DISPERSION OF BUOYANT WASTE WATER DISCHARGED FROM OUTFALL DIFFUSERS OF FINITE LENGTH

by

Philip J. W. Roberts

W. M. Keck Laboratory of Hydraulics and Water Resources
Division of Engineering and Applied Science
CALIFORNIA INSTITUTE OF TECHNOLOGY
Pasadena, California

Report No. KH-R-35 March 1977

DISPERSION OF BUOYANT WASTE WATER

DISCHARGED FROM OUTFALL DIFFUSERS OF FINITE LENGTH

by

Philip J. W. Roberts

Project Supervisor:

Norman H. Brooks
James Irvine Professor of
Environmental and Civil Engineering

Supported by
National Science Foundation
Grant Numbers GK-35774X, ENG75-02985 and ENG75-02985 A01

Environmental Protection Agency
Contract Number 68-03-0434

Rockefeller Foundation
Grant Number RF-72049

Ford Motor Company Fund for Energy Research
(through the Caltech Energy Steering Committee)

W. M. Keck Laboratory of Hydraulics and Water Resources
Division of Engineering and Applied Science
California Institute of Technology
Pasadena, California

Report No. KH-R-35 March 1977

ACKNOWLEDGMENTS

Many people contributed to this study, and I would like to express my gratitude to them.

First and foremost was my adviser, Norman H. Brooks, who suggested this project and provided much encouragement and assistance essential for its completion.

Drs. R. C. Y. Koh and E. J. List made many valuable suggestions during the writing of the thesis. Fellow students E. Naheer and N. Kotsovinos made many useful comments. Greg Gartrell also made many comments, whether wanted or not. Dr. Koh also made many helpful suggestions on the experimental aspects.

I would also like to thank Mr. Elton F. Daly for his invaluable assistance and advice in all practical matters, Joe Fontana who constructed much of the equipment, and Dave Byrum who prepared the drawings.

Dale Johnson and Linda Figueroa assisted with the laboratory experiments, and Bob Shultz and Hugh Ginter assisted with the field experiments.

Mrs. Joan Mathews performed an excellent job in typing the text.

The writer acknowledges support from the following sources at various times during the course of this research: National Science Foundation (Grant Numbers GK-35774X, ENG75-02985 and ENG75-02985 A01), Environmental Protection Agency (Contract Number 68-03-0434), Rockefeller Foundation (Grant Number RF-72049), and Ford Motor Company Fund for Energy Research (through the Caltech Energy Steering Committee).

Finally, I would like to thank Yvette, my wife, for her love and encouragement which were so needed during the course of this study.

This report was submitted in March, 1977 as a thesis for the degree of Doctor of Philosophy in Environmental Engineering Science at the California Institute of Technology.

ABSTRACT

The three-dimensional flow field created by a simple line plume of finite length in a steady current of uniform density was investigated in a laboratory basin. The results can be used to aid in the prediction of dispersion of buoyant waste water released from line diffusers, particularly sewage discharges into the ocean.

The experimental results for minimum surface dilution, S_m, were found to be independent of L/H, in the range $3.7 < L/H < 30$ where L is the diffuser length and H the water depth, and independent of Reynolds number, $Re = 4uH/\nu$, in the range $1190 < Re < 12{,}900$ where u is the current velocity. The results are expressed graphically in the form:

$$\frac{S_m q}{uH} = f(F,\theta) \ ,$$

where q is the volume flux per unit length, and θ the orientation of the line diffuser to the current. F is a type of Froude number defined by $F = u^3/b$, where b is the buoyancy flux per unit length. The initial momentum flux is assumed to be small.

For a current perpendicular to the diffuser, and $F > 0.2$, the effluent mixes over the receiving water depth due to self-induced turbulence. When the diffuser is of finite length, the diluted effluent separates from the bottom at some point downstream and forms a two-layer flow. However, currents parallel to the diffuser do not produce mixing over the depth, and the flow forms a two-layer system immediately, even for Froude numbers as high as 100.

For $F < 0.1$, dilution is independent of current speed and direction. For $F > 0.1$, dilutions when the current is perpendicular to the diffuser are proportional to the current speed. For $0.1 < F < 100$ this dilution is about 60% of that predicted assuming uniform mixing of the effluent over the receiving water depth. This is due to the development of a vertically stable density profile. For $F > 0.1$, a diffuser placed perpendicular to the current will result in greater dilutions than if parallel. The ratio of minimum surface dilution when the current is perpendicular to that when the current is parallel increases with F, and is equal to about 4 at $F = 100$.

Horizontal spreading of the waste field is governed by buoyancy forces rather than ambient turbulence. For $F \geq 1$ the initial surface plume spreading is found to be linear, and independent of L/H and Re for $3.7 < L/H < 15$, and $2{,}900 < Re < 13{,}000$. Beyond this initial linear spreading zone the rate of plume growth decreases. It is speculated that regimes may exist where the surface width grows as the 2/3 or 1/5 power of downstream distance; the results are not adequate to confirm these growth laws. It is believed that ambient turbulence has no significant effect on diluting the waste within several diffuser lengths from the source.

The results have been presented in a manner which makes them immediately applicable for improving outfall designs, and demonstrates the error frequently made in assuming two-dimensional flow fields. This assumption is incorrect even if the diffuser length is an order of magnitude greater than the water depth.

TABLE OF CONTENTS

TABLE OF CONTENTS (Continued)

TABLE OF CONTENTS (Continued)

LIST OF FIGURES

LIST OF FIGURES (Continued)

LIST OF FIGURES (Continued)

LIST OF FIGURES (Continued)

LIST OF FIGURES (Continued)

LIST OF FIGURES (Continued)

LIST OF TABLES

NOMENCLATURE

a_1, a_2, a_3, a_4, a_5	Constants
b	Buoyancy flux per unit length, $\frac{\rho_r - \rho_o}{\rho_o} gq$
B	Slot width
B_o	Buoyancy flux of round jet, $u_e \frac{\pi}{4} D_e^2 g'_o$
c, c_o, c_r	Species concentration in mixture, effluent, and receiving water, respectively
c_p	Specific heat
C	Time averaged effluent concentration, defined as volume fraction of effluent in mixture
C_c	Coefficient of contraction for round jet, $(D_e/D_o)^2$
C_D	Discharge coefficient for basin venturi meter
C_i	Mean concentration at i samples/s, or averaged over i seconds, also i^{th} sample
C_m	Mean concentration at 400 samples/s, or averaged over 512 seconds
C_1, C_2, C_3	Experimental constants
C'	Instantaneous deviation of C from mean
$\sqrt{\overline{C'^2}}$	Standard deviation of C'
d_s	Mean sand grain diameter
d_t, d_u	Throat and upstream pipe diameters of basin venturi meter
D	Depth of ambient water beneath surface layer, H-h
D_e	Diameter of round jet at vena contracta
f	Friction factor, $8u_*^2/u^2$
f( )	Function of variables in parentheses
F	Froude number of line plume in a current, u^3/b

F_e	Froude number of round jet at vena contracta, $u_e/\sqrt{g'_o D_e}$
F_o	Froude number of round jet, $u_o/\sqrt{g'_o D_o}$
F_s	Froude number for two-dimensional stratified flows, $u_1/\sqrt{g'_o h_1}$
F_T	Froude number of multiport diffuser, $q/\sqrt{g'_o H^3}$
g	Acceleration due to gravity
g'	$g(\rho_r-\rho)/\rho_o$
g'_o	$g(\rho_r-\rho_o)/\rho_o$
g'_m	$g(\rho_r-\rho_m)/\rho_o$
h	Thickness of surface layer
h_1	Thickness of surface layer immediately after surface transition zone (Figure 2.5)
H	Water depth
K_1 through K_{10}, K_{1T}	Experimental constants
ℓ	Average port spacing for multiport diffuser, L/n
ℓ_m	Length scale for which momentum flux of line jet dominates over buoyancy flux, $u_j^2 B/b^{2/3}$
L	Diffuser length
L_o	Width of surface waste field at transition from buoyant spreading to horizontal turbulent diffusion
m	Momentum flux per unit length of slot jet, $u_j^2 B$
M_o	Momentum flux of round jet at vena contracta, $u_e^2 \frac{\pi}{4} D_e^2$
n	Total number of ports in multiport diffuser
N	ℓ_m/H
q	Volume flux per unit length
Q	Total volume flux
Q_b	Recirculation rate in basin

Q_o	Volume flux from round jet
R	Basin rotameter reading, percent of full scale
Re	Reynolds number, $4uH/\nu$
s	Coordinate
S	Dilution, 1/C
S_a	Average dilution
S_c	Minimum surface dilution on centerline in three-dimensional flows with a current perpendicular to diffuser
S_m	Minimum surface dilution
t	Time
t_o	Shift in time origin
t_m	Time for vertical mixing due to ambient turbulence to reach surface
T, T_o, T_r	Temperatures of mixture, effluent, and receiving water, respectively
T_m	Averaging time
u	Ambient current velocity
u_e	Velocity of round jet at the vena contracta
u_j	Exit velocity of slot jet
u_o	Exit velocity of round jet
u_p	Local ambient velocity perpendicular to diffuser
u_s	Entrainment velocity due to mixing induced by ambient turbulence
u_1	Horizontal velocity of surface flow immediately after surface transition zone (Figure 2.5)
u_2, u_3	Velocities of lower and upper layers in lock exchange flow
V	Signal voltage recorded on A/D converter

V, V_o, V_r	Volumes of mixture, effluent, and receiving water, respectively
V_T	Volume flux ratio, uH/q
w	Width of surface waste field
w_a	Width of zone of lower boundary attachment
w_b	Width of surface waste field due to buoyant spreading
w_o	Width of surface waste field, bL/u^3
w_t	Measure of surface waste field width due to horizontal turbulent diffusion
W	Basin width
x,y,z	Coordinates (Figure 2.1)
x_a	Length of zone of lower boundary attachment (Figure 3.1)
x_m	Distance from source for vertical mixing of surface waste field due to ambient turbulence to reach surface
x_o	Origin shift
x_r	Estimate of distance from source for interfacial shear to begin affecting surface spreading
x_t	Estimate of distance from source for ambient turbulence to begin affecting horizontal spreading
α	Constant (Eq. 3.44)
β	Average density gradient in surface layer (Eq. 6.22)
γ	L_o/L (Eq. 6.41)
δ, Δ	Difference operator
ΔH	Difference in peizometric head between basin venturi meter taps
Δw	$w - L$
ε	Effective viscosity coefficient (Eq. 3.44)
ε_o	$\lambda L_o^{4/3}$

ε_z	Horizontal diffusion coefficient for ambient turbulence (Eq. 6.38)
η_t	x_t/L
θ	Angle of current relative to line diffuser (Figure 2.1)
λ	$\varepsilon_z w_t^{-4/3}$ (Eq. 6.38)
Λ	Length scale over which initial momentum flux is important relative to buoyancy flux for round jet, $M_o^{3/4}/B_o^{1/2}$
μ	Dynamic viscosity
ν	Kinematic viscosity, μ/ρ_o
ρ, ρ_o, ρ_r	Mass densities of mixture, effluent, and receiving water, respectively
ρ_m	Mass density at point of minimum dilution
σ	Constant (Eq. C11)
σ_T	Experimental constant (Eq. A.7)
τ	Shear stress
ϕ	Constant (Eq. C11)
ψ	d_t/d_u

CHAPTER 1

INTRODUCTION

This report describes experiments which were performed to investigate the dilution and transport of buoyant waste water discharged from a straight diffuser of finite length into a steady current of uniform density and limited depth. This situation occurs in the disposal of sewage and other wastes into coastal oceans.

Modern practice for ocean sewage disposal consists of some degree of treatment followed by discharge through a submarine outfall. An outfall is a pipeline extending some distance offshore along the sea bottom. At the end of the pipeline is a section with ports which discharge the effluent. The length of this perforated section, known as the diffuser, is often of the order of 1000 m which is much greater than the depth of submergence. The outfall and treatment plant constitute a system for wastewater disposal which should be effected to maintain acceptably small changes in the receiving water and to protect public health.

Some of the objectives of waste water disposal are expressed by the ambient water quality standards which must be maintained in the vicinity of the discharge. In California, for example, the State Water Resources Control Board specifies the requirements to be met by waste dischargers. One of the requirements is that the initial dilution achieved by the outfall must exceed 100 for at least 50% of the time and 80 for at least 90% of the time. Also, standards are set which limit the bacterial

content of sea water at and near the shoreline. It is desirable to find the most economical combination of treatment and outfall needed to meet these and other requirements. Thus, knowledge is required of the mechanics of dispersion (defined here as dilution and transport) of the waste water in the ocean.

Dispersion of waste water, and hence ambient water quality, are complex functions of the physical parameters involved. The most important of these are the density difference between the waste and receiving waters, the speed and direction of ambient currents, the density stratification and depth of the receiving water, the effluent discharge rate, and the diffuser length. Knowledge of the natural density stratification often present in the ocean can be used to design diffusers which prevent the effluent from reaching the surface. If the sewage field (the resulting mixture of sewage and sea water) is submerged, the sight of waste water on the surface is virtually eliminated, and the sewage field does not touch the shoreline. At certain times of the year, however, particularly in winter, the stratification may be too weak to maintain a submerged field. If the field surfaces, it may be visible and can reach the shore, possibly violating bacterial standards there. The most probable time for this to occur is when the buoyant spreading of the surface field is most rapid. This occurs when the receiving water is of uniform density.

Methods currently used for the prediction of dispersion in the case of uniform density receiving water suffer from a number of defects. First, dilution is usually estimated by use of the results of studies on buoyant jets in stagnant receiving water. This prediction may considerably

underestimate the actual dilution which occurs in a flowing current. Second, subsequent dispersion of the waste field is usually predicted as if it were passively diffused by the ambient turbulence of the receiving water. This approach ignores the dynamic effect of surface spreading due to the buoyancy of the waste field. Furthermore, previous experimental and theoretical work has been mainly concerned with two-dimensional flows, that is, diffusers of infinite length. There is little information available either on the three-dimensional flows that occur with diffusers of finite length, or on the effects of varying the ambient current direction and speed.

The objectives of this study are to investigate the near field dispersion of buoyant waste water discharged from a line source of finite length into a current which has no density stratification. This near field is defined as the region where the effluent buoyancy affects its dispersion.

The major portion of this study consists of experimental investigations of the flow field created by a source of buoyancy flux only. The source is a submerged line of finite length and the receiving water is of uniform density and finite depth flowing at an arbitrary speed and direction. The results are applicable to diffusers discharging highly buoyant waste water with no net horizontal momentum flux into deep water. These are primarily discharges of effluent whose density is close to that of fresh water into sea water. Sewage and industrial waste disposal into the coastal ocean are examples. Special cases of thermal discharges may be included.

This report is divided into seven chapters. In Chapter 2, previous

work is reviewed. In Chapter 3 the problem is analyzed, in Chapter 4 the experimental equipment and procedures are described, and in Chapter 5 the experimental results are presented and discussed. An example of application of the results to ocean outfall dispersion prediction and comparisons of the results with model and field studies are given in Chapter 6. Also in Chapter 6 the effect of ambient turbulence and the behavior of the waste field at large distances from the source are discussed. Finally, a summary and the conclusions of this study are presented in Chapter 7.

CHAPTER 2

REVIEW OF PREVIOUS STUDIES

2.1 Introduction

The problem under consideration is shown in Figure 2.1. A diffuser of length L, situated in water of depth H, is oriented at an angle θ to a current of uniform density ρ_r, flowing at a steady speed u. The diffuser discharges buoyant effluent with zero net horizontal momentum flux. The problem is to predict the dispersion of the waste water.

The dispersion of effluent has often been considered to consist of several distinct phases. Koh and Brooks (1975), for example, assume three phases. First, they consider an initial dilution zone in which the effect of the ambient current is neglected. Here, the effluent rises, entraining and mixing with the receiving water as a result of self-induced turbulence. The second phase consists of the establishment of the surface field and its buoyant spreading in the vicinity of the diffuser. The final third phase is assumed to be dynamically passive diffusion of the surface field by oceanic turbulence. Although this classification is somewhat arbitrary, inasmuch as the processes can occur simultaneously, it is helpful for discussing the dominant phenomena.

In this chapter previous studies are reviewed. A classification scheme is maintained for the different phases of dispersion. In Section 2.2 initial dilution is considered. The two-dimensional flow field in a stagnant receiving fluid is discussed in Section 2.3. Particular attention is given to the surface transition zone and the

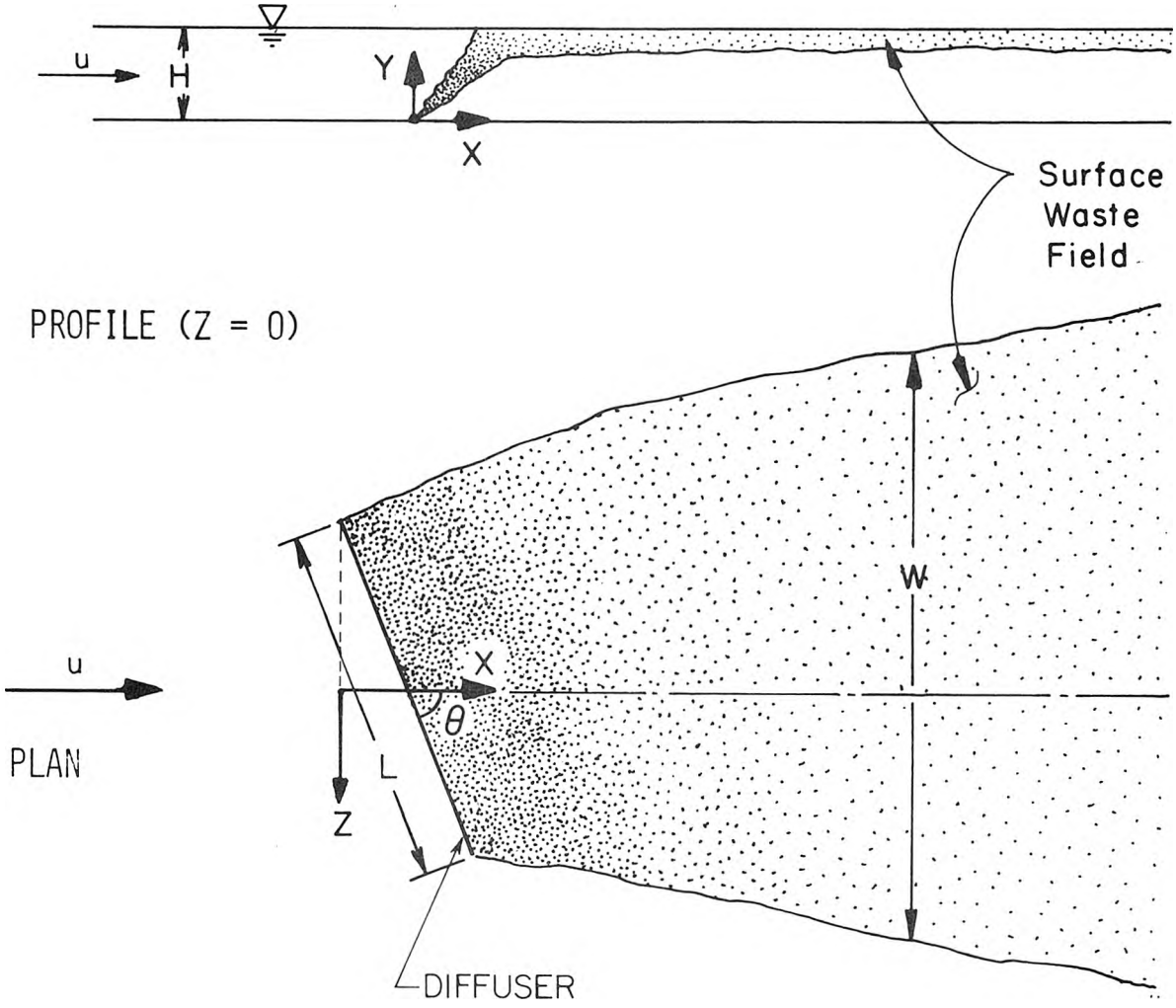

Figure 2.1 Definition diagram.

formation and unsteady buoyant spreading of the surface layer. Attempts to extend these and other results to prediction of surface spreading in the three-dimensional steady flow case are reviewed in Section 2.4. In Section 2.5, the review will be summarized and the objectives of the present study outlined.

2.2 Initial Dilution Region

Diffusers often consist of round pipes with horizontally opposed ports along each side. The effluent is ejected as round turbulent jets from these ports and, being less dense than the receiving water, rises towards the surface. In a stagnant receiving fluid, the column of effluent becomes diluted due to entrainment and grows in size as it rises. Depending on the port spacing, exit velocity, and water depth, the individual jets may merge together before reaching the surface. The resulting surface dilution is usually named the initial dilution.

Early attempts at predicting the initial dilution used the results of experiments on single round buoyant jets issuing horizontally into a stagnant fluid. Since the first systematic experiments on this phenomenon by Rawn and Palmer (1930) many other theoretical and experimental studies have been published. Many of these are summarized in Appendix B.

The flow above a line diffuser in a stagnant medium in which merging of the individual jets has occurred was considered by Pearson (1956). He speculated that the flow would be similar to discharge from a slot. He also pointed out that the dilution

pattern will approach that due to the convective flow developed above a line heat source. This flow is known as a pure plume, whose only source characteristic is the buoyancy flux per unit length, b. For a line diffuser, b is defined as:

$$b = \frac{\Delta\rho}{\rho_o} gq \quad , \tag{2.1}$$

where $\Delta\rho$ is the difference in density, $\rho_r - \rho_o$, between the receiving water and effluent. ρ_r and ρ_o are the densities of the receiving water and effluent, respectively, g is the acceleration due to gravity and q is the volume flux of effluent per unit diffuser length.

By approximating the flow as a line plume, Pearson obtained an estimate for dilution on the centerline (the minimum dilution S_m) for large heights of rise. He used the results of experiments on two-dimensional plumes obtained by Rouse, Yih and Humphreys (1952). Using more recent experimental data from Kotsovinos (1975), the relationship can be written (Appendix B, Eq. 45) as:

$$S_m = 0.42 \left(\frac{\Delta\rho g}{\rho_o}\right)^{1/3} y\, q^{-2/3} \quad , \tag{2.2}$$

where y is the height above the outfall, for y large.

The asymptotic relationship for dilution, Eq. 2.2, was verified by Liseth (1970, 1976), who did experimental work on merging round buoyant jets from a row of ports in a line

diffuser. Dilutions for heights of rise such that the jets have not fully merged to a line plume can be estimated from Figure 5, Appendix B.

The effect of a current flowing perpendicular to a line diffuser of infinite length has been considered by several authors. Pearson (1956) speculated that different flow regimes would exist depending on the relative strength of the ocean current, as shown in Figure 2.2. Pearson attempted to predict dilution for the case where the effluent supposedly remains attached to the ocean floor by applying the results of an analysis by Rouse (1947). Rouse considered the dispersal of heat issuing from a line source of infinite length at ground level perpendicular to a moving air stream of unlimited depth. From a theoretical and experimental study, Rouse obtained an estimate for the local density difference, $\Delta\rho$, as:

$$\frac{\Delta\rho}{\rho_o} g \frac{xF^{1/2}}{u^2} = 2.6 \exp\left[-5.4\left(\frac{y}{x}\right)^2 F\right] . \qquad (2.3)$$

Here, x and y are the horizontal and vertical distances from the source, u is the ambient flow velocity, and F is a type of Froude number defined by

$$F = u^3/b \quad , \qquad (2.4)$$

where b is defined by Eq. 2.1.

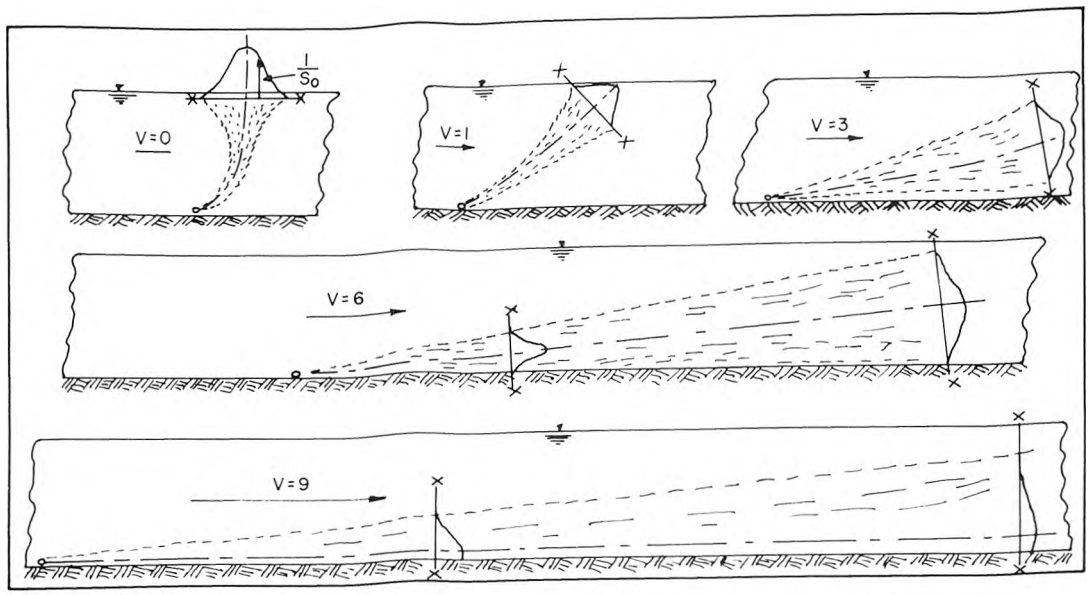

Note: Scale of ordinate from x-x axis represents the reciprocal of dilution, $1/S_o$.

Figure 2.2 Schematic representation (after Pearson (1956)) of possible dispersion patterns from a diffuser in a perpendicular current of varying velocity, V (arbitrary units, not scaled).

The experiments of Cederwall (1971) demonstrated the occurrence of the flow regimes predicted by Pearson and also additional regimes due to the presence of a free surface. Cederwall performed experiments on buoyant slot jets issuing perpendicular to a flowing fluid of finite depth. His source spanned the width of a flume so that the flow was two-dimensional. For jets with negligible initial momentum flux, Cederwall found that the flow could take one of three forms depending on the value of F as defined by Eq. 2.4. These flow regimes are shown in Figure 2.3. For $F < 0.2$, Figure 2.3a, a plume results, and the surface layer spreads up and downstream from the source. This is denoted as the plume regime. For F greater than about 0.2, Figure 2.3b, the plume cannot entrain all the oncoming flow while maintaining the plume flow. The plume breaks up and remains attached to the lower boundary. This is the case that Pearson speculated would exist for strong currents. Cederwall described this regime as forced entrainment. Finally, when F becomes greater than about 1, Figure 2.3c, the upstream wedge is expelled.

An effect of the surface layer is to restrict entrainment into the plume and hence to reduce the surface dilution. Measurements of surface dilutions were made by Bühler (1974). Bühler's experiments were similar to Cederwall's in that a source extended the full width of a flume and the receiving water was moving relative to the diffuser and was of finite depth. Bühler,

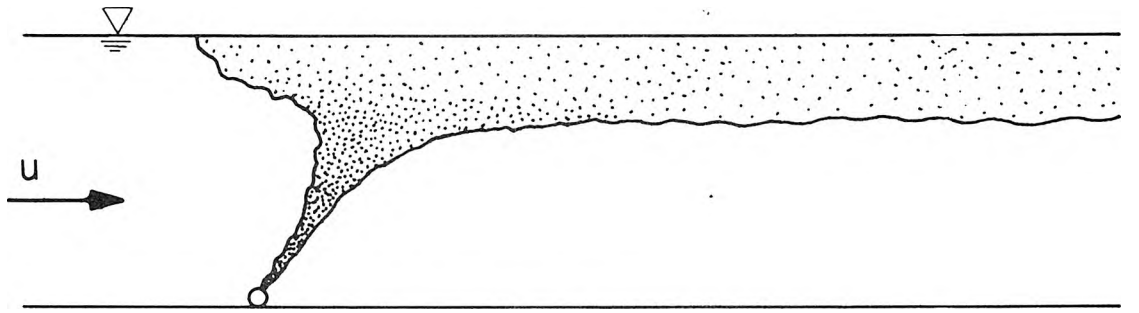

a) $F < 0.2$. Plume and upstream wedge.

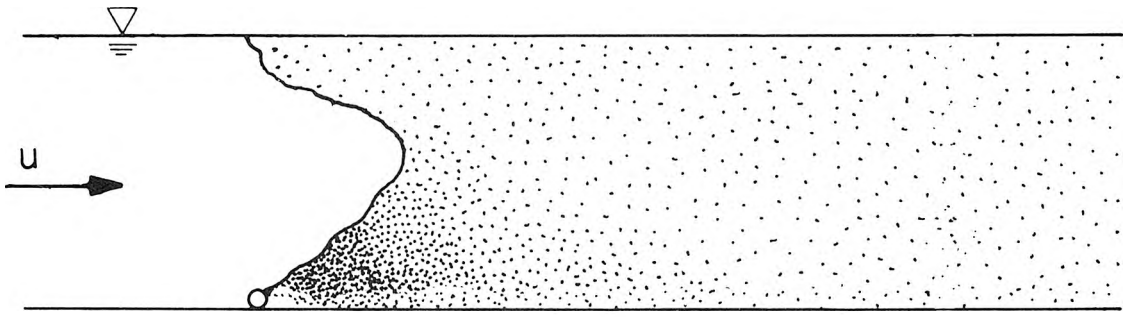

b) $0.2 < F < 1$. Forced entrainment and upstream wedge.

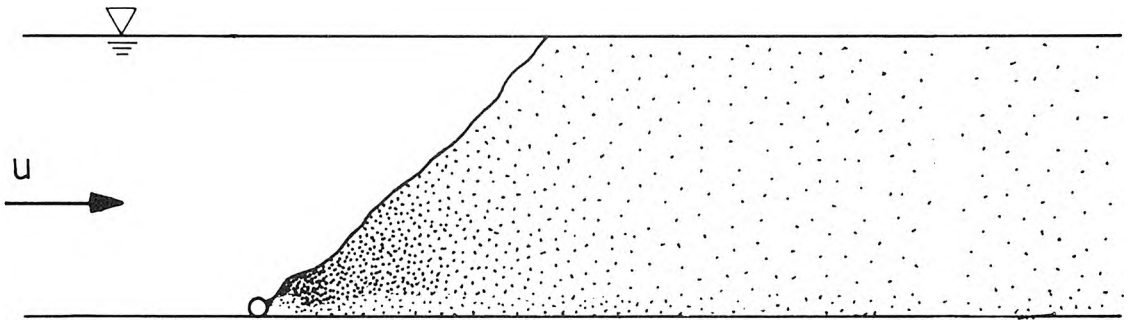

c) $F > 1$. Forced entrainment, no upstream wedge.

Figure 2.3 Flow regimes for a plume of infinite length in a perpendicular current, $F = u^3/b$.

however, used a model multiport diffuser as his source, and found that the same flow regimes observed by Cederwall (Figure 2.3) existed. Bühler measured surface dilutions for a wide range of port spacings, jet densimetric Froude numbers, and ambient current velocities. He found that the minimum surface dilution was primarily a function of the source buoyancy flux, the ambient current velocity, and the receiving water depth. The source momentum flux and port spacing only weakly affected the dilution. By the use of dimensional analysis, Bühler expressed his results in the form:

$$\frac{b^{1/3}H}{S_m q} = f\left(\frac{u}{b^{1/3}}\right) \quad . \tag{2.5}$$

Bühler's results are shown in Figure 2.4. For the plume regime ($F < 0.2$), the dilution is not strongly affected by the current. For the condition of forced entrainment ($F > 0.2$), however, the dilution increases rapidly with current speed. For high current speeds, Bühler assumes an asymptotic solution corresponding to uniform mixing of the effluent over the receiving water depth. S_m is then given by:

$$\frac{b^{1/3}H}{S_m q} = \left(\frac{u}{b^{1/3}}\right)^{-1} \quad . \tag{2.6}$$

Bühler's experiments do not extend to currents of sufficient strength to confirm Eq. 2.6, which is plotted in Figure 2.4. Similar experiments on thermal diffusers in strong currents have been made by Nospal and Tatinclaux (1976). The results of these

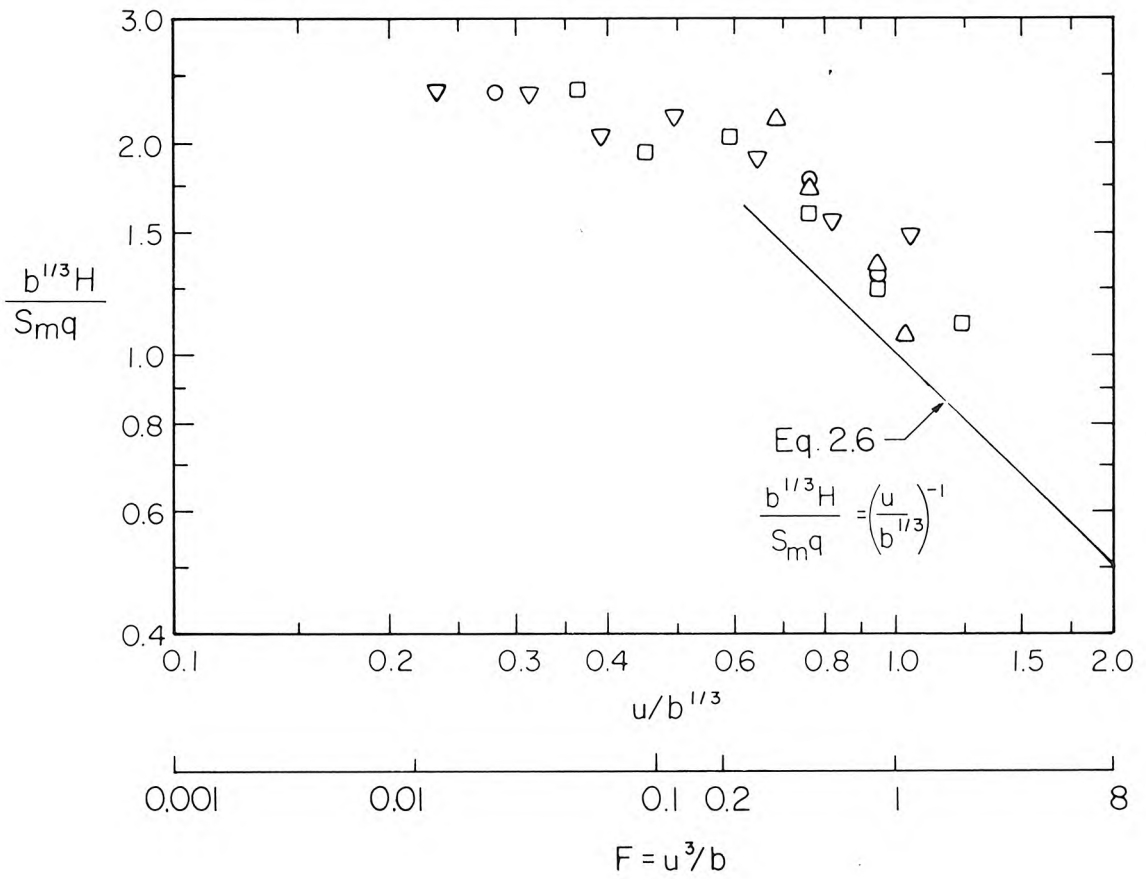

Figure 2.4 Measured minimum surface dilution of buoyant effluent discharged from a multiport diffuser into a perpendicular current, two-dimensional flow (from Bühler (1974)).

experiments and those of Bühler will be discussed further in Chapter 6 in conjunction with the present analysis.

Experimental data on diffusers of finite length are very scarce. Although experimental studies of model thermal outfalls have been made, the results are usually not applicable to sewage outfalls. This is because the source momentum and volume fluxes are relatively large.

Three-dimensional dispersion from outfall diffusers was considered by Jirka and Harleman (1973). They did not attempt to analyze the problem for arbitrary current conditions. For the case of a strong current, however, they proposed that the surface dilution can be predicted by assuming uniform mixing of the effluent over the receiving water depth, as did Bühler. They gave this asymptotic solution, (c.f. Eq. 2.6), as:

$$S_m = \frac{uH}{q} \sin\theta \quad , \tag{2.7}$$

where θ is the angle of the current relative to the diffuser (Figure 2.1). The solution as θ tends to zero is presumably undefined.

Jirka and Harleman performed both two and three-dimensional experiments in which surface dilutions were measured. The two-dimensional experiments with a source having no net horizontal momentum were conducted with a vertically issuing slot jet. It is shown in Section 6.2 that most of their experiments were conducted with a large source momentum flux. The three-dimensional

experiments with no net horizontal momentum were conducted with a diffuser which had widely spaced jets with large individual momentum fluxes. Thus, these results have limited applicability to the situation considered here in which the individual jets merge and have negligible source momentum fluxes. Jirka and Harleman only investigated flows having Froude numbers less than 0.2. This corresponds to the plume regime, Figure 2.3a. Like Bühler, they found that dilutions were not strongly affected by the current in this regime. They found that orientation of the diffuser parallel to the current resulted in a reduction of dilution compared to a perpendicular current of approximately 20%. The results of Jirka and Harleman will be considered further in Chapter 6.

2.3 Two-Dimensional Flow Field in a Stagnant Receiving Fluid

Jirka and Harleman considered the unsteady two-dimensional flow field induced by a line diffuser in a stagnant medium of finite depth. The postulated flow is shown in Figure 2.5. Jirka and Harleman assumed this flow to exist in the center portion of the diffuser. They postulated that three-dimensional flows could be analyzed as a two-dimensional flow bounded by parallel walls of finite length opening at both ends into a large reservoir. This approach is probably reasonable for estimating dilutions in stagnant water, but not for predicting the surface layer extent in three dimensions.

The two-dimensional flow is divided into four regions, as

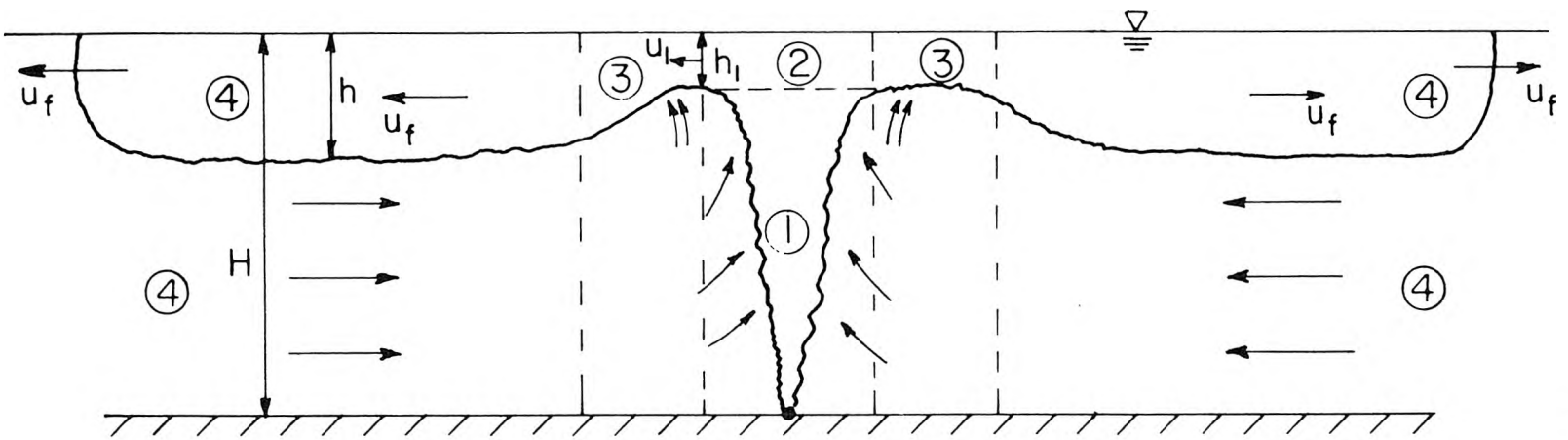

Figure 2.5. Postulated two-dimensional flow field induced at center of diffuser in a stagnant ambient fluid (after Jirka and Harleman (1973)).

shown in Figure 2.5. In the surface transition zone, the motion of the effluent becomes horizontal as the flow spreads laterally due to the force of gravity. For diffusers with negligible initial momentum flux, as considered here, Jirka and Harleman predicted the initial thickness of the surface layer, h_1, as:

$$\frac{h_1}{H} = 0.149 \quad . \tag{2.8}$$

Thus, h_1 is independent of the source buoyancy flux.

An important parameter for two-dimensional stratified flows is a densimetric Froude number, F_s, defined as:

$$F_s = \frac{u_1}{\sqrt{\frac{\Delta\rho}{\rho_o} g h_1}} \quad , \tag{2.9}$$

where u_1 is the mean horizontal velocity of the upper layer, and $\Delta\rho$ is the average density difference between the upper and lower layers. Jirka and Harleman predicted that $F_s = 2.63$ for the flow immediately after the surface transition. This value of F_s, being greater than 1, means that the flow is supercritical and is unaffected by far field conditions. The layer thickness will grow due to turbulent entrainment, and an internal hydraulic jump may occur. This flow, shown as region 3 in Figure 2.5 has been analyzed by Koh (1971), Chu and Vanvari (1976), and others.

After the surface transition region, the flow becomes subcritical and is controlled by conditions at the advancing

front. This is the stratified counterflow region, in which entrainment is not significant. Koh and Fan (1970) analyzed the similar problem of buoyant surface spreading of a continuous source, shown in Figure 2.6.

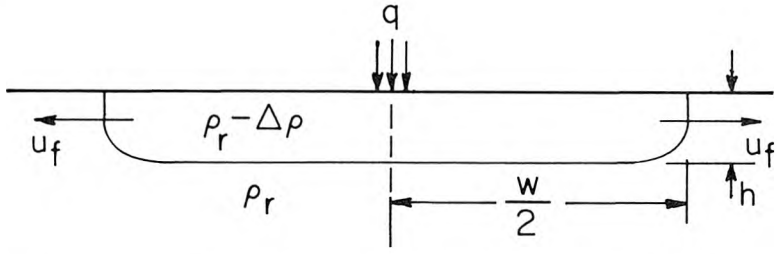

Figure 2.6 Definition sketch of two-dimensional surface spreading problem considered by Koh and Fan (1970).

When w, the length of the surface layer, is small Koh and Fan found that the speed of advance, u_f and the thickness, h are both constant. u_f was predicted as:

$$u_f = K_1 b^{1/3} \quad , \tag{2.10}$$

where b is the flux of buoyancy per unit length, and K_1 is a constant, equal to one. For a submerged source, as shown in Figure 2.5, Eq. 2.10 should still predict u_f, but the value of K_1 would be less than unity due to the current induced in the lower layer by plume entrainment which reduces the rate of surface spreading. The value of K_1 can be obtained from the experiments on multiport diffusers of Bühler (1974). He found that u_f was mainly dependent on b, and was only weakly influenced by the port spacing and jet exit velocities. Roberts (1975) replotted Bühler's data, and estimated the value of K_1 to be 0.66. The results of

two-dimensional experiments performed as a part of the present study (Appendix A) suggest that $K_1 = 0.68$.

The uniformity of the surface layer thickness was observed by Liseth (1970). He estimated this thickness to be about 30% of the water depth. Bühler (1974), however, estimated the thickness as about 40% of the water depth. The results of the present study (Appendix A) suggest that 30% is the more reasonable figure.

Koh and Fan predicted that when the length of the surface layer becomes large, interfacial shear is the dominant mechanism resisting surface spreading. They predicted that for these conditions:

$$u_f \propto t^{-1/5} \quad , \tag{2.11}$$

where t is time. This relationship was confirmed by the results of the present study (Appendix A). The thickness of the surface layer is no longer constant, but grows with time.

2.4 Buoyant Surface Spreading in Three-Dimensional Flow

Several authors have extended the analysis of two-dimensional unsteady surface spreading in order to predict three-dimensional spreading in a steady current. These studies will be reviewed in this section.

Koh and Brooks (1975) estimated the development of the surface field for a current parallel to the diffuser. They assumed that the spreading can be approximated by a time-dependent release.

By applying a Galilean transformation and dimensional analysis, they obtained a result for the width of the field, w, as:

$$w = \frac{K_2 b^{1/3} x}{u} \quad . \tag{2.12}$$

Here, x is the distance along the diffuser, u is the current speed, and K_2 an experimental constant. The field is therefore predicted to grow linearly with distance downstream. From a few experiments, Koh and Brooks found values of K_2 between 1 and 1.5. Comparison of Eqs. 2.10 and 2.12 shows that $K_2 = 2K_1$. The value of K_1 was estimated as 0.68 in the previous section, hence K_2 is about 1.36. Koh and Brooks predicted the thickness of the waste water field to be about 30% of the water depth.

There have apparently been no analyses for the surface spreading rate for the condition of lower boundary attachment, Figure 2.3c.

At some point downstream, the waste field must form a two-layer system (Figure 2.7) if the diffuser is of finite length. An analysis of the buoyant spreading rate in this region was done by Larsen and Sorensen (1968). They neglected the effect of interfacial shear, and assumed a uniformly mixed surface layer. The velocity vector triangle at the surface layer front (Figure 2.7) is defined by the ambient current velocity, u, and a velocity u_f. u_f is the spreading velocity in two-dimensional flow, assumed to be given by:

$$u_f = \sqrt{\frac{g\Delta\rho}{\rho_r} h} \quad . \tag{2.13}$$

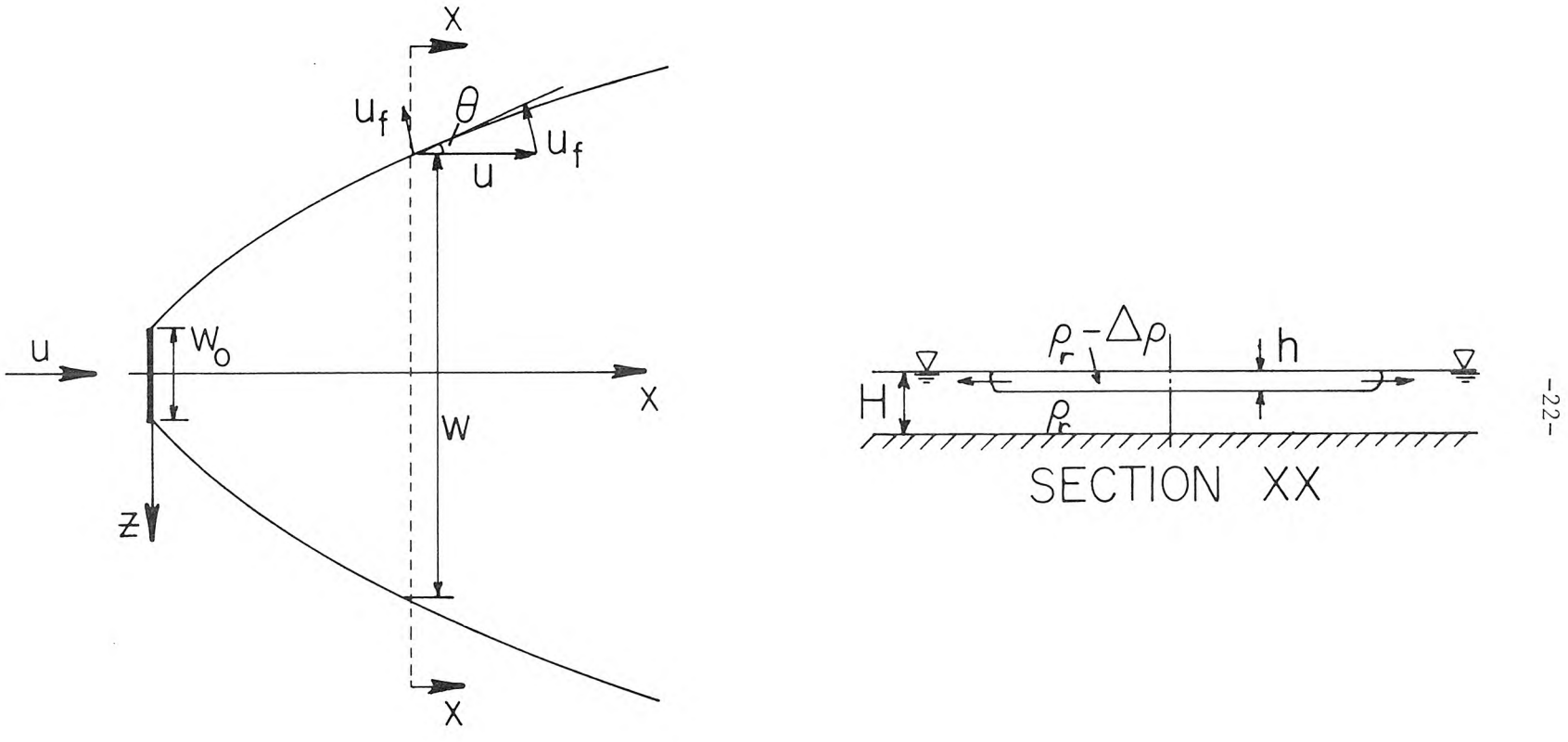

Figure 2.7 Definition diagram for buoyant spreading of surface waste field.

Additional equations are provided by the conservation of buoyancy flux:

$$bL = wu \frac{g\Delta\rho}{\rho_r} h \quad , \tag{2.14}$$

and the kinematic conditions at the front:

$$u \sin\theta = u_f \quad , \tag{2.15}$$

and

$$\frac{dw}{dx} = 2 \tan \theta \quad . \tag{2.16}$$

Larsen and Sorensen obtained the solution to Eqs. 2.13 through 2.16 as:

$$\frac{w}{w_o} = 1.31 \left(\frac{2x}{w_o} \right)^{2/3} + 1 \quad . \tag{2.17}$$

w_o is the original width of the effluent field, obtained by setting the front velocity at this section equal to the ambient current velocity:

$$w_o = \frac{bL}{u^3} \quad . \tag{2.18}$$

Eq. 2.18 is not correct for arbitrary conditions, hence Eq. 2.17 is incorrect, although the asymptotic power law relationship as $x \to \infty$, $w \propto x^{2/3}$, is true within the limits of the assumptions made. However, the assumption of Eq. 2.13 is only valid for infinite receiving water depths. This was shown by Benjamin (1968), who analyzed the two-dimensional problem for a perfect fluid and expressed the spreading rate as:

$$u_f = K_3 \sqrt{\frac{g\Delta\rho}{\rho_r} h} \quad , \tag{2.19}$$

in contrast to Eq. 2.13. He found that K_3 is not constant, but a function of the relative thickness of the surface layer to the water depth. Benjamin found that K_3 increases as the relative layer thickness decreases. K_3 was predicted to vary from $1/\sqrt{2}$ to $\sqrt{2}$ as h/H decreases from 0.5 to 0. This result suggests that the surface layer would grow more rapidly than the 2/3 power law predicted by Eq. 2.17.

Experiments on the surface spreading of a heated surface plume have been reported by Weil and Fischer (1974). They found that the spreading rate followed approximately the 2/3 relationship predicted by Eq. 2.17. The scatter in their data, however, makes the results inconclusive. Weil and Fischer also found that the spreading rate was only weakly affected by background turbulence in the ambient flow.

An alternative approach to predicting surface spreading is given by Bache (1976). He considers the surface spreading to be characterized by two momentum blocks which move apart as shown in Figure 2.8.

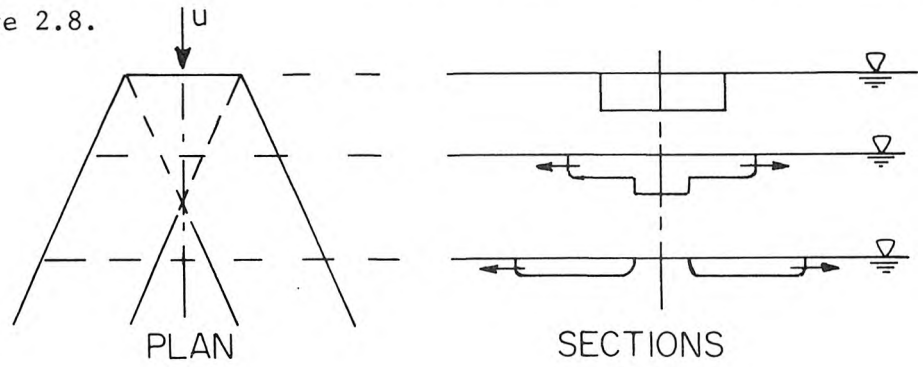

Figure 2.8 Schematic representation of surface spreading due to block motion (after Bache (1976)).

The effect of background turbulence is accounted for by a constant outflow velocity from the blocks. Entrainment into the blocks due to induced mixing is also allowed. By the use of volume and momentum conservation equations, Bache was able to obtain estimates of the surface spreading rate. If this analysis were correct, the individual blocks would subdivide again into two blocks, and this subdivision should continue indefinitely. As this is not accounted for in this model, the analysis of Bache is physically unreasonable.

2.5 Summary and Objectives of Present Study

There are few experimental data available in certain critical areas needed for prediction of dispersion (dilution and transport) of buoyant waste water discharged from finite length diffusers. There is a large uncertainty as to the rate of buoyant spreading of the surface waste field. Also, knowledge is lacking on the effects of finite diffuser length and of current speed and direction. This is partly due to the complexity of the problem resulting from the large number of variables involved. A lengthy model testing program would be required to cover all cases of interest in ocean discharge.

A considerable simplification can be made by considering the results of the experiments of Bühler (1974) and the speculations of Pearson (1956). Pearson suggested that the flow above a diffuser consisting of a row of ports would approach that due to a line source of buoyancy flux only. Bühler performed two-dimensional

experiments on the dispersion of buoyant effluent discharged from a submerged multiport diffuser into moving water. His results verified that the most important source parameter in determining surface dilution and spreading was the source buoyancy flux.

The objective of this study is to investigate experimentally the three-dimensional flow field created by a diffuser of finite length in a cross flow. The diffuser is approximated by a source of buoyancy flux only. The effects on dispersion of varying the water depth, diffuser length, source strength, and current speed and direction will be studied, and the results compared with those from other model and field studies.

The results of this study will aid in the design of outfalls in coastal waters. Furthermore, the study will help in obtaining a more fundamental understanding of the mechanics of dispersion of buoyant discharges, especially as related to the two-dimensional assumption which is often inappropriately made.

CHAPTER 3

ANALYSIS

3.1 Introduction

Normalized parameters for expressing dilution and effluent concentration are obtained by dimensional analysis. The dimensionless parameters of the problem and hence the modeling laws are also derived by this analysis which is presented in Section 3.2. The asymptotic behavior of dilution as the Froude number (F)$\rightarrow$ 0 is also derived. The functional form of the relationship between dilution and the independent variables was investigated experimentally. The results are given in Chapter 5.

Current flow perpendicular to the diffuser is considered in Section 3.3. Particular attention is given to situations where $F \geq 1$. This is the case of lower boundary attachment, Figure 2.3c. The length of the zone of lower boundary attachment and the initial surface spreading rate are estimated. Details of the mixing process are also discussed. Current flow parallel to the diffuser is considered in Section 3.4, and an estimate obtained for the initial surface spreading rate. Finally, in Section 3.5 the buoyant surface spreading rate for two-layer flow is considered.

3.2 Dimensional Analysis

It is assumed that density changes in the flow field are small compared with the absolute density, and affect only the gravitational and not the inertia forces (the Boussinesq assumption). The buoyant weight at any point in the flow field is given by $(\rho_r - \rho)g$, where ρ_r is the receiving water density, ρ is the local density and g the acceleration due to gravity. Since this buoyant weight is a dependent variable, we can write:

$$(\rho_r - \rho)g = f(u, b, \rho_o, L, H, x, y, z, \theta, \nu) , \tag{3.1}$$

where ρ_r is eliminated as a dependent variable by use of the Boussinesq assumption. ρ_o is the effluent density, b the buoyancy flux per unit diffuser length, and ν the kinematic viscosity, assumed equal for effluent and receiving water. The rest of the variables in Eq. 3.1 are defined in Figure 2.1.

A dimensional analysis of Eq. 3.1, in which only steady flow is considered and turbulent fluctuations are averaged out, gives:

$$\frac{(\rho_r - \rho)gHu}{\rho_o b} = f\left(\frac{u^3}{b}, \frac{L}{H}, \frac{x}{L}, \frac{y}{H}, \frac{z}{L}, \theta, \frac{b^{1/3}H}{\nu}\right) . \tag{3.2}$$

Substitution of the definition of buoyancy flux, Eq. 2.1, into Eq. 3.2 gives:

$$\frac{(\rho_r - \rho)\ uH}{(\rho_r - \rho_o)q} = f\left(\frac{u^3}{b}, \frac{L}{H}, \frac{x}{L}, \frac{y}{H}, \frac{z}{L}, \theta, \frac{b^{1/3}H}{\nu}\right) . \tag{3.3}$$

The dilution, S, of a mixture of effluent and receiving water is defined as the reciprocal of the volume fraction of effluent in the mixture. It is shown in Appendix C that if the densities of the effluent (ρ_o), receiving water (ρ_r), and mixture (ρ) vary linearly with the concentration of some species, for example salt, contained in each component, then S is given (by Eq. C9, Appendix C) as:

$$S = \frac{\rho_r - \rho_o}{\rho_r - \rho} \quad . \tag{3.4}$$

Substitution of Eq. 3.4 into Eq. 3.3 and inversion of the left-hand side yields:

$$\frac{Sq}{uH} = f\left(F, \frac{L}{H}, \frac{x}{L}, \frac{y}{H}, \frac{z}{L}, \theta, \frac{b^{1/3}H}{\nu}\right), \tag{3.5}$$

where $F = u^3/b$. Thus, there are only two dynamic parameters needed to describe the system. These are F, as originally found by Rouse, Eq. 2.4, and a Reynolds number, $b^{1/3}H/\nu$. When the Reynolds number is large so that the flow is fully turbulent, the flow pattern depends only on F. This Froude number describes the relative magnitudes of the forces on the effluent due to gravity and the ambient flow. Eq. 3.5 then becomes:

$$\frac{Sq}{uH} = f\left(F, \frac{L}{H}, \frac{x}{L}, \frac{y}{H}, \frac{z}{L}, \theta\right) . \tag{3.6}$$

At some point on the surface the minimum dilution, S_m, occurs. This dilution is not a function of x or z. Hence, with y/H = 1, Eq. 3.6 becomes:

$$\frac{S_m q}{uH} = f\left(F, \frac{L}{H}, \theta\right) . \tag{3.7}$$

The minimum surface dilution for zero current can be obtained by putting u = 0 in Eq. 3.1. Again, x, y, and z are not variables, and neither is θ, as u is zero. Hence, by assuming the plume to be fully turbulent so that the effect of kinematic viscosity can be neglected enables us to write Eq. 3.1 as:

$$(\rho_r - \rho_m)g = f(b, \rho_o, L, H) \quad , \tag{3.8}$$

where ρ_m is the mixture density at the location of the minimum dilution. A dimensional analysis of Eq. 3.8 yields:

$$\frac{(\rho_r - \rho_m)gH}{\rho_o b^{2/3}} = f\left(\frac{L}{H}\right) . \tag{3.9}$$

For $L/H \gg 1$, it would be expected that the flow would be approximately two-dimensional, so L/H drops out of Eq. 3.9, which becomes:

$$\frac{(\rho_r - \rho_m)gH}{\rho_o b^{2/3}} = \frac{1}{K_4} \quad , \tag{3.10}$$

where K_4 is a constant which must be evaluated experimentally. Substitution of the definitions of b and S from Eqs. 2.1 and 3.4, where $S = S_m$ when $\rho = \rho_m$, yields:

$$S_m = K_4 \left(\frac{\rho_r - \rho_o}{\rho_o} g\right)^{1/3} Hq^{-2/3} \quad . \tag{3.11}$$

Eq. 3.11 can be written in terms of the variables of Eq. 3.7 by dividing both sides by u. The result is:

$$\frac{S_m q}{uH} = K_4 F^{-1/3} \quad . \tag{3.12}$$

Eq. 3.12 is the asymptotic solution to Eq. 3.7 as $F \to 0$, for $L/H \gg 1$.

An estimate of the value of K_4 can be obtained by assuming that the effluent mixes like a plume up to the bottom of the surface layer, and that beyond this point no further dilution occurs. By replacing H with H - h in Eq. 3.11 and comparing with Eq. 2.2, the value of K_4 can be estimated as:

$$K_4 = 0.42(1 - h/H) \quad . \tag{3.13}$$

The results of two-dimensional experiments (Appendix A, see also Section 2.3) show the thickness of the surface layer beyond the surface transition zone but before interfacial shear becomes important to be about 30% of the water depth. Eq. 3.13 then becomes:

$$K_4 = 0.42(1 - 0.30) = 0.29 \quad . \tag{3.14}$$

Hence, Eq. 3.11 becomes:

$$S_m = 0.29 \left(\frac{\rho_r - \rho_o}{\rho_o} g \right)^{1/3} Hq^{-2/3} \quad , \tag{3.15}$$

and Eq. 3.12 becomes:

$$\frac{S_m q}{uH} = 0.29 F^{-1/3} \quad . \tag{3.16}$$

Effluent concentration is defined as the reciprocal of dilution. Hence, concentration profiles can be expressed as the inverse of the

left-hand side of Eq. 3.6, thus:

$$\frac{uH}{Sq} = \frac{CuH}{q} = f\left(F, \frac{L}{H}, \frac{x}{L}, \frac{y}{H}, \frac{z}{L}, \theta\right), \tag{3.17}$$

where C(=1/S) is the time-averaged concentration. C and S of the effluent are both equal to 1.

3.3 Dispersion for Current Flow Perpendicular to Diffuser in Forced Entrainment Regime

3.3.1 Extent of Waste Field

Flow regimes for a diffuser of infinite length in a perpendicular current are shown in Figure 2.3. An example of this type of two-dimensional flow is a diffuser extending the full width of a river. For $F > 0.2$, the effluent, which is initially attached to the lower boundary, would be expected to remain attached downstream. In contrast, a diffuser of finite length less than the overall width of the flow field must produce a two-layered flow at some point downstream. This is due to the lateral buoyant spread of the waste field and accompanying movement of the receiving water beneath it, as shown in Figure 3.1.

In order to predict the length of the attached region, x_a, it is assumed that the effluent is uniformly mixed immediately over the receiving water depth. (The effluent actually requires a short distance to reach the surface, and does not quite mix uniformly over the depth. These points will be discussed in Section 3.3.2.) A solution is obtained by applying a Galilean transformation to the lock exchange problem. Lock exchange flow is

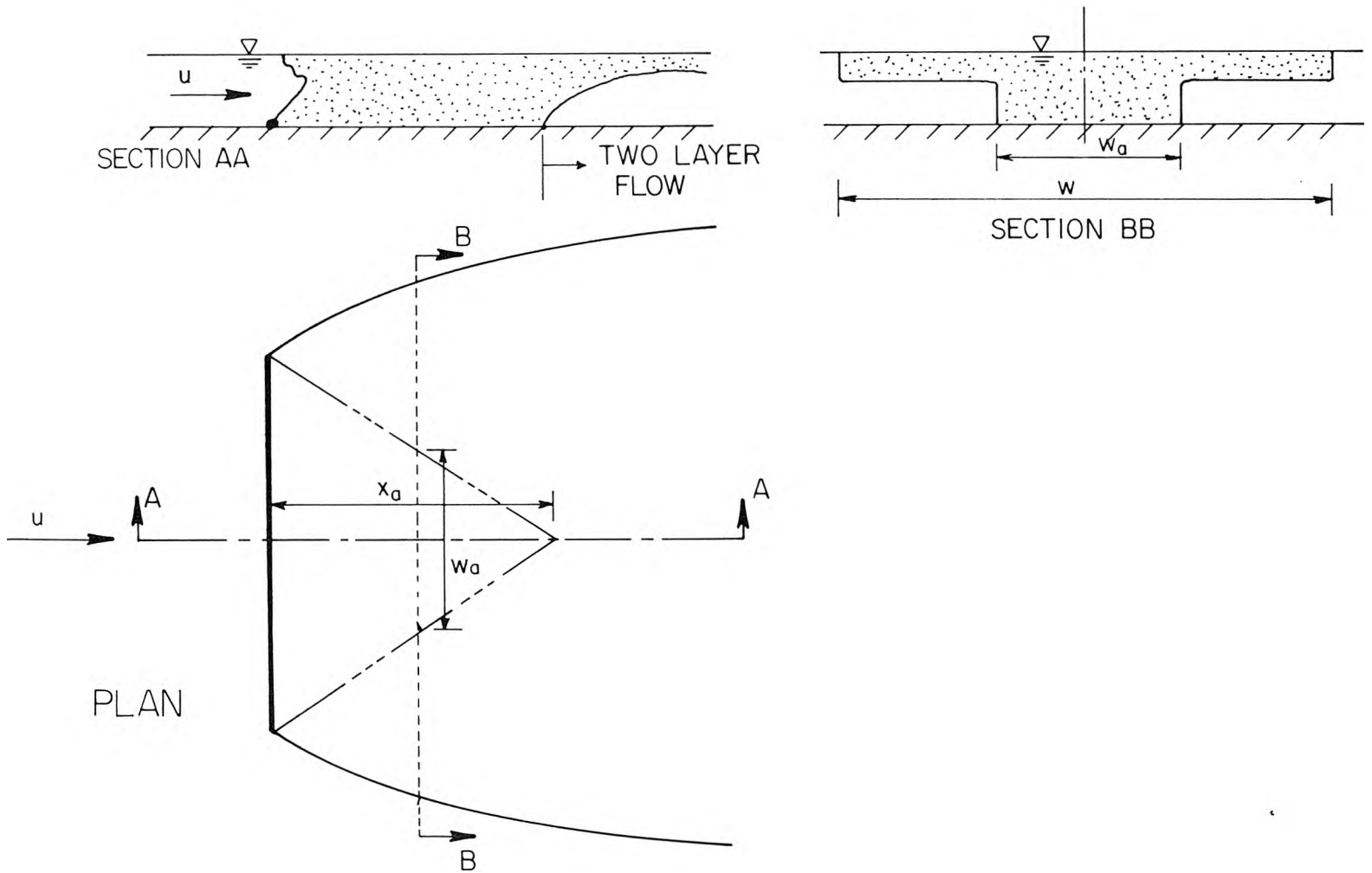

Figure 3.1. Postulated dispersion pattern for F > 1, current perpendicular to diffuser.

two-dimensional and develops after sudden removal of a barrier separating two fluids of slightly differing density and equal but finite depth. O'Brien and Cherno (1932), using a force balance, obtained an estimate for the velocity of advance of the upper and lower layers as:

$$u_3 = K_5 \sqrt{\frac{g\Delta\rho}{\rho_r} H} \quad , \tag{3.18}$$

and

$$u_2 = K_6 \sqrt{\frac{g\Delta\rho}{\rho_r} H} \quad . \tag{3.19}$$

$\Delta\rho$ is the difference in density of the two fluids, H is the water depth and u_3 and u_2 the upper and lower layer velocities. They estimated the value of K_5 and K_6 to be 0.5, and the thickness of the layers to be half the water depth. These results are consistent with the general formulation of Benjamin, Section 2.4. Turner (1973), however, states that in the presence of a free surface, the flow becomes unsymmetrical, with $K_5 = 0.47$ and $K_6 = 0.59$.

The analogy of the lock exchange flow to the present problem is shown in Figure 3.2. The thickness of the upper and lower layers are predicted to be half the water depth. The velocity, u_3, of the lower layer is assumed to be equal to the velocity of the underflow in the lock exchange flow. Consideration of the velocity vector triangle shown in Figure 3.2 then yields:

$$\frac{u_3}{u} = \sin\theta \quad , \tag{3.20}$$

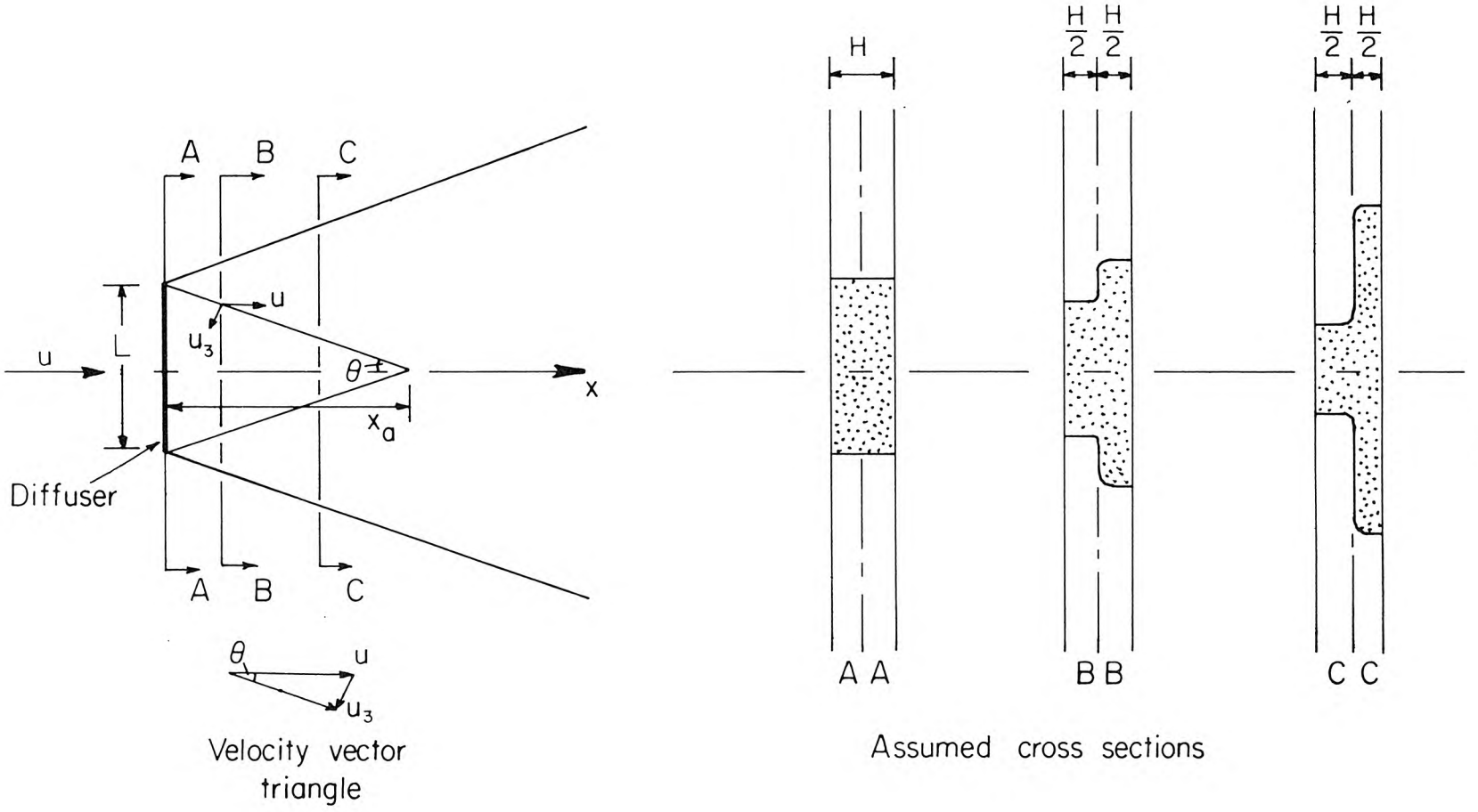

Figure 3.2 Lock exchange analogy for initial dispersion, current perpendicular to diffuser, $F \geq 1$.

and $$\frac{L}{2x_a} = \tan\theta = \frac{\sin\theta}{\sqrt{1 - \sin^2\theta}} \quad . \tag{3.21}$$

The equation for conservation of buoyancy flux is:

$$b = \frac{g\Delta\rho}{\rho_o} uH \quad , \tag{3.22}$$

where $\Delta\rho$ is the difference in density between the two layers. The solution to Eqs. 3.18, 3.20, and 3.21 is:

$$\frac{x_a}{L} = \frac{1}{2K_5} (F - K_5^2)^{1/2} \quad . \tag{3.23}$$

With $K_5 = 0.47$, Eq. 3.23 becomes:

$$\frac{x_a}{L} = 1.06(F - 0.22)^{1/2} \quad . \tag{3.24}$$

A similar analysis for the surface layer yields:

$$\frac{w}{L} = 1 + \frac{2x}{L} K_6 (F - K_6^2)^{-1/2} \quad . \tag{3.25}$$

With $K_6 = 0.59$, Eq. 3.25 becomes:

$$\frac{\Delta w}{x} = 1.18(F - 0.35)^{-1/2} \quad , \tag{3.26}$$

where $\Delta w = w - L$.

An alternate version of Eq. 3.26 is:

$$\frac{w}{L} = 1.18(F - 0.35)^{-1/2} \left(\frac{x + x_o}{L} \right) , \tag{3.27}$$

where x_o is an origin shift given by

$$x_o = \frac{L}{1.18} (F - 0.35)^{1/2} \quad . \tag{3.28}$$

The edges of the zone of lower boundary attachment and the surface plume are thus both predicted to be straight, as shown in Figure 3.2.

3.3.2 Mixing Process

The downstream evolution of the vertical effluent concentration profile on the plume centerline is described by Eq. 3.17, which becomes, with $\theta = 90°$ and $z/L = 0$:

$$\frac{CuH}{q} = f\left(F, \frac{L}{H}, \frac{x}{L}, \frac{y}{H}\right) \quad . \tag{3.29}$$

The form of this relationship varies with distance downstream due to the existence of different mixing regions, as shown in Figure 3.3. These regions, and the form of the concentration profile in each one, are discussed in this section.

Near the diffuser, buoyant elements of effluent rise, and are carried horizontally by the ambient current. It is assumed that this mixing process is two-dimensional. Hence, L is not a variable in Eq. 3.29, which becomes:

$$\frac{CuH}{q} = f\left(F, \frac{x}{H}, \frac{y}{H}\right) \quad . \tag{3.30}$$

The process is the same as gravitational diffusion from a boundary source in a semi-infinite fluid, analyzed by Rouse (1947), and

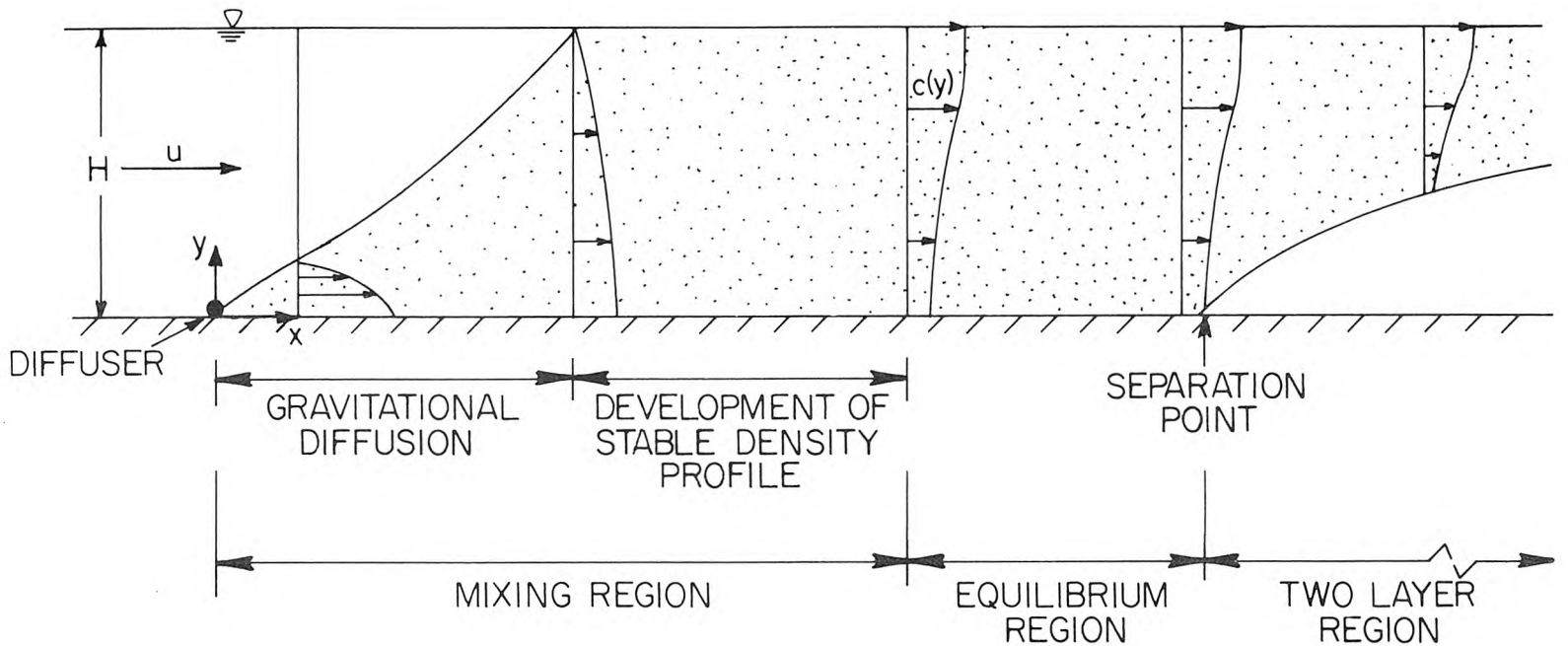

Figure 3.3 Schematic representation of time-averaged concentration profiles on centerline of diffuser in a current perpendicular to diffuser, $F \geq 1$.

discussed in Section 2.2. His solution, Eq. 2.3, can be written in the notation of Eq. 3.30 as:

$$\frac{CuH}{q} = \frac{2.6F^{1/2}}{x/H} \exp\left\{-5.4 \frac{(y/H)^2}{(x/H)^2} F\right\} . \tag{3.31}$$

Eventually, some of the buoyant fluid elements reach the free surface. A stable density profile then begins to develop, damping further buoyancy induced turbulent concentration fluctuations. At some point downstream these fluctuations will be completely suppressed, and no further mixing due to buoyancy occurs. Thus, the presence of the free surface results in confinement of the mixing region to a finite horizontal distance, as shown in Figure 3.3. Again, the assumption of two-dimensional mixing requires that Eq. 3.30 must describe the evolution of the stably developing concentration profile.

At the end of the mixing region a stable density, or concentration, profile has developed. This profile will not change shape downstream until further mixing due to molecular diffusion or ambient turbulence occurs. This profile is denoted as the equilibrium profile, and the region where it occurs as the equilibrium region. Thus, the shape of this profile is independent of downstream distance, and Eq. 3.30 becomes:

$$\frac{CuH}{q} = f\left(F, \frac{y}{H}\right) . \tag{3.32}$$

As discussed in the preceding section, the waste field must separate at some point downstream when the diffuser length is less

than the flow width. A two-layer region then forms, as shown in Figure 3.3. The concentration profile is then given by the original form of Eq. 3.29:

$$\frac{CuH}{q} = f\left(F, \frac{L}{H}, \frac{x}{L}, \frac{y}{H}\right) . \tag{3.33}$$

The stable density profile develops from the free surface downwards. The surface dilution may thus reach its limiting (minimum) value while mixing still proceeds beneath it. If this limiting dilution is reached before the flow separates, it would be expected to equal that measured in two-dimensional flow. The minimum centerline dilution for three-dimensional flows, S_c, is in this case independent of L/H, as for two-dimensional flows. Eq. 3.7, with $\theta = 90°$, then becomes:

$$\frac{S_c q}{uH} = f(F) . \tag{3.34}$$

This relationship should be valid for all F, with $L/H \gg 1$. In the forced entrainment regime, the only restriction is that the minimum surface dilution must occur in a shorter distance than required for the waste field to separate from the bottom.

To summarize, the concentration profile on the plume centerline for three-dimensional forced entrainment flow is described by several different relationships. First, near the source, Eq. 3.31 is applicable. When the presence of the free surface is felt, Eq. 3.30 applies. Farther downstream an equilibrium profile may develop whose shape is defined by Eq. 3.32. When three-dimensional effects, that is, flow separation,

occur, Eq. 3.33 is applicable. The functional forms of these equations were evaluated experimentally. The results are presented in Section 5.3.4.

By means of a dimensional analysis similar to that leading up to Eq. 3.17 a relationship for the intensity of the buoyancy-induced turbulent concentration fluctuations can be derived. By analogy with Eq. 3.17, this relationship can be written:

$$\frac{\sqrt{\overline{C'^2}}\, uH}{q} = f\left(F, \frac{L}{H}, \frac{x}{H}, \frac{z}{L}, \frac{y}{H}\right) . \tag{3.35}$$

Near the surface on the centerline, and assuming two-dimensional flow, Eq. 3.35 becomes:

$$\frac{\sqrt{\overline{C'^2}}\, uH}{q} = f\left(F, \frac{x}{H}\right) . \tag{3.36}$$

By dividing Eq. 3.36 by Eq. 3.30, with y/H = 1, we find:

$$\frac{\sqrt{\overline{C'^2}}}{C} = f\left(F, \frac{x}{H}\right) , \tag{3.37}$$

for the forced entrainment regime.

3.4 Initial Surface Spreading Rate When Current Flow is Parallel to Diffuser

Initial spreading of the surface field is predicted by applying a Galilean transformation to the solution of the unsteady two-dimensional buoyant surface spreading problem. This is similar to the approach of Koh and Brooks (1975) discussed in Section 2.4, except that the frontal

velocity vector is taken as being perpendicular to the front rather than perpendicular to the current direction as they assumed.

The velocity vector triangle is shown in Figure 3.4. The kinematic

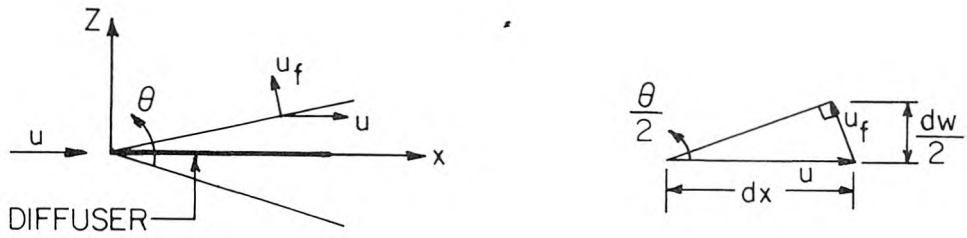

Figure 3.4 Definition diagram for formation of surface field in parallel current.

condition at the front is given by:

$$\frac{u_f}{u} = \sin\frac{\theta}{2} \quad . \tag{3.38}$$

It is assumed that u_f is the same as the initial two-dimensional surface spreading rate of buoyant effluent discharged from a submerged line source. As discussed in Section 2.3, this velocity is constant, and can be predicted by Eq. 2.10, with $K_1 = 0.68$. Substitution of Eq. 2.10 into Eq. 3.38 yields:

$$\sin\frac{\theta}{2} = \frac{0.68b^{1/3}}{u} \quad , \tag{3.39}$$

and substitution of the definition of F, Eq. 2.4, into Eq. 3.39 gives:

$$\sin\frac{\theta}{2} = 0.68F^{-1/3} \quad , \tag{3.40}$$

thus

$$\theta = 2\sin^{-1}(0.68F^{-1/3}) \quad . \tag{3.41}$$

The plume is therefore predicted to grow linearly. The total included angle, θ, is given by Eq. 3.41. θ is analogous to the Mach angle in supersonic flow, with the characteristic velocity $b^{1/3}$ analogous to the speed of sound. The width of the field, w_o, at the end of the diffuser is:

$$w_o = 1.36LF^{-1/3}\left[1 - \left(0.68F^{-1/3}\right)^2\right]^{-1/2}, \qquad (3.42)$$

and the width of the field at any distance downstream, x, is:

$$\frac{w}{L} = 1.36\,\frac{x}{L}\,F^{-1/3}\left[1 - \left(0.68F^{-1/3}\right)^2\right]^{-1/2}, \text{ for } F \geq 1\,, \qquad (3.43)$$

in the initial stages.

3.5 Buoyant Surface Spreading Rate in Two-Layer Flow

As discussed in Section 3.3.1 the wastewater field must always form a surface layer at some point downstream if the diffuser length is less than the width of the oncoming flow. The spreading rate of this surface flow is considered in this section.

First, we consider a regime in which the total buoyancy, bL, is the only important source parameter. It is assumed that initial dilution, variations in water depth, and interfacial shear are unimportant. This is the problem analyzed by Larsen and Sorensen, discussed in Section 2.4. The current velocity, u, can be eliminated as an independent parameter by use of the Galilean transformation u = x/t, and assuming the buoyant spreading velocity to be a function only of bL and x, thus:

$$u \frac{dw}{dx} = f(x,bL) \quad . \tag{3.44}$$

Dimensional analysis of Eq. 3.44 yields:

$$\left(\frac{x}{bL}\right)^{1/3} u \frac{dw}{dx} = K_{10} \ , \tag{3.45}$$

where K_{10} is an experimental constant. The solution to Eq. 3.45 can be written:

$$\Delta w = \frac{3K_{10}}{2} \frac{(bL)^{1/3}}{u} (x^{2/3} - x_o^{2/3}) \quad , \tag{3.46}$$

where $\Delta w = w - L$,

and x_o is a constant origin shift. At large distances from the source x/x_o becomes large, and Eq. 3.46 can be written:

$$\frac{\Delta w}{L} = \frac{3K_{10}}{2} F^{-1/3} \left(\frac{x}{L}\right)^{2/3} \quad . \tag{3.47}$$

Eqs. 3.46 and 3.47 might be expected to apply beyond the region where the diffuser length is important, i.e., $x/L \gg 1$, and/or beyond the zone of lower boundary attachment in forced entrainment flow, i.e., $x/L \gg F^{1/2}$ (c.f. Eq. 3.24). The spreading rate in this regime is governed by a balance of the pressure force caused by the density difference between the upper and lower layers and inertia force.

Interfacial shear is assumed to be the only force resisting buoyant spreading of the surface waste field much farther from the source. This is the assumption made by Koh and Fan (1970) for two-dimensional flow (see Section 2.3). The results of their analysis predicts the width of the surface layer to grow as $t^{4/5}$ where t is time. This was verified

by the results of the present study, presented in Appendix A. The following analysis is an adaptation of their approach, and is intended only to deduce approximate solutions.

We consider first the unsteady two-dimensional problem for an instantaneous source. This is the same as the problem shown in Figure 2.6 with zero inflow, that is q = 0. The force driving the surface spreading is a pressure difference induced by the density difference between the surface layer and ambient water. For a uniformly mixed layer, this force is:

$$\frac{1}{2} g(\rho_r - \rho)h^2 \quad ,$$

where ρ and ρ_r are the densities of the upper and lower layers and h the surface layer thickness. The resistive force of shear is $\frac{\tau w}{2}$, where τ is the average shear on the interface across the half-width, and w is total layer width. It is assumed that

$$\tau = \frac{\alpha\varepsilon}{2h} \frac{dw}{dt} \quad , \tag{3.48}$$

where α is a constant, and ε a constant effective viscosity coefficient. Equating the driving and resistive forces, we obtain:

$$\frac{1}{2} g(\rho_r - \rho)h^2 = \frac{\alpha\varepsilon w}{4h} \frac{dw}{dt} \quad . \tag{3.49}$$

In three-dimensional steady-state flow, the total buoyancy flux crossing any plane normal to the current direction is equal to the source buoyancy flux, i.e.:

$$\frac{uhw(\rho_r - \rho)g}{\rho_o} = bL \quad , \tag{3.50}$$

and the average initial dilution, S_a, is given by:

$$S_a = \frac{\rho_r - \rho_o}{\rho_r - \rho} \quad . \tag{3.51}$$

By combining Eqs. 3.49, 3.50, and 3.51, we find:

$$w^4 \frac{dw}{dt} = \frac{2g_o' Q^3 S_a^2 \rho_o}{\alpha \varepsilon u^3} \quad , \tag{3.52}$$

where $$g_o' = \frac{\rho_r - \rho_o}{\rho_o} g \quad ,$$

and Q is the total effluent volume flux. The solution to Eq. 3.52 is

$$w^5 - w_o^5 = 10 \frac{g_o' Q^3 S_a^2 \rho_o}{\alpha \varepsilon u^3} t \quad , \tag{3.53}$$

where w_o is the field width at t = 0. To apply this result to the three-dimensional steady problem, we use the Galilean transformation, t = x/u. Eq. 3.53 then becomes:

$$w^5 - w_o^5 = 10 \frac{g_o' Q^3 S_a^2 \rho_o x}{\alpha \varepsilon u^4} \quad . \tag{3.54}$$

For large distances downstream, $w \gg w_o$, and Eq. 3.49 becomes:

$$w \approx \left(10 \frac{g_o' Q^3 S_a^{\,2} \rho_o x}{\alpha \varepsilon u^4} \right)^{1/5} . \tag{3.55}$$

Also,

$$\Delta w \approx \left(\frac{10 g_o' Q^3 S_a^{\,2} \rho_o x}{\alpha \varepsilon u^4} \right)^{1/5} , \tag{3.56}$$

where $\Delta w = w - L$.

For current flow perpendicular to the diffuser in the forced entrainment regime ($F \geq 1$, Figure 2.3c), the <u>average</u> dilution S_a is given by:

$$S_a = \frac{uH}{q} , \tag{3.57}$$

also

$$q = \frac{Q}{L} , \tag{3.58}$$

by definition. Substituting Eqs. 3.52 and 3.53 into Eq. 3.51 yields:

$$w = \left(10 \frac{g_o' q L^3 H^2 \rho_o x}{\alpha \varepsilon u^2} \right)^{1/5} . \tag{3.59}$$

On substituting the definitions of buoyancy flux, b from Eq. 2.1 and F from Eq. 2.4, Eq. 3.54 becomes:

$$\frac{w}{L} = 10^{1/5} \, F^{-1/5} \left(\frac{uH^2 \rho_o}{\alpha \varepsilon L} \right)^{1/5} \left(\frac{x}{L} \right)^{1/5} . \tag{3.60}$$

Eq. 3.55 can be written as:

$$\frac{w}{L} = \left[\left(\frac{10}{4\alpha}\right)\left(\frac{1}{F}\right)\left(\frac{4uH}{\nu}\right)\left(\frac{\nu\rho_o}{\varepsilon}\right)\left(\frac{H}{L}\right)\left(\frac{x}{L}\right)\right]^{1/5} . \tag{3.61}$$

On substitution of the definitions of Reynolds number,

$$Re = \frac{4uH}{\nu} ,$$

and dynamic viscosity,

$$\mu = \nu\rho_o ,$$

Eq. 3.56 becomes:

$$\frac{w}{L} = \left[\left(\frac{10}{4\alpha}\right)\left(\frac{Re}{F}\right)\left(\frac{L}{H}\right)^{-1}\left(\frac{\mu}{\varepsilon}\right)\left(\frac{x}{L}\right)\right]^{1/5} . \tag{3.62}$$

The effective viscosity coefficient in Eq. 3.48 may not be constant. In turbulent flows, for example, ε may be proportional to $h\frac{dw}{dt}$ or some other function. Different assumptions of the nature of ε lead to differing exponents in Eq. 3.55.

The buoyant surface spreading rate downstream is described by several different growth laws. This is due to changes with distance downstream both of geometrical effects and dominant forces. Three regimes and growth laws are identified in this chapter; they are shown in Figure 3.5 for $F \geq 1$. Spreading in the first two regimes is governed by a balance of the driving pressure force and the retarding inertia force. Near to the source the diffuser geometry is important, resulting

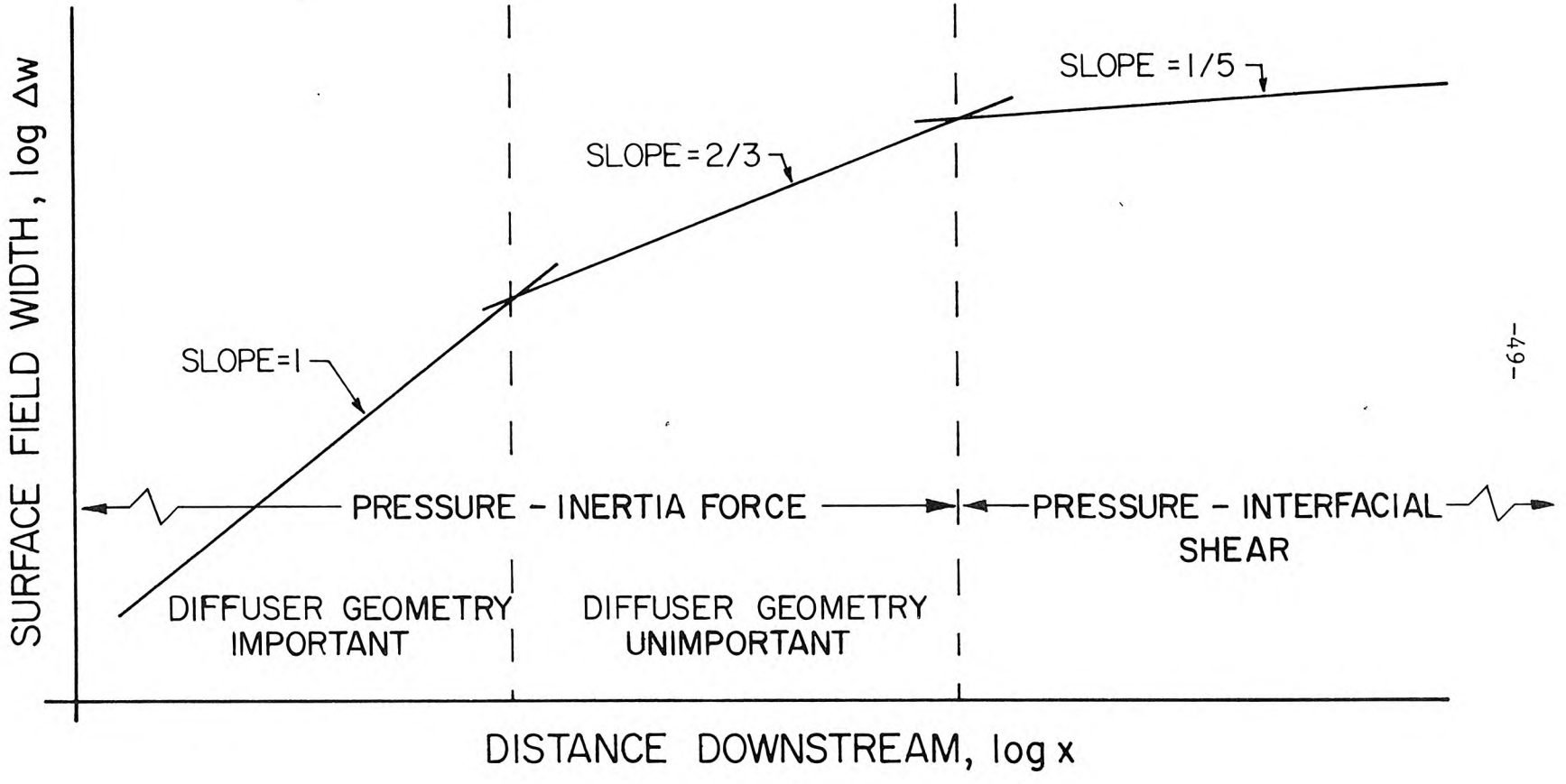

Figure 3.5 Speculated regimes for buoyant spreading of surface waste field, $F \geq 1$. $\Delta w = w - L$, w is field width, L is diffuser length, and x is distance downstream.

in a linear growth rate which is predicted by Eqs. 3.43 or 3.26 for current directions parallel or perpendicular to the diffuser, respectively. Further from the source, i.e., $x/L \gg 1$, the diffuser geometry is unimportant and the 2/3 power law, Eq. 3.47, may apply. Finally, at great distances from the source the driving pressure force is balanced by interfacial shear and the surface layer is predicted by Eq. 3.56 to grow as the 1/5 power of distance downstream. The transition distances between the different regimes are, in general, functions of F, L/H, μ/ε, and Reynolds number. Because of the complexity of the problem due to the many variables involved, no attempt will be made to predict these distances. It is possible that the first two regimes may not exist in certain cases, as interfacial shear may be important near the source. This is probably so for $F < 1$, in which case an upstream wedge forms (Figure 2.3) whose length and width are dependent on interfacial shear.

The aim of the analysis of the chapter has been to show that many surface spreading regimes can exist, causing different rates of growth of the surface waste field downstream, but not to investigate these regimes in detail.

CHAPTER 4

LABORATORY EXPERIMENTS

4.1 Objectives

The experimental objectives were to investigate the flow field created by a line plume of finite length in a steady current. Dimensionless parameters of the flow were derived in Section 3.2. The most important of these are a Froude number, $F = u^3/b$; the ratio of diffuser length to water depth, L/H; and the angle, θ, of the current relative to the line source (see Figure 2.1).

The results are to be used for prediction of dispersion of buoyant waste water discharged from ocean outfalls in their immediate vicinity. Hence, the parameters were varied over a range typical of this situation. Consideration of outfalls suggested this range to be: Froude numbers from 0.01 to 100; L/H from 3.75 to 30; and θ from 0° to 90°. Nominal experimental values were Froude numbers of 0.01, 0.1, 1, 10, and 100; and L/H of 3.75, 7.5, 15, and 30. Most experiments were conducted at the limiting current directions of θ = 0° (parallel) and 90° (perpendicular). A few experiments were done at θ = 45°.

4.2 Description of Apparatus

4.2.1 Basin

The experiments were performed in a rectangular recirculating basin, Figure 4.1, located in the W. M. Keck Laboratories at Caltech. The basin is 20 feet (6.1 m) wide by 36 feet (11.0 m) long,

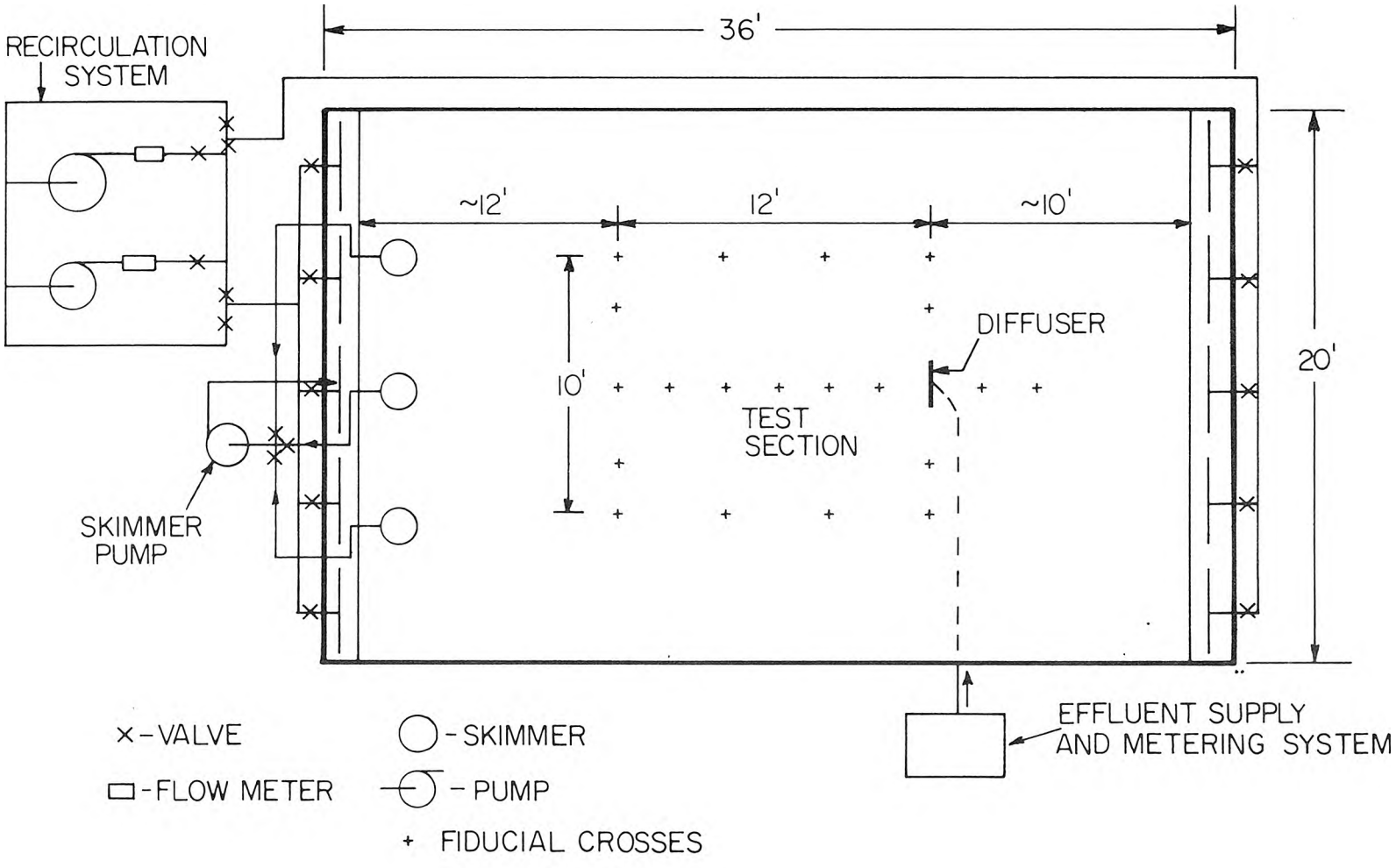

Figure 4.1 Schematic drawing of basin and diffuser.

and is described in Koh, et al. (1974). The basin walls consist of concrete blocks mortared onto the concrete laboratory floor. A shaped plastic sheet prevents any leakage. Approximately twenty tons of sand (median diameter = 0.8 mm) sits on the plastic sheet. The sand surface was leveled to about ±1 mm of the mean with a horizontal grader. A recirculation system consisting of two pumps used singly allows the simulation of a wide range of current speeds. Flow rates can be measured with a venturi meter for discharges above 0.1 ft^3/s (2.8×10^{-3} m^3/s), and by a rotameter for those below. The maximum discharge rate was about 0.8 ft^3/s (2.3×10^{-2} m^3/s). The intake and discharge of the recirculation system consists of five manifolds at each end of the basin. Each manifold has a throttling valve for flow distribution control. Immediately in front of the manifolds is a cradle containing rubberized hair to ensure even flow distribution. Photographs of various subcomponents are shown in Figures 4.2 through 4.5.

Dust fallout on the basin resulted in the accumulation of a surface layer. This layer caused the water near the surface to stagnate and affected the buoyant spreading of the waste field. The problem was solved by means of three swimming pool skimmers attached to a common pump. The skimmers were situated across the downstream end of the basin. The action of withdrawal through the skimmers caused them to float just below the water surface so that only the surface layer was pumped. This water was circulated back to the downstream end of the basin so that the net basin flow rate was unaffected. The skimmers did an

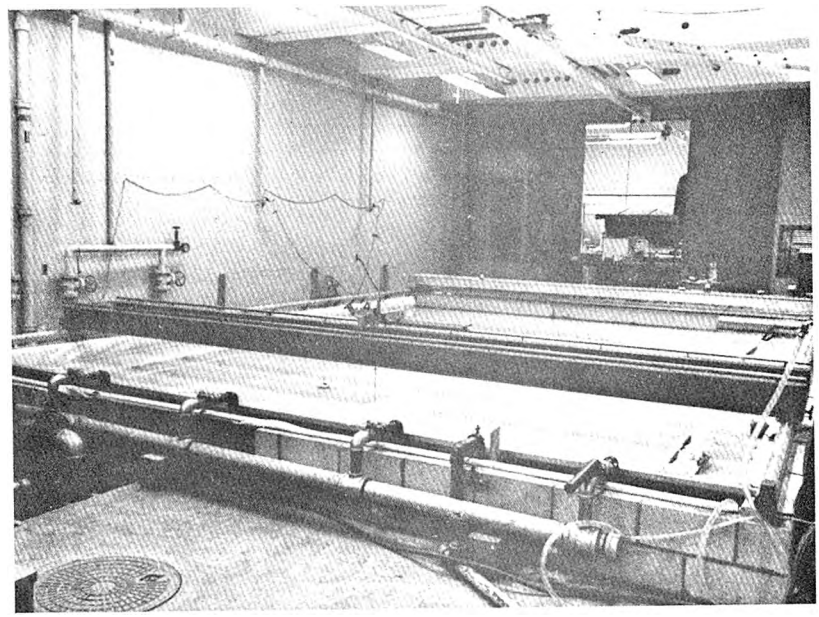

Figure 4.2. Overall view of test basin.

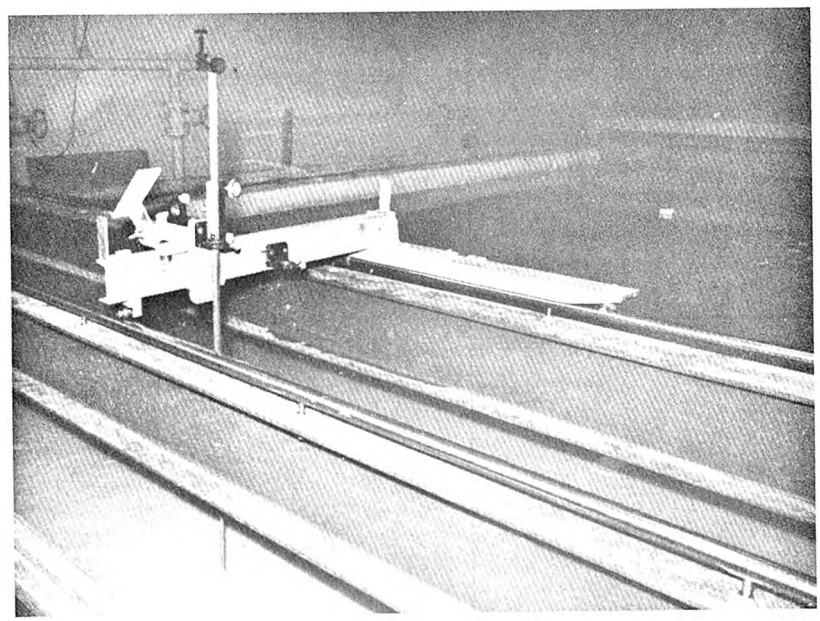

Figure 4.3. Test carriage and depth probe.

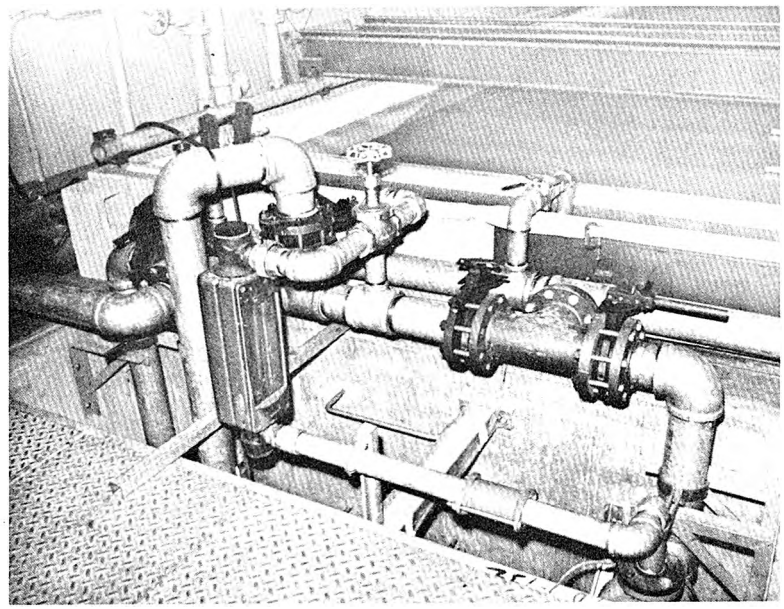

Figure 4.4. Piping and valves for controlling flow direction and rate. Pumps and venturi meter are out of sight in the pump well.

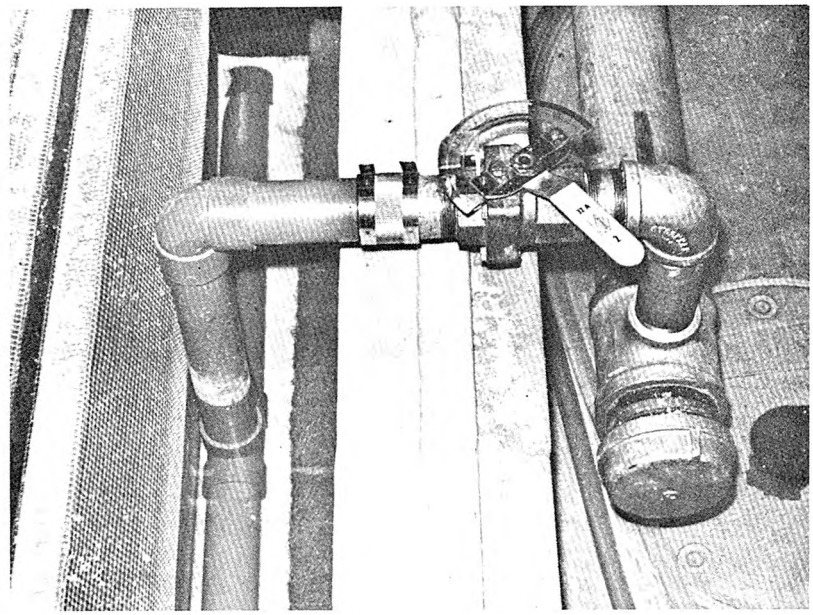

Figure 4.5. Manifold control valve and rubberized hair screen (extreme left).

excellent job in cleaning the water surface, and were usually left running during the course of the experiments.

An instrument carriage spans the width of the basin. This carriage, visible in Figures 4.2 and 4.3, moves on rails mounted on the basin walls. The carriage has rails along its length on which smaller carriages run traversely. One of these carriages is shown in Figure 4.3. Three were used to support the conductivity probes.

4.2.2 Diffuser, Effluent, and Injection System

The diffuser must produce a good approximation to a line plume. This means that the relative source volume and momentum fluxes be small, but that the flow be fully turbulent. A simple slot was first considered. If the volume flux is q per unit length, the slot Reynolds number is q/ν, where ν is the kinematic viscosity. For turbulent flow q/ν should be greater than about 1000, or $q \gtrsim 10$ cm^2/s. For surface dilutions to be unaffected by the initial volume and momentum fluxes, the ratios $q/b^{1/3}H$ and $m/b^{2/3}H$ must both be much less than one, where m and b are the momentum and buoyancy fluxes per unit length, and H is the water depth. For water depths of 8 cm and less, initial density differences, $\Delta\rho/\rho_o$, greater than 0.2 are required to satisfy the volume flux and Reynolds number constraints. Density differences this large cannot be used for the present experiments as the Boussinesq assumption made in the analysis of Section 3.2 would be violated. Smaller density differences must therefore be used and the requirements that $q/\nu > 10^3$ and $q/b^{1/3}H \ll 1$ cannot be simultaneously satisfied. Hence, a simple vertical slot cannot be used for these experiments.

The problem was solved by discharging an approximately 2% buoyant methanol solution through the diffuser shown in Figure 4.6. The diffuser consists of a box about 2 feet (61 cm) long which sits flush with the basin floor. Inside the box is an effluent injector which is fed by three hoses to ensure uniform flow along the pipe. The uniformity is further aided by means of an internal baffle. The effluent escapes from the injector as a jet through a 0.022 ± 0.001 inch (0.56 ± 0.0025 mm) slot which is 2 feet (61 cm) long. The jet is laminar (Reynolds number, $q/\nu \approx 20$), it strikes one of the vertical box walls and ascends due to its buoyancy. This flow is unstable and becomes turbulent near to the top edge of the wall. Beyond this point, the flow becomes a free turbulent plume.

The momentum and volume fluxes of the plume at separation must be calculated and so are not known exactly. Also, the turbulence is probably not fully developed. For these reasons, a separate series of two-dimensional experiments was performed. These experiments are discussed in Appendix A. The results, when compared with those of larger scale plume studies, confirmed the flow to be a close approximation to a pure plume. The difference in dilution compared to that of a fully turbulent pure plume is less than 20%. The results also verified that the primary source parameter governing the effluent surface spreading rate is the buoyancy flux per unit length.

The effective diffuser length is 2 feet (61 cm). For some experiments the injector was taped at the ends to form a 30.5 cm length. Also, a few experiments were done with a false wall at one end of the diffuser. The diffuser was perpendicular to the current, making an effective

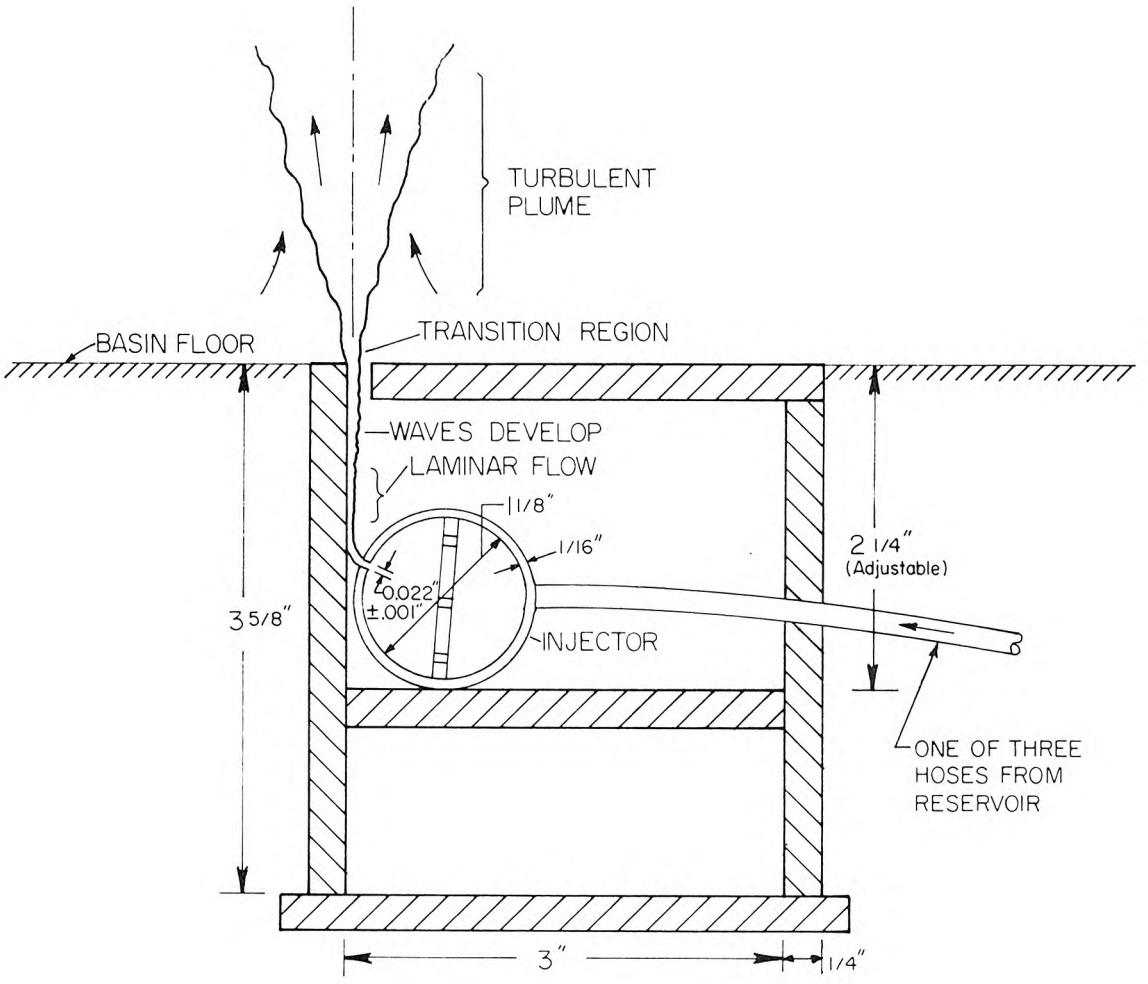

Figure 4.6 Vertical cross section through diffuser.

diffuser length of 122 cm.

The effluent was a mixture of water, methanol, sodium chloride and a small amount of blue dye for flow visualization. The sodium chloride was a tracer; dilutions of the order of several hundred to one could be easily measured with conductivity probes. Typical ratios of effluent constituents were 11 liters of water to 4 liters methanol to 150 g of salt. The water was cooled so that the temperature rise due to chemical reactions between the methanol and water resulted in a mixture temperature of about 20°C. The typical specific gravity of this mixture was 0.975. Densities of the effluent, ρ_o, and basin water, ρ_r, were measured to four decimal places with a Troemner Model S-100 specific gravity balance. The absolute accuracy of these measurements was better than 1/10%. However, the error in computing the density difference, $\Delta\rho/\rho_o$, was typically about ± 2%. Surface tension effects caused by the methanol were removed by the addition of detergent to the basin water; the procedure is described in Section 4.4.

Effluent was supplied to the diffuser via a constant head tank and metering system. A schematic diagram of the arrangement is shown in Figure 4.7. The effluent was contained in a large reservoir and was kept well-mixed by a motor-driven paddle. The flow rate was measured by a Fischer and Porter precision flowmeter No. FP-1/4-37-G-6 $\frac{3}{4}$ /61, Laboratory Number Q-53. The flowmeter was calibrated with effluent up to its maximum flow rate of 21 cm^3/s. The accuracy of the flow measurements was about ± 1%. The effluent, after passing through the flowmeter, entered a cylindrical chamber with three outflows which led directly to the diffuser.

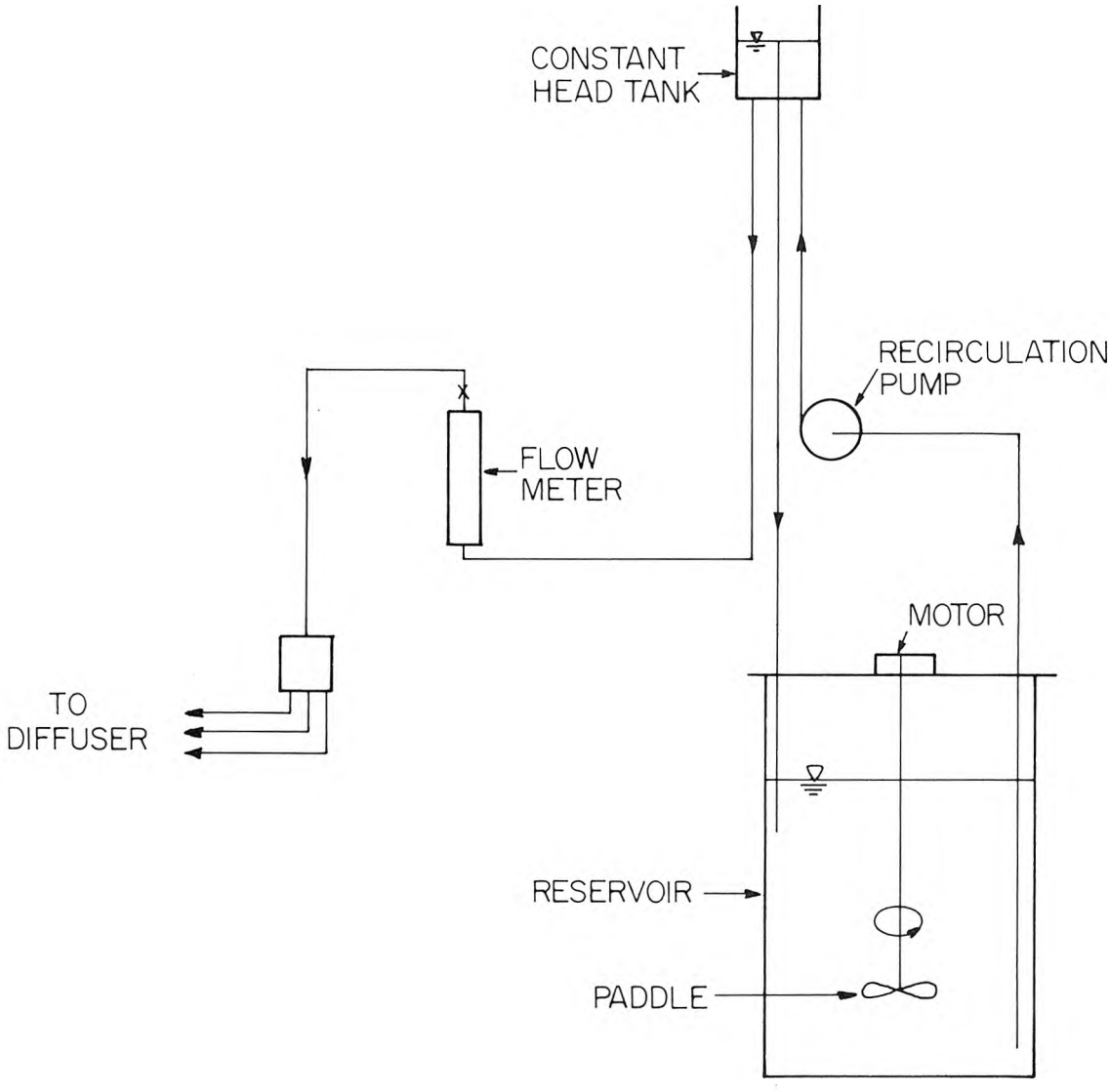

Figure 4.7 Schematic drawing of effluent supply and metering system.

4.2.3 Photographic Equipment

Overhead photographs of the flow were taken with a Nikon F camera equipped with a 17 mm lens. The wide angle of the lens enabled a large fraction of the basin to be covered. The camera was equipped with a motor drive and could be triggered remotely. Lighting was obtained by means of several synchronized electronic flashes located on each side of the basin. The original photographs were taken on color slide film. Photographs contained in this report were made from black and white negatives copied from the slides.

4.2.4 Dilution Measurement System

a. Overall system

Dilutions were computed from measured changes in electrical conductivity resulting from variations in sodium chloride concentration due to the mixing of effluent and ambient water.

Four conductivity probes were used simultaneously. The probes were mounted on three carriages which in turn were mounted on the main carriage traversing the basin. The carriages, similar to that shown in Figure 4.3, were mounted on rails so that traverses perpendicular to the ambient current could be obtained. Two of the probes were fixed together with a horizontal separation of 3 cm. The vertical spacing could be varied, but was fixed for any individual experiment. The purpose of this was to obtain simultaneous samples at two different heights. All of the probes could be moved vertically by means of remotely controlled Selsyn motors. Thus, each probe could

be moved in all three coordinate directions. A sketch of the probe arrangement is shown in Figure 4.8. In general, the two solitary probes were not moved vertically, but were kept just submerged to obtain horizontal traverses near the surface. The other two probes were usually kept on the plume centerline and moved to obtain vertical traverses.

Each conductivity probe forms part of a Wheatstone bridge circuit. The other elements of the bridge are housed inside a grounded bridge box. Excitation of the bridge circuit was provided by a preamplifier-recorder system, which also amplified and recorded the output continuously on a strip chart, and simultaneously relayed it to an analog-to-digital (A/D) converter. The digitized information was recorded on magnetic tape by a synchronous tape recorder. A schematic representation of the system is shown in Figure 4.9. The components of this system are described below.

b. Conductivity probes

The conductivity probes used were the same as those used by Fischer (1966), and Okoye (1970). A drawing of one of the probes is shown in Figure 4.10. Much of the remainder of this section is excerpted from these reports.

The probes, nominally 15 inches long, consist of three platinum plate electrodes firmly set into a 7052 kovar sealing which blends into Corning 3320 canary glass. This seals the lower end of a streamlined 7740 Pyrex glass casing which tapers off at the top where it is glued

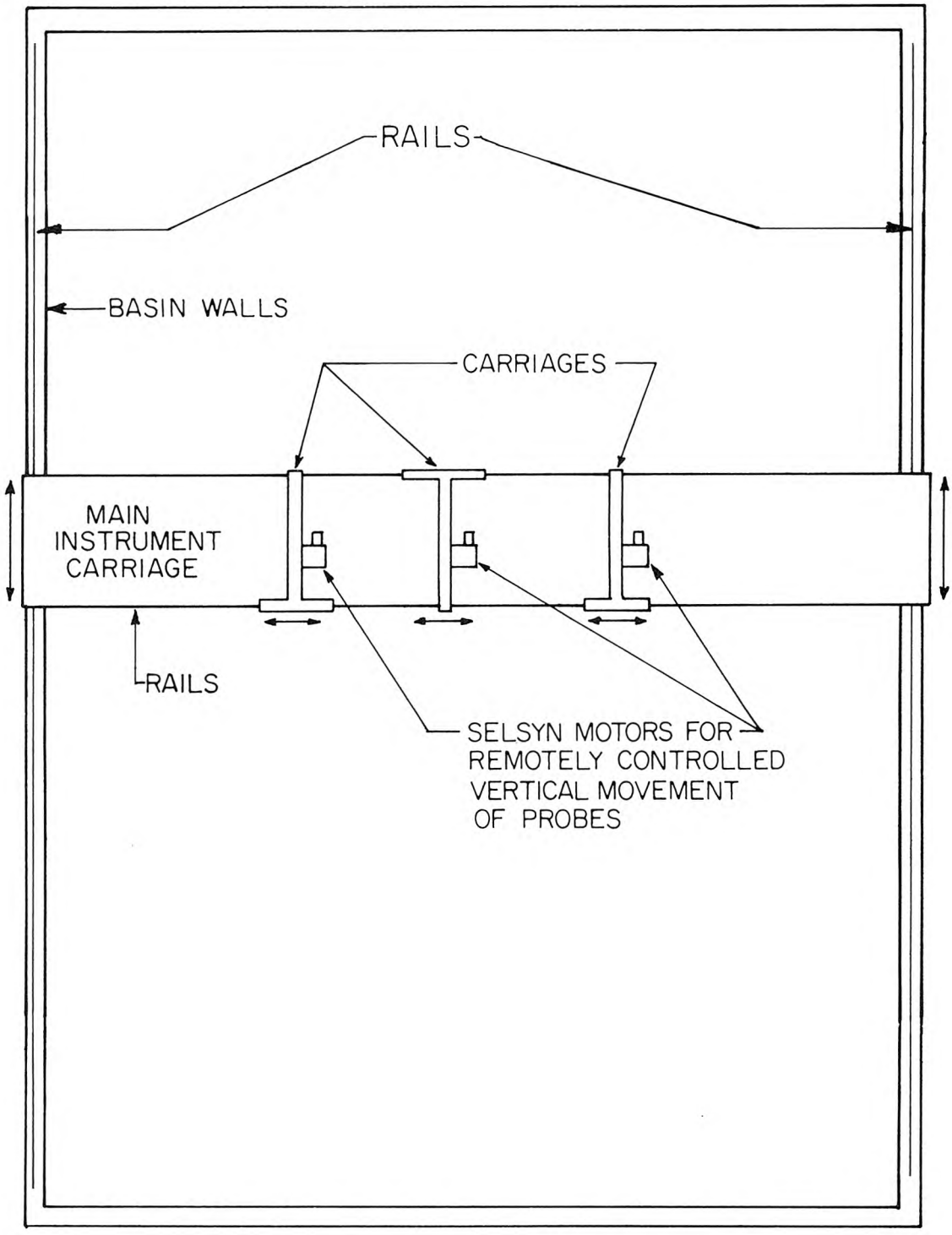

Figure 4.8 Schematic drawing of conductivity probe mountings.

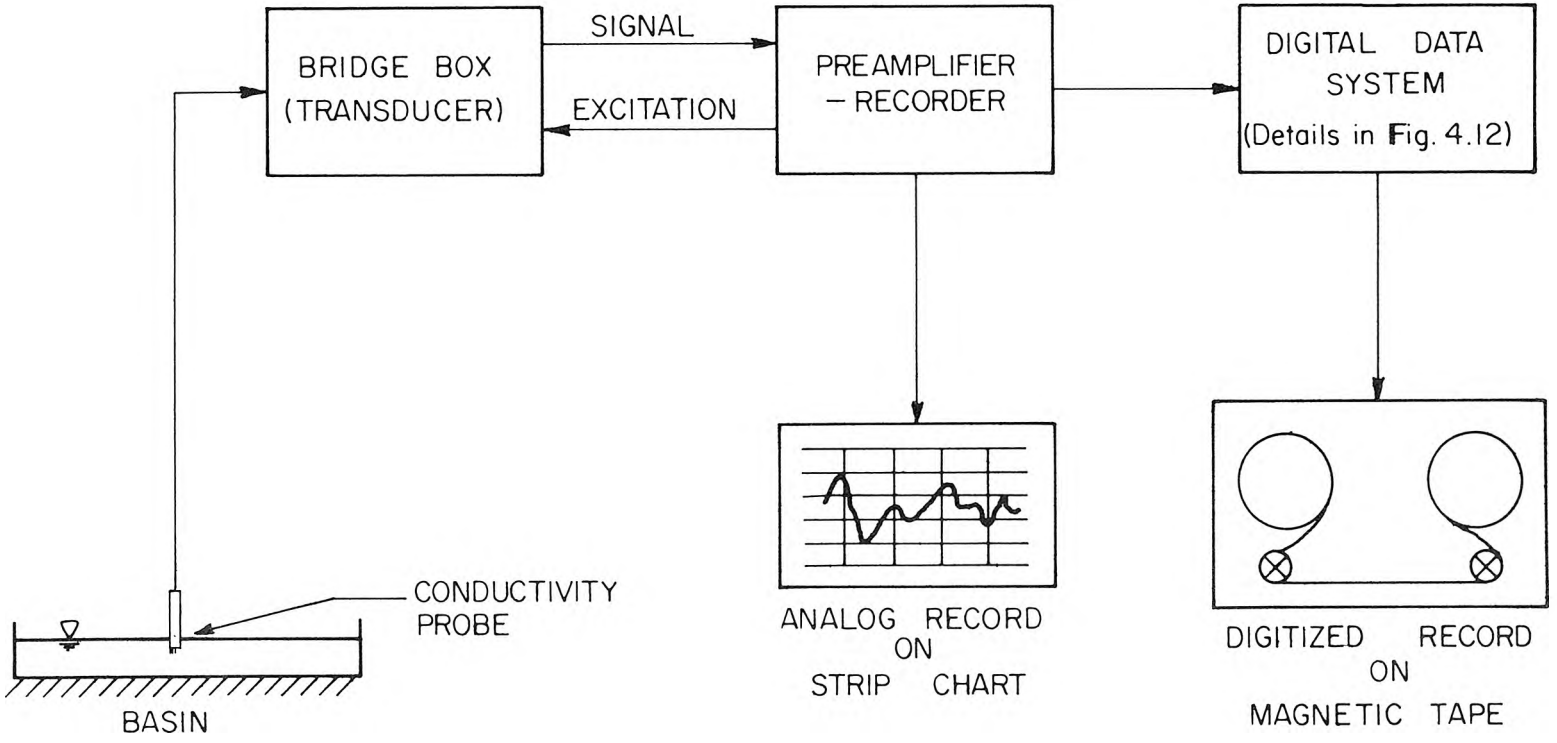

Figure 4.9 Schematic drawing of dilution measuring system (after Okoye (1970)).

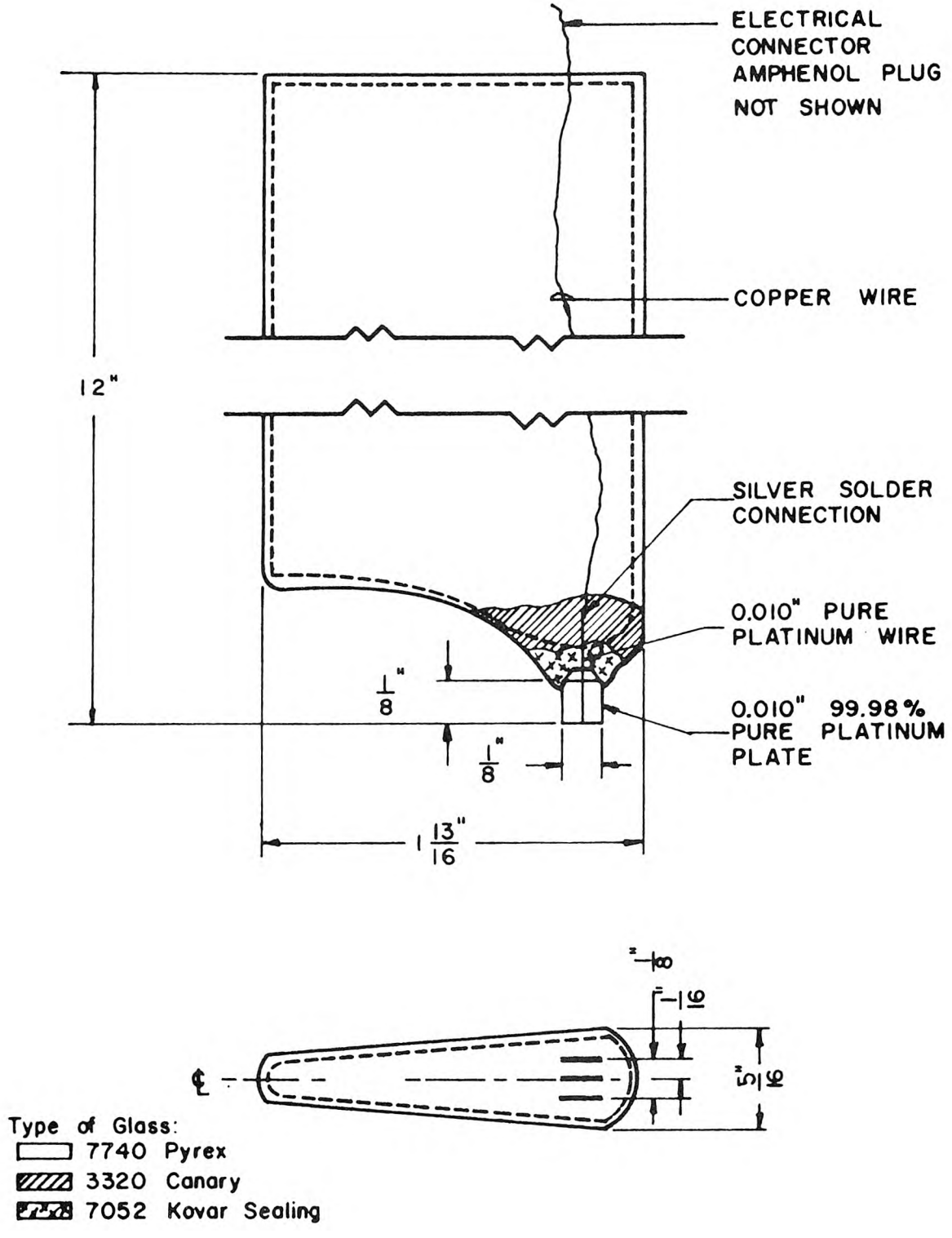

Figure 4.10 Design of the conductivity probes (after Fischer (1966)).

to an amphenol connector with Reziweld epoxy. The casing is 1/32-inch thick.

Each electrode, 1/8 inch by 1/8 inch and 0.005 inch thick, is spot-welded to a two-inch long pure platinum wire. The copper wires leading to the amphenol connector are each silver soldered to the platinum wires. The central wire is insulated from the outer two, and the three wires enclosed in a continuous metallic shield. The center lead is soldered to the center pin of the amphenol connector and the outer leads to the connector base.

The three electrodes are aligned such that the outer ones are 1/8 inch apart with the center plate exactly midway between them. Thus the generated electric field is confined to a small region within the outer plates, in contrast to the large field which a conventional two-plate system induces. The three-plate arrangement therefore offers greater sensitivity and better response to concentration variations at a point than a dual electrode configuration. The response times of the probes were measured by Okoye (1970) and found to be about 15 milli-seconds.

The probe electrodes were regularly cleaned with a chromic-sulfuric acid solution and platinized according to a standard procedure (American Public Health Association (1971)). During storage, the electrodes were immersed in distilled water.

c. Bridge circuit

The probes were connected to the bridge circuits by two-conductor shielded cables (Belden 8402 or 8422) leading from the amphenol connectors to two-prong connectors which were plugged into but insulated from the metallic bridge boxes. As shown in the block diagram of Figure 4.9, the recorder supplied the excitation voltage for the bridge and received the input signal of the probe via the bridge circuit.

Details of the elements of the full-bridge circuit and the external connections to the recorder are shown in Figure 4.11. The probe was connected across a 25-ohm resistor which could be replaced by a variable potentiometer in order to vary the probe sensitivity if desired. Increasing the potentiometer resistance at this point would decrease probe sensitivity, and vice versa. The 1K-ohm variable resistor on the opposite arm of the bridge aided in the initial balancing of the bridge circuit. The bridge was connected to the recorder via the signal and excitation circuits, each of which was a two-conductor shielded cable.

d. Analog recording system

A four channel Sanborn recording system series 150 was used. This system supplies an excitation voltage of 4.5 volts at 2400 hertz to the bridge box. An analog record of the signal returned from the conductivity probes is made onto a strip chart. Thus, a hard copy of the conductivity data was obtained. From the Sanborn recorder, the signal was fed into an analog-to-digital converter.

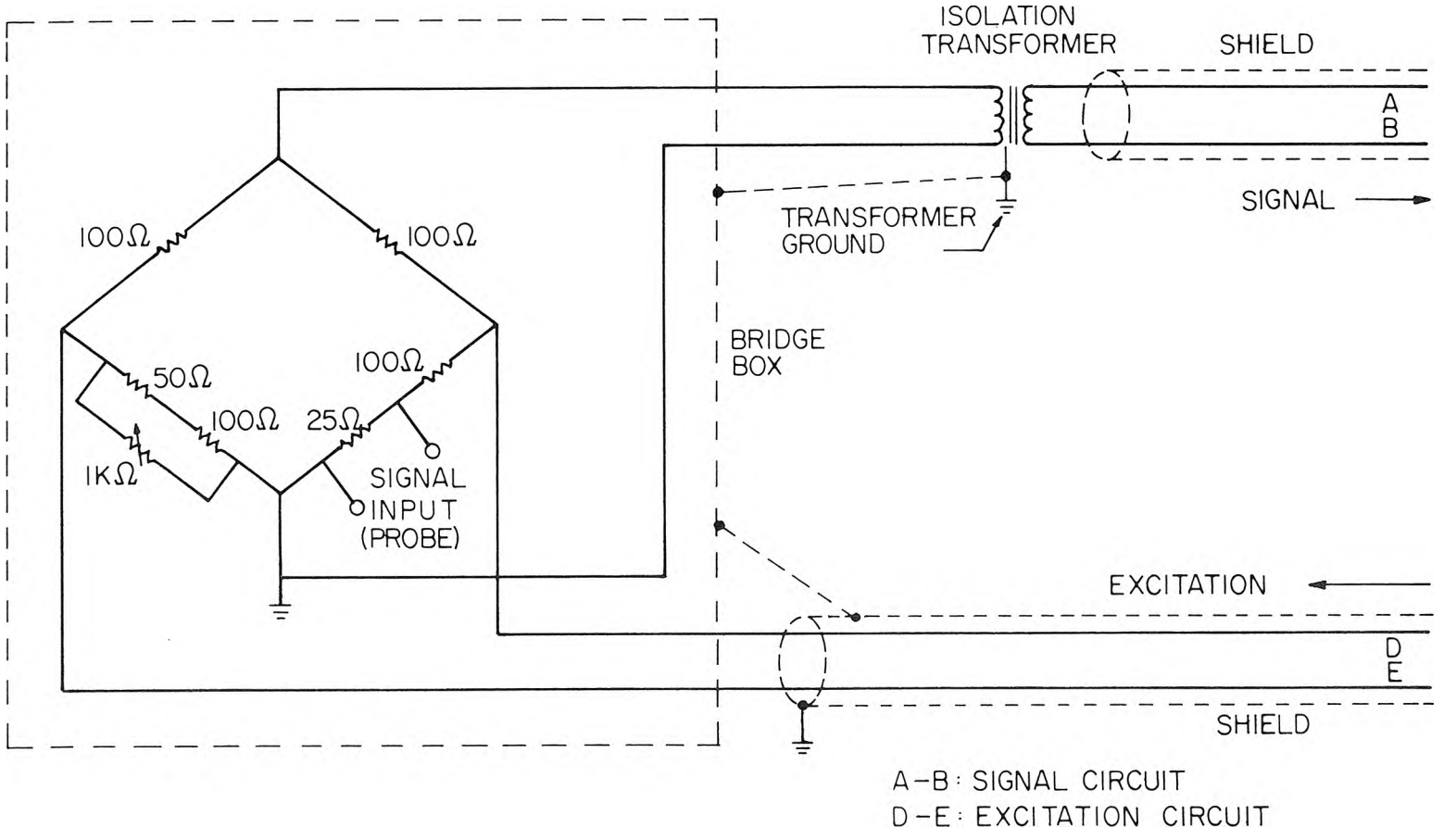

Figure 4.11 Details of bridge circuit and external connections to Sanborn analog recorder (after Okoye (1970)).

e. Analog to digital (A/D) data acquisition system

A flow diagram of the A/D system is shown in Figure 4.12. The A/D system (series 1103) manufactured by Digital Data Systems, Northridge, California, accepted eight channels of analog voltages which ranged to a maximum of ± 10 volts. The channels were sampled by an analog multiplexer which scanned the eight channels in about 4.4 milliseconds. The sample-and-hold amplifier, receiving the sampled voltage, had an aperture of 0.17 microseconds. This represents the period over which the input voltage was digitized. Both the scanning rate and the aperture were constants for the system. However, the sampling rate, which denotes the rate at which the analog voltage was digitized, was selected by the operator by use of the BASE FREQ and DIVIDE BY controls. The maximum sampling rate was 1600 samples per second (s/sec) for one channel. Thus if eight channels were being used, the maximum rate was 200 s/sec per channel.

Sampled voltage was fed to the A/D converter where it was converted to a binary signal and then to binary-coded-decimal (BCD). Meanwhile the header data received by the control logic were coded appropriately. The header data consisted of (i) identification information from the analog multiplexer, (ii) digital clock data, (iii) a four-digit number termed the header constant, and (iv) manual identification inputs. The BCD of the converter and the header data from the control logic were received by a digital multiplexer and transferred to one of two memory units for storage. Each unit has a capacity of 1024 tape characters.

Since the system utilized a synchronous tape transport, as

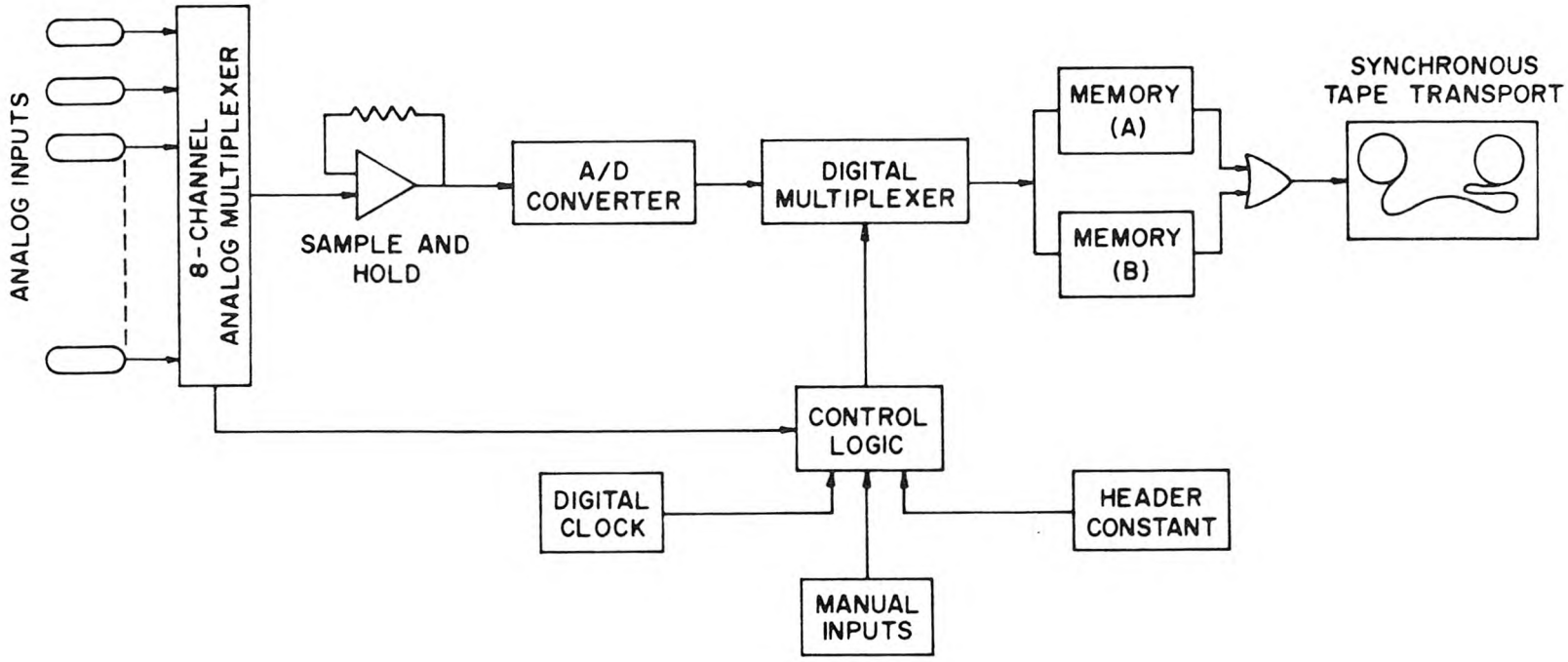

Figure 4.12 Flow diagram of the digital data system (after Okoye (1970)).

opposed to an incremental recorder, data were first collected in one memory unit at the sampling rate, and then transferred to the tape at the maximum transport rate of the recorder. Meanwhile the other memory unit accepted data from the digital multiplexer while data in the full unit were being recorded on tape. Thus no information was lost while digitized data were being recorded on tape.

Digitized information was packed on the magnetic tape in a language and format compatible with the IBM 370/158 high speed computer. Data from a set of measurements, such as concentration monitored at a fixed point over a given length of time, were stored on tape as a file. The files were separated from each other by END OF FILE marks. Each file was composed of records separated from one another by INTER RECORD GAPS. A record length was 1024 tape characters and comprised the storage of each memory unit. In each record, the first sixteen tape characters identified the header data from the control logic; the remaining 1008 characters were digitized data. Since voltages were recorded as 3-digit values, each sample consisted of three tape characters; thus 336 samples were stored in every record.

By use of subroutines, the recorded information was retrieved by the IBM 370/158 computer; thus digitized concentration data were available for reduction and analysis by the main computer program.

4.3 Determination of Sampling Rate and Time

A representative dispersion experiment was performed to determine a suitable sampling rate and averaging time for measuring mean and standard deviations of concentration.

The averaging time, T_m, must be large enough that these quantities are essentially independent of it. Okoye (1970) pointed out that the required averaging time increases with the size of the largest eddy effecting mixing, hence longer averaging times are needed for deeper water. Thus, the sampling rate and averaging time were determined for the deepest water anticipated in the subsequent experiments. This depth was 16.3 cm. The diffuser was perpendicular to the current, and the Froude number approximately equal to one. This results in the largest vertical mixing eddy size, in the present experiments, as the effluent mixes over the receiving water depth (Figure 2.3). All four probes were simultaneously sampled.

The probes were sampled at 400 samples/s each for sixty seconds. Means were formed of every sample, every other sample, every third sample, etc., up to every four hundredth sample. This is equivalent to taking 400, 200, 133,...., 1 samples/s. The ratios C_i/C_m were then computed, where C_i is the mean at i samples/s and C_m the mean at 400 samples/s. Similarly, values of the standard deviation $\sqrt{\overline{C_i'^2}}$ and the ratios $\sqrt{\overline{C_i'^2}}/\sqrt{\overline{C_m'^2}}$ were formed. The results are plotted in Figure 4.13. The means and standard deviations become independent of the sampling rate for rates greater than about 10 samples/s. This rate was chosen for all subsequent experiments.

In order to determine T_m, the probes were sampled at 10 samples/s each for nine minutes. The samples were averaged over 2, 4, 8,...., 512 seconds. Ratios C_i/C_m were then calculated where C_i is the mean

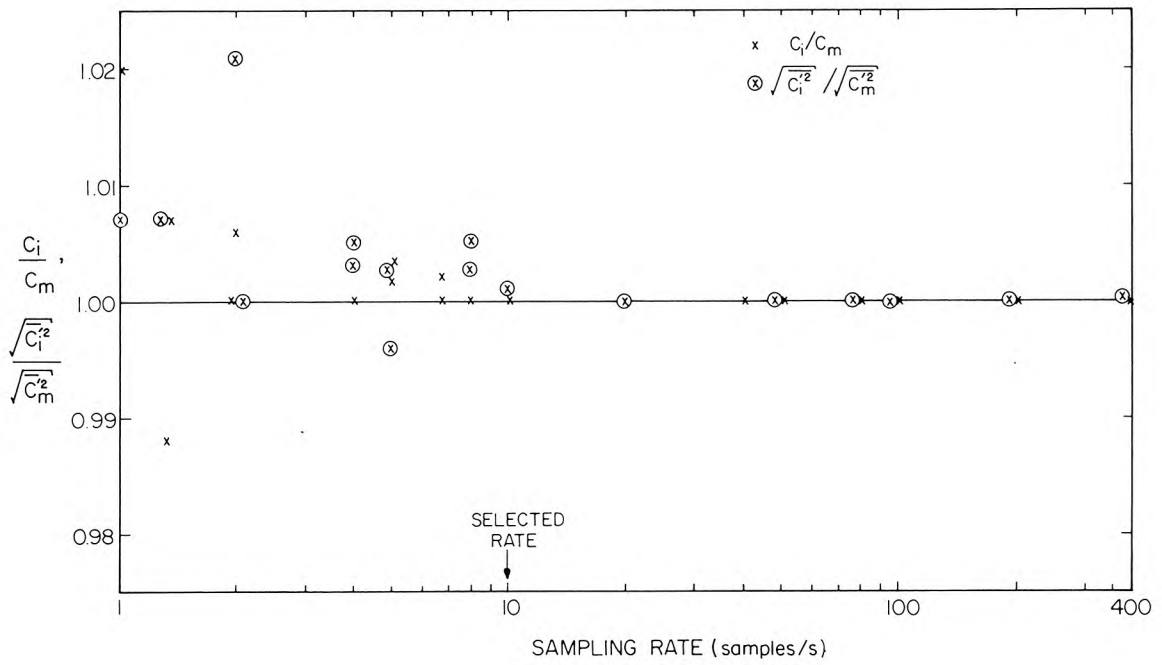

Figure 4.13 Mean and standard deviations of concentrations as a function of sampling rate, one minute average.

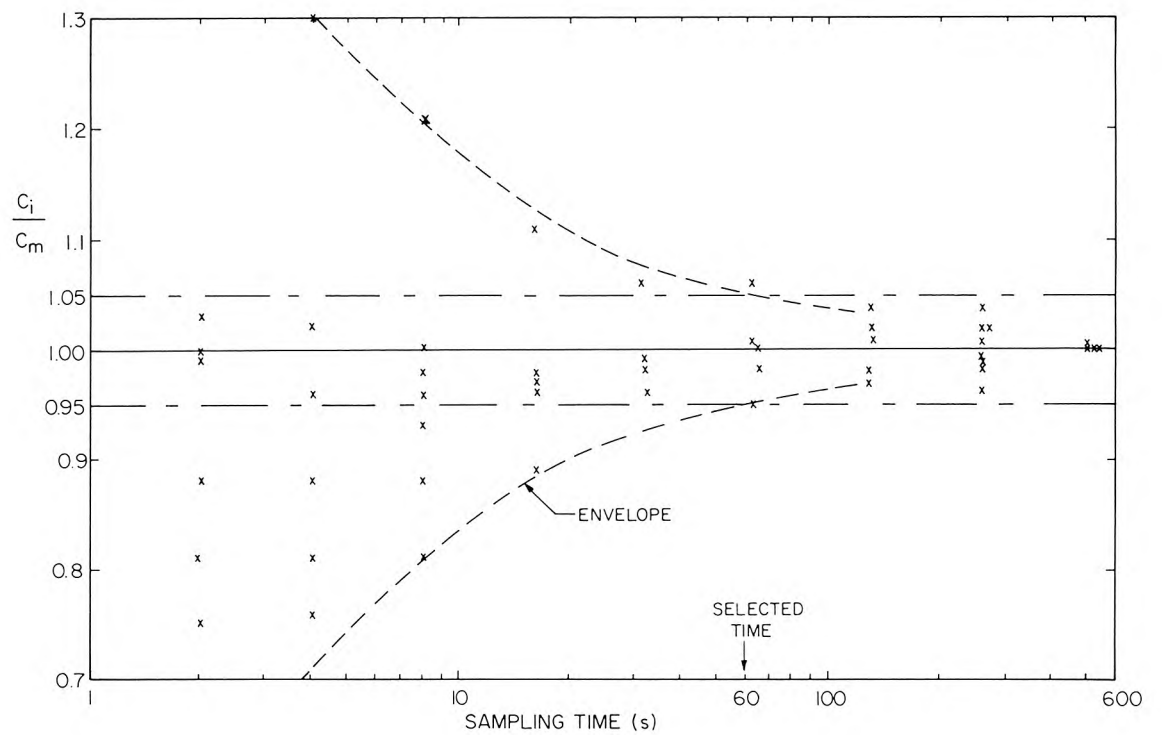

Figure 4.14 Mean concentration as a function of sampling time, sample rate is 10 per second.

concentration averaged over i seconds, and C_m is the 512 second mean. The results are plotted in Figure 4.14. It was decided to take the averaging time T_m such that most of the means fell within ± 5% of the asymptotic value. The envelope of the means plotted in Figure 4.14 falls within this range for $T_m \approx 60$ seconds. Hence, a one minute averaging time was chosen for all subsequent experiments.

To summarize, a sampling rate of ten per second and an averaging time of one minute was chosen for all concentration measurements. These values are based on experiments whose results are plotted in Figures 4.13 and 4.14.

4.4 Experimental Procedure

The following procedure was followed for all three-dimensional experiments. First, the electrical equipment was turned on to allow warm-up time. The Sanborn recorder requires about ninety minutes. The main basin recirculating pump and skimmers were then turned on. This was to mix the basin water uniformly and to clean the water surface. Air was flushed from the recirculation system if the basin had been previously emptied. The diffuser and associated plumbing were then flushed rapidly with tap water and the diffuser slot carefully cleaned with a razor blade. This was to remove air bubbles from the system and any particles which may have caught in the slot. This was necessary to ensure uniform diffuser flow.

Water was then drained or added to the basin until the desired depth was obtained. Valves on the basin recirculation system were

adjusted to achieve the desired current velocity. The effluent was then mixed, and the temperature adjusted to ± 1°C from the basin water.

The surface tension difference between the basin water and effluent was neutralized as follows. The diffuser was turned on at the anticipated flow rate and the surface plume observed. Surface tension differences were very apparent, as the elements of effluent hitting the surface would spread rapidly, almost bursting, as they hit the surface. If this occurred, detergent was added to the basin water and allowed to mix thoroughly. Ivory dishwashing liquid was found to be suitable. This procedure was repeated until the bursting was just suppressed. There was then no surface tension difference to affect the spreading of the plume on the surface. The amount of detergent required was of the order of 50 mℓ.

The conductivity probes were then calibrated. This was done by placing them in a beaker containing 3000 mℓ of basin water. The bridge circuit for each probe was balanced and the pen deflections on the Sanborn recorder zeroed. Measured amounts of effluent were added sequentially, and the resulting solution mixed thoroughly with a magnetic stirrer. After each addition, the pen deflections were noted, and the signals recorded on the A/D converter. When full scale deflections on the Sanborn recorder were reached, the probes were removed from the beaker and placed in the basin. They were positioned just touching the water surface. All probes were then lowered a further 5 mm so that the electrodes were submerged. This is defined as the surface position.

The Sanborn recorder appeared to be the largest source of error in dilution measurements. Due possibly to the age of the equipment, the baseline drifted. This introduced a constant error whose relative magnitude increased as measured dilutions increased. By choosing a suitable NaCl concentration and adjusting the Sanborn sensitivity so that large deflections were maintained, this error was reduced to about ± 5%.

The camera was loaded with film and placed in position. The flash and camera operations were then tested and an identification letter and number for the experiment was placed within the camera view.

The basin water depth was measured with a point gage to an accuracy of ± 1/10 mm. The temperatures and densities of the effluent and basin water and the basin flow rate were then measured. Using this information, the exact diffuser flow required to achieve the desired Froude number was calculated and the experiment begun.

The probes were sampled for at least one minute. They were then moved to their next locations, the probe coordinates noted, and sampling begun again. This was repeated about fourteen times. Thus, with four probes, concentrations were measured at about sixty locations for each experiment.

The basin is a closed circuit. Hence, the effluent is eventually recirculated to the head of the basin, causing the background concentration to increase. This background concentration was regularly monitored.

After the experiment was completed, the densities were rechecked. If further experiments were to be done that day, the procedure

described above was repeated. However, the diffuser was not reflushed nor were the probes recalibrated for each experiment.

At the end of the day the diffuser was flushed with clean water. To prevent algal growth, chlorine was added to the basin water and mixed thoroughly. The probes were removed and the calibration rechecked. The probes were then placed in distilled water.

4.5 Data Reduction

Data recorded on the A/D converter was reduced on an IBM 370/158 computer. The program reduced the data in the following way.

A least squares fit to the calibration data for each probe was made by means of a Caltech subroutine "LSQUAR", to evaluate the constants a_1, a_2, and a_3 in the formula

$$C = a_1 + a_2 V + a_3 V^2 \quad , \tag{4.1}$$

where C is the concentration of effluent in the mixed fluid, and V the voltage recorded by the A/D converter. C is computed by

$$C = \frac{V_o}{V_o + V_r} \quad , \tag{4.2}$$

where V_o is the total volume of effluent added to a volume V_r of basin water. C is then the reciprocal of dilution, S. A typical calibration curve is shown in Figure 4.15.

The basin flow rate was then calculated. For the venturi meter, this was done by the formula

$$Q_b = C_D \frac{\pi d^2}{4} \sqrt{\frac{2g\Delta H}{1 - \psi^4}} \quad , \tag{4.3}$$

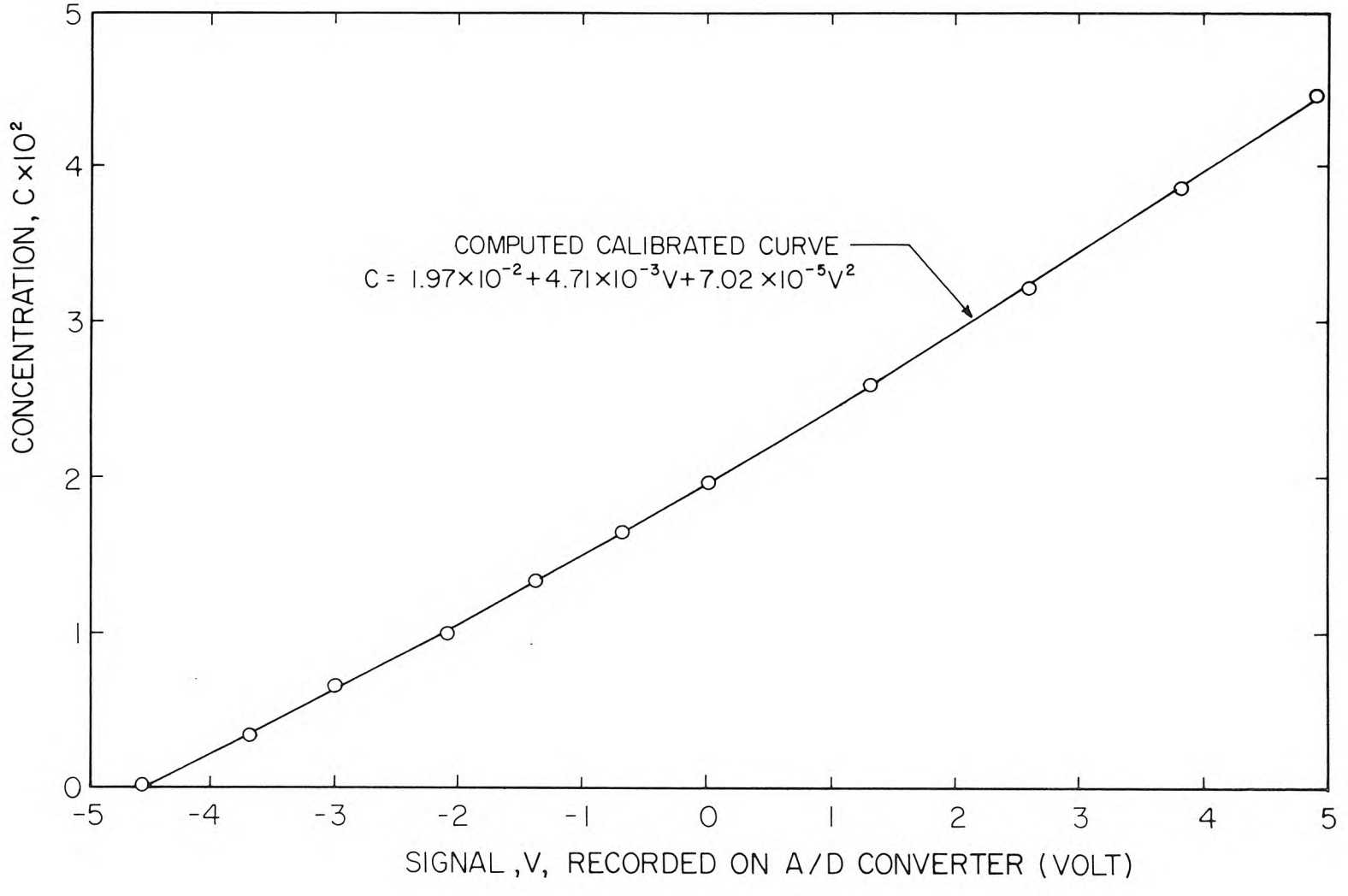

Figure 4.15 Typical conductivity probe calibration curve (concentration is volume fraction of effluent in mixture).

where C_D is a discharge coefficient; g the acceleration due to gravity; ΔH the difference in piezometric head between the venturi meter taps, measured by manometer; and $\psi = d_t/d_u$, where d_t is the throat diameter, and d_u the upstream pipe diameter. The venturi meter used was Keck Laboratory number Q-35, with d_t = 3.25 inch (8.25 cm), and d_u = 4.00 inch (10.2 cm). A discharge coefficient, C_D = 0.980 ± 2% was assumed. Hence, Eq. 4.3 becomes

$$Q_b = 0.603\sqrt{\Delta H} \quad , \tag{4.4}$$

where Q_b is in ft^3/s, and ΔH in feet. The rotameter is a Fischer Porter Flowrator model 1735, Keck Laboratory number Q-27. The meter is scaled in percent of full flow. Previous laboratory calibrations have verified this relation, where 100% is 0.105 ft^3/s (3.0×10^{-3} m^3/s) ± 2%. Hence, the relationship

$$Q_b = 0.105R/100 \tag{4.5}$$

was used, where Q_b is in ft^3/s, and R is percent of full flow. Thus, the measurement error for both flowmeters is about ± 2%.

The ambient current velocity, u, was calculated from the formula

$$u = \frac{Q_b}{WH} \quad , \tag{4.6}$$

where W is the basin width, and H the water depth. Q_b is given by Eq. 4.4 or 4.5. The error in depth measurement is about ± 1 mm due to the unevenness of the sand bottom. Hence, the error in H is usually less

than ± 2%, and the total error in u is ± 4%, assuming a ± 2% error in flow measurement. The Froude number is then calculated from:

$$F = u^3 L \Big/ \left(\frac{\Delta\rho}{\rho_o} g Q \right) , \tag{4.7}$$

where u is given by Eq. 4.6, and L is the diffuser length. $\Delta\rho/\rho_o$ is computed from the density measurements, and Q is the effluent flow rate. By summing up the individual errors in the quantities of Eq. 4.7, the error in F is estimated at ± 15%.

In order to compute dilutions, the concentration of each sample, C_i, is computed from Eq. 4.1. A one minute average was then obtained from:

$$C = \frac{1}{N} \sum_{i=1}^{N} C_i \quad , \tag{4.8}$$

where N = 600. Background concentrations were computed by linear interpolation between measured values. The mean concentration, Eq. 4.8, was then corrected by subtracting the background. The dilution, S, was then computed as:

$$S = \frac{1}{C} \quad . \tag{4.9}$$

The variance was computed by the equation:

$$\overline{C'^2} = \frac{1}{N} \sum_{i=1}^{N} (C_i - C)^2 \quad . \tag{4.10}$$

Finally, the ratios Sq/uH, C u H/q, and $\sqrt{\overline{C'^2}}/C$ were computed for each probe at each sampling point. The error in the first two ratios due to

errors in measurement of the individual quantities is about ± 12% and in the last ratio about ± 10%.

The spreading rate of the surface waste field was measured from the photographs. This was done by projecting each slide in an enlarger and tracing the plume outline. The scale was measured from the grid markings. The error in measuring w due to the difference in height between the surface plume and the grid marks was less than + 5%.

4.6 Summary of Experimental Errors

The parameters of primary interest in this study are the ratios Sq/uH and its inverse CuH/q; a Froude number, $F = u^3/b$; and the extent of the waste field. A source of error is the variation of u over the basin width; this variation is about ± 5% of the mean. The limited averaging time of one minute introduces an error of ± 5% in the measurements of mean concentrations compared to their asymptotic values. The relative error in the ratios Sq/uH and CuH/q is assumed to be the square root of the sum of the squares of the relative errors in each quantity, and is equal to 9%. Similarly, the relative error in F is 11%. A further systematic error results from the small plume Reynolds numbers of these experiments. This error is highest in the plume regime, where it may be as high as ± 20% (Appendix A).

The measurements of surface plume width systematically overestimate the true width by less than 5%. This is due to the difference in heights of the water surface and fiducial marks.

CHAPTER 5

EXPERIMENTAL RESULTS

5.1 Summary of Experiments

The expression for dilution with no ambient current is deduced in Section 5.1, and hence an estimate of the asymptotic expression for dilution as the Froude number, $F \to 0$ is obtained. Results for dispersion in currents perpendicular, parallel, and at intermediate angles to the diffuser, respectively, are presented in Sections 5.3, 5.4, and 5.5. In Section 5.6 the results for minimum surface dilution are presented.

All experiments are identified by a letter and number which enables values of experimental variables to be found from the data summary, Table 5.1. In all photographs the grid spacing on the centerline is equal to the diffuser length, L.

5.2 Dilution with No Ambient Current

Five experiments were performed with no ambient current in order to measure minimum surface dilutions. The results are plotted in Figure 5.1 in a form suggested by Eq. 3.11, that is:

$$S_m = f\left(g_o'^{1/3} H q^{-2/3}\right) ,$$

where

$$g_o' = \frac{\rho_r - \rho_o}{\rho_o} g .$$

The results confirm the prediction of Eq. 3.15:

Table 5.1 Summary of data for three-dimensional experiments.

Experiment Number	H Water Depth cm	L Diffuser Length cm	u Current Velocity cm/s	$\Delta\rho/\rho_o$ Density Difference $\times 10^3$	q Effluent Flow Rate cm^2/s	θ Current Direction	L/H	F Froude Number $u^3/\left(\frac{\Delta\rho}{\rho_o} gq\right)$	Re Reynolds Number $4uH/\nu$
G1	16.29	61	1.78	28.5	0.172	90°	3.74	1.17	11,600
G2	16.28	61	0.857	25.0	--	90°	3.75	--	5,580
G3	8.21	61	3.74	26.3	0.187	90°	7.43	10.8	12,290
G4	8.21	61	1.82	26.0	0.187	90°	7.43	1.26	5,980
G5	8.16	61	0.826	25.7	0.181	90°	7.48	0.124	2,700
G6	4.07	61	8.15	25.1	0.187	90°	15.0	117	13,270
G7	4.05	61	3.80	25.0	0.187	90°	15.1	11.9	6,150
G8	4.08	61	1.78	24.8	0.187	90°	15.0	1.24	2,900
G9	4.04	61	0.785	24.9	0.187	90°	15.1	0.106	1,270
H1	16.36	61	1.71	26.2	0.160	90°	3.73	1.22	11,210
H2	16.29	61	0.826	26.7	0.179	90°	3.74	0.120	5,380
H3	8.11	61	3.80	29.3	0.168	90°	7.52	11.4	12,340
H4	8.16	61	1.80	25.8	0.181	90°	7.48	1.27	5,860
H4(R1)	8.12	61	1.80	26.4	0.231	90°	7.51	0.98	5,850
H5	8.16	61	0.861	27.2	0.196	90°	7.48	0.122	2,810
H5(R1)	8.12	61	0.859	26.6	0.194	90°	7.51	0.125	2,790
H7	4.08	61	3.66	26.3	0.196	90°	15.0	9.69	5,980
H8	4.05	61	1.91	25.8	0.226	90°	15.1	1.22	3,090
H9	4.07	61	0.779	25.5	0.189	90°	15.0	0.100	1,270
H10	4.05	61	5.47	26.4	0.175	90°	15.1	36.1	8,870
H11	8.10	61	0.367	26.7	0.189	90°	7.53	0.0100	1,190
H12	8.10	61	0.602	26.7	0.189	90°	7.53	0.0440	1,951
N1	4.05	30.5	3.61	25.8	0.193	90°	7.53	9.65	5,850
N2	4.07	30.5	7.65	25.8	0.180	90°	7.49	98.4	12,450

Table 5.1 (Continued)

Experiment Number	H Water Depth cm	L Diffuser Length cm	u Current Velocity cm/s	$\Delta\rho/\rho_o$ Density Difference $\times 10^3$	q Effluent Flow Rate cm^2/s	θ Current Direction	L/H	F Froude Number $u^3/\left(\frac{\Delta\rho}{\rho_o} gq\right)$	Re Reynolds Number $4uH/\nu$
N3	8.17	30.5	1.62	26.6	0.167	90°	3.73	0.976	5,280
N4	8.19	30.5	3.57	26.0	0.184	90°	3.72	9.71	11,700
J0	16.27	61	1.92	27.1	0.183	0°	3.75	1.45	12,500
J1	16.30	61	1.66	27.5	0.174	0°	3.74	0.973	10,800
J1(R1)	16.27	61	1.66	26.2	0.185	0°	3.75	0.963	10,830
J2	16.30	61	0.753	26.6	0.168	0°	3.74	0.0974	4,910
J2(R1)	16.25	61	0.767	25.4	0.185	0°	3.75	0.0977	4,980
J3	8.14	61	3.66	23.3	0.220	0°	7.49	9.77	11,900
J3(R1)	8.13	61	3.60	23.6	0.207	0°	7.50	9.72	11,690
J4	8.13	61	1.62	23.1	0.189	0°	7.50	0.991	5,270
J4(R1)	8.13	61	1.60	22.7	0.187	0°	7.50	0.983	5,210
J5	8.14	61	0.769	23.9	0.200	0°	7.49	0.0972	2,500
J6	4.06	61	7.72	23.4	0.209	0°	15.0	95.8	12,620
J6(R1)	4.10	61	7.68	24.6	0.192	0°	14.9	97.9	12,590
J7	4.06	61	3.60	23.4	0.207	0°	15.0	9.81	5,840
J7(R1)	4.04	61	3.56	23.4	0.189	0°	15.1	10.4	5,750
J8	4.04	61	1.63	22.6	0.196	0°	15.1	1.00	2,630
J8(R1)	4.08	61	1.54	24.9	0.153	0°	15.0	0.978	2,500
J9	4.06	61	0.781	25.1	0.198	0°	15.0	0.0978	1,270
J11	6.38	61	0.612	24.2	0.207	0°	9.56	0.0467	1,560
J11(R1)	6.39	61	0.595	23.8	0.194	0°	9.55	0.0466	1,520
B1	8.12	30.5	1.72	25.0	0.214	0°	3.76	0.970	5,600
B1(R1)	8.15	30.5	1.66	24.7	0.193	0°	3.74	0.978	5,420
B2	8.12	30.5	3.71	24.3	0.219	0°	3.76	9.79	12,040
B2(R1)	8.12	30.5	3.64	24.5	0.206	0°	3.76	9.74	11,830
B3	4.05	30.5	3.51	24.9	0.180	0°	7.53	9.83	5,680
B4	4.07	30.5	7.82	25.4	0.197	0°	7.49	97.3	12,740

Table 5.1 (Continued)

Experiment Number	H Water Depth cm	L Diffuser Length cm	u Current Velocity cm/s	$\Delta\rho/\rho_o$ Density Difference $\times 10^3$	q Effluent Flow Rate cm^2/s	θ Current Direction	L/H	F Froude Number $u^3/\left(\frac{\Delta\rho}{\rho_o} gq\right)$	Re Reynolds Number $4uH/\nu$
B4(R1)	4.08	30.5	7.90	24.7	0.210	0°	7.48	96.9	12,892
B5	8.12	30.5	0	24.5	0.214	0°	3.76	0	0
B6	4.08	30.5	0	24.7	0.214	0°	7.48	0	0
R3	8.14	61	3.67	24.4	0.211	45°	7.49	9.80	11,940
R3(R1)	8.13	61	3.61	23.5	0.207	45°	7.50	9.85	11,730
R4	8.13	61	1.67	23.9	0.202	45°	7.50	0.982	5,430
R4(R1)	8.17	61	1.70	23.2	0.224	45°	7.47	0.963	5,570
R5	8.08	61	0.805	23.5	0.231	45°	7.55	0.0979	2,600
R6	4.07	61	7.76	23.8	0.205	45°	15.0	97.4	12,640
R10	8.07	61	0	23.5	0.194	45°	7.56	0	0
R17	8.07	61	0	23.5	0.194	45°	7.56	0	0
L1	16.26	122	1.64	24.8	0.185	90°	7.50	0.979	10,640
L1(R1)	16.29	122	1.69	25.3	0.198	90°	7.49	0.981	11,020
L2	16.25	122	0.745	25.0	0.167	90°	7.51	0.101	4,840
L3	8.16	122	3.500	25.0	0.179	90°	15.0	9.76	11,430
L4	4.07	122	7.71	24.2	0.198	90°	30.0	97.6	12,540
L4(R1)	4.05	122	7.66	26.0	0.181	90°	30.1	97.5	12,410
L5	4.07	122	3.71	24.2	0.220	90°	30.0	9.78	6,030
L5(R1)	4.08	122	3.60	25.6	0.192	90°	29.9	9.66	5,810
L6	4.07	122	1.56	25.5	0.155	90°	30.0	0.978	2,540
L6(R1)	4.10	122	1.55	25.7	0.153	90°	29.8	0.967	2,540
L7	4.04	122	0.771	25.6	0.187	90°	30.2	0.0975	1,250
L7(R1)	4.12	122	0.756	25.3	0.179	90°	29.6	0.0971	1,250
L8	6.38	122	0.682	24.9	0.176	90°	19.1	0.0737	1,740
L9	16.26	122	0	24.9	0.189	90°	15.0	0	0

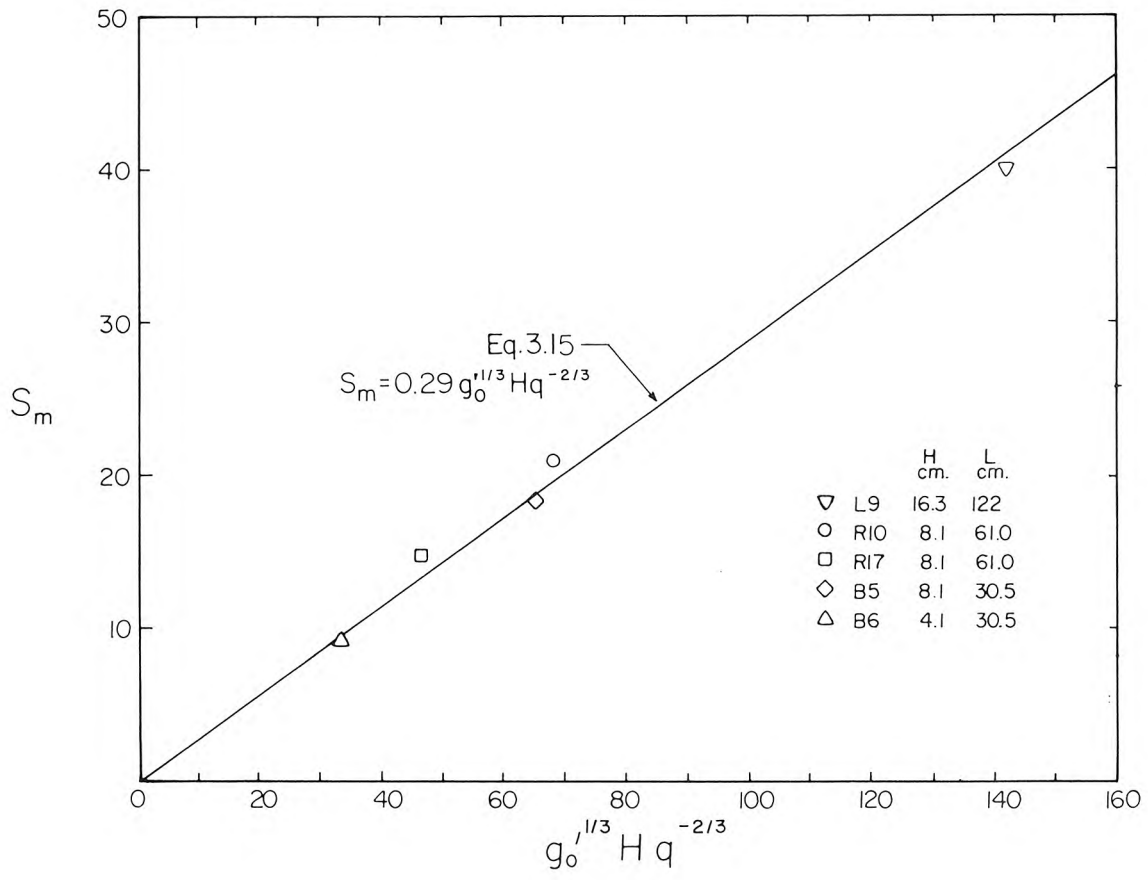

Figure 5.1 Measured minimum surface dilution in stagnant ambient fluid.

$$S_m = 0.29\ g_o'^{1/3} H q^{-2/3} \quad , \tag{5.1}$$

which is also plotted. This suggests that Eq. 3.16:

$$\frac{S_m q}{uH} = 0.29 F^{-1/3} \quad , \tag{5.2}$$

is the asymptotic expression for dilution in a moving current as $F\ (= u^3/b) \rightarrow 0$. However, the assumption made that the surface layer thickness is uniform with no ambient current is only true for an initial period. For long times, the layer thickness grows with time due to interfacial shear. Hence, the dilution decreases with time due to the reduced height of plume rise. Eq. 5.1 is therefore a time dependent solution, only valid for an initial period. The value of the coefficient in Eq. 5.2 is therefore only an approximation.

5.3 Dispersion in a Perpendicular Current

5.3.1 Photographs of Surface Plumes

As discussed in Section 2.2, there exist three flow regimes for dispersion from a line plume of infinite length discharging into a current flowing perpendicular to the source. These flow regimes depend only on the magnitude of the Froude number, F, and are illustrated in vertical cross section in Figure 2.3. The photographs shown in this chapter are all plan views.

An example of the plume flow regime (Figure 2.3a) is shown in Figure 5.2. Here, $F \approx 0.1$ and an upstream wedge forms, causing the

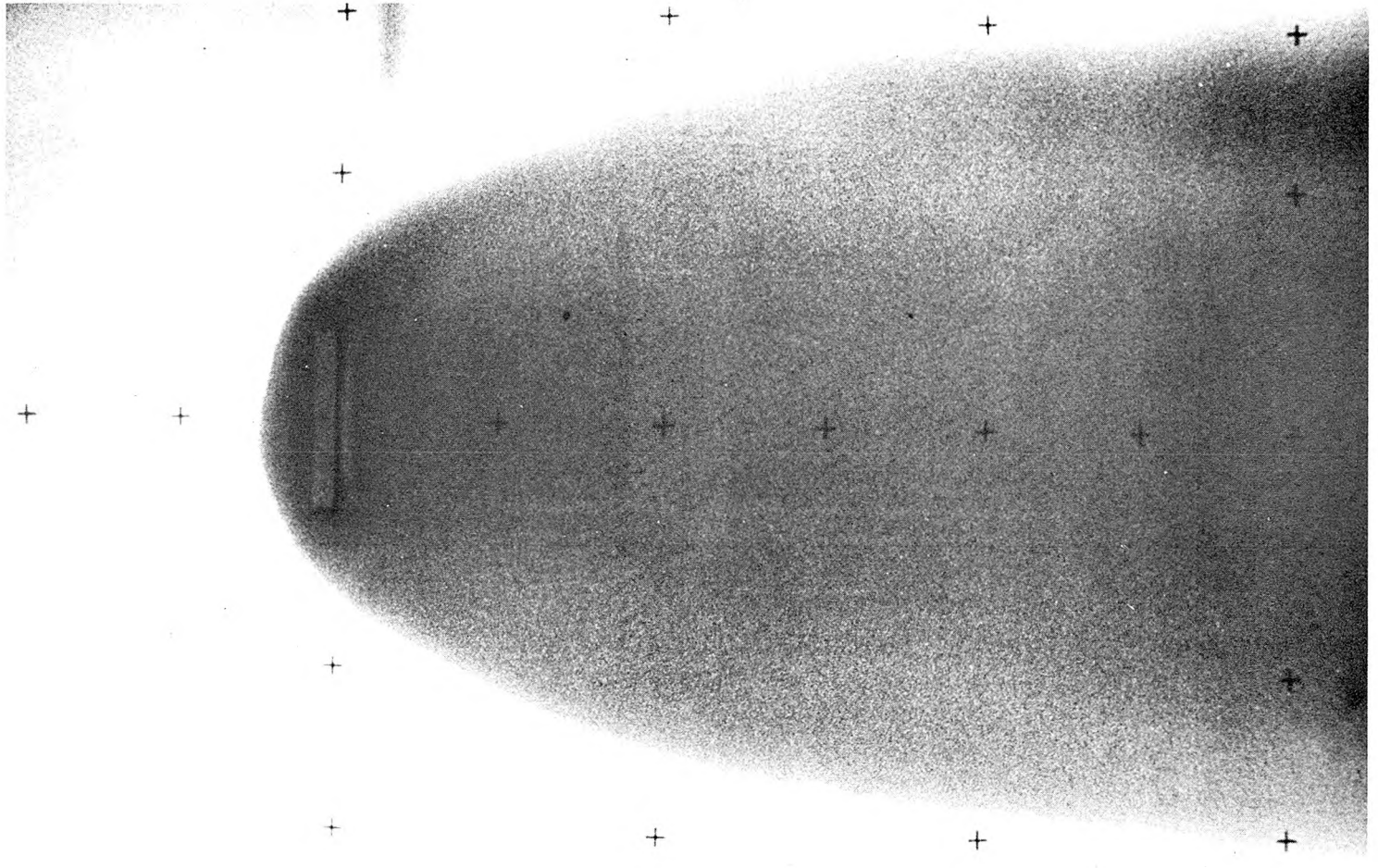

Figure 5.2 Photograph of surface plume: G9, $F \approx 0.1$.

width of the surface plume at the diffuser to be greater than the diffuser length.

For $F \geq 1$, the upstream wedge is swept away, and the effluent remains attached to the lower boundary, as shown in Figure 2.3c. The three-dimensional case was discussed in Section 3.3.1; it was predicted that the effluent would remain attached to the lower boundary for some distance downstream, as shown in Figure 3.1. This can be seen in the example shown in Figure 5.3. The zone of lower boundary attachment is the dark triangle extending about three diffuser lengths downstream.

The effect on the surface plume of varying the Froude number for otherwise fixed conditions (L = 61 cm, $H \approx 4$ cm) is shown in Figure 5.4. Experiment number G9 is in the plume regime ($F \approx 0.1$) where the upstream wedge can be seen. When F is increased to about 1.2, G8, the upstream wedge is swept away. The forced entrainment regime is entered, and a zone of lower boundary attachment forms, extending about one diffuser length downstream. For $F \approx 12$, G7, the zone of attachment extends further downstream, and the size of the surface field is smaller. Finally, for $F \approx 120$, G6, the current is so strong that little surface spreading results. The fuzzy plume edges suggest that ambient turbulence is beginning to affect dispersion.

The effect on the surface plume of varying the water depth for $F \approx 1$, and L = 61 cm, is shown in Figure 5.5. The spreading near the diffuser is unaffected by the water depth, as predicted by Eq. 3.26. For the 4 cm water depth, interfacial shear greatly retards the surface spreading rate compared to the case of 16 cm depth. This is predicted

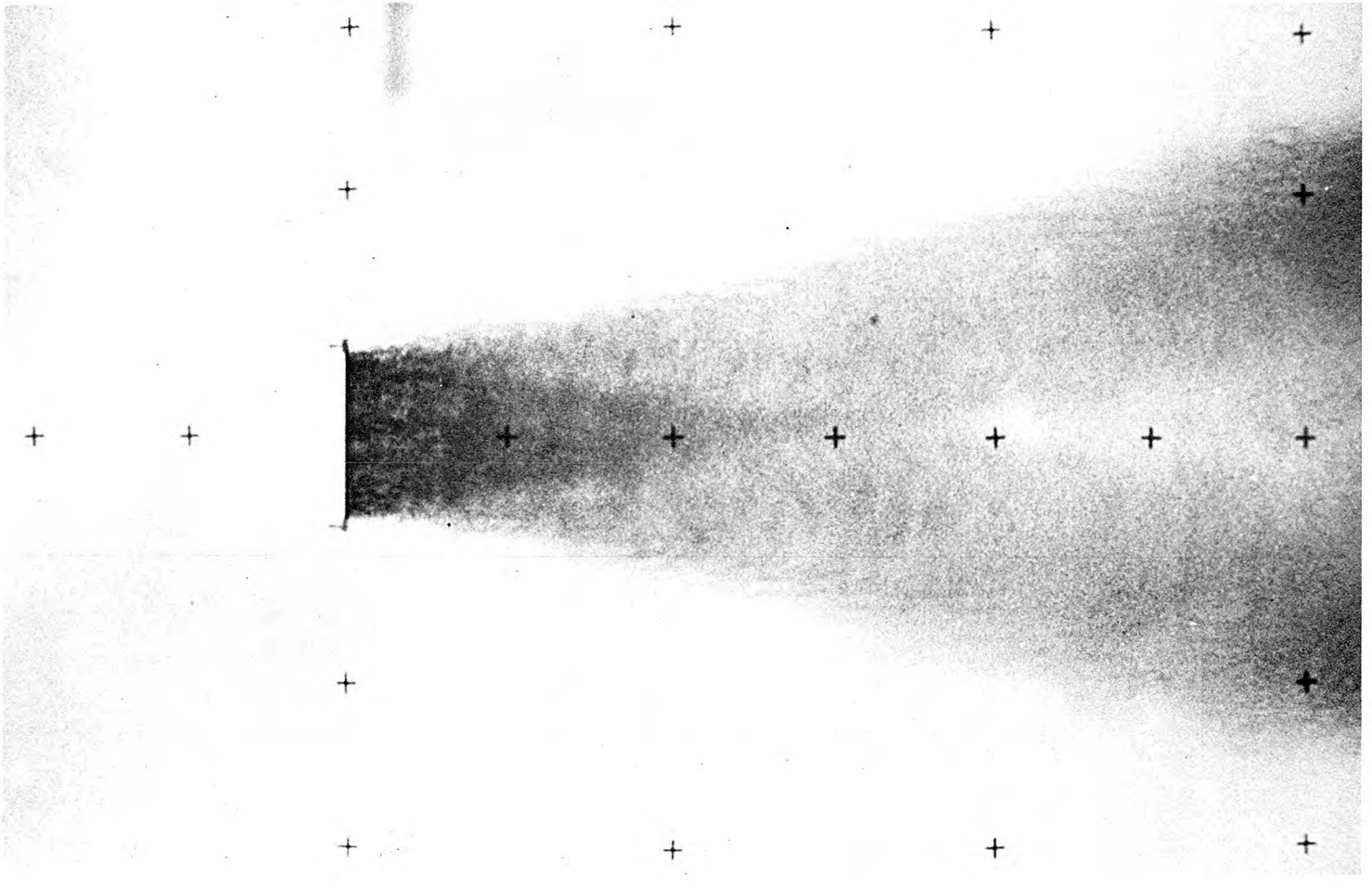

Figure 5.3 Photograph of surface plume: G3, F ≈ 11.

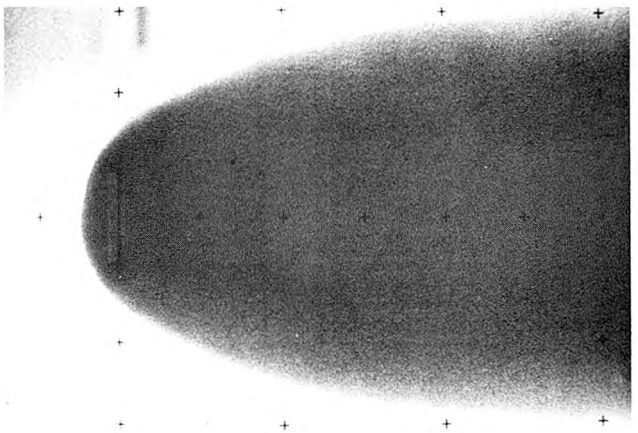

G9, $F \approx 0.1$

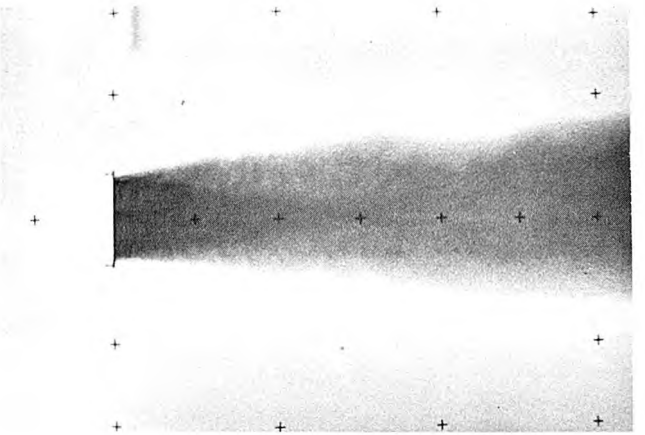

G7, $F \approx 12$

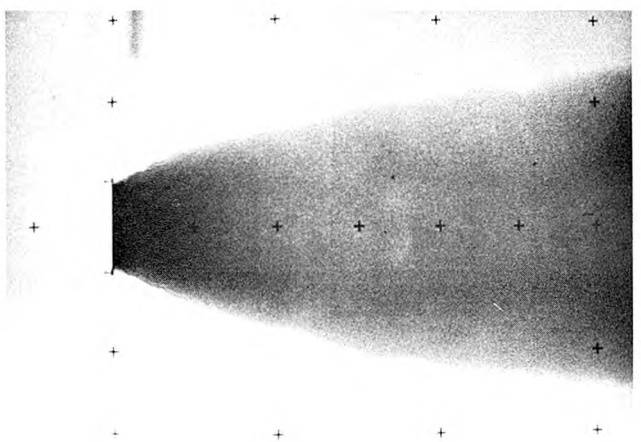

G8, $F \approx 1.3$

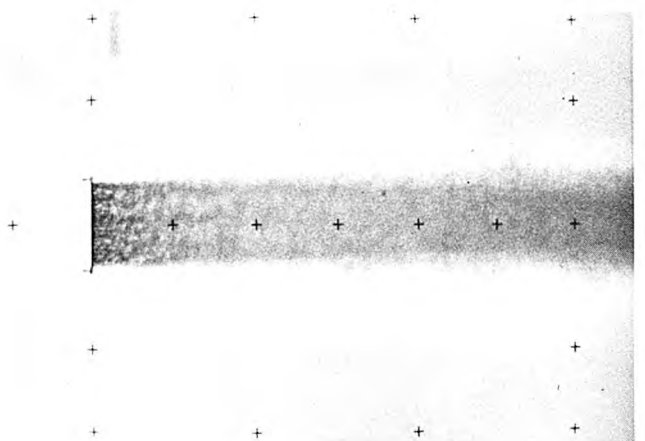

G6, $F \approx 120$

Figure 5.4 Photographs of surface plumes at different values of the Froude numbers, F.

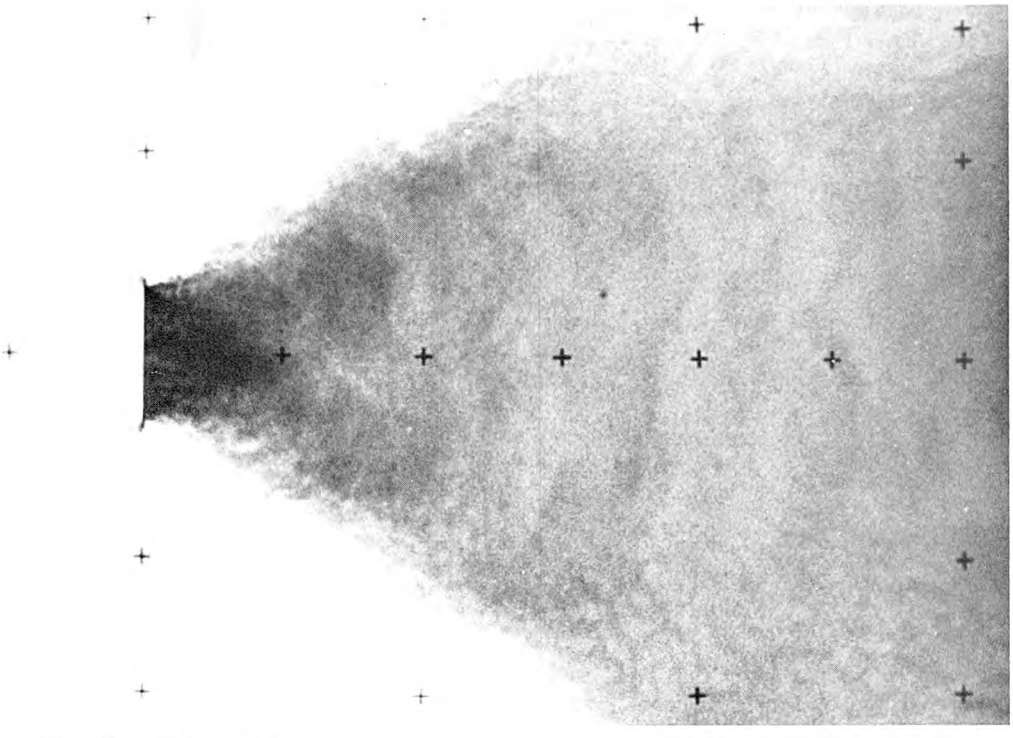

G1, H = 16.3 cm

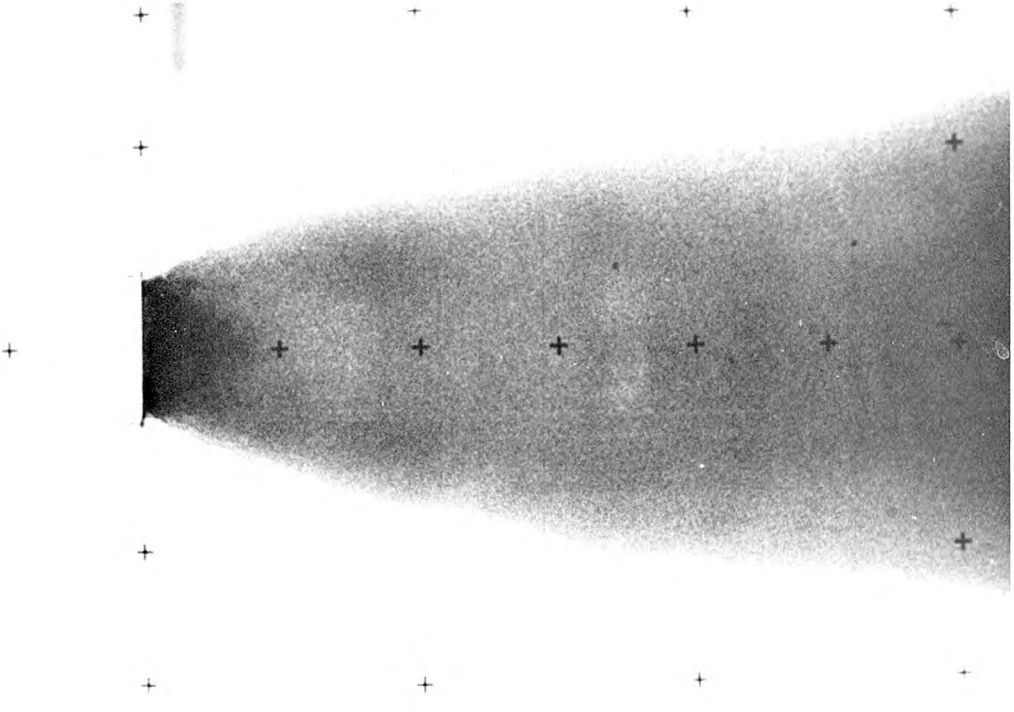

G8, H = 4.1 cm

Figure 5.5 Photographs of surface plumes at different water depths, H. $F \approx 1$, L = 61 cm.

by Eq. 3.44, as the shear stress, τ, increases as the water depth decreases. The length of lower boundary attachment is about one diffuser length, and is unaffected by the change in water depth, as predicted by Eq. 3.24.

5.3.2 Length of Lower Boundary Attachment

For experiments in which $F \geq 1$, the length of the zone of lower boundary attachment, x_a (defined in Figures 3.1 and 3.2) was measured from the photographs. The results are plotted in dimensionless form in Figure 5.6. The prediction, Eq. 3.24, which is also plotted, shows good agreement with the results. Figure 5.3 is a good example of a photograph from which x_a was measured. Here, $x_a \approx 3L$.

5.3.3 Buoyant Surface Spreading Rate

Buoyant surface spreading was discussed in Section 3.5. For $F \geq 1$ it was speculated that three spreading regimes might exist as shown in Figure 3.5. In order to test this hypothesis the results were plotted in the form Δw $(= w - L)$ versus x in Figures 5.7, 5.8, 5.9, and 5.10 for F = 0.1, 1, 10, and 100, respectively. Lines with slopes of 1, 2/3, and 1/5, are also marked. $\Delta w/x$ for the initial linear spreading portion of each experiment with $F \geq 1$ was measured from these figures and the results plotted versus F in Figure 5.11.

The initial spreading rate for $F \geq 1$ was predicted to be linear and independent of Reynolds number and L/H for $L/H \gg 1$. The results show this to be true and confirm the prediction, Eq. 3.26 (Figure 5.11), for $3.75 < L/H < 15$, and $2900 < Re < 12{,}300$. Within the range of validity $(F \geq 1)$, only for $F \approx 100$ do the results differ appreciably

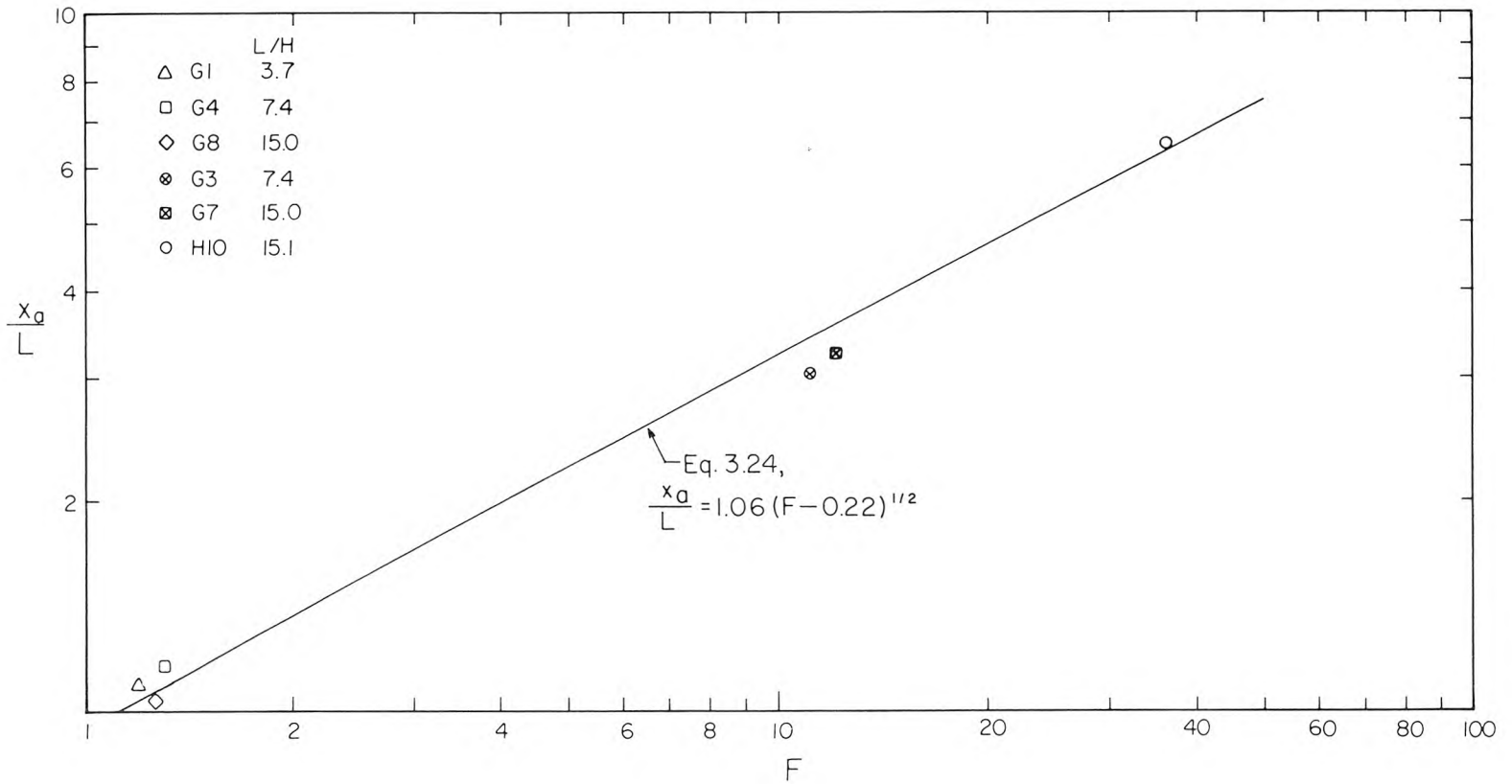

Figure 5.6 Length of lower boundary attachment (see Figures 3.1 and 3.2 for definition sketches).

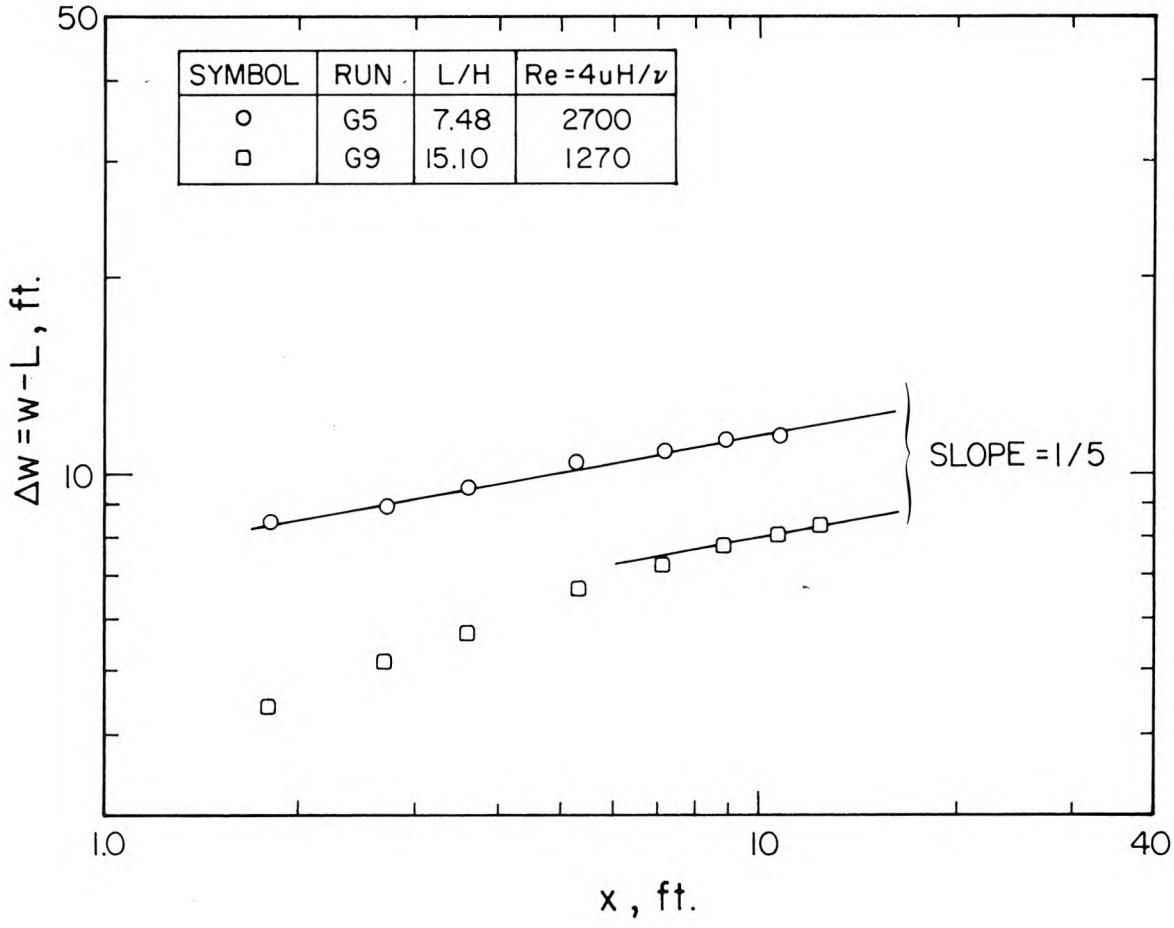

Figure 5.7 Growth of surface field downstream; current perpendicular to diffuser, F ≈ 0.1 (1 ft = 0.305 m).

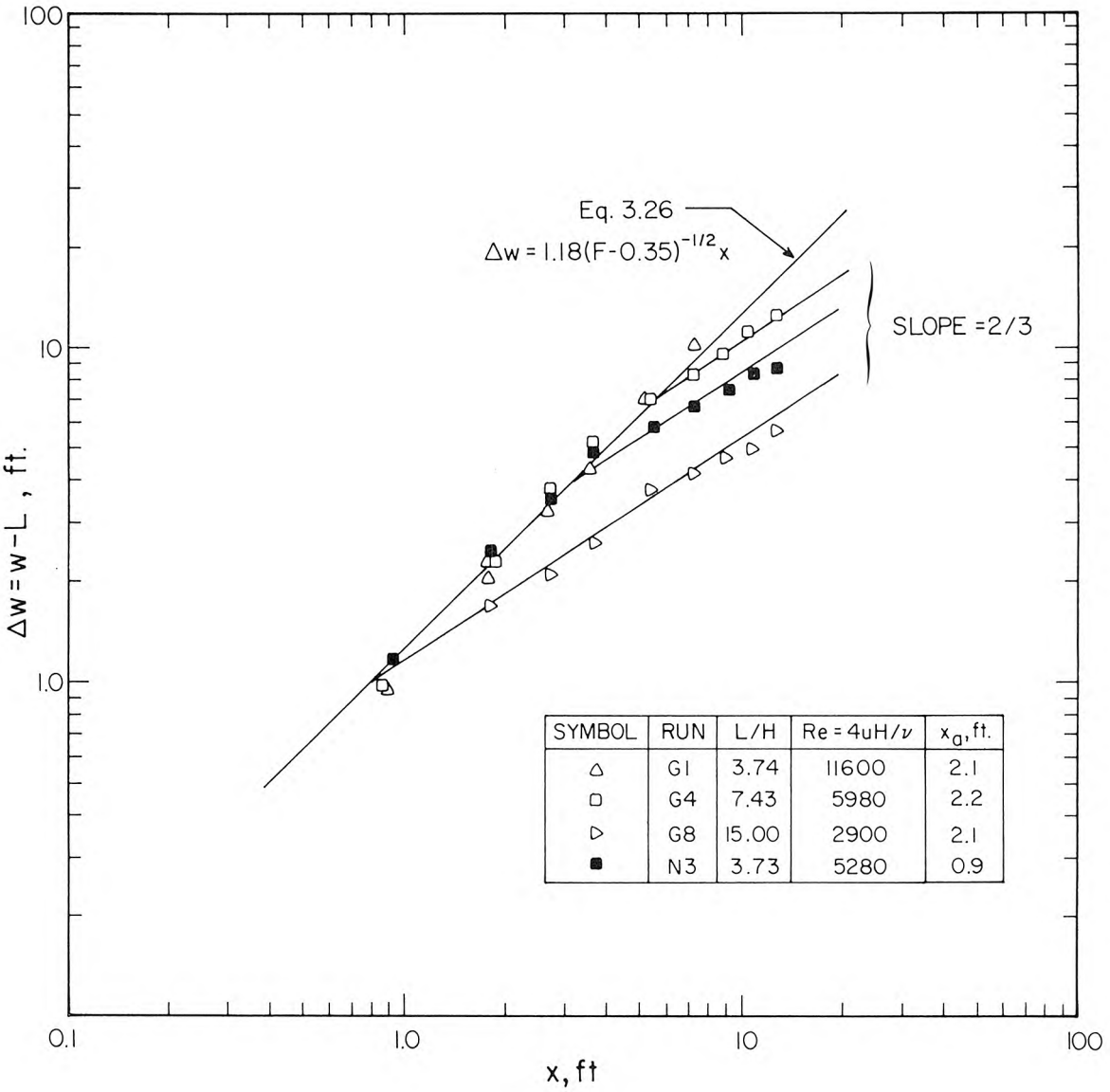

Figure 5.8 Growth of surface field downstream, current perpendicular to diffuser, $F \approx 1$. (x_a is length of zone of lower boundary attachment, predicted by Eq. 3.24.)(1 ft = 0.305 m)

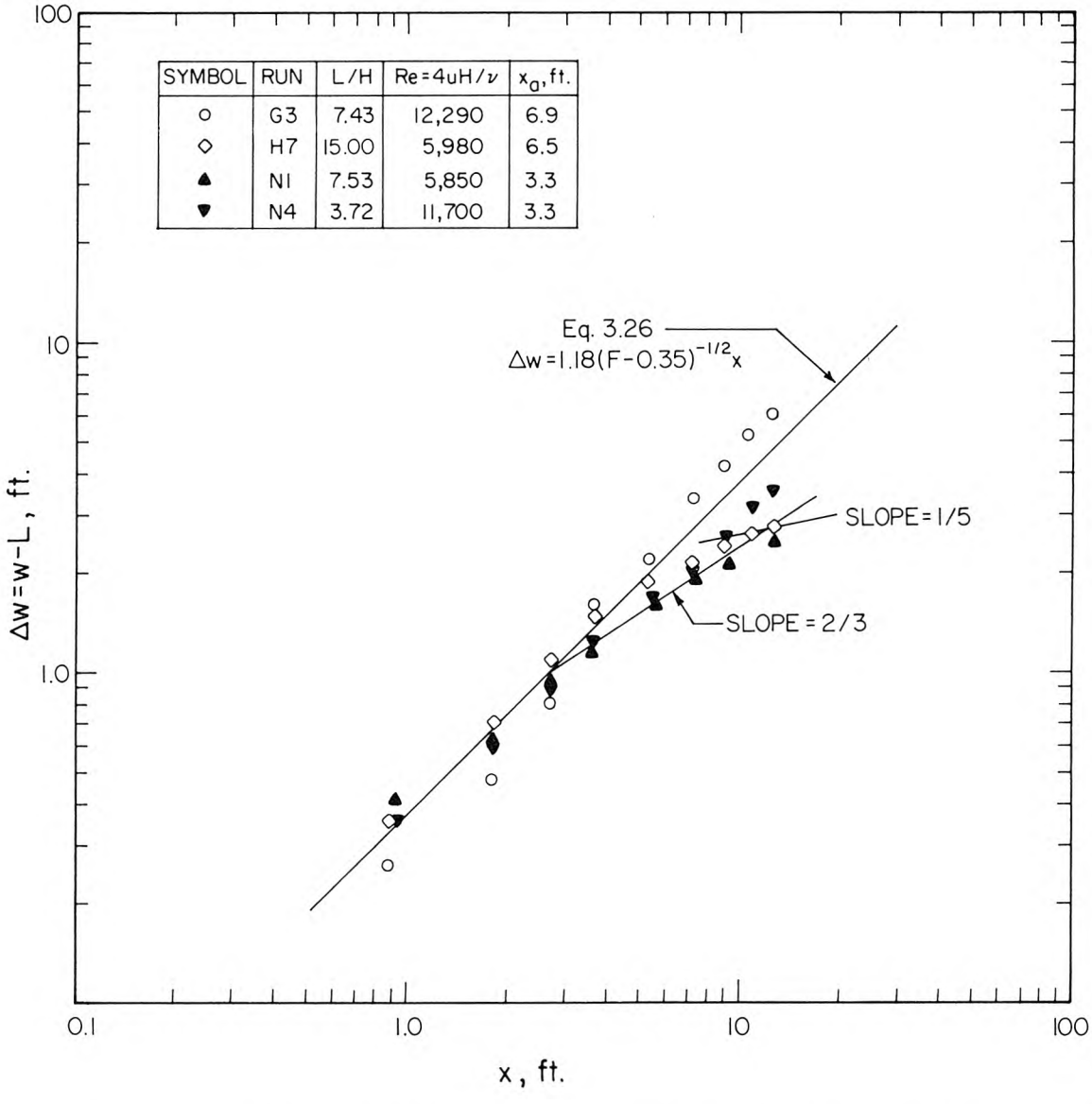

Figure 5.9 Growth of surface field downstream, current perpendicular to diffuser, $F \approx 10$. (x_a is length of zone of lower boundary attachment, predicted by Eq. 3.24.)(1 ft = 0.305 m)

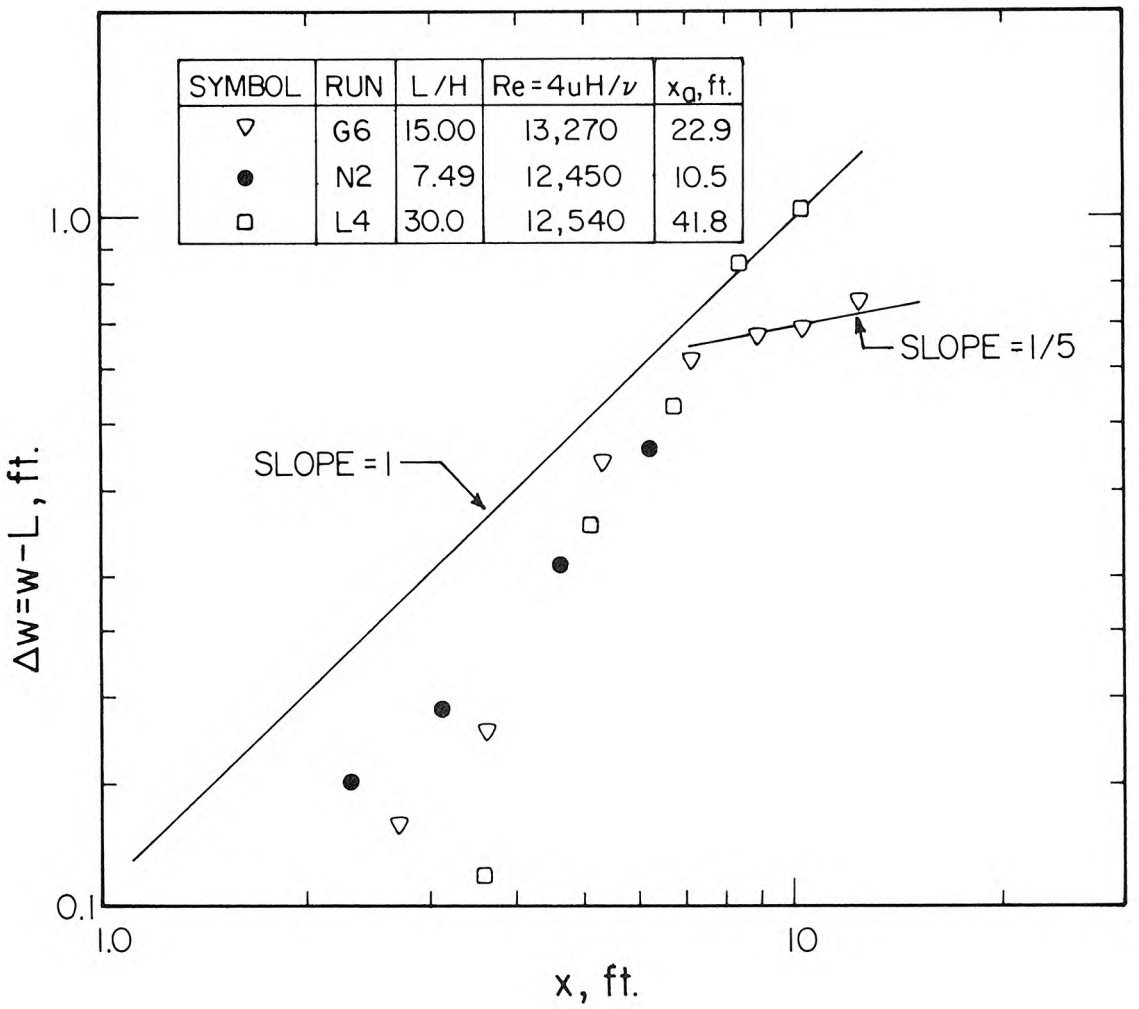

Figure 5.10 Growth of surface field downstream, current perpendicular to diffuser, $F \approx 100$. (x_a is length of zone of lower boundary attachment, predicted by Eq. 3.24.)(1 ft = 0.305 m)

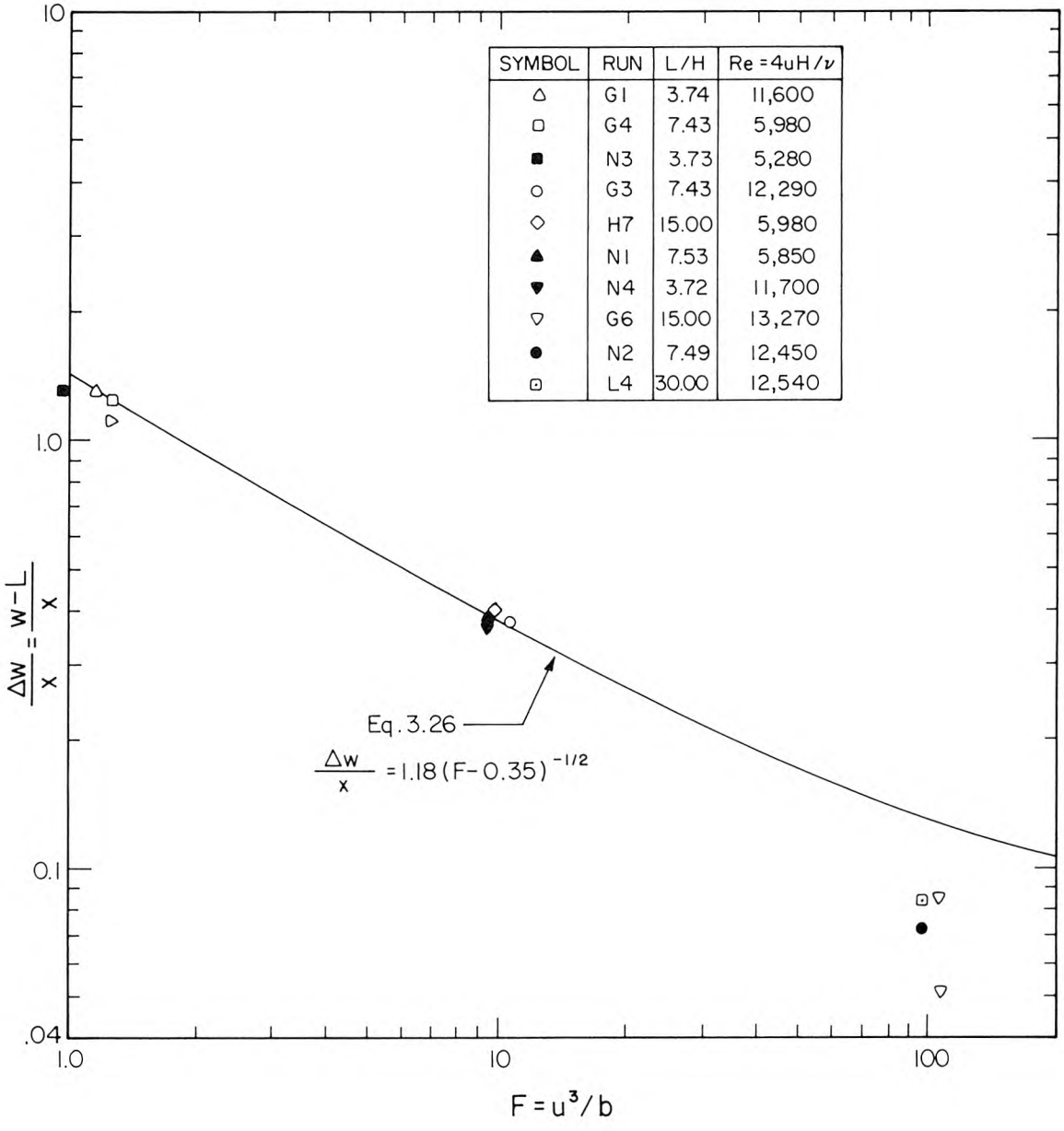

Figure 5.11 Initial spreading rate of surface field, current perpendicular to diffuser.

from Eq. 3.26. This is probably not significant, however, as the spreading rate here is very small and the measurements subject to considerable error (see, for example, Figure 5.4, G6).

The spreading is usually linear at least up to the point of lower boundary separation. Only for experiment G8 does the spreading depart significantly from linear before separation. This flow has a very low Reynolds number (2900, see Figure 5.5). It can be concluded that the initial spreading rate is linear at least up to flow separation (whose length, x_a, can be predicted by Eq. 3.24, and is marked on Figures 5.8, 5.9, and 5.10) and is independent of L/H and Reynolds number in the range $3.74 < L/H < 15$, $5{,}280 < Re < 12{,}300$ and $1 < F < 20$ (this excludes experiment G8 with Re = 2900).

The spreading rate appears to show the 2/3 slope predicted by Eq. 3.46 at greater downstream distances. This is particularly apparent for flows with $F \approx 1$, Figure 5.8 and some with $F \approx 10$, Figure 5.9. Few of these flows show the 1/5 slope predicted by Eq. 3.56, except possibly H7, Figure 5.9, which may be approaching a 1/5 slope, and G6, Figure 5.10. These results suggest that these experiments do not extend far enough downstream to reach the regime where spreading is resisted mainly by interfacial shear.

For $F < 1$ an upstream wedge forms (for example, Figure 5.2). The length of the wedge, and hence the initial width of the surface field at the origin is strongly influenced by interfacial shear. Thus, it would be expected that the surface spreading is everywhere affected by shear. This is found in experiments G5 and G9, Figure 5.7. Experiment G5 shows the 1/5 slope predicted by Eq. 3.56, and G9 becomes a 1/5 slope

downstream from the source. Experiment G9 can, however, be made to fit a line of 1/5 slope exactly by means of a suitable origin shift.

Although the results show the linear, 2/3 and 1/5 slopes as predicted, the data are inadequate to definitely confirm these growth laws. Also, the transition coordinates between the regimes cannot be reliably predicted. The initial linear spreading for $F \geq 1$ predicted by Eq. 3.26 is confirmed, however, at least within the specified limits of F, L/H, and Reynolds number.

5.3.4 Profiles of Effluent Concentration

Profiles for $F \approx 0.1$ are shown in Figure 5.12. The profiles shown were measured vertically on the plume centerline and transversely just beneath the surface at several distances downstream. The results are plotted according to Eq. 3.17 with $\theta = 90°$, that is:

$$\frac{CuH}{q} = f\left(F, \frac{L}{H}, \frac{x}{L}, \frac{y}{H}, \frac{z}{L}\right) .$$

The results are found to be independent of L/H for $7.5 < L/H < 15$, so the profiles can be plotted as:

$$\frac{CuH}{q} = f\left(F, \frac{x}{L}, \frac{y}{H}\right) ,$$

for the vertical centerline profiles, and

$$\frac{CuH}{q} = f\left(F, \frac{x}{L}, \frac{2z}{L}\right)$$

for the surface profiles.

The thickness of the surface layer near the diffuser is about half the water depth, H. This is greater than the 0.3H layer thickness found for the two-dimensional frictionless flow (Section 2.3). The reason for this greater thickness and the slope of the interface apparent in Figure 5.12 is probably interfacial shear, which is more important in the three-dimensional case due to the formation of the upstream wedge and lateral spreading.

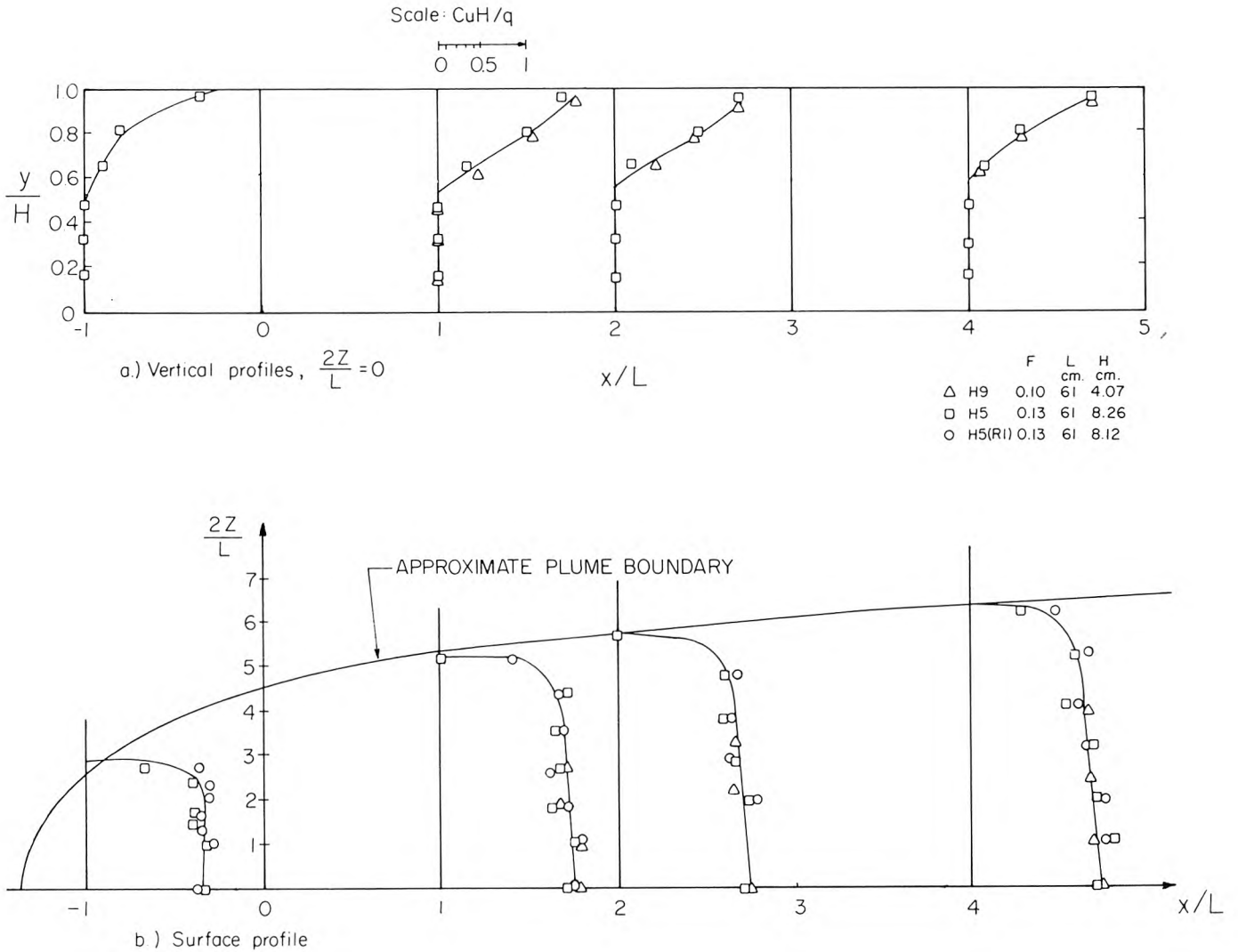

Figure 5.12 Normalized profiles of effluent concentration, C, for current flow perpendicular to diffuser, F ≈ 0.1. Distances of ordinates from axes are proportional to CuH/q: scale at top.

The surface effluent concentration varies slightly across the plume width, reaching a maximum at the centerline. The variation is due to three-dimensional effects resulting from the finite diffuser length. The plume was observed to be nearly vertical at the center, but to lean downstream at an angle which became increasingly steep towards the diffuser ends. Thus, the dilution increases, and hence concentration decreases towards the ends due to the longer entrainment path there. This effect can be seen in the photograph of Figure 5.2 as the curved light-colored band which is an indicator of the plume surfacing zone just downstream of the diffuser. (This light band also appears in the two-dimensional flow with no ambient current, region 3, Figure 2.5, visible also in the photograph, Figure A-3, Appendix A.)

The mixing process for $F \geq 1$ was discussed in Section 3.3.2. It was hypothesized, and confirmed by the results of the previous section, that the effluent would remain attached to the lower boundary for some finite distance downstream from the source. This is also apparent in the vertical centerline concentration profiles plotted in Figure 5.13 for $F \approx 1$, and Figure 5.14 for $F \approx 10$. These profiles correspond to those shown schematically in Figure 3.3. The results are plotted according to Eq. 3.30 close to the diffuser, that is:

$$\frac{CuH}{q} = f\left(F, \frac{x}{H}, \frac{y}{H}\right) .$$

Further from the diffuser Eq. 3.33 is applicable. However, the results are found to be independent of L/H and can be plotted as:

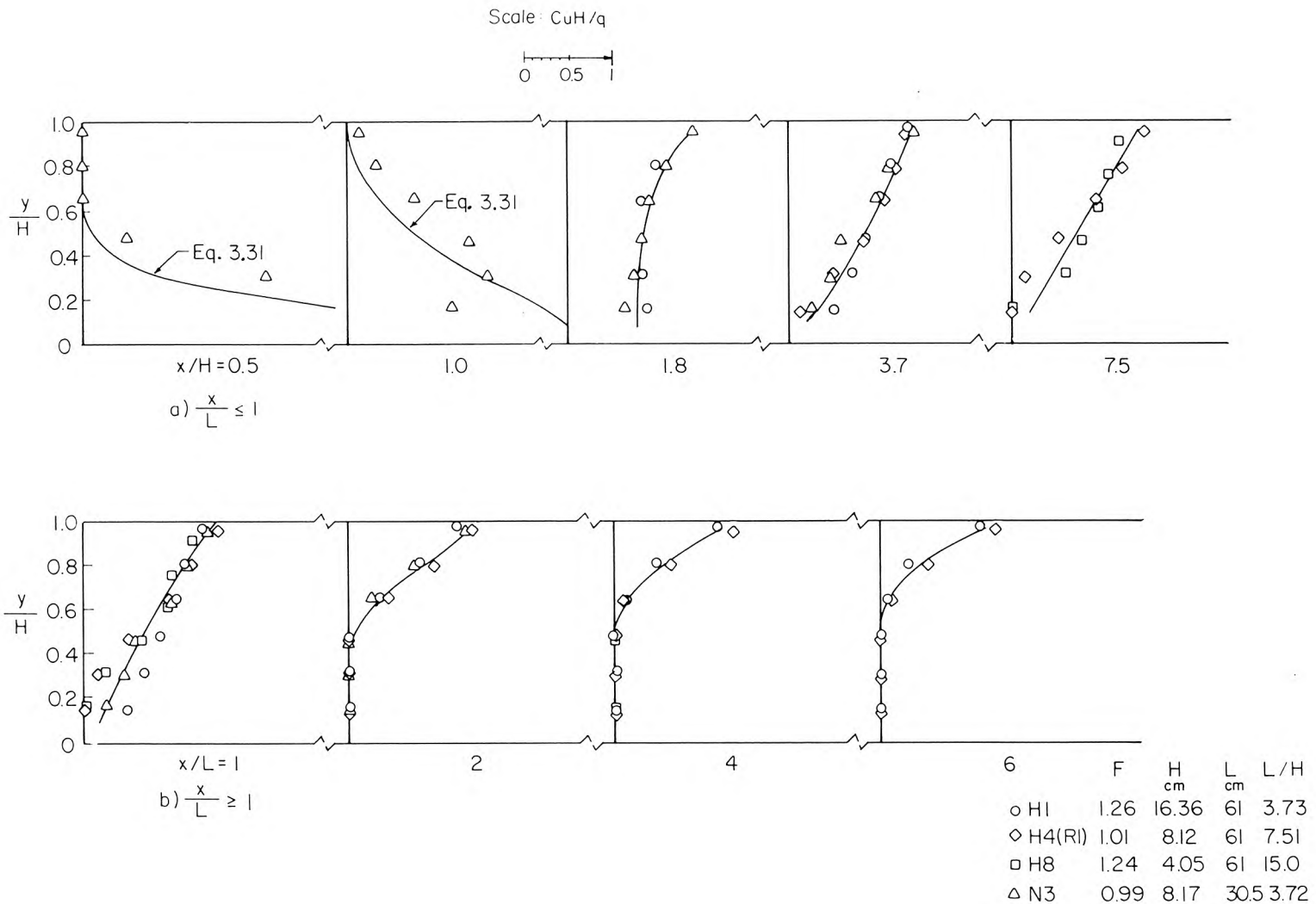

Figure 5.13 Normalized vertical profiles of effluent concentration, C, on centerline for current flow perpendicular to diffuser, F ≈ 1. Distances of ordinates from axes are proportional to CuH/q: scale at top.

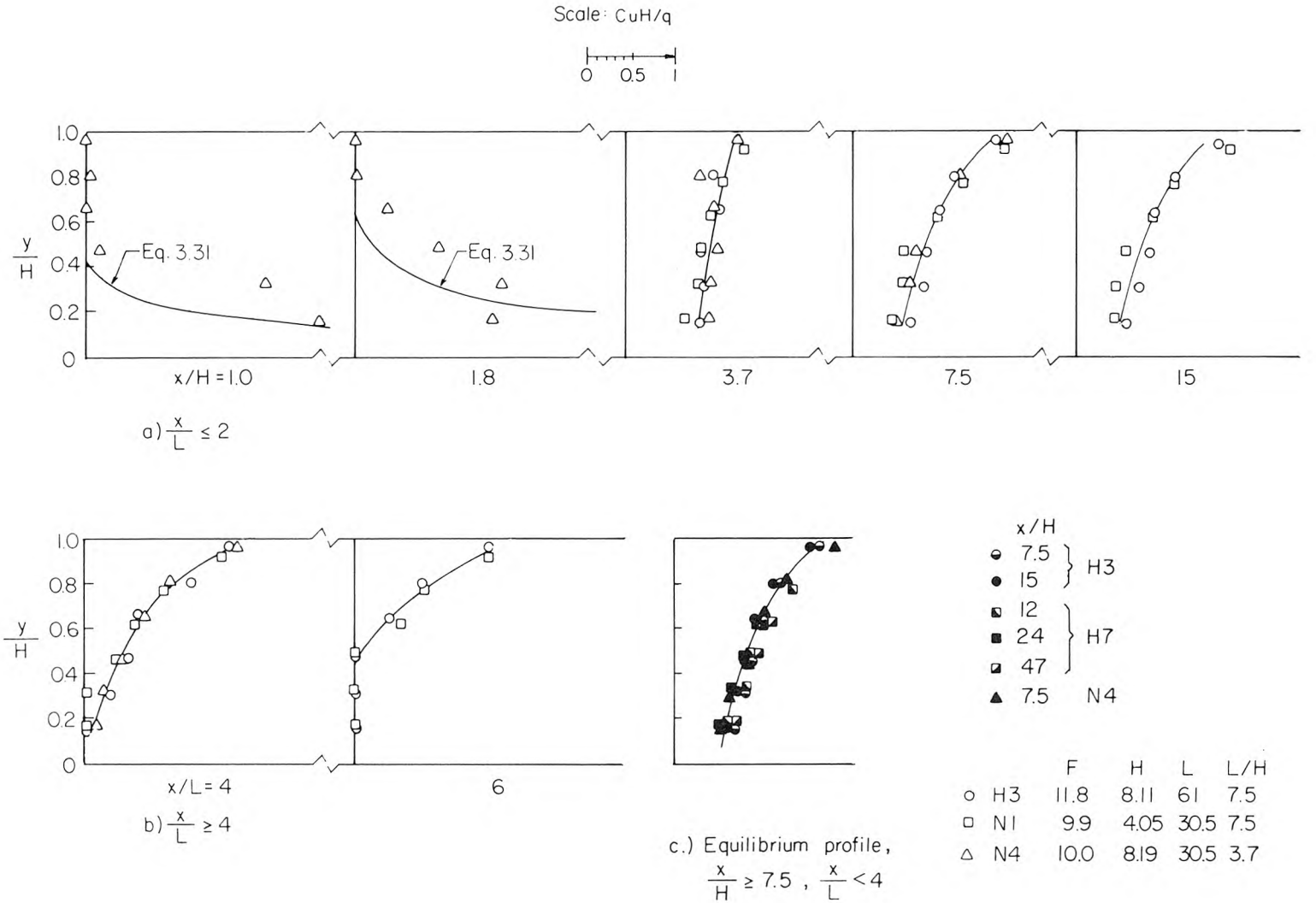

Figure 5.14 Normalized vertical profiles of effluent concentration, C, on centerline for current flow perpendicular to diffuser, F ≈ 10. Distances of ordinates from axes are proportional to CuH/q: scale at top.

$$\frac{CuH}{q} = f\left(F, \frac{x}{H}, \frac{y}{L}\right) .$$

Also plotted for the smallest values of x/H are the solutions for gravitational diffusion due to Rouse (1947), Eq. 3.31.

Rouse's solution does not give an accurate prediction in its region of validity. This is probably due to his assumption that the maximum concentration at any downstream distance occurs on the lower boundary. Examination of Rouse's data, and those presented by Taylor (1961), suggest that the maximum concentration occurs away from the lower boundary. These data show a shape more in agreement with the present results.

The decay in intensity of the buoyancy-induced fluctuations in concentration near the water surface are plotted in Figure 5.15. The results are plotted according to Eq. 3.37, that is:

$$\frac{\sqrt{\overline{C'^2}}}{C} = f\left(F, \frac{x}{H}\right) .$$

For $F \approx 1$, the relative concentration fluctuation intensity falls to 0.1 in a distance of about 4H. This distance is an estimate of the

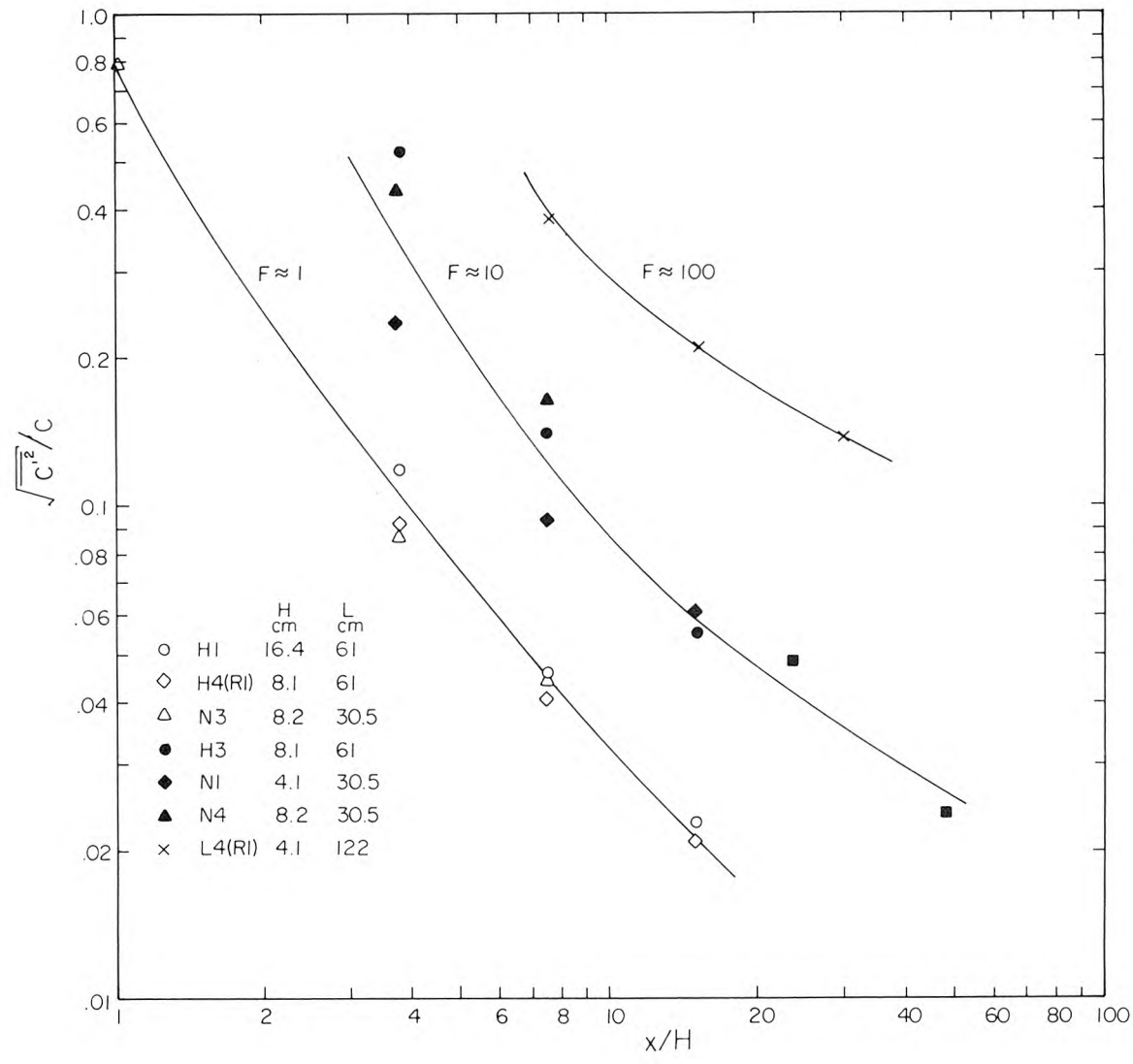

Figure 5.15 Decay in intensity of buoyancy-induced fluctuations of concentration on plume centerline near surface, perpendicular current.

mixing region length (Figure 3.3) which agrees with that found from the concentration profiles, Figure 5.13. For $x/H \geq 3.7$, the profile near the surface does not change with increasing distance downstream, x. The data nearer the lower boundary show considerable scatter, however, and the postulated equilibrium profile (Section 3.3.2) does not occur. This is probably due to three-dimensional effects with the ambient water reaching the center line before the mixing process is complete.

The equilibrium profile does, however, occur for F = 10, Figure 5.14. This is because the distance required for $\sqrt{\overline{C'^2}}/C$ to fall below 0.1 is now about 9H (Figure 5.15), which is considerably less than the distance for separation in these experiments. The equilibrium profile, Figure 5.14c, is seen to occur for $x \geq 7.5H$, a distance which agrees approximately with the 9H deduced above.

Several authors have proposed asymptotic expressions for dilution as $u \to \infty$. These expressions are based upon the assumption that the effluent becomes uniformly mixed over the receiving water depth at high current speeds. However, the vertical concentration profiles in the forced entrainment regime, Figures 5.13 and 5.14, show that for some Froude numbers this uniform mixing does not occur. For example, the equilibrium profile, Figure 5.14c, is clearly not uniform over the depth. This profile must be stable, hence the density must increase, and so the effluent concentration decrease, with depth below the free surface. Therefore, the minimum dilution at the surface must always

be less than that predicted by Eq. 2.7 (with $\theta = 90°$):

$$S_m = \frac{uH}{q} \quad ,$$

which assumes uniform mixing. Nonetheless, as $F \to \infty$, ambient turbulence should produce a uniform mixture ($S_m q/uH = 1$), but the present experiments do not show this result for $F \leq 10$. The results for minimum surface dilution will be discussed in Section 5.6.

Pearson (1956)(see Section 2.2) attempted to predict dilution in the forced entrainment regime by use of Rouse's gravitational diffusion analysis. As previously discussed, the effect of the free surface is to cause a stable layer of buoyant fluid to build up, which shifts the concentration maximum to the surface. Rouse's analysis, which only applies to a receiving fluid of infinite depth, is therefore not applicable.

The thickness of the surface layer after separation, Figures 5.13 and 5.14, is about half the receiving water depth. This is in agreement with the lock exchange analogy used in predicting the length of the lower boundary attachment, Section 3.3.1.

5.4 Dispersion in a Parallel Current

5.4.1 Photographs of Surface Plumes

A photograph of the surface plume produced when a current flows parallel to the line diffuser is shown in Figure 5.16. Photographs showing the effect of varying the Froude number are presented in Figure 5.17.

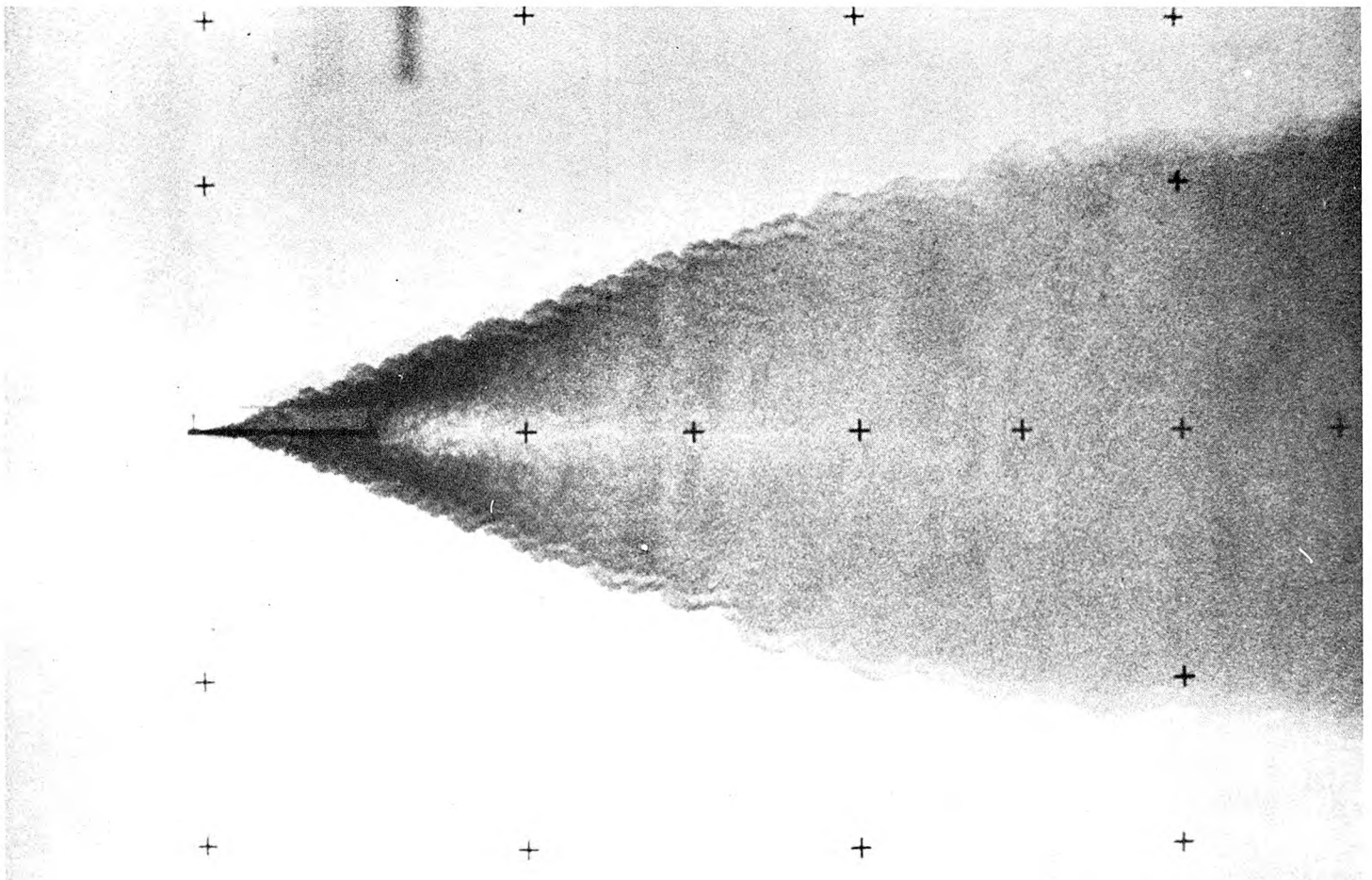

Figure 5.16 Photograph of surface plume in a parallel current: J3, F ≈ 10.

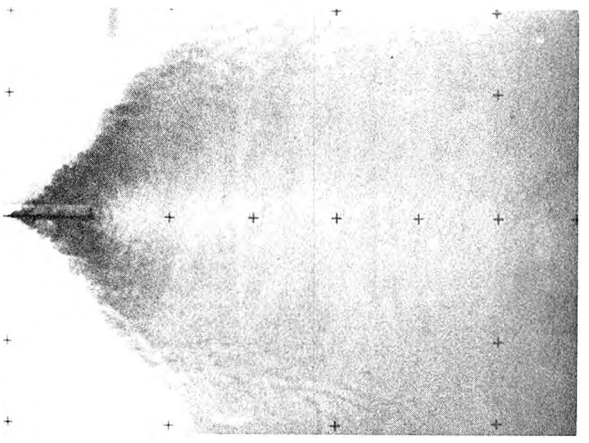

J1, $F \approx 1$

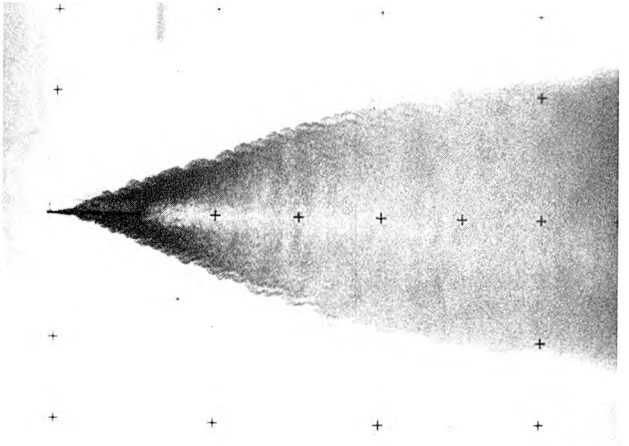

J3, $F \approx 10$

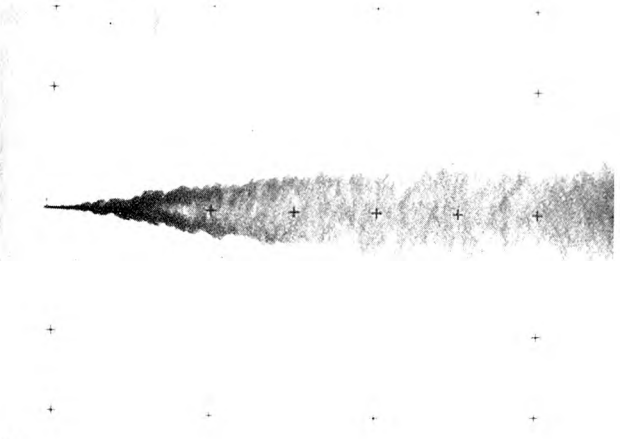

J6, $F \approx 100$

Figure 5.17 Photographs of surface plumes in a parallel current.

5.4.2 Initial Surface Spreading

The photographs of Figure 5.17 show the initial surface spreading to be linear, as predicted by the analysis of Section 3.4. The width of the surface field, w_o, at the end of the diffuser was measured from the photographs. The results and the prediction, Eq. 3.42, are plotted in Figure 5.18. The results confirm the analysis, and show the initial spreading to be independent of L/H at least for $3.75 < L/H < 15$ and Reynolds number at least for $2500 < Re < 12{,}740$.

5.4.3 Effluent Concentration Profiles

Vertical and near surface effluent concentration profiles for parallel currents are shown in Figure 5.19 through 5.22. The results are plotted according to Eq. 3.33. Again, the results are found to be independent of L/H for $3.75 < L/H < 15$, and can be expressed as:

$$\frac{CuH}{q} = f\left(F, \frac{y}{H}, \frac{x}{L}\right) .$$

A characteristic feature of dispersion in a current parallel to the diffuser are the light areas centered immediately behind the diffuser. These are visible in the photographs, Figures 5.16 and 5.17, and are also manifest in the concentration profiles. This area is thinner and more highly diluted than the rest of the surface layer, and possibly results from two effects. The first is the production of a wake by the buoyant discharge, similar to that produced by a flat plate in a uniform flow. The second is vortices induced by the vertical motions of the buoyant effluent. Thus, the ambient flow immediately behind the diffuser is a paired vortex, with a downstream velocity less than u. This

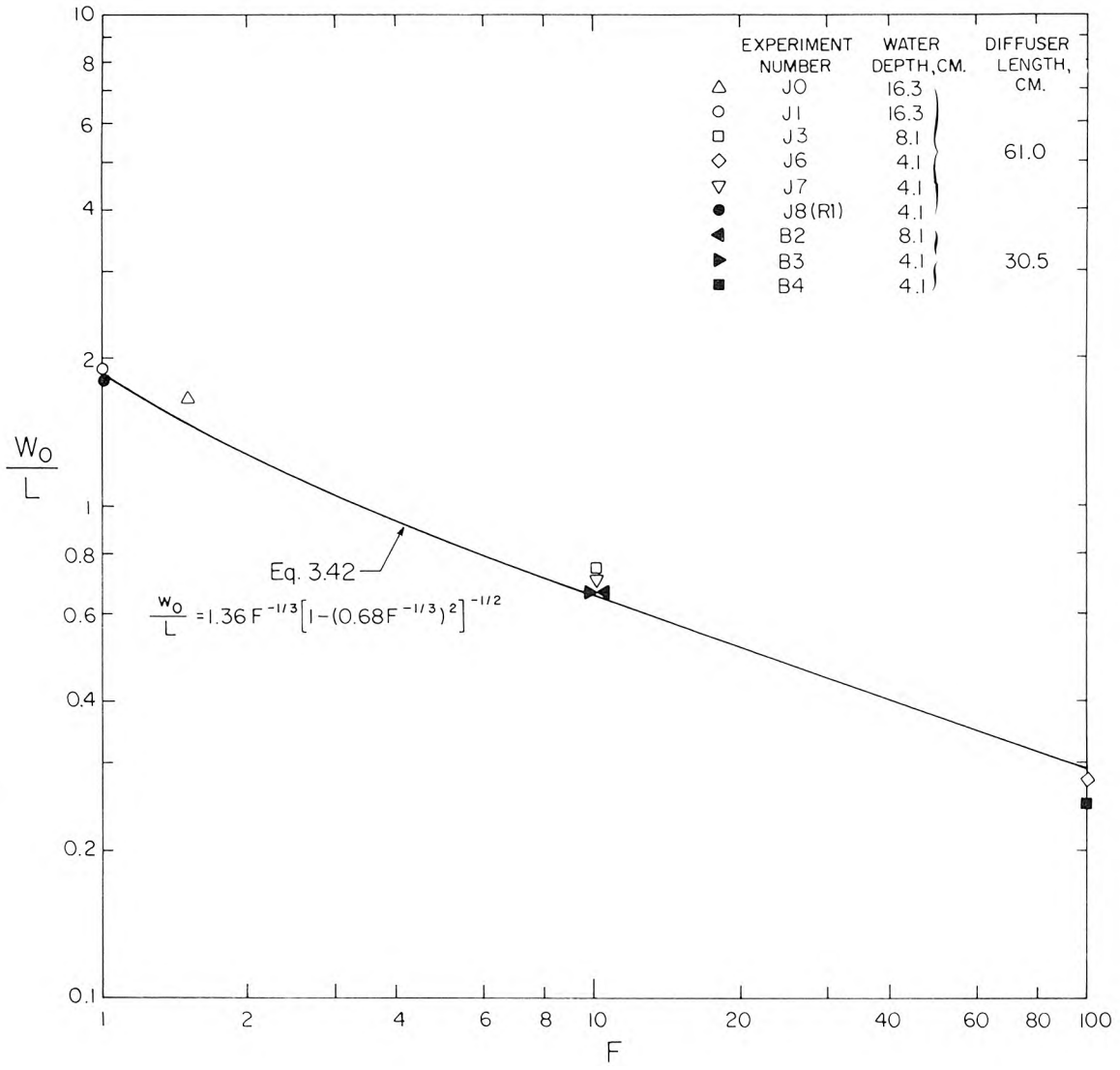

Figure 5.18 Surface field width (w_o) at downstream end of line diffuser for current parallel to diffuser.

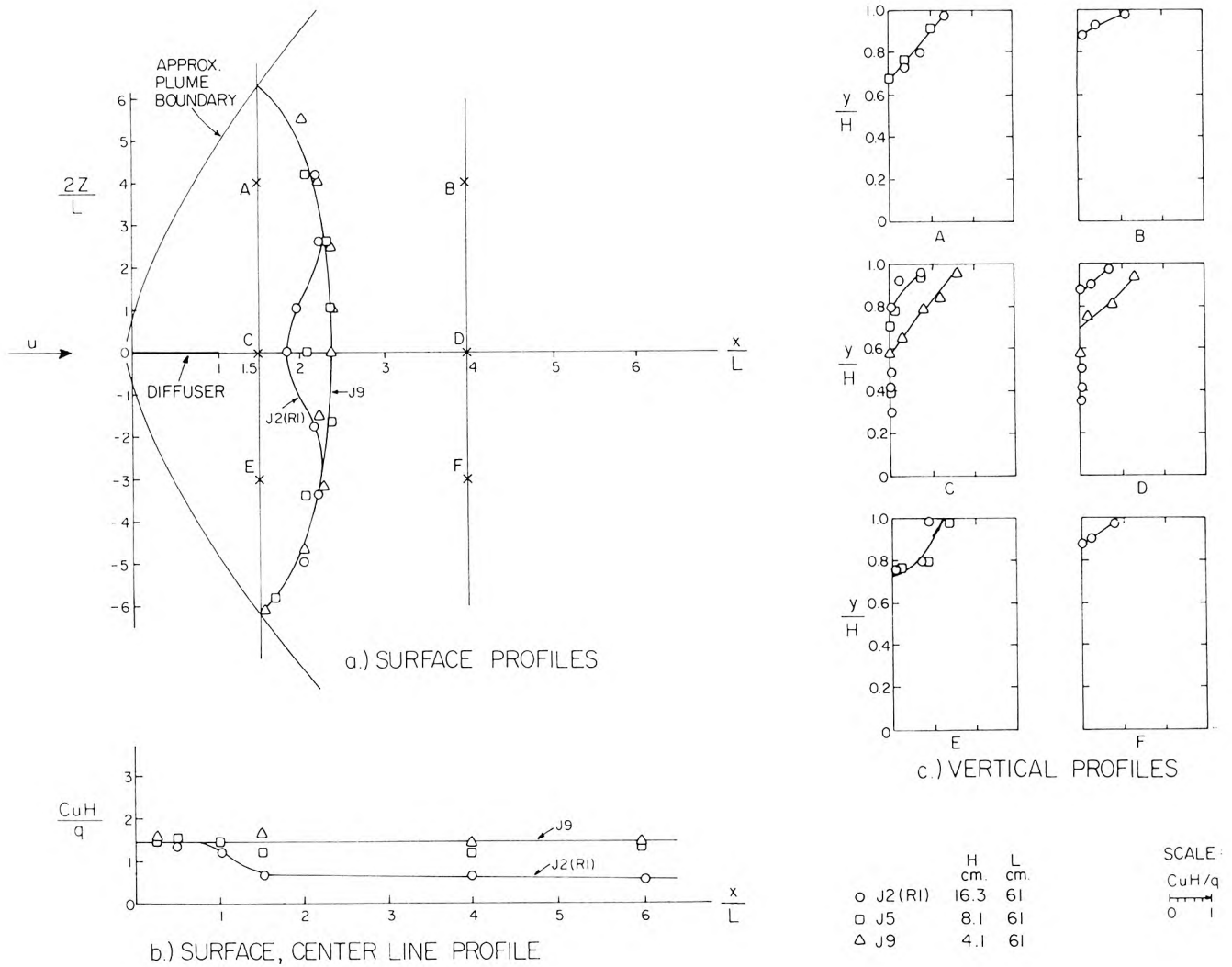

Figure 5.19 Normalized profiles of effluent concentration, C, for current flow parallel to diffuser, F ≈ 0.1. Distances of ordinates from axes are proportional to CuH/q: scale at lower right.

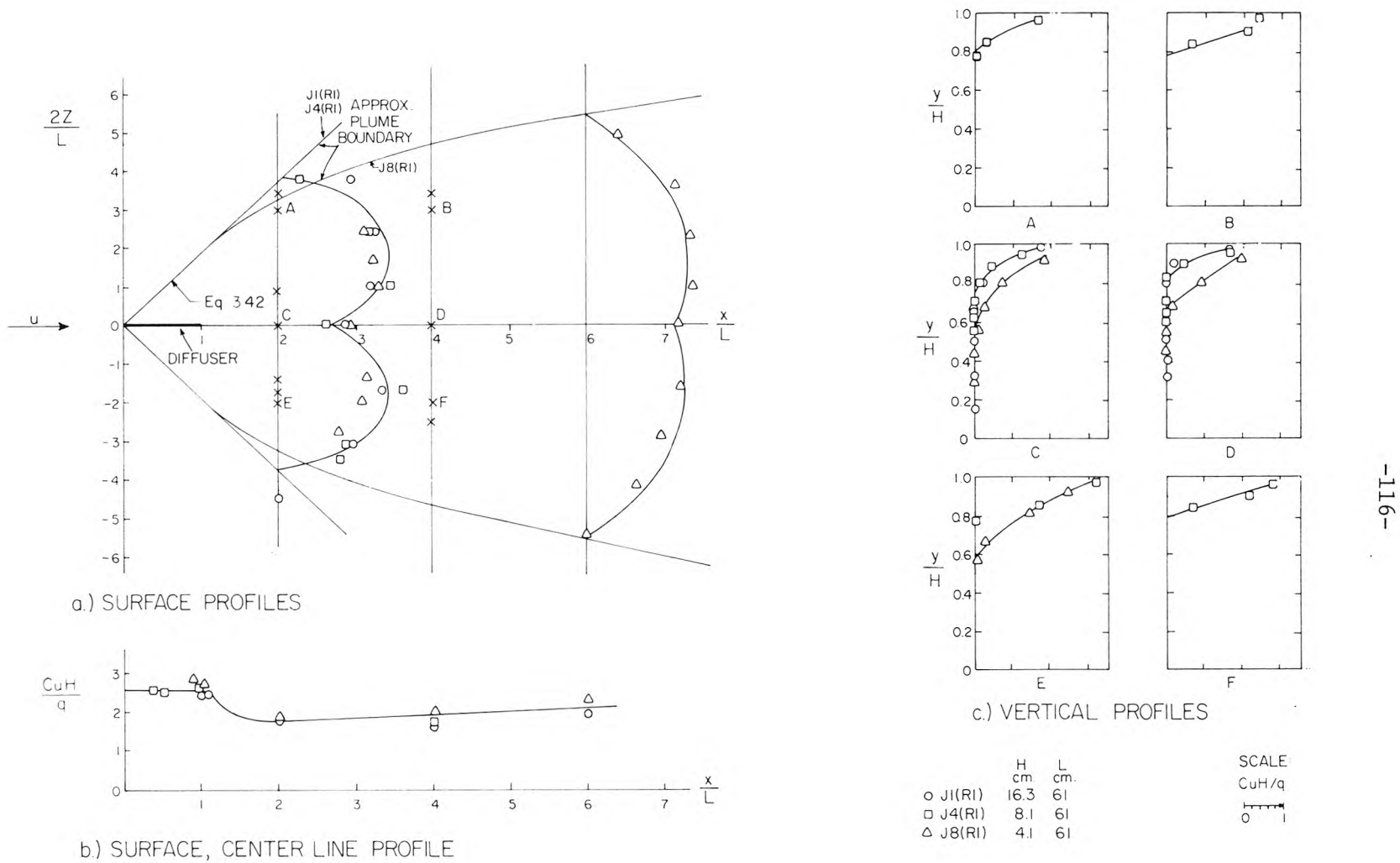

Figure 5.20 Normalized profiles of effluent concentration,C, for current flow parallel to diffuser, F ≈ 1. Distances of ordinates from axes are proportional to CuH/q: scale at lower right.

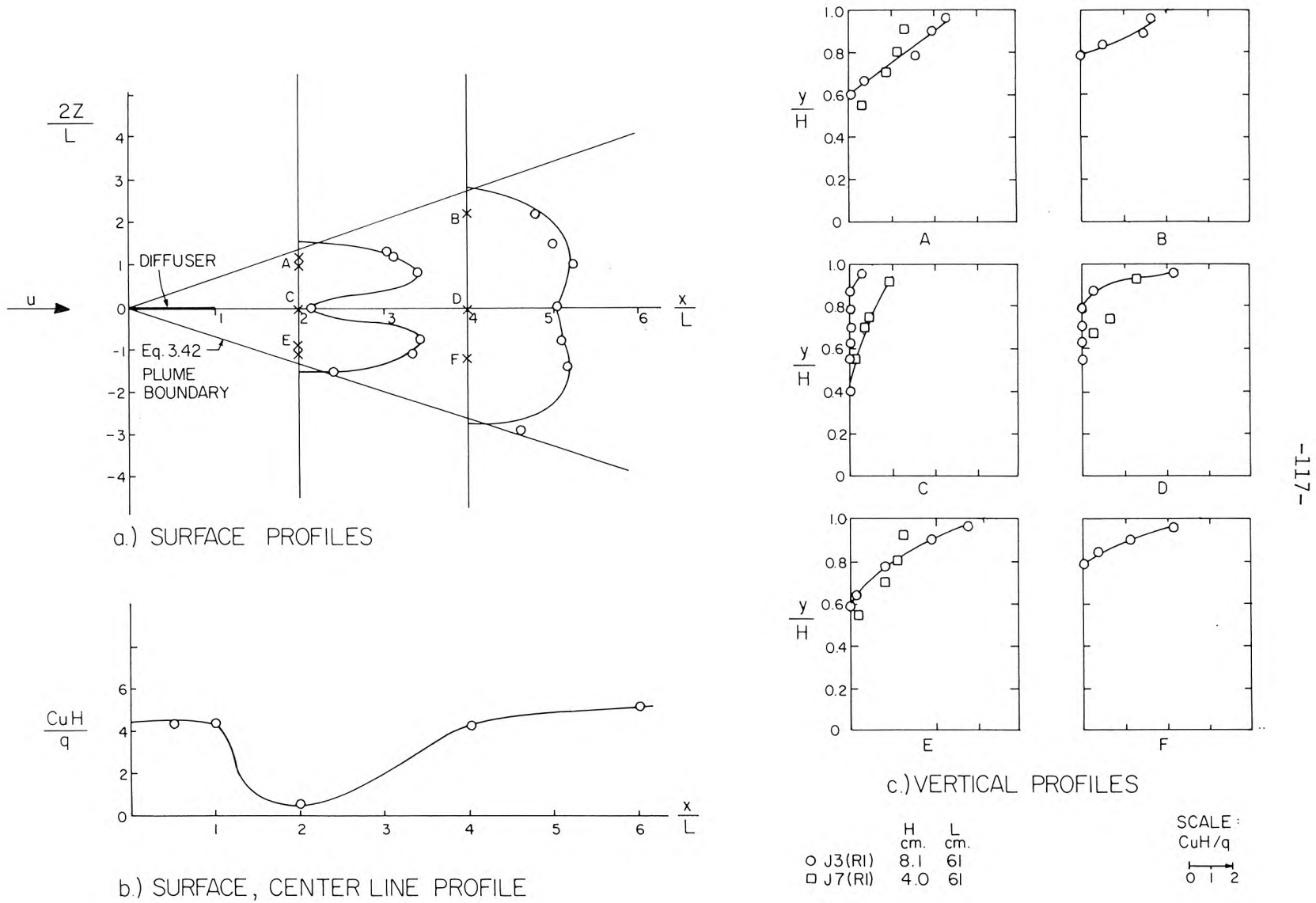

Figure 5.21 Normalized profiles of effluent concentration, C, for current flow parallel to diffuser, F ≈ 10. Distances of ordinates from axes are proportional to CuH/q: scale at lower right.

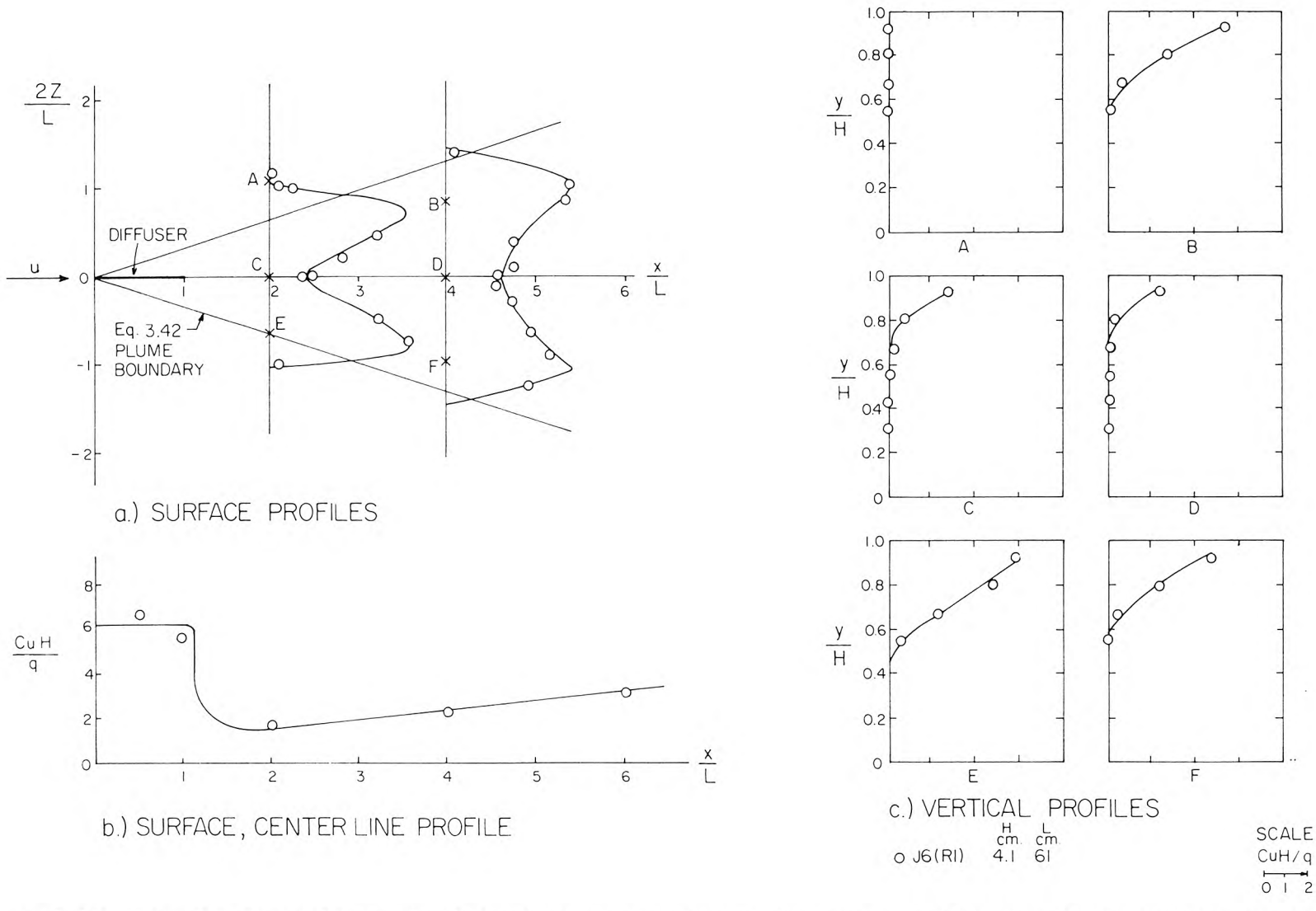

Figure 5.22 Normalized profiles of effluent concentration, C, for current flow parallel to diffuser, $F \approx 100$. Distances of ordinates from axes are proportional to CuH/q: scale at lower right.

flow is illustrated in Figure 5.23. The vertical motion of the ambient flow

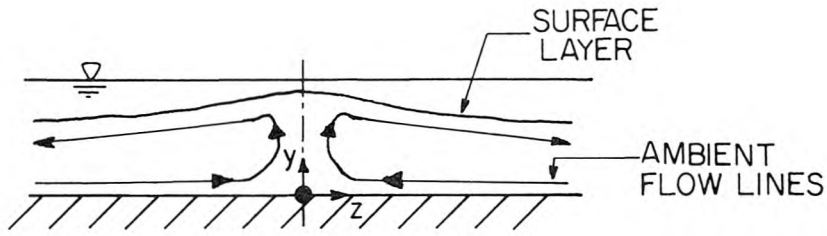

Figure 5.23 Vertical profile at downstream end of diffuser showing postulated flow field.

near the centerline possibly causes the thinning of the surface layer there. Only the shallow-water low-Froude number experiment (J9, Figure 5.19) does not show this effect. This is probably due to the greater relative effect of viscosity at shallower depths. It is possible that the friction damps the vortices and reduces the lateral surface spreading rate, resulting in elimination of this lighter zone.

The centerline surface concentration is fairly uniform up to the end of the diffuser. Beyond that point, the concentration drops suddenly as the "light" zone is reached. Thereafter, the concentration increases slowly with distance downstream due to horizontal mixing and spreading, as illustrated in the surface profiles of Figures 5.20, 5.21, and 5.22. Only for F = 0.1, Figure 5.19 (J9) is this increase with distance not observed. This is due to the rapid outward spreading for this case, which apparently reduces the inward spreading and mixing. In general, the surface concentration profiles transverse to the flow direction have a bimodal shape, becoming more uniform with distance downstream. The minimum surface dilution occurs to the sides of the

diffuser, before any significant horizontal mixing has occurred. The minimum surface dilution will be discussed further in Section 5.6.

The effluent forms a two-layer flow immediately, even for very strong current speeds. This two-layer flow can be seen in the vertical concentration profiles of Figure 5.19 through 5.22. Even for a Froude number of 100 (Figure 5.22), the two-layer flow still forms immediately. This is in contrast to the dispersion pattern produced by a current perpendicular to the diffuser. In this situation, the effluent remains attached to the lower boundary for some distance downstream if $F > 0.2$.

The initial surface layer thickness is about 40% of the water depth for $F \geq 1$, Figures 5.20 to 5.22. This is greater than the 30% predicted by Koh and Brooks (1975). However, the thickness, h, is not uniform in a plane transverse to the current direction, particularly just downstream of the diffuser where it can be as small as 0.1H. At greater distances downstream, the layer becomes thinner and more uniform as it spreads horizontally. The relative layer thickness, h/H, may be larger at shallower water depths due to an interfacial slope which develops to overcome shear. For example, the experiments performed at 4 cm water depths show larger values of h/H than those in deeper waters (see Figures 5.19 to 5.21).

5.5 Dispersion at Intermediate Angles

5.5.1 Photographs of Surface Plumes

A few experiments were performed with the diffuser orientated at a 45° angle to the current. A photograph of the surface plume for $F = 1$ is shown in Figure 5.24. Photographs of the surface

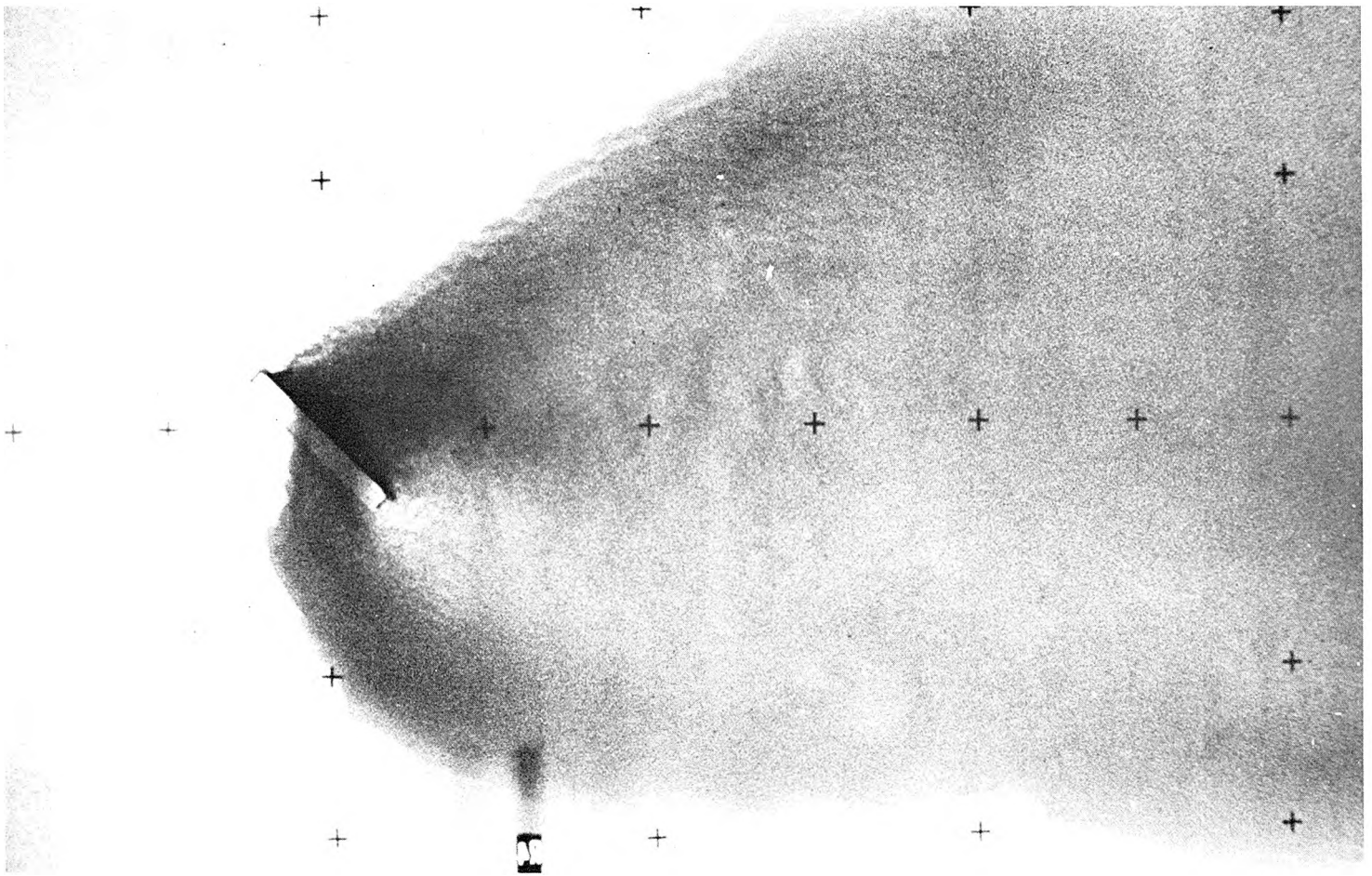

Figure 5.24 Photograph of surface plume in a 45° current. R4, $F \approx 1$.

plume for F = 1, 10, and 100 are shown in Figure 5.25.

For F = 1, Figures 5.24 and 5.25a, the surface layer forms not only an upstream wedge but also a light zone immediately behind the diffuser. The upstream wedge is characteristic of a perpendicular current for $F < 1$ (Figure 2.3). For $\theta = 45°$, however, it forms only along part of the diffuser length. Also, the plume leans more steeply downstream at the leading edge. These observations suggest that the ambient flow is deflected, becoming more parallel to the diffuser as it approaches the downstream diffuser end. Thus, the ratio u_p^3/b, where u_p is the local velocity perpendicular to the diffuser, probably varies along the diffuser length. It may fall below 1 at some point, causing the upstream wedge formation. Because the ambient flow is more nearly parallel to the diffuser at the end, the light zone forms there, as in the parallel current case discussed in Section 5.4. This flow ($\theta = 45°$, $F \approx 1$) is therefore of a "hybrid" nature, having characteristics common to current flows both perpendicular and parallel to the diffuser.

For stronger currents the flow becomes more like that found in flows perpendicular to the diffuser. For example, in Figure 5.25b (R3), a zone of lower boundary attachment is seen, extending the full diffuser length. A similar flow is seen for F = 100, Figure 5.25c (R6).

5.5.2 Effluent Concentration Profiles

Profiles for F = 10 are shown in Figure 5.26. The flow is similar to that for a current flowing perpendicular to a diffuser whose length is equal to the projected length of the oblique diffuser. The vertical profiles show the effluent to remain initially attached to the

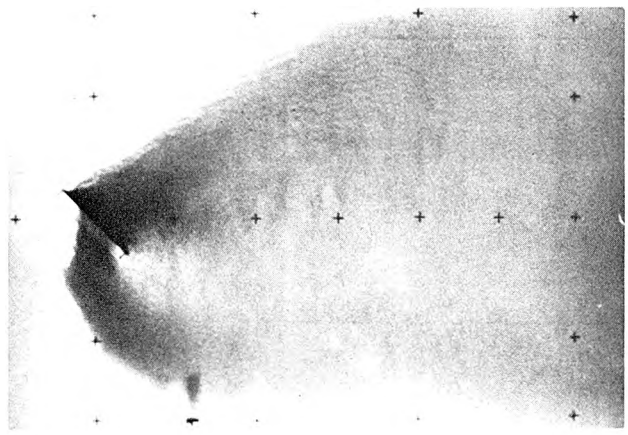

R4, $F \approx 1$

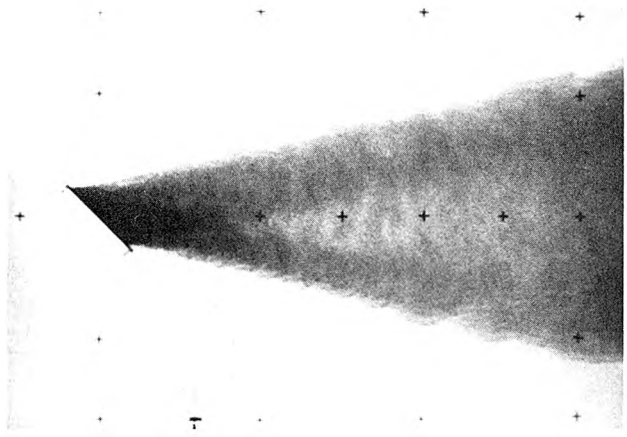

R3, $F \approx 10$

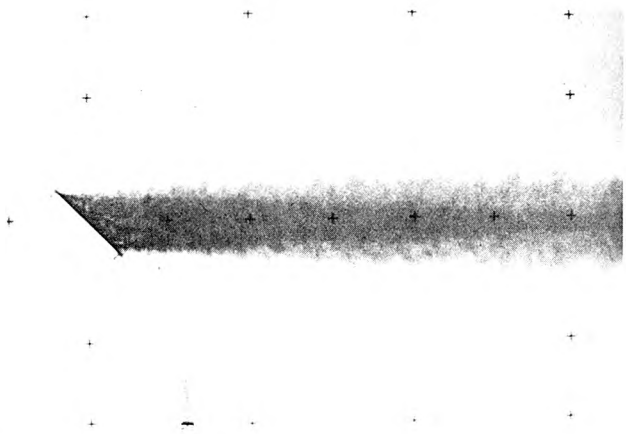

R6, $F \approx 100$

Figure 5.25 Photographs of surface plume in a 45° current at different values of the Froude number, F.

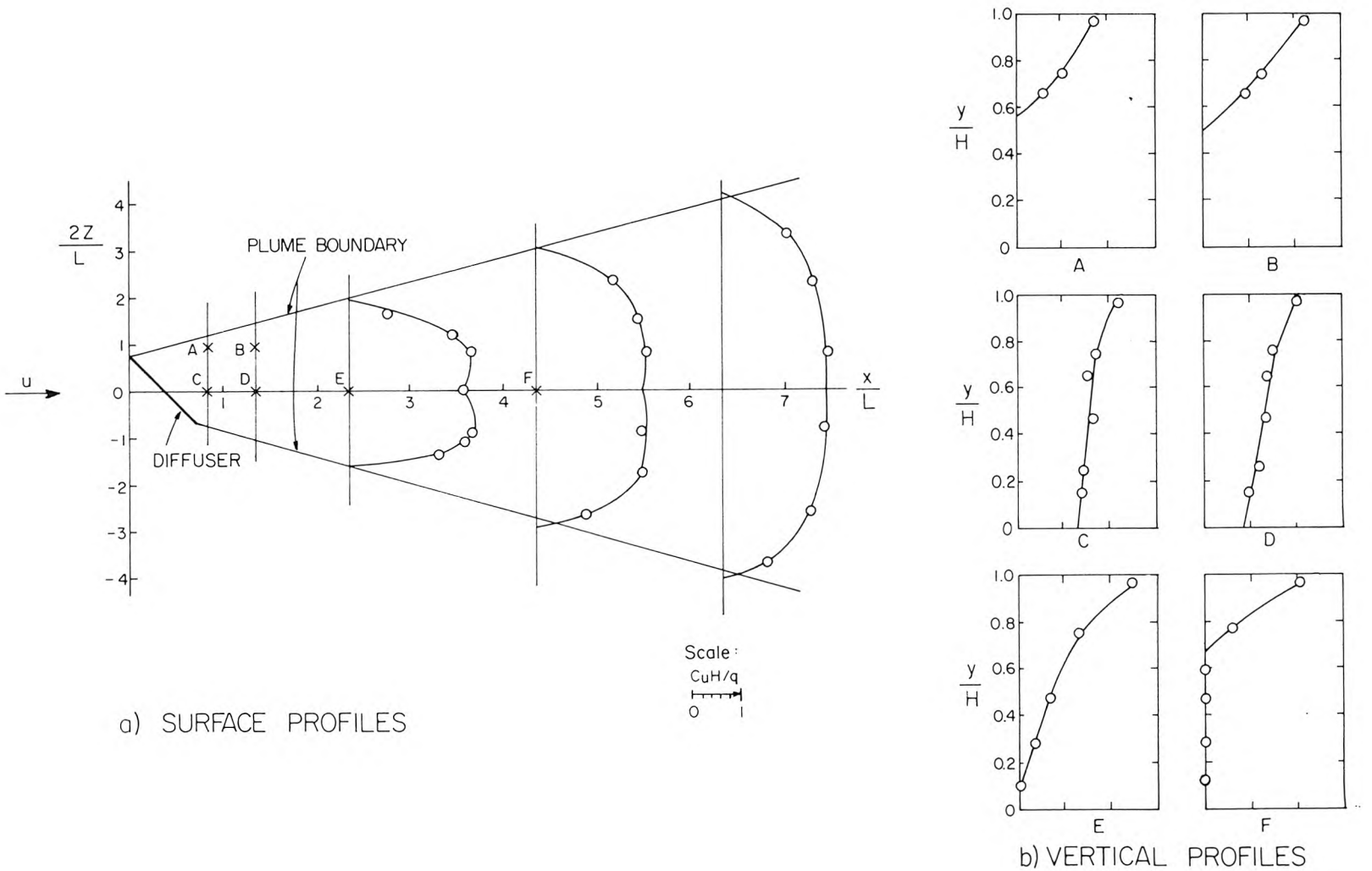

Figure 5.26 Normalized profiles of effluent concentration, C, for current flow at a 45° angle to the diffuser. Distances of ordinates from axes are proportional to CuH/q: scale in middle.

lower boundary and to form a two-layer flow further downstream. The thickness of the surface layer outside the zone of lower boundary attachment, but before separation has occurred is about 50% of the water depth, as in the perpendicular case.

5.6 Minimum Surface Dilution

The measurements of minimum surface dilution are plotted in Figure 5.27 according to Eq. 3.7. The results are independent of L/H for $3.75 < L/H < 30$ within the limits of experimental error, and so can be expressed as:

$$\frac{S_m q}{uH} = f(F, \theta) \quad . \tag{5.4}$$

Eq. 3.12, the asymptotic solution as $F \to 0$ is also plotted. A value of K_4 equal to 0.27 fits the data better than the 0.29 value predicted by assuming two-dimensional flow in a stagnant ambient fluid. Hence, the asymptotic solution is:

$$\frac{S_m q}{uH} = 0.27F^{-1/3} \tag{5.5}$$

or

$$\frac{S_m q}{H} = 0.27b^{1/3} \quad .$$

This solution applies for F less than about 0.1 (Figure 5.27). In other words, the current does not affect dilution for $F < 0.1$. In the forced entrainment regime, the minimum surface dilution was often observed to lie off the centerline. This can be seen in the surface profiles of Figure 5.26. This may be due to the flow of ambient water towards the centerline, causing the elements of effluent to rise more rapidly to the surface than would occur for two-dimensional gravitational

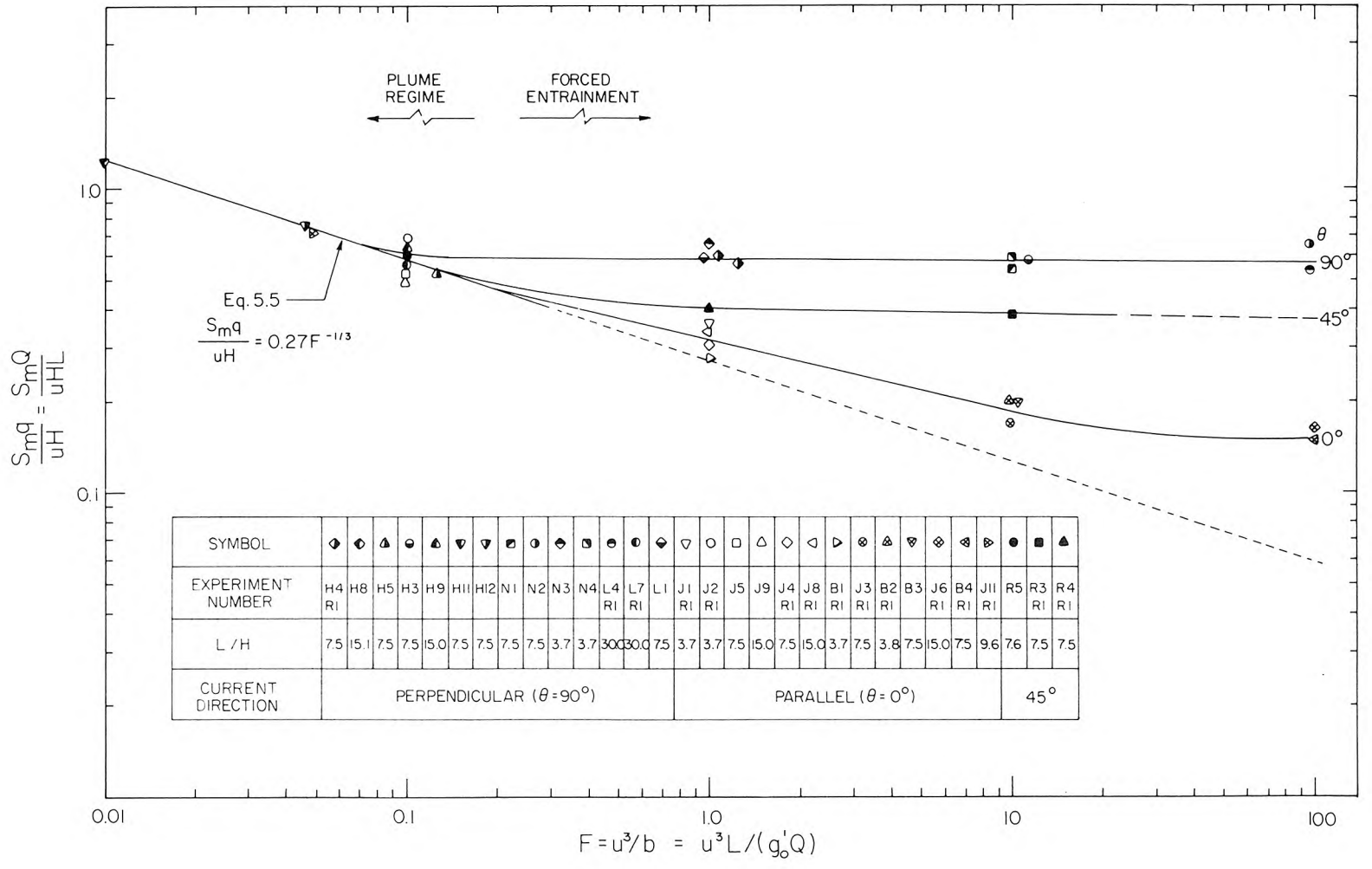

Figure 5.27 Experimental measurements of minimum surface dilution for a finite line source of buoyancy flux in a current.

diffusion. This forced rate of rise may afford the effluent less opportunity to mix and hence to become less diluted than on the centerline. However, this transverse variation of surface concentration was comparable with the experimental errors, so this effect may not be real.

Values of $S_m q/uH$ lying above the asymptotic solution, Eq. 5.5, represent an increase in dilution due to the current. This increase for current flow parallel to the diffuser is much less than for a perpendicular current. The difference becomes more pronounced as the Froude number increases. In the parallel case, the effect of current on dilution is not significant until F is greater than about 1. For a Froude number of 100, the dilution is about 2.5 times greater than with no ambient current. If the flow is perpendicular to the diffuser, the dilution is about 10 times greater than that with no current for $F = 100$. Hence, at $F = 100$, a diffuser four times as long would be required for equal dilutions if the ambient flow is parallel to the diffuser compared to flow perpendicular to it.

Photographs of the surface plume in currents perpendicular and parallel to the current, respectively, are shown in Figures 5.3 and 5.16. Other conditions are equal, and $F \approx 10$. The width of the surface field beyond a distance of 3L downstream is independent of the current direction (see also Figure 5.25, R3 for $\theta = 45°$, $F \approx 10$). The vertical concentration profiles of Figures 5.14 and 5.21 show the surface layer to be thinner in the parallel case than the perpendicular one. In general, a diffuser oriented parallel to the ambient flow results in a thinner,

more concentrated surface waste field of comparable lateral extent than a diffuser perpendicular to the current.

The asymptotic expression as $F \to \infty$ for dilution with current flow perpendicular to the diffuser was discussed in Section 5.3.4. It was shown that there is a range of Froude numbers where the effluent does not mix uniformly over the receiving water depth. This is due to the development of a stable density profile. The asymptotic solution assuming uniform mixing which has been proposed by several authors is

$$\frac{S_m q}{uH} = 1 \quad . \tag{5.6}$$

Although this equation probably applies for very large values of F (u large or b small), the range of F (up to 100) in these experiments did not show this result. Values of $F > 100$ are probably not of practical interest for sewage outfalls in the ocean. The observed ratio $S_m q/uH$ is essentially constant at about 0.58 for $0.1 < F < 100$, $3.7 < L/H < 30$, and $2{,}800 < \frac{4uH}{\nu} < 12{,}000$. Furthermore, this uniformity suggests that the shape of the equilibrium profile discussed in Section 3.3.2 and shown in Figure 5.14c is not a strong function of F.

The results for $\theta = 0°$ and $90°$ are limiting cases. Intermediate current directions result in dilutions lying between them as do those for $\theta = 45°$ (Figure 5.27).

CHAPTER 6

DISCUSSION

6.1 Example of Procedure for Predicting Dilutions for Multiport Diffusers

The present study has investigated the dispersion of buoyant effluent from a line approximating a source of buoyancy flux only. The receiving fluid is of uniform density and moves at a steady speed in an arbitrary direction relative to the line source. The minimum surface dilution, S_m, can be expressed as

$$\frac{S_m q}{uH} = f(F,\theta) \quad , \tag{6.1}$$

where q is the volume flux of effluent per unit diffuser length, u the current speed, H the water depth, and θ the angle of the current to the diffuser, as shown in Figure 2.1. F is a type of Froude number defined by $F = u^3/b$, where b is the buoyancy flux per unit diffuser length, defined by Eq. 2.1. The experimental results are plotted in Figure 5.27. In this section procedures which should be followed in using these results to predict dilution for a multiport diffuser are outlined and an example is given.

The flow has different regimes depending on the values of F and θ. In order to predict dilution, the first step is to find which regime the flow belongs to by computing F and θ. If F is less than about 0.1 the flow is in the plume regime, Figure 2.3a, and dilutions can be estimated by neglecting the current. The asymptotic solution as $F \to 0$,

Eq. 5.5:

$$\frac{S_m q}{uH} = 0.27F^{-1/3} \quad , \tag{6.2}$$

can be used as a first estimate provided the diffuser is well represented as a line source of buoyancy.

The degree to which the flow approaches that due to a line plume depends primarily on the source momentum flux of each port, the port spacing, and the receiving water depth. An estimate of dilution which takes account of these factors can be made by following the methods of Roberts (1975)(reproduced as Appendix B). It is shown there that the minimum dilution, S_m, at height y above a multiport diffuser discharging round jets whose diameter and velocity at the vena contracta are D_e and u_e can be expressed as

$$\frac{S_m}{F_e} = f\left(\frac{y/D_e}{F_e} , \frac{y}{\ell}\right) . \tag{6.3}$$

ℓ is the average port spacing, given by:

$$\ell = L/n \quad , \tag{6.4}$$

where L is the diffuser length and n the total number of ports. F_e is an effective jet Froude number defined at the vena contracta by

$$F_e = \frac{u_e}{\sqrt{\frac{\Delta\rho}{\rho_o} g D_e}} = \frac{u_e}{\sqrt{g_o' D_e}} \quad . \tag{6.5}$$

If C_c is the coefficient of jet contraction, defined by

$$C_c = \left(\frac{D_e}{D_o}\right)^2 \quad , \tag{6.6}$$

where D_o is the port diameter, then from mass conservation:

$$u_e = u_o/C_c \quad , \tag{6.7}$$

where u_o is the jet velocity at the port. It then follows that the jet Froude number at the port, F_o, where

$$F_o = \frac{u_o}{\sqrt{g_o' D_o}} \quad , \tag{6.8}$$

is related to the effective Froude number F_e by:

$$F_e = C_c^{-5/4} F_o \quad . \tag{6.9}$$

Eq. 6.3 is only valid if the initial jet volume flux is negligible. This is true for $F_e > 8$, which covers most sewage outfalls. The functional relationship of Eq. 6.3 is shown in Figure 5, Appendix B, as contours of constant values of S_m/F_e on a plot of $(y/D_e)/F_e$ versus y/ℓ.

To estimate dilution, the values of y/ℓ and $(y/D_e)/F_e$ are first computed. For $y/\ell < 5$ no dilution reduction due to jet interaction occurs, Figure 5, Appendix B, and results for isolated round buoyant jets, Figure 4, Appendix B, should be used. For $y/\ell > 5$ the dilution is reduced compared to that of an individual jet at the same height due to jet interference, and Figure 5 should be used for dilution estimation. The closer the upper right corner of Figure 5 is approached,

the closer is the flow to that due to a line plume. This is the region where Eq. 6.2 gives a reliable estimate. Whereas Eq. 6.2 includes the reduction in dilution due to the surface layer, Figure 5, Appendix B, does not, so corrections should be made to account for this effect. An example of the procedure outlined above is given in Section 6.3.

The effect of the ambient current on dilution cannot be neglected if F ($= u^3/b$) is greater than about 0.1. The minimum surface dilution then depends on F and the orientation, θ, of the diffuser to the current; the results of the present study, Figure 5.23, should be used if $H/\ell > 5$ and $F > 0.1$.

As an example of dilution prediction the 120 inch outfall of the Los Angeles County Sanitation Districts is considered. The diffuser, shown in Figure 6.1, has a length, L, of 4440 feet (1353 m), and is oriented parallel to the coast except for a small portion on the near-shore end. The ratio of water depth to port spacing, H/ℓ is 32, and $(H/D_e)/F_e$ is greater than 20 (Roberts (1975)). Hence, with no ambient current, the effluent flow and dilution near the surface should closely approximate that resulting from a line plume (Figure 5, Appendix B). It follows that the line plume approximation should be even better when the receiving water is moving, as the resulting longer jet trajectories afford better opportunity for merging of the individual jets.

The average daily flow rate, Q, through the outfall is about 210 million gallons per day (9.20 m^3/s). A density difference of 0.026 g/cc between the sewage and sea water is assumed. The buoyancy flux, b, per unit length is then given by Eq. 2.1 as

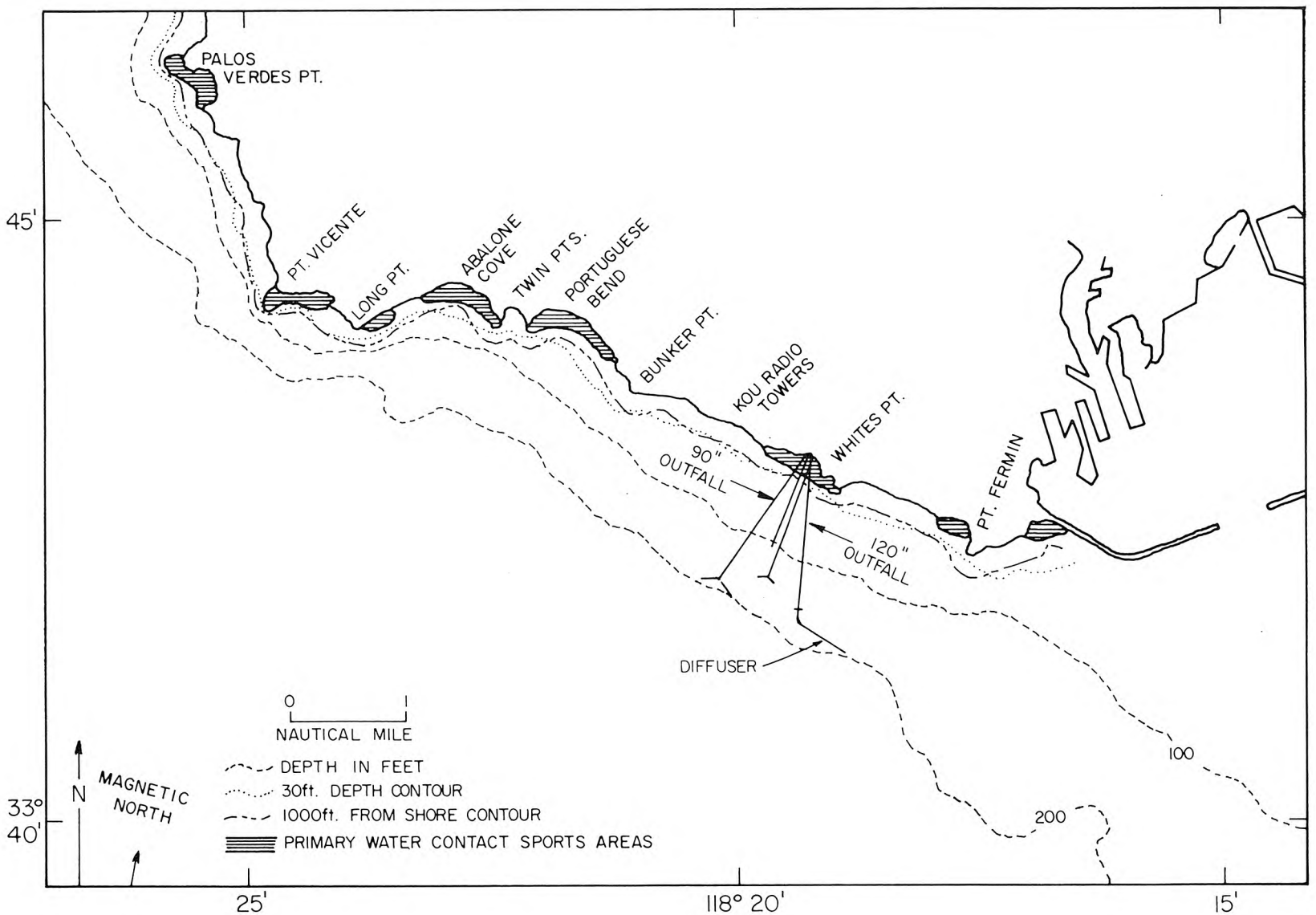

Figure 6.1 Ocean outfalls of the Los Angeles County Sanitation Districts.

$$b = \frac{\Delta\rho}{\rho_o} g \frac{Q}{L} = \frac{0.026}{1.000} \times 9.81 \times \frac{9.20}{1353}$$

$$= 1.73 \times 10^{-3} \ m^3/s^3 \quad .$$

The expected dilutions can now be computed from Figure 5.23. For example, a current speed, u, of 0.3 knot (0.154 m/s) corresponds to a Froude number, F of

$$F = \frac{u^3}{b} = \frac{(0.154)^3}{1.73 \times 10^{-3}} = 2.11 \quad .$$

For currents flowing perpendicular and parallel to the diffuser, Figure 5.23 gives $S_m q/uH$ as 0.58 and 0.26, respectively. The minimum surface dilution S_m in a water depth, H, of 200 feet (61.0 m) is then estimated as:

$$S_m = 0.58 \frac{uHL}{Q} = 0.58 \frac{0.154 \times 61.0 \times 1353}{9.20}$$

$$= 800, \text{ for a perpendicular current,}$$

and

$$S_m = 0.26 \frac{uHL}{Q} = 0.26 \times \frac{0.154 \times 61.0 \times 1353}{9.20}$$

$$= 360, \text{ for a parallel current.}$$

Similarly, dilutions for other current speeds were estimated. The results are shown in Figure 6.2. This figure is an updated version of Figure 12 in Roberts (1975). (The reader is reminded that these results are for the case of no ambient density stratification; with stratification, the effluent cloud usually does not rise to the surface, and lower initial dilutions would be expected.)

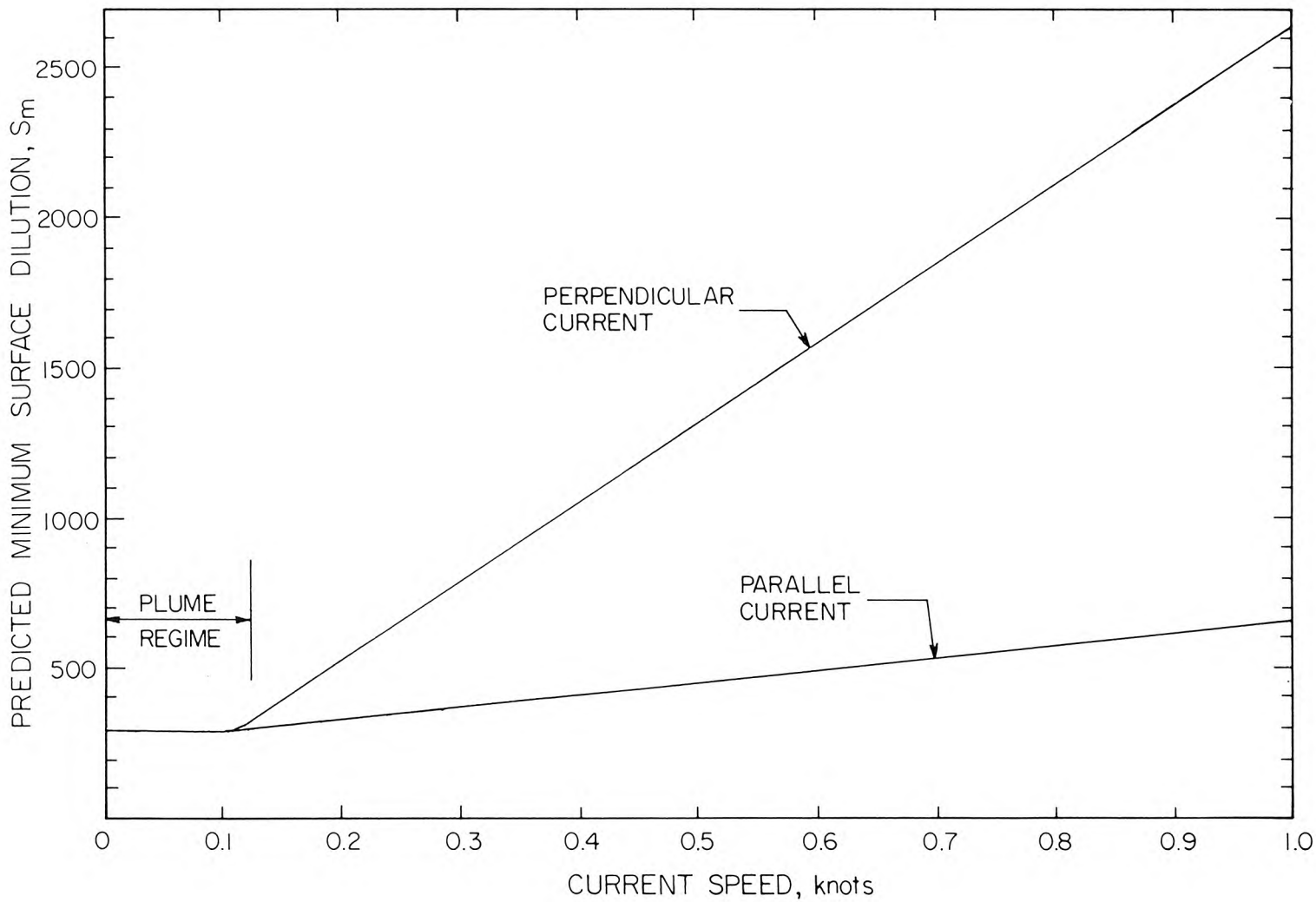

Figure 6.2 Predicted minimum surface dilution for the 120 inch outfall, Los Angeles County Sanitation Districts, flow = 210 mgd (9.2 m^3/s), no density stratification in ocean.

6.2 Comparison of Results with Other Model Studies

A few model studies have been made of dispersion from diffusers into a flowing current, as discussed in Section 2.2. In this section the measurements of minimum surface dilution obtained in these investigations will be compared with those of the present study.

Jirka and Harleman (1973) performed two-dimensional experiments with hot water escaping vertically from a slot. They expressed their results as:

$$\frac{\Delta T_o}{\Delta T_m} = S_m = f(F_T, V_T) \quad , \tag{6.10}$$

where

$$F_T = q/\sqrt{\frac{\Delta\rho}{\rho_o} g H^3} \tag{6.11}$$

and

$$V_T = \frac{uH}{q} \quad , \tag{6.12}$$

where $\Delta\rho$ is the density difference resulting from the temperature difference ΔT_o between the effluent and receiving water, and ΔT_m is the maximum temperature rise at the surface. The identity used in Eq. 6.10, $S_m = \Delta T_o/\Delta T_m$, is derived in Appendix C, Eq. C13. The variables can be expressed in terms of those used in the present study as:

$$\frac{S_m q}{uH} = \frac{S_m}{V_T} \quad ,$$

and

$$F = F_T^2 V_T^3 \quad .$$

The momentum of the ambient current relative to that of the source is given by M (Cederwall (1971)), where

$$M = \frac{u_j^2 B}{u^2 H} \quad , \tag{6.13}$$

and u_j is the jet exit velocity and B the source width. With no current, the momentum flux, $u_j^2 B$, of the source is important relative to the buoyancy flux over a length ℓ_m where

$$\ell_m = \frac{u_j^2 B}{b^{2/3}} \quad . \tag{6.14}$$

Thus, for the source momentum flux to have no effect on surface dilution, the ratio N, where

$$N = \frac{\ell_m}{H} \quad , \tag{6.15}$$

must be much less than one. N is also given by

$$N = F^{2/3} M \quad , \tag{6.16}$$

and is thus not an independent variable of the problem. Hence, a better choice of variables to express the minimum surface dilution than those of Eq. 6.10 is:

$$\frac{S_m q}{uH} = f(F,M) \quad ,$$

where the influence of the source momentum flux should disappear as $M \to 0$. The results of Jirka and Harleman are replotted in this way in Figure 6.3. In addition, the results for currents perpendicular to

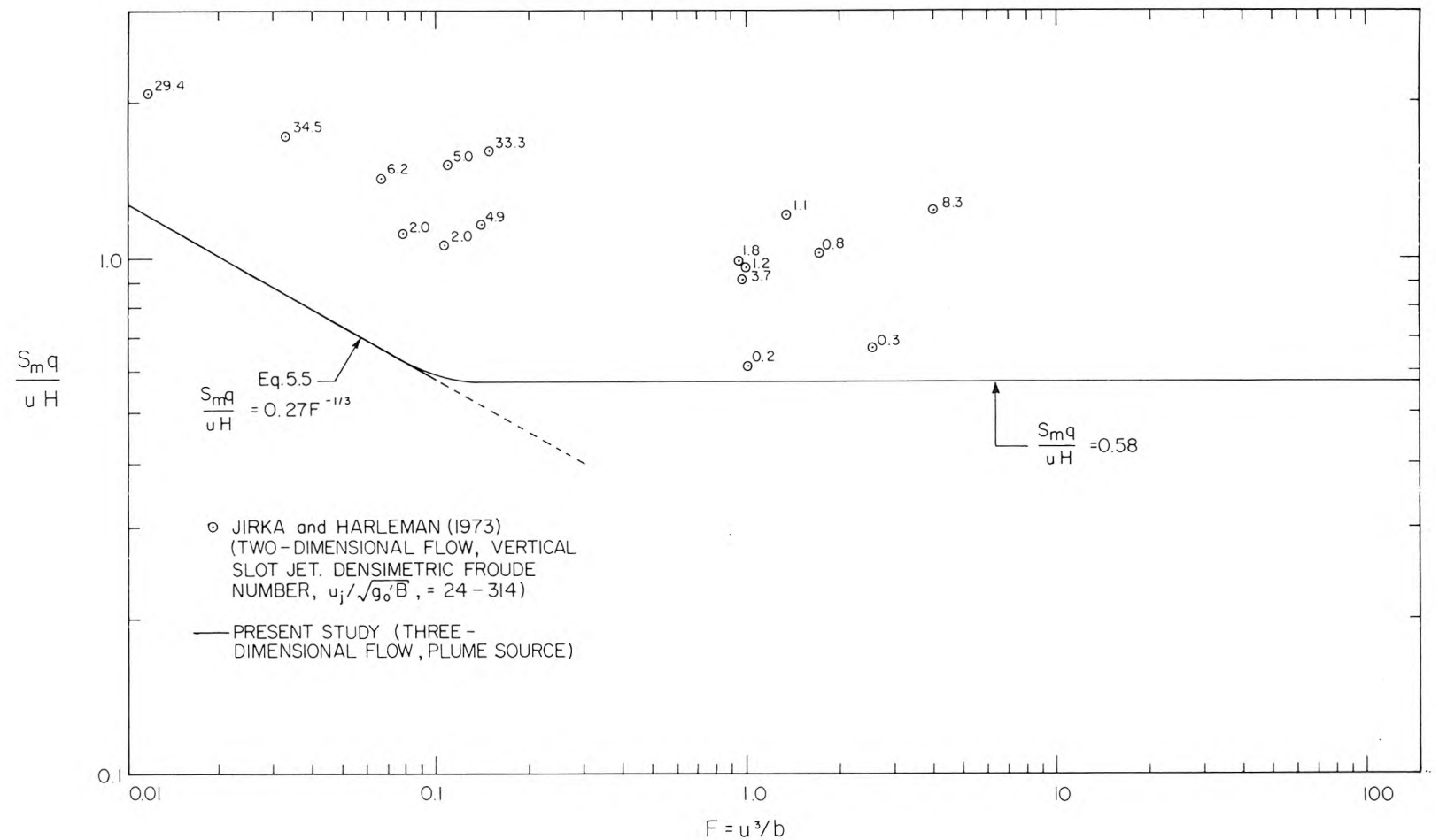

Figure 6.3 Comparison of minimum surface dilution measurements for diffuser in a perpendicular current from present study with two-dimensional studies of Jirka and Harleman (1973). Numbers are momentum flux parameters, $M = u_j^2 B/(u^2 H)$.

the diffuser obtained in the present study, Figure 5.27, are plotted. The number written next to each datum point is the value of M.

The effect of the source momentum flux is to increase the dilution above that for an equivalent line plume. In general, the data with the highest values of M show dilutions which are largest compared with those found in the present study. This also illustrates the problems discussed in Section 4.2.2 which could have arisen if a simple slot jet were used for the present experiments. It is concluded that the results of the two-dimensional experiments of Jirka and Harleman cannot be used for comparison with those of the present study due to the high source momentum flux and the two-dimensional configuration.

Jirka and Harleman also performed three-dimensional experiments, discussed briefly in Section 2.2, in which surface dilutions were measured. Tests were conducted in a basin with line multiport diffusers of finite length discharging hot water into an ambient flow. They expressed their results as for the two-dimensional studies, Eq. 6.10. Two-dimensional experiments with multiport diffusers were done by Bühler (1974) and Nospal and Tatinclaux (1976), as discussed in Section 2.2. Bühler expressed his results for minimum surface dilution in the form of Eq. 2.5; they are plotted in Figure 2.4. Nospal and Tatinclaux expressed their results in the form of Eq. 6.10.

The results of Bühler, Nospal and Tatinclaux, and Jirka and Harleman are replotted in Figure 6.4 according to the analysis of the present study, Eq. 5.2:

$$\frac{S_m q}{uH} = f(F,\theta) \quad .$$

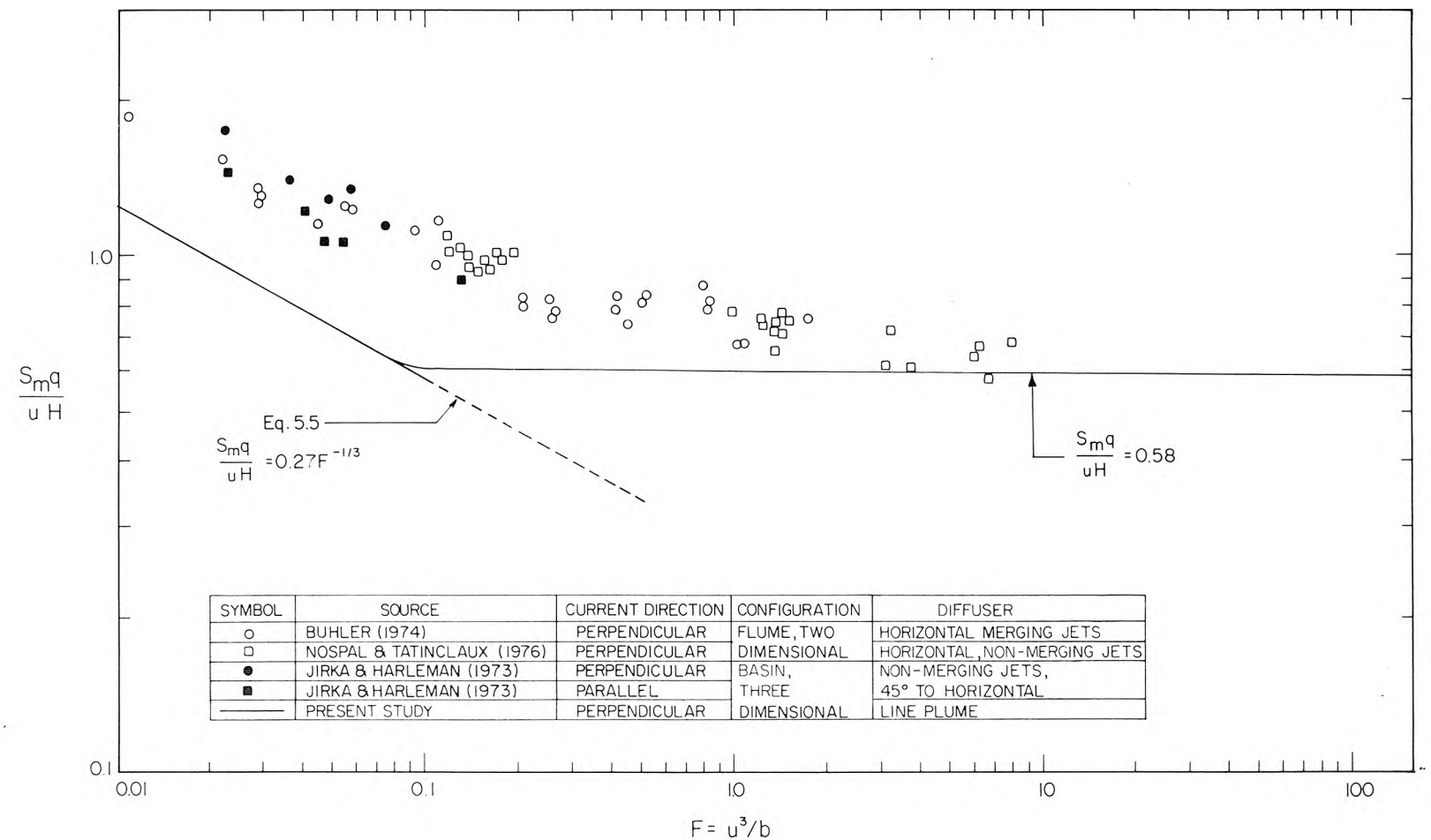

Figure 6.4 Comparisons of minimum surface dilution measurements of a line plume from present study with investigations of multiport diffusers.

The results approach those of the present study as F increases. This would be expected as the effects of the initial momentum flux and port spacing decrease as the current velocity increases. For smaller Froude numbers, measured dilutions for multiport diffusers are higher than those found in the present study by about 50%. This discrepancy is larger than the 20% limit on scaling errors for the present study (Appendix A), so other reasons for the difference must exist. The experiments of Jirka and Harleman were conducted with a water depth to nozzle spacing ratio, H/ℓ, of either 3.1 or 4.2. This spacing is too large for any merging of the jets to occur before reaching the free surface, as discussed in Section 6.1. Also, the momentum flux of the jets was appreciable and the nozzles were pointing upwards at an angle of 45°. Hence, the assumptions made in the present study, that the individual jets have merged into a line plume and the source momentum flux is negligible, are invalid for Jirka and Harleman's experiments.

Bühler conducted his experiments over a range of source Froude numbers, F_o, between 12 and 96. The port spacing, ℓ, was varied from 3.2 to 25 cm, the water depth, H, was 124.8 cm, and the orifice diameter, D_o, was 0.318 cm. Thus, the range of $(H/D_o)/F_o$ and H/ℓ was:

$$4.1 < \frac{H/D_o}{F_o} < 32.7 \quad ,$$

and

$$5.0 < H/\ell < 39.0 \quad .$$

The location of these points on Figure 5, Appendix B, suggests that the line plume approximation should be reasonable for these conditions.

However, the ratio of water depth to port spacing, H/ℓ, in the experiments of Nospal and Tatinclaux was about 3. Hence, the jets would not be expected to merge before reaching the free surface with no current and so the line plume approximation is not reasonable.

The experiments of Bühler and Nospal and Tatinclaux were both two-dimensional with the source extending the full width of the flume. This is the most probable reason for the difference in dilutions observed in their studies and the present one. In two-dimensional flows at small Froude numbers, the supply of diluting water at the downstream side of the diffuser must be supplied from the downstream end of the flume as ambient flow cannot come around the diffuser ends. In the three-dimensional case, the supply of entrained water at the downstream plume end can be supplied by flow around the ends of the diffuser, Figure 5.2. Furthermore, these two-dimensional flows are unsteady and the thickness of the surface layer is initially less than that in three-dimensional flows due to the importance of interfacial shear in the latter case. Two and three-dimensional flows at small Froude numbers are thus fundamentally different but should become similar as $F \to \infty$. These dissimilarities may be the reasons for the differences in dilutions apparent in Figure 6.4 at small Froude numbers. However, the results do agree with those of the present study at higher Froude numbers, confirming that the effluent does not become uniformly mixed over the receiving water in strong currents perpendicular to the diffuser. For smaller Froude numbers or current directions other than perpendicular, there are no suitable data for comparison.

6.3 Comparison of Results with Field Studies

There are very few field data available with which to compare the results of the present study. The few studies on line diffusers which have been made generally lack good current speed and direction data. The dependence of dilution on these parameters has been demonstrated by the present study. Because of this lack of data, a series of field experiments was performed on the outfalls of the Los Angeles County Sanitation Districts. The results of these studies will be discussed at the end of this section.

Data suitable for comparison are contained in the reports of Burgess and James (1970, 1971). These authors studied the dispersion of pulp mill effluent from outfalls in Northern California and Oregon. Aerial photographs of the plumes were obtained, and dilutions measured by photodensimetric methods and by boat sampling. The characteristics of the three outfalls studied are given in Table 6.1, and their locations and configurations are shown in Figures 6.5, 6.6, and 6.7.

The water depth-to-port spacing ratio, H/ℓ, varies from 2.0 to 3.8 for these outfalls. Thus, if the receiving water is stagnant, it would be expected that the individual jets would not merge before reaching the surface, Figure 5, Appendix B. Hence, the line plume approximation would not be good for predicting dilutions at low current speeds. A summary of experimental observations from Burgess and James (1970) is given in Table 6.2 along with computed values of F, $S_m q/uH$, $(H/D_o)/F_o$ and also S_m estimated for non-merging jets from Figure 4, Appendix B. The results are plotted for comparison with those of the present study as $S_m q/uH$ versus F and θ in Figure 6.8.

Table 6.1 Characteristics of paper mill outfall diffusers studied by Burgess and James (1970, 1971).

Location	Newport, Oregon	Gardiner, Oregon	Samoa, California
Diffuser configuration	Y, 140° angle between legs	Line	Line
D_o. Port diameter, inches	3	5	6
Q. Effluent flow rate, ft^3/s	8.91-20.1	~22.3	~37.9
H. Water depth, feet	40	25	22-38
ℓ. Port spacing, feet	20	7.5	10
L. Diffuser length, feet	560	182	500
H/ℓ	2.0	3.3	2.2-3.8

Some of the data agree with those of the present study, and some do not. The largest discrepancies are for those measured at the Newport outfall on 8-8-68 and 8-16-68. These dilutions are between a half and a third of those predicted from this study. However, they are about half the predicted dilutions for non-merging jets in a stagnant current and

Table 6.2 Experimental results from field experiments of Burgess and James (1970) on surfacing plumes.

Date	Location	Q Effluent Flow Rate ft^3/s	S_m Measured Minimum Surface Dilution	u Current Speed ft/s	θ Approx. Current Direction*	F Froude Number $= u^3/b$	$\frac{S_m q}{uH}$ +	$\frac{H/D_o}{F_o}$ +	F_o Jet Froude Number $= \frac{u_o}{\sqrt{g'_o D_o}}$	S_m Predicted for no Current#
8-8-68	Newport	12.4	67	0.26	Parallel	1.10	0.142	7.2	22.3	89
8-14-68	Newport	16.9	48	-	-	-	-	5.2	30.6	86
8-16-68	Newport	16.8	43	0.42	Parallel	3.41	0.077	5.3	30.4	85
8-21-68	Newport	16.5	50	-	-	-	-	5.4	29.8	83
9-12-68	Newport	15.0	100	-	-	-	-	5.9	27.2	84
7-8-69	Newport	20.1	100	0.5	Parallel	4.83	0.18	4.4	36.2	72
8-12-69	Newport	18.5	100	0.1	45°	0.042	0.83	4.8	33.4	90
9-8-69	Newport	18.7	100	0.2	Parallel	0.331	0.42	4.7	33.8	91
7-16-69	Gardiner	22.3	43	0.26	Perpendicular	0.20	0.81	4.9	12.2	34
8-19-69	Gardiner	22.5	45	0.1	45°	0.011	2.23	4.9	12.3	33
8-20-69	Gardiner	16.7	45	0.13	45°	0.033	1.27	6.6	9.1	32
8-6-69	Samoa	41.4	56	0.45	Perpendicular	1.52	0.47	6.4	6.9	21
8-7-69	Samoa	36.8	56	0.50	Perpendicular	2.36	0.37	7.2	6.1	20

*Estimated from photos and plots.

#Predicted from Figure 4, Appendix B, for individual round buoyant jets without interference.

+q = effluent volume flux per unit length, H = water depth, u_o = jet exit velocity, D_o = port diameter, $g'_o = \frac{\rho_r - \rho_o}{\rho_o} g$.

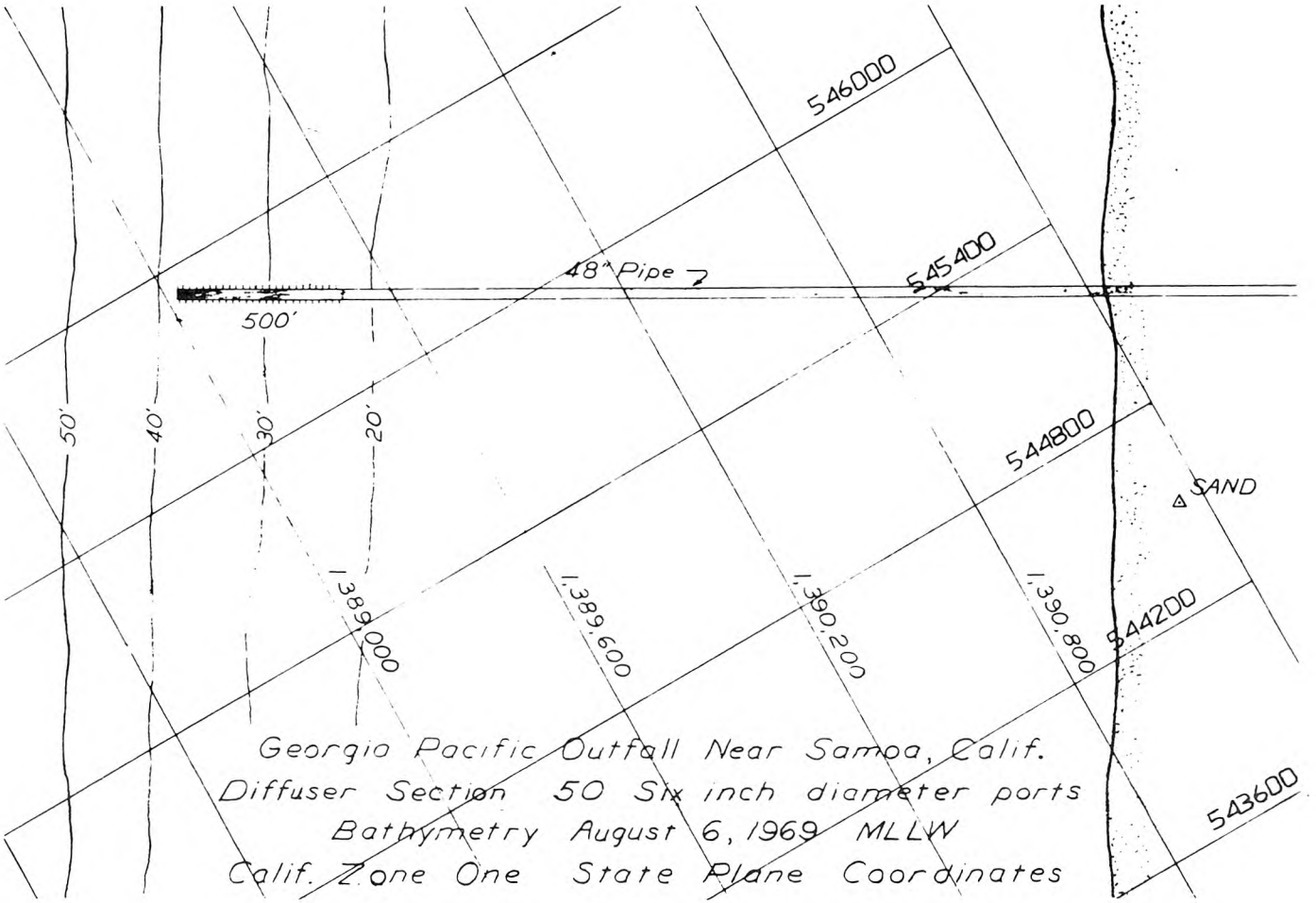

Figure 6.5 Sketch of outfall near Samoa, California (after Burgess and James (1970)).

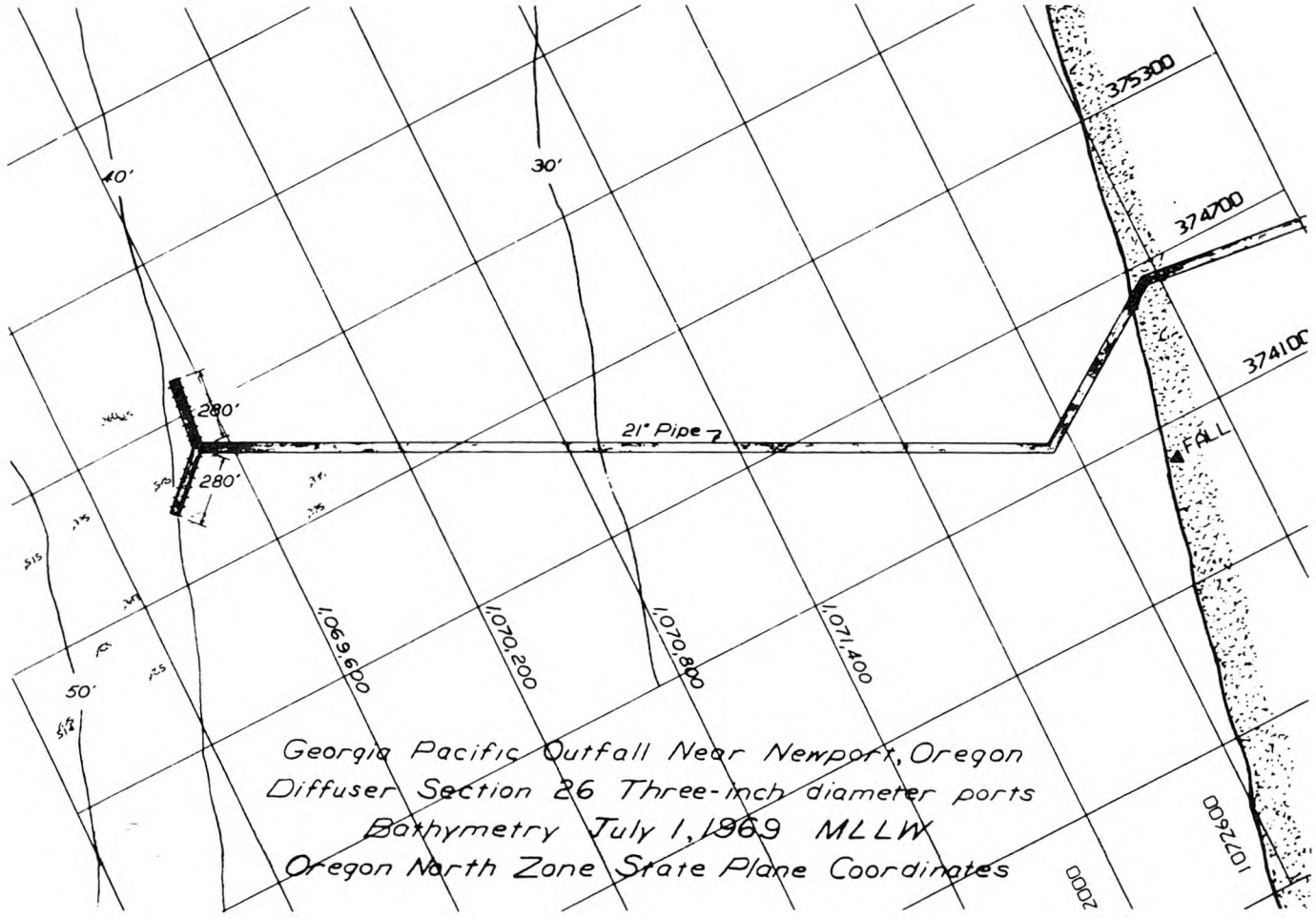

Figure 6.6 Sketch of outfall near Newport, Oregon (after Burgess and James (1970)).

Figure 6.7 Sketch of outfall near Gardiner, Oregon (after Burgess and James (1970)).

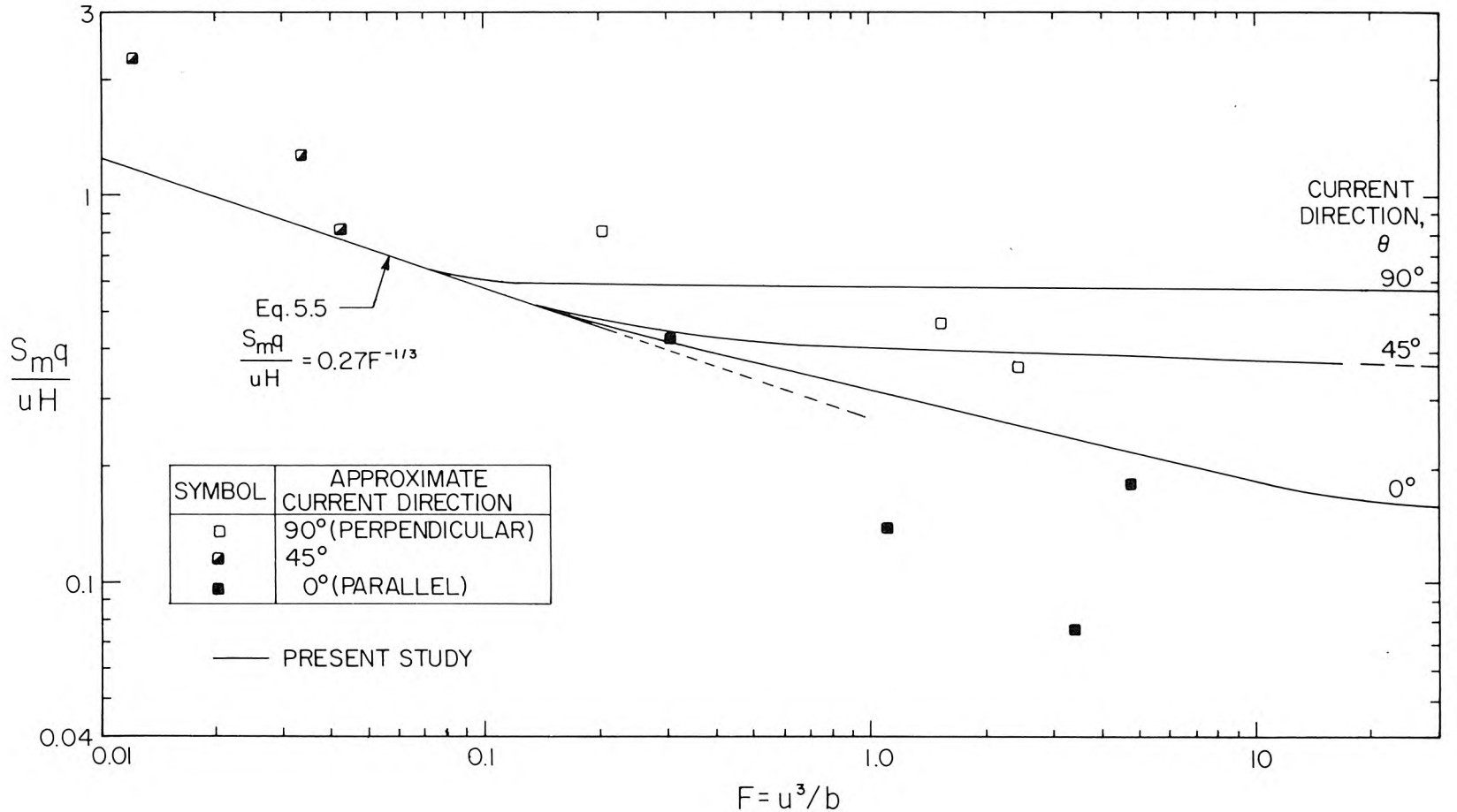

Figure 6.8 Comparison with results of present study of dilution measurements for pulp mill outfalls obtained by Burgess and James (1970)(see Table 6.2).

dilutions were much higher for similar conditions. The data obtained on 7-8-69, 8-12-69, and 9-8-69 agree well with the present results. The ratios $S_m q/uH$ obtained over the Samoa outfall are also low. The dilutions, however, are higher than those predicted for non-merging jets. The increase is probably due to the current effect, but is less than predicted by the results of this study.

These inconsistencies between field and laboratory results could be due to the inadequacy of the ocean current data. Burgess and James measured only surface currents for a short period, whereas the analysis of the present study is based on the depth-averaged current velocity, which is assumed to be steady. The unsteadiness and shear of ocean currents affects effluent dispersion. In order to assess these effects, a series of current meters at different depths operating over a longer period would be necessary. The lack of this type of data makes the comparisons between field and laboratory results difficult.

For the same reasons, the surface spreading results cannot be compared, but some general observations can be made. Burgess and James found that one of the surface floats in the experiment of 7-16-69 at Gardiner moved downstream with the waste field but that the second float remained stationary just upstream of the outfall. The Froude number, F, was 0.20, Table 6.2, so the flow should then be similar to that of Figure 5.2. The stationary float is consistent with a stagnant region due to the arrested upstream wedge. A further example is the photograph of the plume on 8-6-69 at Samoa, Figure 6.9. The Froude number, F, was 1.5, Table 6.2. The location of the outfall is shown

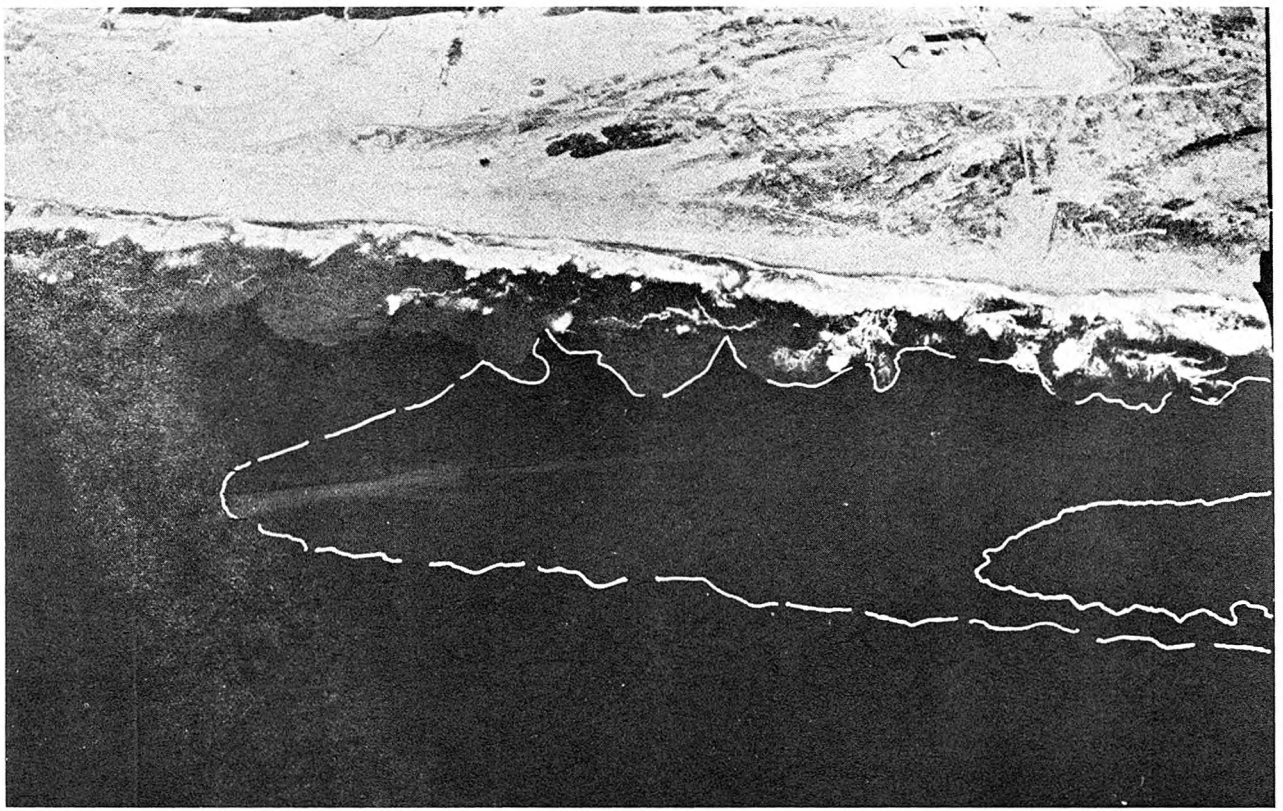

Figure 6.9 Aerial photograph of waste plume on 8-6-69 at Samoa, California. F = 1.5. From Burgess and James (1970), outlining by them.

in Figure 6.5. The shape of the plume suggests the current direction to be about 10° from a normal to the diffuser. The aerial photograph was taken at an oblique angle, so direct comparisons with the present study cannot be made. However, the plume appears to be similar to those observed in the present study. Further examples are given in Figure 6.10. The Froude number of the plume shown in Figure 6.10a is 4.8, a fairly high value resulting in a narrow surface plume which is comparable with that for F = 10 shown in Figure 5.3. Conversely, the small Froude number of 0.033 of Figure 6.10b results in rapid surface spreading and "laking" of the effluent around the diffuser which can be compared with the plume for F = 0.1, Figure 5.2.

As part of this study, a series of experiments was performed over the 120-inch outfall of the Los Angeles County Sanitation Districts, shown in Figure 6.1. Aerial photographs were made, and the surface current computed from the movement of surface dye patches. Attempts to assess dilutions by means of ammonia measurements in seawater samples were also made.

These experiments were largely unsuccessful due to the infrequent surfacing of the plumes. No satisfactory dilution measurements were obtained, and the only clear photograph of the surfacing plume was obtained at about 2:00 p.m. on 21 February 1975; it is shown in Figure 6.11. The measured surface current velocity and direction at this time was 0.29 knots (0.149 m/s) approximately parallel to the diffuser and shoreline. The effluent flow rate through the diffuser was about 270 mgd (11.8 m^3/s). The diffuser length is 4440 feet

a) 7-8-69 at Newport, Oregon. F = 4.8.

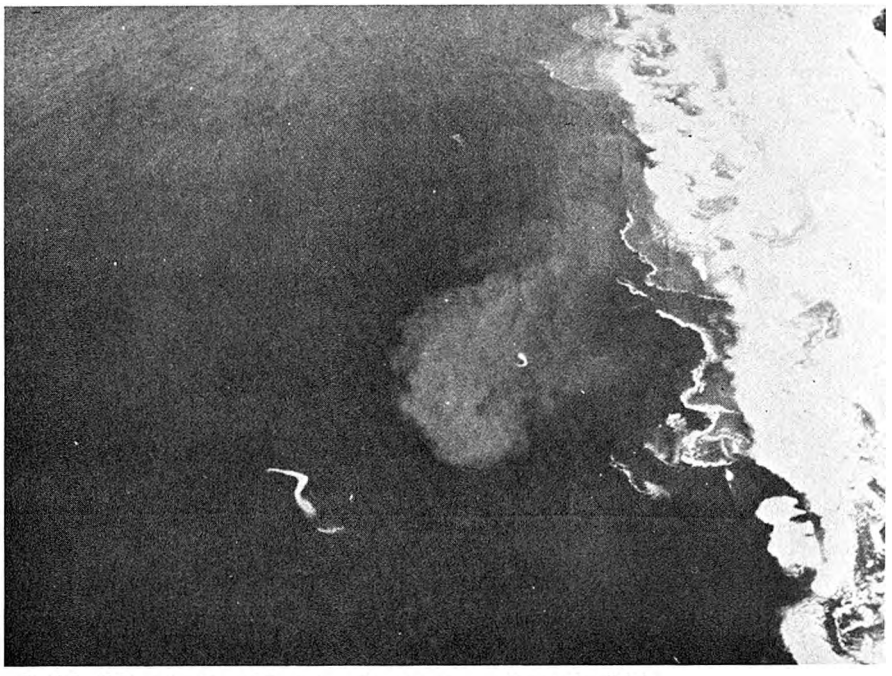

b) 8-20-69 at Gardiner, Oregon. F = 0.033.

Figure 6.10 Aerial photographs of waste plumes (from Burgess and James (1970).

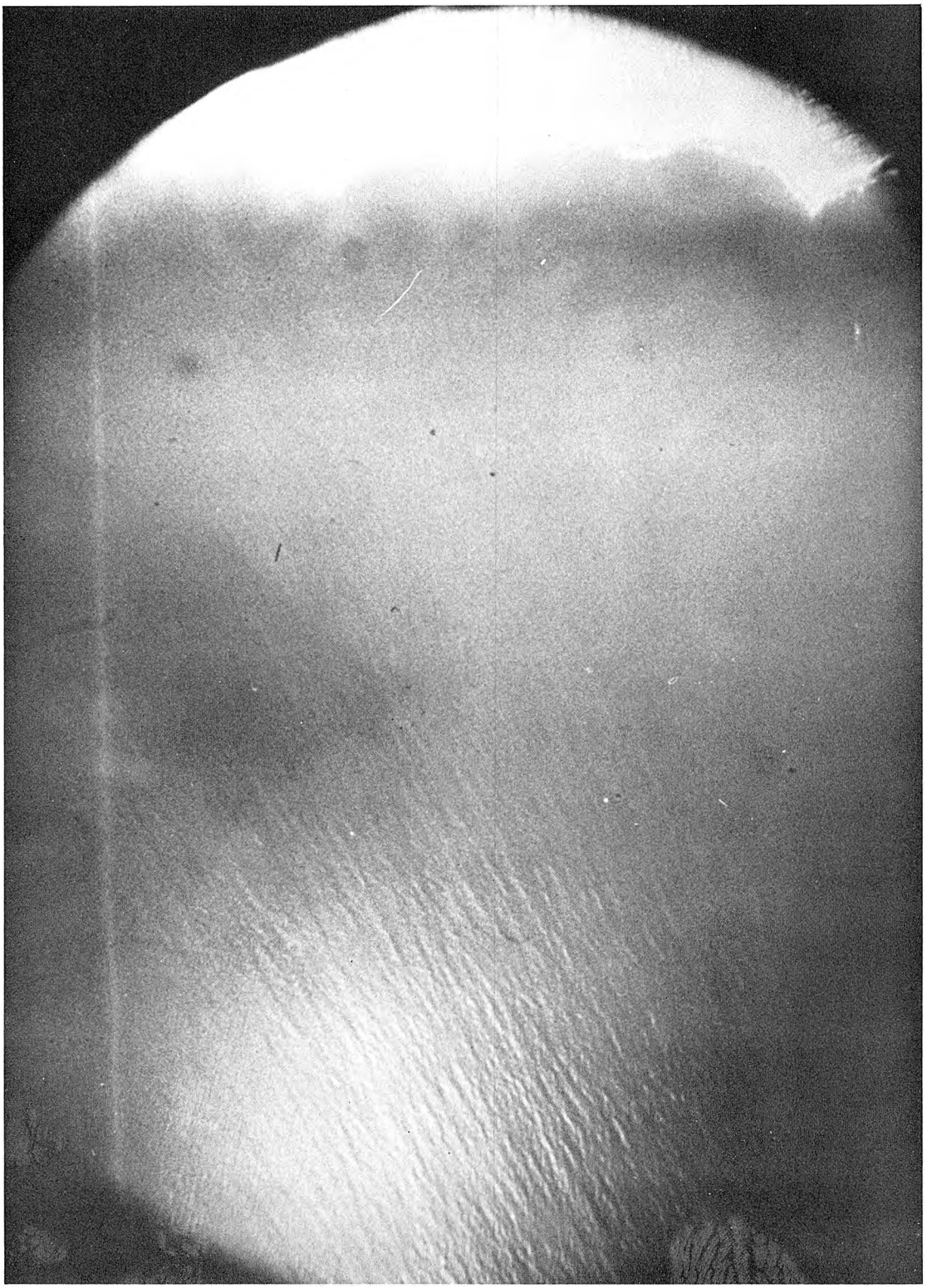

Figure 6.11 Aerial photograph of surface plume from 120 inch outfall, Los Angeles County Sanitation Districts, 21 February 1975.

(1353 m) and the density difference, $\Delta\rho/\rho_o$ is about 0.026, therefore the Froude number is

$$F = \frac{u^3}{b} = \frac{u^3 L}{\frac{\Delta\rho}{\rho_o} g Q} = \frac{(0.149)^3 \times 1353}{0.026 \times 9.81 \times 11.8} = 1.5 \ .$$

An experiment was performed to simulate these conditions in the laboratory. Photographs of the laboratory and field plumes are shown in Figure 6.12. Tracings of these plumes, and comparison with the theoretical prediction of the shape, Eq. 3.43, are shown in Figure 6.13.

Although the agreement between the field and laboratory observations is excellent, the photograph of the field plume is not what it seems. Analysis of the location of the plume with respect to the diffuser indicates that the surface plume to be displaced about 3000 feet downstream from the upstream end of the diffuser. This displacement may be due to ambient stratification causing the waste field to form beneath the surface. After this initial formation, the plume may continue to drift to the surface, and appear west of the diffuser. Another possibility is that the plume rises more slowly due to ambient stratification, gradually spreading as it rises. In either case, the surface field is not strictly comparable to those observed in the present study. The general shape of the field plume, however, suggests that the dispersion of effluent from these very large outfalls has a mechanism similar to that found in the present study.

6.4 Behavior of Waste Field at Large Distances from the Diffuser

The analysis and results presented in Chapters 3 and 5 are concerned with dispersion close to the diffuser. It was found that beyond the

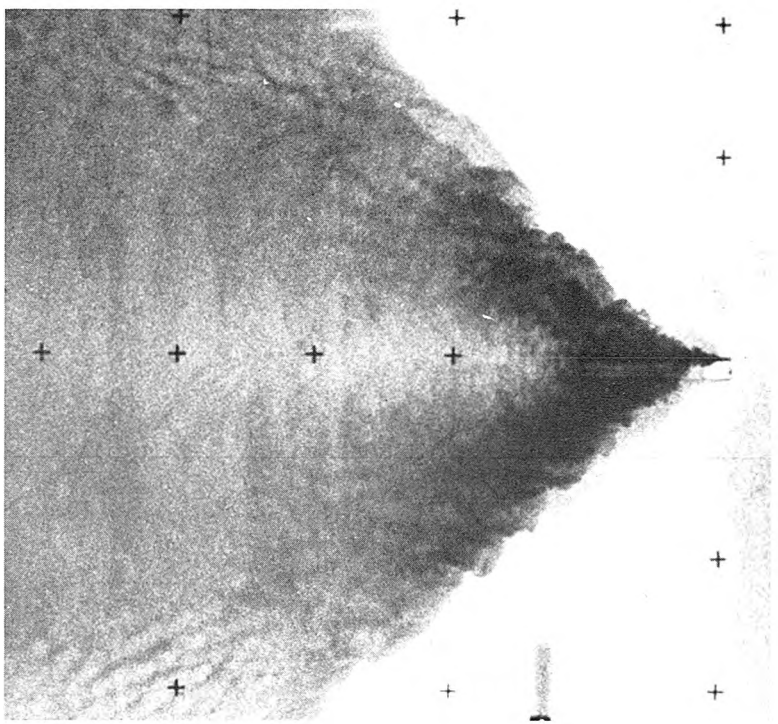

Experiment number JO

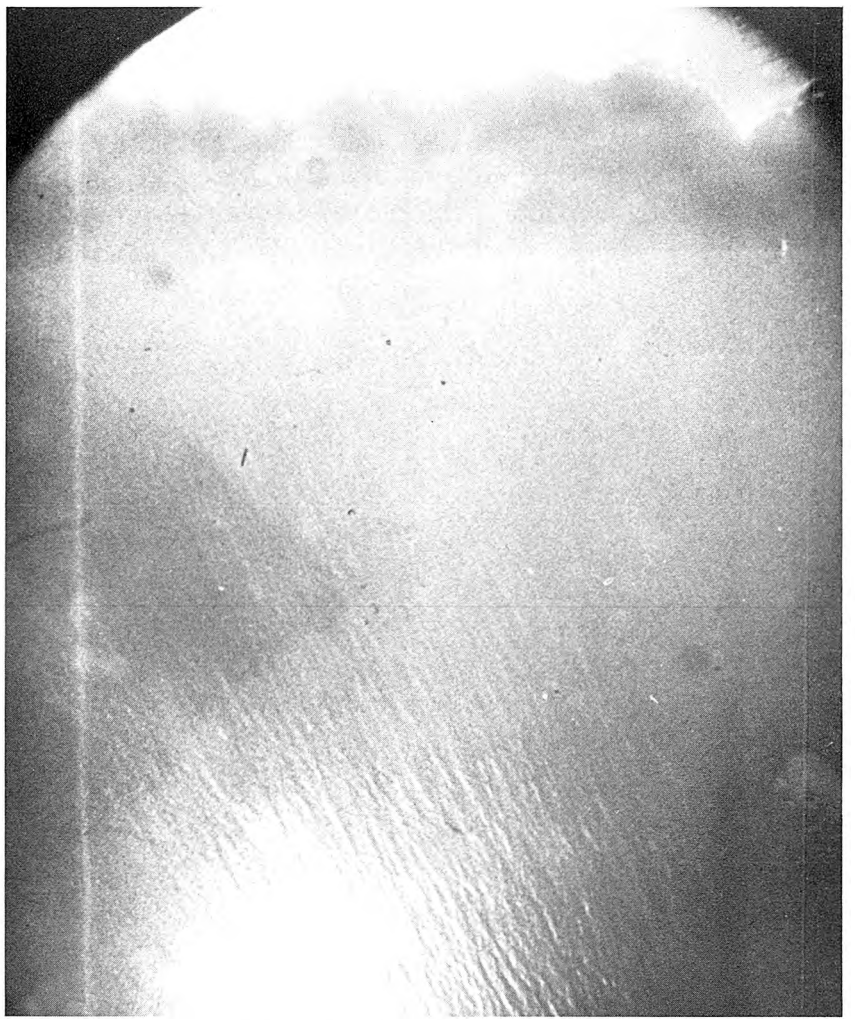

Field plume (see Figure 6.11)

Figure 6.12 Photographs of laboratory and field surface plumes, F = 1.5.

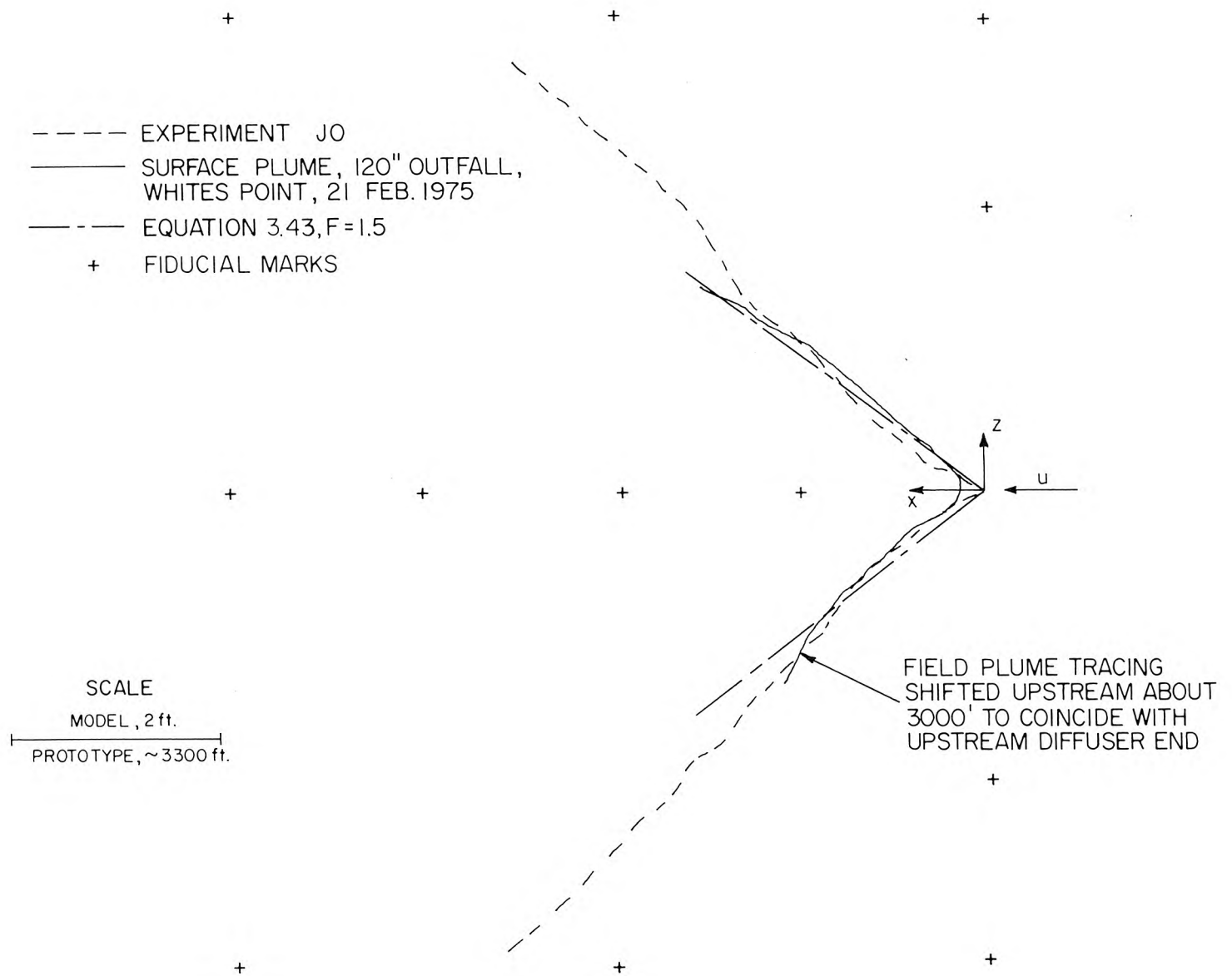

Figure 6.13 Tracings of surface plumes observed in the laboratory and field, and comparison with theory.

initial mixing region, the effluent forms a surface layer whose stability impedes further vertical mixing. This surface layer then spreads horizontally due to its buoyancy, with little additional dilution occurring. At large distances from the outfall, however, dispersion is dominated by diffusion due to ambient turbulence. This turbulence increases the size of the effluent field and causes additional dilution by both horizontal and vertical mixing. These effects are discussed in this section, with vertical and horizontal mixing considered separately.

Vertical mixing of the surface field due to ambient turbulence is more rapid if the density stratification is weak. This density gradient is inversely proportional to the initial dilution, and so the effect of vertical mixing should be most pronounced for higher dilutions. The highest dilutions occur when the diffuser is perpendicular to the current in the forced entrainment regime. This limiting condition for vertical mixing will now be considered.

When the diffuser is of finite length and the receiving water of finite depth, the effluent must form a buoyant surface layer at some point downstream (Figure 3.1). This surface layer has a stable density profile which suppresses further vertical mixing. Nevertheless, ambient turbulence will gradually erode this surface layer by vertical mixing, and at some distance downstream the mixing will penetrate to the surface, reducing the surface concentration. This distance will now be estimated.

It is assumed that the ambient turbulence results only from shear at the lower boundary. Experimental studies of the similar problem

shown in Figure 6.14 have been made by Kato and Phillips (1969). They applied a constant stress $\tau = \rho u_*^2$ at the upper boundary of a fluid having an initially linear density profile and found that the resulting turbulent mixing proceeded as shown in Figure 6.14. The entrainment velocity, u_s, of fluid from the lower layer to the upper was found to be described by

$$\frac{u_s}{u_*} = 2.5 \frac{\rho_r u_*^2}{g\delta\rho D} \quad , \tag{6.17}$$

where $\delta\rho$ is the density jump across the interface. As the total fluid volume is conserved, the rate of advance of the interface is given by:

$$\frac{dD}{dt} = u_s \quad . \tag{6.18}$$

These results can be used to predict the surface waste field erosion by vertical mixing. It is assumed that the density profile in the surface layer is linear. This is reasonable, since the effluent concentrations are almost linear (see Figures 5.9 and 5.10). The lower layer is assumed to be always well-mixed leading to the development of the density profiles as shown in Figure 6.15. The density of the lower layer gradually reduces until the effluent is uniformly mixed over the receiving water depth.

The density difference, $\delta\rho$, is given by

$$\delta\rho = \rho_r - \rho(s) \quad . \tag{6.19}$$

Conservation of mass states that:

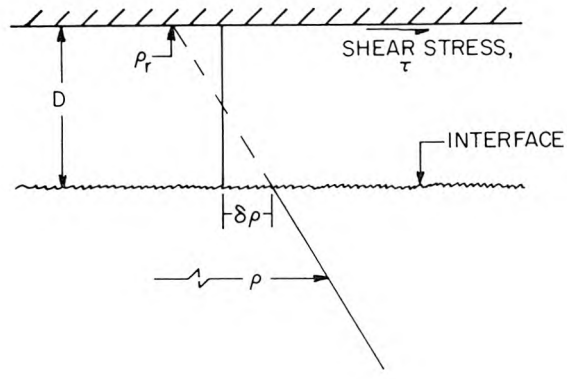

Figure 6.14 Schematic of experiment by Kato and Phillips (1969) on mixing of a stratified fluid due to boundary shear generated turbulence.

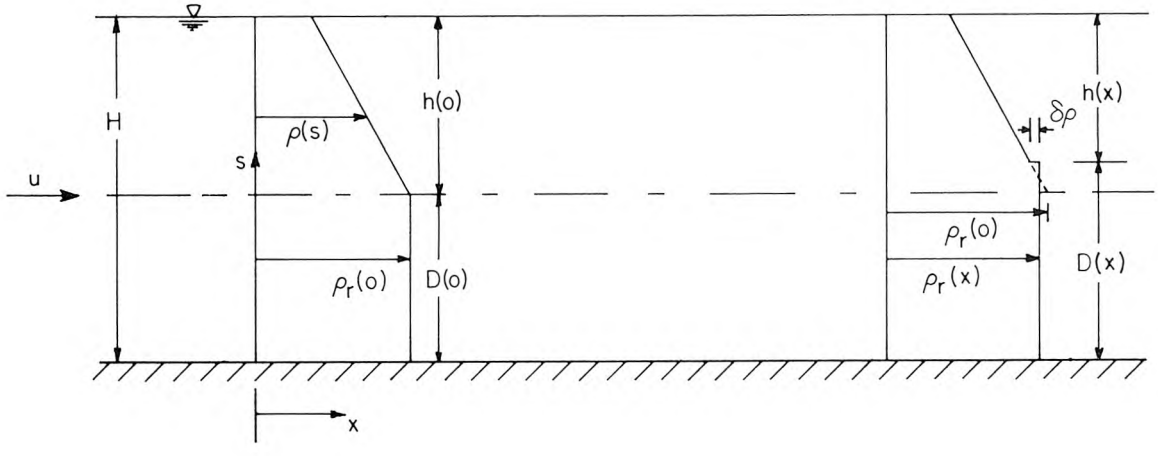

Figure 6.15 Postulated erosion of surface waste field due to vertical mixing. Thickness of surface layer, h = H-D.

$$\rho_r D = \rho_r(0)D(0) + \int_o^{D-D(0)} \rho(s)ds \quad . \tag{6.20}$$

The thickness of the surface layer just after separation is half the water depth (see Sections 3.3.1 and 5.3). Thus:

$$D(0) = H/2 \quad . \tag{6.21}$$

The density distribution in the upper layer is assumed to be linear, hence:

$$\rho(s) = \rho_r(0) + \beta s \quad , \tag{6.22}$$

where

$$\beta = \frac{\partial \rho}{\partial s} \quad .$$

Substitution of Eqs. 6.21 and 6.22 into 6.20 gives:

$$\rho_r(x)\, D = \rho_r(0)\, \frac{H}{2} + \int_o^{D-H/2} [\rho_r(0) + \beta s]ds$$

$$= \rho_r(0)\, \frac{H}{2} + \rho_r(0)(D - \frac{H}{2}) + \frac{\beta}{2}(D - \frac{H}{2})^2$$

$$= \rho_r(0)D + \frac{\beta}{2}(D - \frac{H}{2})^2 \quad ,$$

hence,

$$\rho_r(x) = \rho_r(0) + \frac{\beta}{2D}(D - \frac{H}{2})^2 \quad . \tag{6.23}$$

Now,

$$\rho(s) = \rho_r(0) + \beta(D - \frac{H}{2}) \quad , \tag{6.24}$$

hence, substitution of Eqs. 6.23 and 6.24 into 6.19 gives:

$$\delta\rho = \rho_r(0) + \frac{\beta}{2D}\left(D-\frac{H}{2}\right)^2 - \rho_r(0) - \beta\left(D-\frac{H}{2}\right)$$

$$= -\frac{\beta}{2D}\left(D-\frac{H}{2}\right)\left(D+\frac{H}{2}\right) \quad . \tag{6.25}$$

Substitution of Eq. 6.25 into 6.17 gives:

$$\frac{u_s}{u_*} = -2.5\,\frac{\rho_r u_*^2 2D}{g\beta\left(D-\frac{H}{2}\right)\left(D+\frac{H}{2}\right)} \quad . \tag{6.26}$$

Combining Eqs. 6.18 and 6.26 we find:

$$\frac{dD}{dt} = u_s = -5\,\frac{\rho_r u_*^3}{g\beta\left(D-\frac{H}{2}\right)\left(D+\frac{H}{2}\right)} \quad , \tag{6.27}$$

whose solution is

$$\frac{D^3}{3} - \frac{H^2 D}{4} + \frac{H^3}{12} = -5\,\frac{\rho_r u_*^3}{g\beta}\,t \quad . \tag{6.28}$$

The interface reaches the free surface when D = H, in a time t_m, thus

$$\frac{H^3}{3} - \frac{H^3}{4} + \frac{H^3}{12} = -5\,\frac{\rho_r u_*^3}{g\beta}\,t_m \quad ,$$

or

$$t_m = -\frac{H^3 g\beta}{30\rho_r u_*^3} \quad . \tag{6.29}$$

The distance downstream for this to occur is given by the Galilean

transformation $x_m = ut_m$, hence:

$$x_m = -\frac{1}{30}\frac{H^3 g\beta}{\rho_r u_*^3}\, u \quad . \tag{6.30}$$

The slope of the density profile is given by

$$\frac{\beta g}{\rho_r} = \frac{g}{\rho_r}\frac{\partial \rho}{\partial s} = -\, g\, \frac{\Delta\rho_m/\rho_r}{H/2} \quad , \tag{6.31}$$

where $\Delta\rho_m = \rho_m - \rho_r(0)$, and ρ_m is the density at the free surface. From the definition of minimum surface dilution (Eq. C9):

$$S_m = \frac{\Delta\rho}{\Delta\rho_m} \quad ,$$

hence,

$$\Delta\rho_m = \frac{\Delta\rho}{S_m} \quad . \tag{6.32}$$

The measurements of minimum surface dilutions (Figure 5.27) show that for currents perpendicular to the diffuser and $F > 0.1$:

$$\frac{S_m q}{uH} \approx 0.6 \quad ,$$

hence

$$S_m \approx 0.6\,\frac{uH}{q} \quad . \tag{6.33}$$

Substitution of Eqs. 6.33 and 6.32 into 6.31 yields:

$$\frac{\beta g}{\rho_r} = -\,\frac{2}{0.6}\,\frac{\Delta\rho g q}{\rho_r u H^2} \quad . \tag{6.34}$$

Substitution of the definition of buoyancy flux per unit length, b, from Eq. 2.1 with Eq. 6.34 assuming $\rho_o \approx \rho_r$, gives:

$$\frac{\beta g}{\rho_r} = -\frac{2}{0.6}\frac{b}{uH^2} \quad , \tag{6.35}$$

and substitution of Eq. 6.35 into 6.30 yields:

$$\frac{x_m}{H} = \frac{1}{9}\frac{b}{u_*^3} \quad . \tag{6.36}$$

Eq. 6.36 can be written:

$$\frac{x_m}{H} = \frac{1}{9}\frac{b}{u^3}\frac{u^3}{u_*^3}$$

$$= \frac{1}{9F}\left(\frac{8}{f}\right)^{3/2} \quad , \tag{6.37}$$

where f is a friction factor defined by

$$f = 8\frac{u_*^2}{u^2} \quad .$$

It is instructive to compare the values of x_m computed from Eq. 6.37 with the distance required for the completion of vertical mixing due to gravitational diffusion. For example, experiment H3 (similar to G3, Figure 5.3) has F = 11.4, Re = 12,340, and H = 8.1 cm (Table 5.1). The basin surface roughness, $d_s/4H$, where d_s is the sand grain diameter is $0.08/4 \times 8.1 = 0.0025$, hence from the Moody friction factor diagram, we find f = 0.034. Eq. 6.37 becomes:

$$\frac{x_m}{H} = \frac{1}{9 \times 11.4}\left(\frac{8}{0.034}\right)^{3/2}$$

$$= 35,$$

hence $$x_m = 35H.$$

The distance for the dilution at the surface to reach its limiting (minimum) value is about 7H (Figure 5.10). As the distance for completion of gravitational mixing is much less than that predicted for ambient turbulence to affect vertical mixing, it is concluded that ambient turbulence will not affect the initial dilution for $F < 10$. However, we now consider the case of higher Froude numbers, for example experiment L4(R1). From Table 5.1 we find: $F = 98$; $H = 4.05$ cm; $Re = 12{,}540$. The basin surface roughness is $0.08/4 \times 4.05 = 0.005$, and from the Moody diagram we find $f = 0.038$. Eq. 6.37 then becomes:

$$\frac{x_m}{H} = \frac{1}{9 \times 98}\left(\frac{8}{0.038}\right)^{3/2}$$

$$= 3.5,$$

hence $$x_m = 3.5H.$$

This very short distance implies that ambient vertical mixing is affecting the initial dilution in this case. This conclusion is supported by the photograph of a similar plume, G6, Figure 5.4, which shows fuzzy edges presumably due to the ambient turbulence. Also, the shape of the decay curve of concentration fluctuations for experiment

L4(R1), Figure 5.11, is not parallel to those for F $\approx$ 1 or 10. The slower decay rate is further evidence of the effects of ambient turbulence. Finally, by using an analysis similar to that of Cederwall (1971), it can be shown that the distance downstream for the buoyant effluent to reach the surface (about 1H for F = 1, Figure 5.9, and 2H for F = 10, Figure 5.10) are much less than those expected for ambient turbulent diffusion. Only as F approaches 100 do these distances become comparable.

It is concluded that ambient turbulence only affects initial dilutions in the model for F $\gg$ 10. This conclusion is based on the assumption that ambient turbulence is generated only by shear at the lower boundary. If the turbulence is generated by other means, for example wind shear, the conclusion may not be valid. Friction factors in the ocean are generally less than those of the basin, so the effects of ambient turbulence generated by lower boundary shear on vertical mixing would be less in the ocean than in the model. Hence, the conclusion that initial dilutions are only affected by ambient turbulence generated by lower boundary shear for F $\gg$ 10 should also apply in the ocean.

Horizontal mixing due to ambient turbulence will now be considered. The horizontal diffusion coefficient of ambient turbulence, ε_z, increases with the size of the effluent field. Koh and Brooks (1975) assume the 4/3 power law to be applicable, that is,

$$\varepsilon_z = \lambda w^{4/3} \quad , \tag{6.38}$$

where w is a measure of the size of the effluent field. λ is a constant whose value has been estimated to lie between 6.8×10^{-5} and 2.3×10^{-3} $m^{2/3}/s$. Brooks (1960) obtained a solution for horizontal spreading from a line source of length L_o due to ambient turbulence as:

$$\frac{w_t}{L_o} = \left(1 + \frac{2}{3} \frac{12\varepsilon_o}{uL_o} \frac{x}{L_o}\right)^{3/2} , \tag{6.39}$$

where w_t is a measure of the plume width, and $\varepsilon_o = \lambda L_o^{4/3}$. The rate of plume growth due to ambient turbulence is obtained by differentiating Eq. 6.39 with respect to x. The result is

$$\frac{dw_t}{dx} = \frac{12\lambda}{u} \left(L_o^{2/3} + \frac{8\lambda x}{u}\right)^{1/2} . \tag{6.40}$$

The initial plume width, L_o, should be greater than L due to buoyant spreading, but be of order L, hence we assume

$$L_o = \gamma L , \tag{6.41}$$

where γ is a constant probably lying between 1 and 10.

It is assumed that the distance downstream for ambient turbulence to begin affecting horizontal spreading is so large that the buoyant spreading is in the regime governed by interfacial shear (see Section 3.5). The rate of surface plume growth due to buoyant spreading is then given by Eq. 3.60 as:

$$\frac{dw_b}{dx} = \frac{2}{F} \left(\frac{L^3 H^2 \rho_o u}{\alpha \varepsilon w_b^4}\right) , \tag{6.42}$$

where w_b is the plume size due to buoyant spreading. Eq. 6.42 applies only for a current perpendicular to the diffuser in the forced entrainment regime. The rate of plume growth is given by Eq. 3.55, hence Eq. 6.42 becomes:

$$\frac{dw_b}{dx} = \frac{2}{10^{4/5}} F^{-1/5} \left(\frac{L^3 H^2 \rho_o u}{\alpha \varepsilon} \right)^{1/5} x^{-4/5} \quad . \tag{6.43}$$

An estimate of the distance from the source where ambient turbulence begins to affect horizontal spreading can be obtained by finding the point at which the plume growth rates due to turbulence and buoyant spreading are equal. Denoting this distance by x_t, setting Eqs. 6.42 and 6.40 equal, and substituting Eq. 6.41, we find:

$$\left(1 + \frac{8\lambda L^{1/3}}{\gamma^{2/3} u} \eta_t \right)^{1/2} \eta_t^{4/5} = \frac{10^{-4/5}}{6} \left(\frac{\lambda \gamma^{1/3} L^{1/3}}{u} \right)^{-1} F^{-1/5} \left(\frac{H^2 u \rho_o}{\alpha \varepsilon L} \right)^{1/5} , \tag{6.44}$$

where $$\eta_t = \frac{x_t}{L} \quad .$$

Eq. 6.44 must be solved numerically for η_t.

To give an example, we consider the plume from the Samoa outfall shown in Figure 6.9. The following data are extracted from Tables 6.1 and 6.2: F = 1.52; L = 500 ft (152 m); u = 0.45 ft/s (0.137 m/s); $H \approx$ 30 ft (9.14 m).

The estimated value of x_t/L depends strongly on the value of λ. Taking the extremes of $\lambda = 6.8 \times 10^{-5}$ and 2.3×10^{-3} $m^{2/3}/s$ yields values of x_t/L of 105 and 1.6, respectively. An intermediate value of $\lambda = 4.64 \times 10^{-4}$ $m^{2/3}/s$ (0.01 $cm^{2/3}/s$) yields a value of $x_t/L = 11$. These

values were calculated for $\gamma = 1$ (i.e., $L_o = L$) and $\varepsilon/\rho_o = 10^{-6}$ m^2/s. x_t/L is less dependent on γ and ε. Changing γ from 1 to 5 changes x_t/L from 11 to 8 and changing ε/ρ_o from 10^{-6} to 10^{-4} m^2/s changes x_t/L from 11 to 5. Thus, there is considerable uncertainty in the transition distance for turbulent diffusion due primarily to the uncertainty in the turbulent diffusion coefficient. However, the intermediate value of λ, = 4.64×10^{-4} $m^{2/3}/s$ is probably a reasonable estimate, suggesting a value of x_t of about 10L. This point is approximately the beginning of the second plume shown in Figure 6.9. The friction factor, f, was estimated to lie between 0.018 and 0.028, resulting in estimates of x_m for vertical mixing from Eq. 6.37 of between 21L and 41L. These results imply that the portion of the surface plume shown in Figure 6.9 is unaffected by ambient turbulence.

It is also of interest to compute x_t for the 120 inch outfall of the Los Angeles County Sanitation Districts, where L = 4440 ft (1353 m), H = 200 ft (61 m), and the average daily flow is 210 mgd (9.2 m^3/s). Assuming intermediate parameter values of: $\lambda = 4.64 \times 10^{-4}$ $m^{2/3}/s$; $\gamma = 2$; $\varepsilon = 10^{-5}$ m^2/s, the transition distance, x_t is predicted to increase from 2L to 6L as the current speed increases from 0.1 knot to 0.5 knot. The distance of the diffuser from the shoreline is roughly 2L (Figure 6.1), suggesting that horizontal mixing will not significantly affect dispersion in the vicinity of the shoreline.

The results of this section suggest that horizontal spreading is governed by buoyancy forces and not by ambient turbulence in the vicinity of the shoreline. Furthermore, the surface dilution at the shoreline may be the same as that resulting from the initial dilution, as the

subsequent vertical or horizontal mixing due to ambient turbulence may be negligible. Although these conclusions are very tentative, the importance of the shoreline area merits further investigation of the relative roles of ambient turbulence and buoyancy forces in effluent dispersion.

CHAPTER 7

SUMMARY AND CONCLUSIONS

7.1 Introduction

Experiments were performed to investigate the flow field created by a simple line plume of finite length in a steady current of uniform density. The results can be used to aid in the prediction of dispersion of buoyant waste water released from line diffusers of length, L, much greater than the water depth, H. The range of variables investigated was chosen to cover those typical of sewage discharges into the ocean.

7.2 Flow Regimes

The dispersion pattern for currents perpendicular to the diffuser can take one of three forms depending on the value of a Froude number, F, defined by:

$$F = u^3/b \quad ,$$

where u is the current speed, and b the buoyancy flux per unit length, defined by Eq. 2.1. These regimes are shown in Figure 2.3 for a line diffuser between two parallel walls. For $F < 0.2$ a plume pattern results and a surface wedge forms which spreads upstream against the current. For $F > 0.2$ the plume mixes over the receiving water depth, a situation denoted as forced entrainment, Figure 2.3b, and for $F > 1$ the upstream wedge is swept away, Figure 2.3c.

When the diffuser is of finite length, and $F < 1$, a resulting upstream wedge causes the width of the surface field at the diffuser to

be greater than the diffuser length, for example, Figure 5.2. For $F > 0.2$, the diluted effluent is first attached to the lower boundary, but separates at some point downstream, as shown for $F \approx 10$ in the photograph of Figure 5.3. The region of lower boundary attachment is the dark triangle extending about three diffuser lengths downstream. The limits of the zone of lower boundary attachment are straight. The length of the lower boundary attachment was predicted to be proportional to the diffuser length and independent of cross-flow Reynolds number, $Re = \frac{4uH}{\nu}$. This prediction, Eq. 3.24, was verified by the experiments in the range $1 < F < 36$, $3.7 < L/H < 15$, are $2900 < Re < 12{,}300$.

In the case of a diffuser parallel to the current, the two-layer flow formed immediately without lower boundary attachment. This occurred for all Froude numbers up to the maximum observed value of 100.

7.3 Dilutions

The normalized surface dilution, $S_m q/uH$, where S_m is the minimum surface dilution, q is the volume flux of effluent per unit diffuser length, and H is the water depth, was found to be independent of L/H in the range $3.7 < L/H < 30$, and Re in the range $1190 < Re < 12{,}900$. The results could be expressed as:

$$\frac{S_m q}{uH} = f(F,\theta) \quad ,$$

where θ is the angle of the diffuser to the current (Figure 2.1). The experimental results are shown in Figure 5.27. For F less than about 0.1, dilution is independent of the current speed and direction. For $F > 0.1$, dilutions depend on the current direction, and for a

current flowing perpendicular to the diffuser, dilution is proportional to current speed. When the diffuser is parallel to the current, dilution does not increase so rapidly with current speed. In general, a diffuser oriented parallel to the current results in a thinner, more concentrated surface waste field than one perpendicular to the current. For F greater than about 10, the dilution achieved by a diffuser parallel to the current is about four times smaller than one perpendicular to the current. Conversely, a diffuser approximately four times as long would be required for equal dilutions if the diffuser is parallel, rather than perpendicular to the current.

7.4 Internal Structure

The forced entrainment ($F > 0.2$) initial mixing process is discussed in Section 3.3.2. Buoyancy-induced mixing is limited to a finite horizontal distance downstream because the free surface, which causes a vertically stable density profile to develop, damps the mixing and causes it to decrease with distance from the source. Because of the development of the stable density profile, surface dilutions are only 58% of those predicted by assuming uniform mixing over the receiving water depth in the range $0.1 < F < 100$. Beyond the mixing zone is an equilibrium region where the shape of the vertical concentration profile does not change with distance downstream. Examples of concentration profiles are shown in Figures 5.13 and 5.14. The surface layer thickness outside the zone of lower boundary attachment up to the point of separation is half the receiving water depth. Beyond this point the surface layer thins as it spreads horizontally.

Dispersion when the current is parallel to the diffuser has several characteristics. Profiles transverse to the current show the surface layer thickness and effluent concentrations to be least on the centerline immediately downstream of the diffuser, resulting in a clear zone, Figure 5.16, which persists for some distance downstream for $1 < F < 100$. The effluent concentration on the centerline near the surface is approximately constant until the downstream diffuser end. It then suddenly drops in the clear zone and subsequently increases downstream due to horizontal mixing. Hence, the transverse surface concentration profiles are bimodal, with the minimum surface dilution occurring off the centerline at the sides of the diffuser, for example, Figure 5.21. The thickness of the surface layer is everywhere less than half the receiving water depth.

Flows for intermediate current directions can possess characteristics of both parallel and perpendicular currents, for example, Figure 5.24. Here, for $F \approx 1$, an upstream wedge forms, as for a perpendicular current, but a clear zone forms also, as for a parallel current. For stronger currents (Figure 5.25) the flow becomes similar to that for a perpendicular current, with a zone of lower boundary attachment extending some distance downstream.

7.5 Buoyant Surface Spreading

The dynamics of buoyant surface spreading were discussed in Sections 3.3, 3.4, and 3.5. It was predicted that various growth laws could apply due to the changing with distance downstream of both the influence of source geometry and the types of forces dominating the spreading. Three growth laws were identified; they are shown in Figure 3.5.

For $F \geq 1$ it was predicted that near to the source spreading would be controlled by a balance of pressure and inertia forces. The source geometry would be important, resulting in a linear growth rate of the surface field with distance downstream. The growth rate was predicted to be independent of L/H, for $L/H \gg 1$, and Re. The results, Figure 5.18, confirmed the prediction for spreading in a parallel current Eq. 3.43, for $1 < F < 100$, $3.7 < L/H < 15$, and $2500 < Re < 12{,}740$. For this range of variables the surface field was linear at least up to the downstream diffuser end. The results for flow perpendicular to the diffuser, Figure 5.11, confirmed the prediction, Eq. 3.26, for $3.7 < L/H < 15$, and $2{,}900 < Re < 12{,}300$.

Beyond this initial linear spreading region, it was speculated that a flow regime might exist where the effect of source geometry is unimportant. This results in a region where the plume width grows as the 2/3-power of distance downstream, Eq. 3.47. The results for surface spreading for perpendicular currents, Figures 5.7, 5.8, and 5.9, showed some of the plumes to display this 2/3-power growth law.

Far from the diffuser the surface spreading is assumed to be resisted primarily by interfacial shear; a 1/5-power growth law is predicted, Eq. 3.62. The results suggested that none of the plumes extended fully into this regime.

Locations of these transitions between the different regimes are, in general, functions of F, L/H, and Re. The surface plume was found to be linear at least up to the point of lower boundary separation for perpendicular currents for $1 < F < 10$, $3.7 < L/H < 15$ and $5{,}300 < Re < 12{,}300$. Only for a very low Re flow (G8, $Re = 2900$) did the plume become nonlinear

in a shorter distance.

For $F < 1$ an upstream wedge forms, and the surface field is predicted to be strongly affected by interfacial shear and hence to grow as the 1/5-power of distance downstream. The results, Figure 5.7, show this result.

The data are inadequate to fully confirm the predicted far-field spreading rates. Only the predicted initial linear growth rates for $F \geq 1$ are confirmed by the results within the specified limits of F, L/H, and Re. However, the far-field growth rate must be less than the initial rate, so the prediction of the initial growth rate, Eq. 3.43 for parallel currents, or Eq. 3.26 for perpendicular currents, can be used to predict an upper limit to the size of the surface waste field.

7.6 Effects of Ambient Turbulence

At large distances from the source, mixing is effected by ambient turbulence. An estimate was made for the distance required for the surface dilution to be affected, assuming that vertical mixing results from turbulence generated by shear at the lower boundary. It was concluded that ambient turbulence in the model only affects the initial dilution for $F \gg 10$. The effect on horizontal dispersion was estimated by considering the asymptotic solution for horizontal diffusion due to ambient turbulence. At distances of practical interest from very long diffusers (e.g. to the shoreline), it is possible that ambient turbulence could have no significant effect on dilution of the waste field or on horizontal spreading (which is dominated by buoyancy forces).

7.7 Comparisons with Other Studies

There are few data available on multiport diffusers with which to compare the present results. There are no data available on three-dimensional dispersion for F greater than about 0.1. Comparisons with two-dimensional studies show the results to approach those of the present study for $F > 1$. For smaller Froude numbers, however, dilutions measured in two-dimensional studies are about 50% higher than those found in the present study. This is probably due to differences in flow patterns between two and three-dimensional flows.

Field studies of paper mill outfalls obtained dilution measurements which sometimes agreed and sometimes disagreed with the results of the present study. The field measurements were inconsistent, however, and the discrepancies may be due to uncertainties in the field measurements, particularly in current data. The behavior of the surface plumes showed qualitative agreement with that reported here.

7.8 Conclusions

The effect of a finite diffuser length is important in determining effluent dispersion in an ambient current. Even though the length may be very much greater than the water depth, the flow cannot be considered to be two-dimensional. The orientation of the diffuser to the current also affects dispersion. In general, a diffuser parallel to the current results in a thinner, more concentrated surface layer than a diffuser perpendicular to the current. For a perpendicular current when $F > 0.2$, the effluent initially mixes over the receiving water depth; however, it does not become uniformly mixed for $0.2 < F \leq 100$, with the minimum

surface dilution in this range being about 60% of that predicted for complete uniform mixing.

7.9 Recommendations

It is recommended that the results of the present study be used in ocean outfall design. Field studies of operating outfalls should be conducted to assess the scaling errors inherent in applying laboratory measurements to full size conditions. The effects of ambient turbulence and the mechanism of interfacial shear should also be investigated in the field.

7.10 Significance of Results for Practical Applications

The present research should have significant impact on outfall design because it conclusively demonstrates the error in assuming two-dimensional flow for line diffusers perpendicular to a current, even when the length of the diffuser is an order of magnitude greater than the depth. The three-dimensional flow field has been defined here in a manner which makes the results immediately applicable to ocean sewer outfall design. These results should be much more reliable than any previous models based on two-dimensional flows. Also, for the first time the effect of diffuser orientation has been experimentally measured. The reader is cautioned that the results are found to be independent of Reynolds number only for $Re < 1.3 \times 10^4$; they have not been verified for $Re \approx 10^6$, which is more typical of ocean conditions.

REFERENCES

Abraham, G. (1965), "Horizontal jets into stagnant fluid of other density," J. Hyd. Div., ASCE, 94(HY4):138-154.

American Public Health Association (1971), "Standard methods for the examination of water and wastewater," New York.

Anwar, H. O. (1972), "Measurements on horizontal buoyant jets in calm ambient fluid, with theory based on variable coefficient of entrainment determined experimentally," Houille Blanche, 27(4): 311-319.

Bache, D. H. (1976), "Density current surges, Parts I and II," J. Hyd. Res., 14(1):1-16.

Benjamin, T. B. (1968), "Gravity currents and related phenomena," J. Fluid Mech., 31(2):209-248.

Brooks, N. H. (1960), "Diffusion of sewage effluent in an ocean current," Proceedings of First International Conference on Waste Disposal in the Marine Environment, Pergamon Press, New York.

Bühler, J. (1974), "Model studies of multiport outfalls in unstratified, stagnant or flowing receiving water," Ph.D. Thesis, University of California at Berkeley.

Burgess, F. J. and James, W. P. (1970), "Aerial photographic tracing of pulp mill effluent in marine waters," Federal Water Quality Office, U. S. Environmental Protection Agency, Water Pollution Control Research Series, 12040 EBY.

REFERENCES (Continued)

Burgess, F. J. and James, W. P. (1971), "Airphoto analysis of ocean outfall dispersion," U. S. Environmental Protection Agency, Water Pollution Control Research Series, 16070 ENS.

Cederwall, K. (1967), "Jet diffusion. Review of model testing and comparison with theory," Chalmers Institute of Technology, Division of Hydraulics, Publication Number 35.

Cederwall, K. (1971), "Buoyant slot jets into stagnant or flowing environments," W. M. Keck Laboratory of Hydraulics and Water Resources, California Institute of Technology, Report No. KH-R-25.

Chu, V. H. and Vanvari, M. R. (1976), "Experimental study of turbulent stratified shearing flow," J. Hyd. Div., ASCE, 102(HY6):691-706.

Fan, L. N. and Brooks, N. H. (1969), "Numerical solutions of turbulent buoyant jet problems," W. M. Keck Laboratory of Hydraulics and Water Resources, California Institute of Technology, Report No. KH-R-18.

Fischer, H. B. (1966), "Longitudinal dispersion in laboratory and natural streams," W. M. Keck Laboratory of Hydraulics and Water Resources, California Institute of Technology, Report No. KH-R-12.

Hansen, J. and Schroder, H. (1968), "Horizontal jet dilution studies by use of radioactive isotopes," Acta Polytechnica Scandinavia, Copenhagen, Publication No. 49.

Jirka, G. and Harleman, D. R. F. (1973), "The mechanics of submerged multiport diffusers for buoyant discharges in shallow water," Ralph M. Parsons Laboratory for Water Resources and Hydrodynamics, Massachusetts Institute of Technology, Report No. 169.

REFERENCES (Continued)

Kato, H. and Phillips, O. M. (1969), "On the penetration of a turbulent layer into a stratified fluid," J. Fluid Mech., 37:643-655.

Koh, R. C. Y. (1971), "On buoyant jets," IAHR Fourteenth Congress, Paris, Paper No. A18.

Koh, R. C. Y. (1971), "Two-dimensional surface warm jets," J. Hyd. Div., ASCE, 97(HY6):819-836.

Koh, R. C. Y. and Brooks, N. H. (1975), "Fluid mechanics of waste water disposal in the ocean," Ann. Rev. of Fluid Mech., 7:187-211.

Koh, R. C. Y., et al. (1974), "Hydraulic modeling of thermal outfall diffusers for the San Onofre Nuclear Power Plant," W. M. Keck Laboratory of Hydraulics and Water Resources, California Institute of Technology, Report No. KH-R-30.

Koh, R. C. Y. and Fan, L. N. (1970), "Mathematical models for the prediction of temperature distributions resulting from the discharge of heated water into large bodies of water," Environmental Protection Agency, Water Pollution Control Research Series, 16130 DWO.

Kotsovinos, N. E. (1975), "A study of the entrainment and turbulence in a plane buoyant jet," W. M. Keck Laboratory of Hydraulics and Water Resources, California Institute of Technology, Report KH-R-32.

Larsen, J. and Sorensen, T. (1968), "Buoyancy spread of wastewater in coastal regions," Eleventh Conference on Coastal Engineering, London, 2:1397-1402.

REFERENCES (Continued)

Liseth, P. (1970), "Mixing of merging buoyant jets from a manifold in stagnant receiving water of uniform density," University of California, Berkeley, Hydraulic Engineering Laboratory, Tech. Rept. HEL 23-1.

Liseth, P. (1976), "Wastewater disposal by submerged manifolds," J. Hyd. Div., ASCE, 101(HY1):1-13.

Nospal, A. and Tatinclaux, J. C. (1976), "Design of alternating diffuser pipes," J. Hyd. Div., ASCE, 120(HY4):553-558.

O'Brien, M. P. and Cherno, J. (1934), "Model law for motion of salt water through fresh," Trans. ASCE, 99:576-609.

Okoye, J. K. (1970), "Characteristics of transverse mixing in open-channel flows," W. M. Keck Laboratory of Hydraulics and Water Resources, California Institute of Technology, Report No. KH-R-23.

Pearson, E. A. (1956), "An investigation of the efficacy of submarine outfall disposal of sewage and sludge," State Water Pollution Control Board, Sacramento, California, Publ. No. 14.

Prych, E. A. (1970), "Effects of density differences on lateral mixing in open-channel flows," W. M. Keck Laboratory of Hydraulics and Water Resources, California Institute of Technology, Report No. KH-R-21.

Rawn, A. M. and Palmer, H. K. (1930), "Pre-determining the extent of a sewage field in sea water," Trans. ASCE, 94:1034-1060.

REFERENCES (Continued)

Roberts, P. J. W. (1975), "The diffusion of buoyant effluent from outfall diffusers of finite length - Progress Report," W. M. Keck Laboratory of Hydraulics and Water Resources, California Institute of Technology, Tech. Memo. 75-1.

Rouse, H. (1947), "Gravitational diffusion from a boundary source in two-dimensional flow," J. of Appl. Mech., ASME, A225-A228.

Rouse, H., Yih, C. S., and Humphreys, H. W. (1952), "Gravitational convection from a boundary source," Tellus, 4:201-210.

Shirazi, M. A. and Davis, L. R. (1972), "Workbook on thermal plume prediction, Vol. I: Submerged discharges," U. S. Environmental Protection Agency, Water Pollution Control Research Series, EPA-R2-72-005a.

Taylor, G. I. (1961), "Fire under influence of natural convection," International Symposium on the Use of Models in Fire Research, NAS-NRC, Washington, D.C., 1961, Publ. 786.

Turner, J. S. (1973), "Buoyancy effects in fluids," Cambridge University Press.

Weil, J. and Fischer, H. B. (1974), "Effect of stream turbulence on heated water plumes," J. Hyd. Div., ASCE, 100(HY7):951-969.

APPENDIX A

TWO-DIMENSIONAL EXPERIMENTS

a. Introduction

The analysis of the experiments described in this report assumes the source to produce a pure line plume in a state of fully developed turbulence. In order to assess these assumptions, a series of experiments was performed. Vertical, parallel walls were placed perpendicular to each end of the diffuser to produce a two-dimensional flow. Concentration profiles across the rising plume and the rate of surface spreading were measured in stagnant receiving water. The results were compared with those obtained from larger scale studies. These experiments and the results obtained are summarized in this appendix.

b. Analysis

A pure, fully turbulent plume is characterized only by the source buoyancy flux per unit length, b. For a source discharging a small volume flux, q, b is defined by Eq. 2.1 as:

$$b = \frac{\rho_r - \rho_o}{\rho_o} gq \quad , \tag{A.1}$$

where ρ_r and ρ_o are the densities of the receiving water and effluent, and g is the acceleration due to gravity. It is assumed that density changes in the flow field are small compared with the absolute density, and affect only the gravitational and not the inertia forces (the Boussinesq assumption). The buoyant weight $(\rho_r - \rho)g$, is then a dependent

variable, and we can write:

$$(\rho_r - \rho)g = f(b,x,y,\rho_o) \quad , \tag{A.2}$$

where ρ_r is eliminated as a dependent variable by use of the Boussinesq assumption. y and x are the vertical and horizontal distances from the source, respectively. A dimensional analysis of Eq. A.2 yields:

$$\frac{(\rho_r - \rho)gy}{\rho_o b^{2/3}} = f(\frac{x}{y}) \quad . \tag{A.3}$$

On substituting the definitions of dilution, S (Eq. C9):

$$S = \frac{\rho_r - \rho_o}{\rho_r - \rho} \quad ,$$

and b (Eq. A.1) into Eq. A.3, and rearranging, we obtain:

$$\frac{yg_o'^{1/3}}{Sq^{2/3}} = f(\frac{x}{y}) \quad , \tag{A.4}$$

where $$g_o' = \frac{\rho_r - \rho_o}{\rho_r} g \quad .$$

Experiments to determine the form of Eq. A.4 have been performed by Rouse, Yih, and Humphreys (1952), who measured temperatures and velocities in the convective flow above a line burner. Although their data showed considerable scatter, they expressed the result for temperature and density distribution as:

$$(\rho_r-\rho)g = 2.6\left[\frac{\rho_r(b\rho_r)^2}{y^3}\right]^{1/3} \exp\left\{-41\,\frac{x^2}{y^2}\right\}, \qquad (A.5)$$

where b was computed from the thermal energy per unit width, H, convected away from the source by the relation:

$$b = \frac{\omega g H}{c_p},$$

where c_p is the specific heat and ω the coefficient of thermal expansion. It is assumed that the buoyancy flux is produced by a source volume flux, q, of hot water of mass density ρ_o. b is then given by Eq. A.1 and, by assuming $\rho_r \approx \rho_o$, defining S as in Eq. C9, then Eq. A.5 can be written in the form of Eq. A.4 as:

$$\frac{y g_o'^{1/3}}{Sq^{2/3}} = 2.6 \exp\left\{-41\,\frac{x^2}{y^2}\right\}. \qquad (A.6)$$

More recent experiments have been performed by Kotsovinos (1975). He measured velocities with a laser Doppler velocimeter and temperature by fast response thermistors above a two-dimensional heated water jet. Kotsovinos varied the source parameters to cover flow conditions ranging from a pure jet to a pure plume. Kotsovinos' results for plumes at large distances from the origin can be expressed in the same form as Eq. A.5, assuming $\rho_o \approx \rho_r$, as:

$$\frac{(\rho_r-\rho)g}{\rho_o} = \frac{b^{2/3}}{\sigma_T y} \exp\left\{-\ell n 2\left(\frac{x}{K_{1T} y}\right)^2\right\}, \qquad (A.7)$$

where σ_T and K_{1T} are experimental constants. By following the same arguments outlined above, Eq. A.7 can be written as:

$$\frac{yg_o'^{1/3}}{Sq^{2/3}} = \frac{1}{\sigma_T} \exp\left\{ - \ell n 2 \left(\frac{x}{K_{1T} y} \right)^2 \right\} . \qquad (A.8)$$

Kotsovinos recommends values of σ_T and K_{1T} as 0.42 and 0.14, respectively, and so Eq. A.8 becomes:

$$\frac{yg_o'^{1/3}}{Sq^{2/3}} = 2.38 \exp\left\{ - 35 \frac{x^2}{y^2} \right\} , \qquad (A.9)$$

in contrast to the result of Rouse, Yih, and Humphreys, Eq. A.6. Kotsovinos showed that the method used by Rouse, et al. to compute b was incorrect in neglecting the turbulent heat flux, and also in assuming a constant value of the thermal expansion coefficient. Kotsovinos computed b from the known heat flux at the source and used a variable thermal expansion coefficient computed at the local temperature. Hence, the expression for dilution in a pure plume in a stagnant medium due to Kotsovinos, Eq. A.9, is probably more reliable than that due to Rouse, Yih, and Humphreys, Eq. A.6.

After the flow reaches the surface, the motion of the effluent becomes horizontal as it spreads laterally under the force of gravity (see Figure 2.5). The surface spreading rate can be predicted in a manner similar to that used by Koh and Fan (1970) in analyzing the problem shown in Figure 2.6. Although the submerged source case differs from the surface source in that the former has entrained flow in the

lower layer, the same power laws would be expected to apply in both situations.

The initial spreading rate, u_f, is predicted to be constant, and is given by Eq. 2.10 as

$$u_f = K_1 b^{1/3} \quad , \tag{A.10}$$

where K_1 is a constant. If the length of the surface layer is w, Eq. A.10 becomes:

$$\frac{w}{2b^{1/3}t} = K_1 \quad , \tag{A.11}$$

where t is time. As discussed in Section 2.3, the thickness of the surface layer, h, in this initial spreading period is constant, hence:

$$h = f(H,b) \quad , \tag{A.12}$$

where the effect of viscosity is neglected. A dimensional analysis of Eq. A.12 gives:

$$\frac{h}{H} = K_8 \quad , \tag{A.13}$$

where K_8 is a constant. The value of K_8 is estimated to lie between 0.3 and 0.4 based on the experimental results of Bühler (1974) and Liseth (1970), discussed in Section 2.3.

For long times, Koh and Fan predict that interfacial shear is the dominant force resisting the surface spreading, hence:

$$w = f(b,H,\nu,t) \quad , \tag{A.14}$$

where ν is the kinematic viscosity. A dimensional analysis of Eq. A.14 yields:

$$\frac{w}{2b^{1/3}t} = f\left(\frac{\nu t}{H^2}, \frac{b^{1/3}t}{H}\right) . \qquad (A.15)$$

The second parameter, $b^{1/3}t/H$, is the ratio of flow time to the time required for the plume to reach the surface after starting. Hence, after the plume reaches the surface the effect of this parameter is lost. Eq. A.15 then becomes:

$$\frac{w}{2b^{1/3}t} = f\left(\frac{\nu t}{H^2}\right) . \qquad (A.16)$$

Koh and Fan predict w to grow in proportion to $t^{4/5}$ in the shear dominated phase (Eq. 2.11), and so Eq. A.16 must have the form:

$$\frac{w}{2b^{1/3}t} = K_9\left(\frac{\nu t}{H^2}\right)^{-1/5} , \qquad (A.17)$$

where K_9 is an experimental constant.

c. Description of Experiments

The basin, diffuser, and effluent metering system described in Sections 4.2.1 and 4.2.2 were used. In addition, vertical walls were installed perpendicular to the ends of the diffuser, forming a channel whose ends opened into the basin, Figure A.1. The center section of the channel was formed by clear lucite panels and a mirror installed at approximately 45° to the vertical enabled a horizontal view of the flow to be obtained in the overhead photographs. Fiducial marks were placed

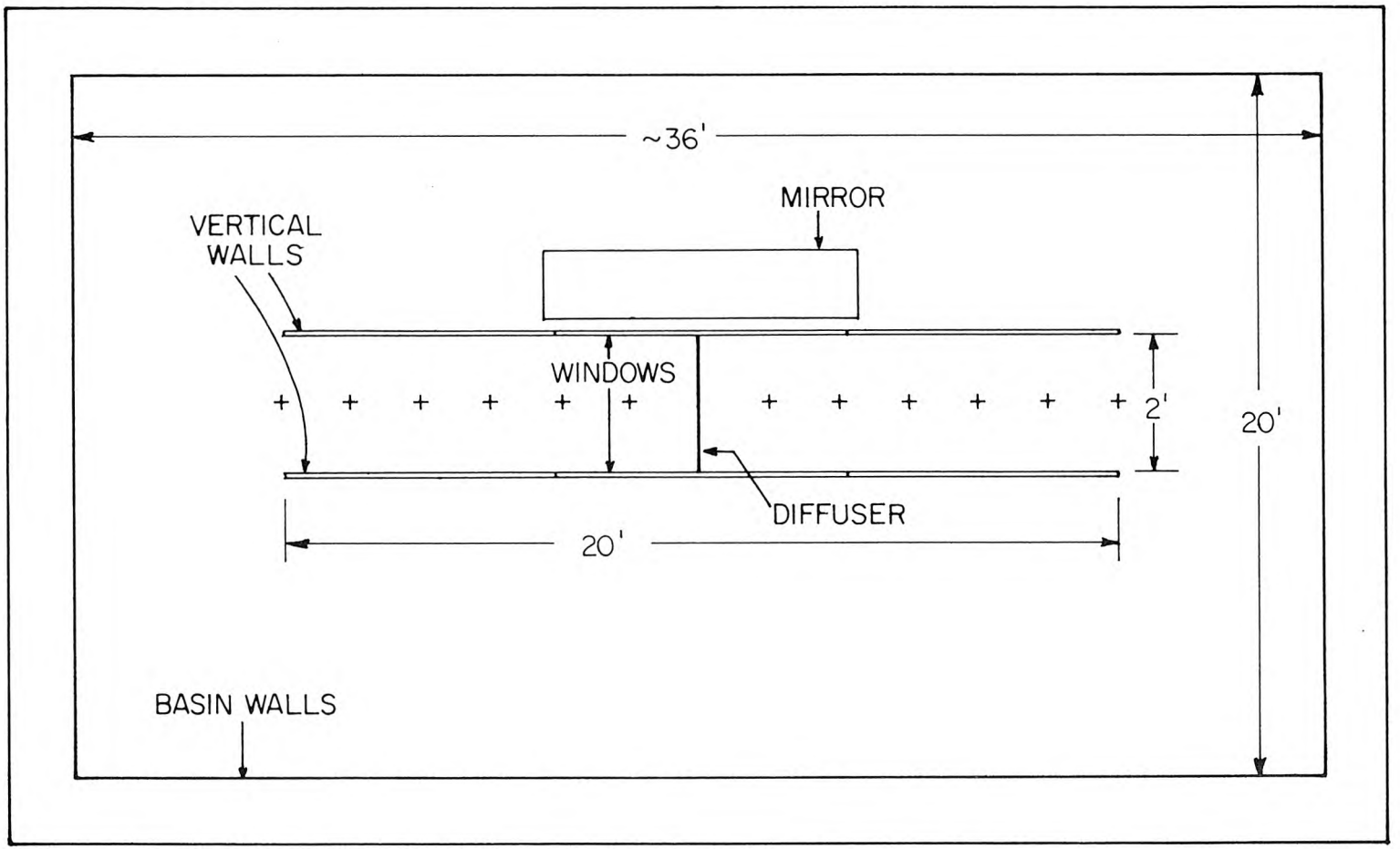

Figure A.1 Configuration for two-dimensional experiments (not to scale).

at one foot intervals along the channel centerline.

Dilutions were measured with the same system used for the three-dimensional experiments, Section 4.2.4, except that the twin electrode conductivity probe shown in Figure A.2 was used. The probe was mounted on a test carriage (Figure 4.3) such that traverses perpendicular to the plume axis could be made. The probe position was measured to ± 1/10 mm by means of a vernier gage. Traverses were made across the plume beneath the surface layer. Two minute averages were taken at each of nine points at a rate of 10 samples per second.

Overhead photographs were taken at regular intervals during the course of the experiments. The length of the surface layer was measured from each photograph, and the growth of the layer as a function of time computed.

Experiments were performed at three values of the buoyancy flux per unit length, b, of about 2.6, 4.7, and 8.0 cm^3/s^3. The density difference was maintained nominally constant at 0.025 g/cc, and the variation in buoyancy flux was achieved by changing the discharge rate. For the surface spreading experiments, water depths of 4, 8, and 16 cm were used, and concentration traverses at probe heights of about 4, 8, and 14 cm were made. Hence, there were nine dilution traverses, and nine surface spreading experiments. A summary of the experimental data is given in Table A.1.

d. Results

Figure A.3 shows a photograph of an experiment at a water depth of 16 cm, and a buoyancy flux of 8.8 cm^3/s^3. The appearance of the flow

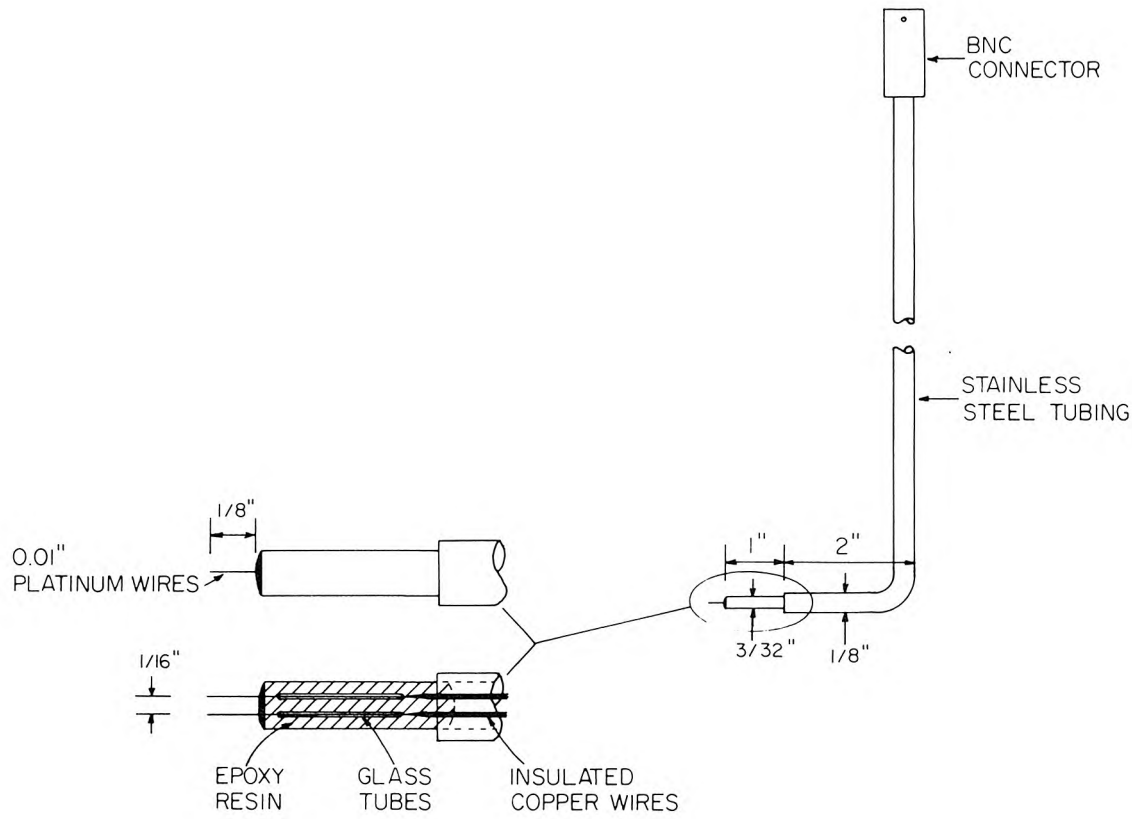

Figure A.2 Conductivity probe used in two-dimensional experiments.

Table A.1 Summary of data for two-dimensional experiments.*

Experiment Number	H Water Depth cm	$\Delta\rho/\rho_o$ Density Difference x 10^3	q Effluent Flow Rate cm^2/s	b Buoyancy Flux $= q \frac{\Delta\rho}{\rho_o} g$ cm^3/s^3
D2	16.30	24.6	0.104	2.55
D4	8.09	25.3	0.106	2.67
D5	8.14	26.1	0.184	4.80
D7	4.05	25.7	0.103	2.65
D8	4.04	25.5	0.181	4.61
D10	16.14	26.0	0.180	4.67
D11	16.25	25.4	0.330	8.39
D12	8.14	25.1	0.329	8.26
D14	4.03	26.0	0.327	8.50
D16	16.0	26.0	0.339	8.81
E31	13.29	24.5	0.313	7.67
E32	13.29	24.5	0.180	4.40
E33	13.29	24.5	0.104	2.54
E41	19.36	25.5	0.280	7.13
E42	19.36	25.5	0.179	4.57
E43	19.36	25.5	0.104	2.64
E51	24.03	24.9	0.278	6.91
E52	24.03	24.9	0.182	4.53
E53	24.03	24.9	0.105	2.62

* D denotes surface spreading experiments, and E dilution experiments.

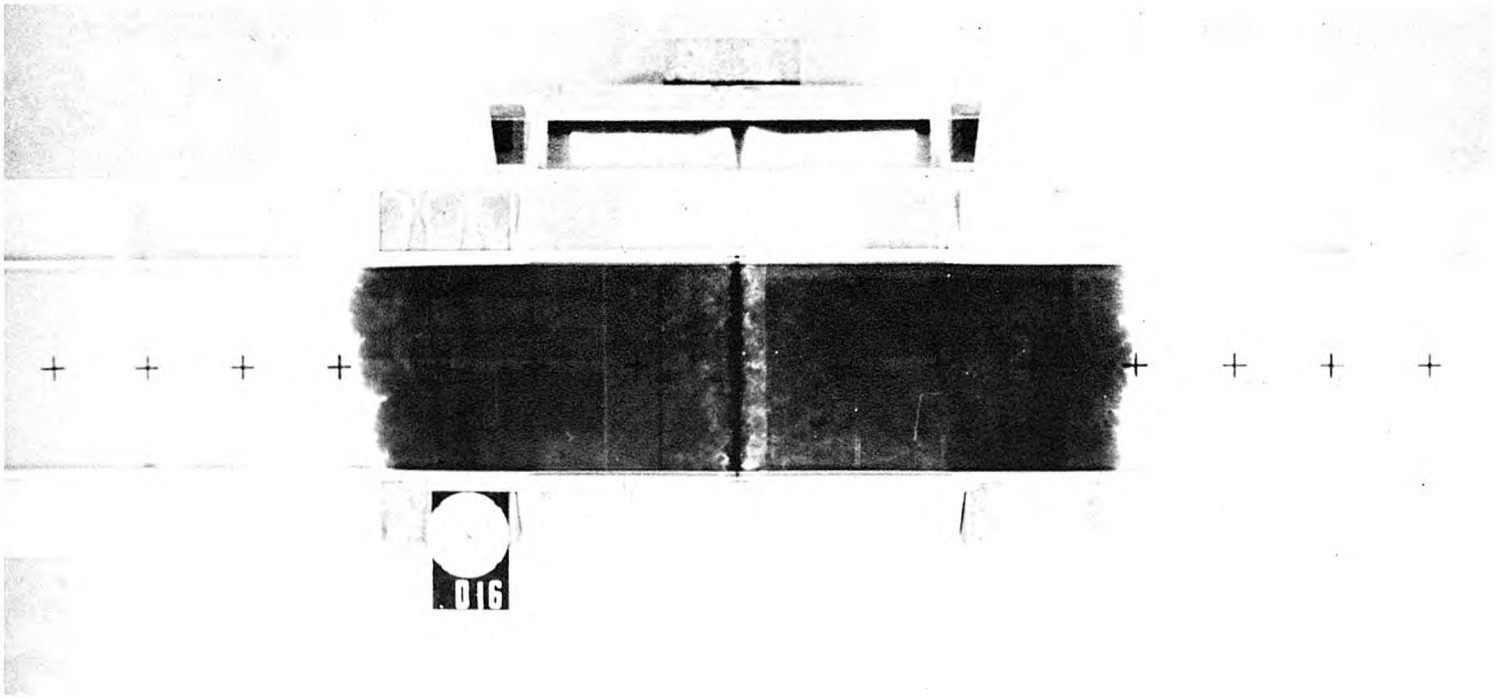

Figure A.3 Overhead photograph of two-dimensional dispersion of a submerged line source of buoyancy flux. Oblique mirror at top shows horizontal view of flow.

in the horizontal view through the mirror is very similar to the postulated flow in the center portion of a diffuser, Figure 2.5. The thickness of the surface layer is about 30% of the water depth, as was found for all flow rates and water depths. Hence, the value of the constant K_8 in Eq. A.13 is approximately 0.3.

The surface spreading results are plotted in the form of Eq. A.16 in Figure A.4 in addition to the predictions, Eqs. A.11 and A.17. The results are plotted with a time shift, t_o, which was chosen to shift the results for small t onto the predicted curves. t_o does not affect the results for longer times. The values of the experimental constants K_1 and K_9 are 0.68 and 0.27, respectively. The value of 0.68 for K_1 is in close agreement with that of 0.66 obtained from Bühler's experiments with a multiport diffuser, discussed in Section 2.3.

The results of the concentration traverses are shown in Figure A.5, plotted in the form of Eq. A.4. Also plotted are the results of Kotsovinos (1975), Eq. A.9, and those of Rouse, et al. (1952), Eq. A.6.

e. Discussion and Conclusions

The analysis of Koh and Fan predicts the initial surface spreading rate of buoyant effluent discharged from a line source to be constant, and determined primarily by the source buoyancy flux. For longer times, the length of the surface layer is predicted to grow as the 4/5 power of time. The results, Figure A.4, confirm these predictions. Further, the results show close agreement with those of the experiments of Bühler (1974) on multiport diffusers at water depths up to 40 times greater than those used in the present study. This confirms that the surface

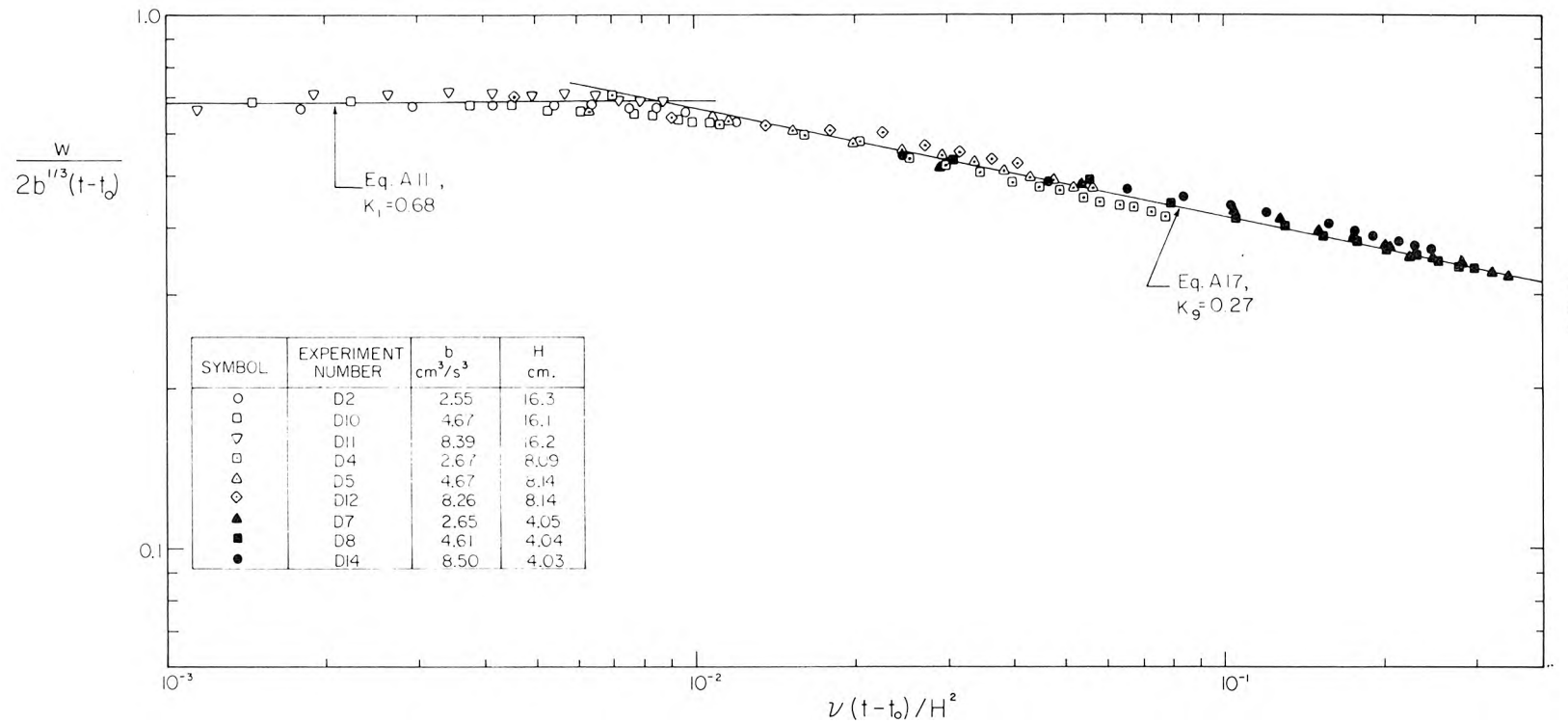

Figure A.4 Surface spreading rate of buoyant effluent discharged from a submerged line source in two-dimensional flow.

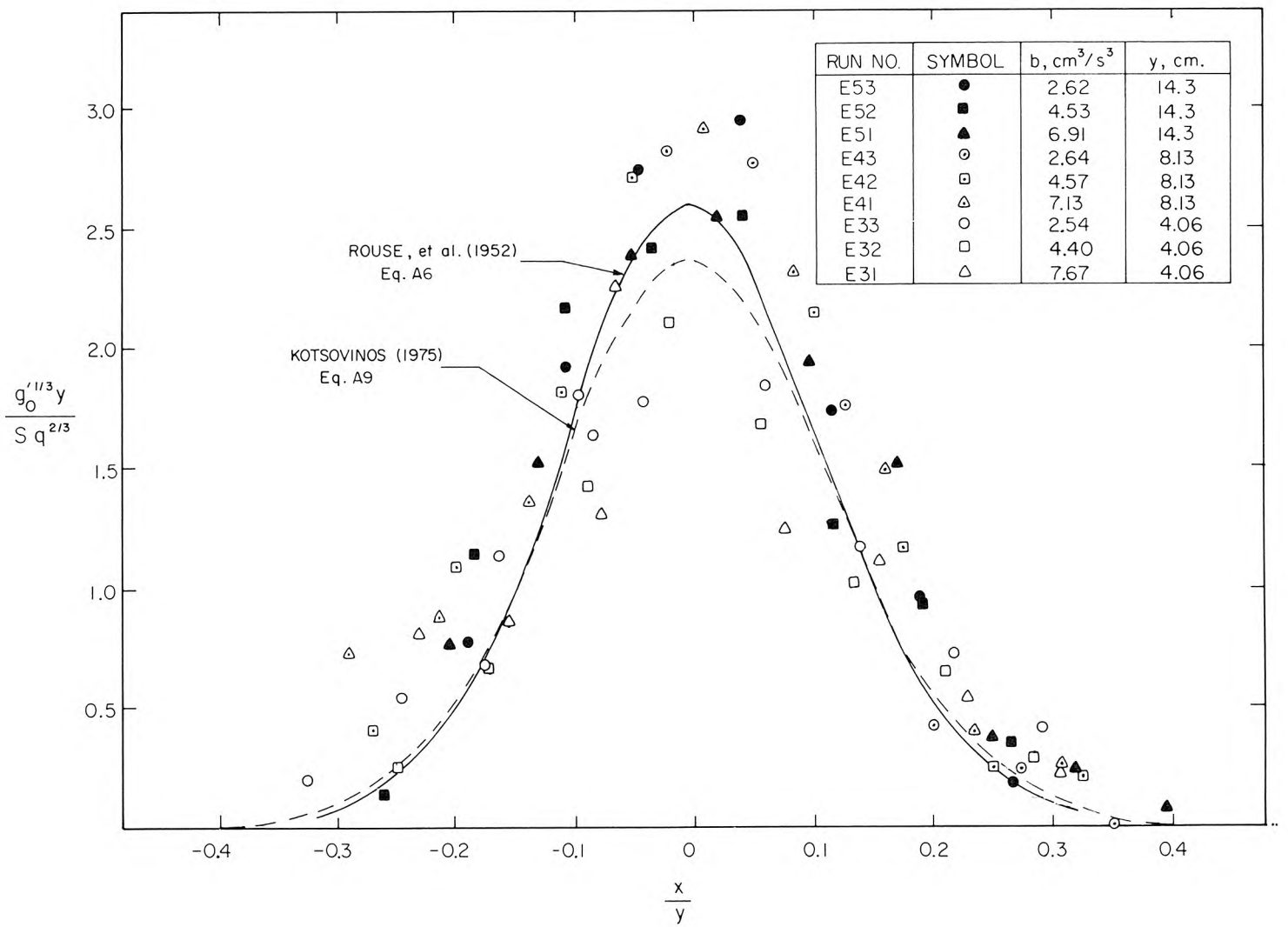

Figure A.5 Horizontal dilution traverses across plume, two-dimensional flow.

spreading rate of effluent discharged from multiport diffusers is primarily governed by the source buoyancy flux per unit length and that it is possible to reproduce these results at the very small scale of the present experiments.

Normalized concentrations measured in horizontal traverses across the plume are shown in Figure A.5. The data show a scatter of about ± 20% from the results of the larger scale experiments of Rouse, et al. (1952), and Kotsovinos (1975). Part of the scatter is probably due to the difficulty in achieving a completely stagnant ambient fluid. Small circulations in the basin occurred which affected the plume due to the low buoyancy fluxes used. Other sources of experimental error may exist. These were not investigated as it was not the purpose of these experiments to make very careful measurements. It is concluded that the source produces a good approximation to a line plume with dilutions which are within ± 20% of those obtained from larger scale studies.

APPENDIX B

DILUTION PREDICTION FOR A MULTIPORT DIFFUSER IN STAGNANT, UNIFORM FLUID

This Appendix consists of Sections III-1 and III-2 of:

Roberts, P. J. W. (1975), "The Diffusion of Buoyant Effluent from Outfall Diffusers of Finite Length - Progress Report," Tech. Memo. 75-1, W. M. Keck Laboratory of Hydraulics and Water Resources, California Institute of Technology.

III. SUMMARY OF PREVIOUS WORK

III-1. Introduction

The basic hypothesis of this study is that for estimation of dilution and size of the surface waste field, many diffusers can be replaced by an equivalent source of buoyancy flux only. A means for estimating the degree of this approximation in any particular instance is given below. In Section III-3 the results of experimental studies on line buoyant jets and diffusers in a flowing fluid are discussed.

III-2. Prediction of dilution above a multiport diffuser in a stagnant, uniform fluid

The diffuser illustrated in Figure 1 consists of a pipe with circular ports along each side through which the effluent escapes. The following analysis is derived principally for this type of diffuser although it can also be applied to others in which the effluent is discharged as horizontal round buoyant jets, e.g. through risers.

Near the point of discharge, the effluent behaves as if it were an unrestricted horizontal round buoyant jet, and the minimum dilution can be predicted from a consideration of this type of flow. At some point above the diffuser the jets begin to merge. The centerline dilution is then reduced below what would be expected for individual jets, and the flow approaches that which would be produced by a two-dimensional plume. The following analysis provides a means of predicting the minimum dilution at any point above a diffuser in a stagnant, uniform environment. This dilution can then be compared with that predicted by assuming the diffuser is replaced by its equivalent source of buoyancy flux only. Thus the degree of the approximation involved in making this assumption can be assessed.

First consider the horizontal round buoyant jet in a stagnant, uniform fluid of infinite extent, as shown in Figure 3. By making use of the Boussinesq assumption, i.e., that changes in density are small compared with the absolute density, we can write:

$$g' = f(Q_o, M_o, B_o, x, y, z). \tag{12}$$

Where

$$Q_o = u_e \frac{\pi}{4} D_e^2, \text{ volume flux,} \tag{13}$$

$$M_o = u_e^2 \frac{\pi}{4} D_e^2, \text{ momentum flux,} \tag{14}$$

$$B_o = u_e \frac{\pi}{4} D_e^2 g_o', \text{ buoyancy flux,} \tag{15}$$

$$D_e = \sqrt{C_c}\, D_o, \text{ diameter of the jet at the vena contracta,} \tag{16}$$

C_c = coefficient of contraction,

and

$$u_e = u_o (D_o/D_e)^2, \text{ mean jet velocity at the vena contracta.} \tag{17}$$

An effective densimetric Froude number of the jet which accounts for the increase in momentum flux due to the vena contracta is defined as:

$$F_e = u_e / \sqrt{g_o' D_e} \ . \tag{18}$$

By combining Equations 18, 17, and 16, we obtain:

$$F_e = C_c^{-5/4} F_o \ , \tag{19}$$

where

$$F_o = u_o / \sqrt{g_o' D_o}, \text{ the usual definition of the densimetric Froude number.} \tag{20}$$

A characteristic length scale Λ which gives the length over which the initial momentum flux is important compared to the buoyancy flux is given by:

$$\Lambda = M_o^{3/4} / B_o^{1/2} \ . \tag{21}$$

Dimensional analysis of Equation 12 then gives:

$$\frac{g' M_o^{5/4}}{B_o^{3/2}} = f\left(\frac{y}{\Lambda}, \frac{x}{\Lambda}, \frac{z}{\Lambda}, \frac{Q_o B_o^{1/2}}{M_o^{5/4}} \right) \tag{22}$$

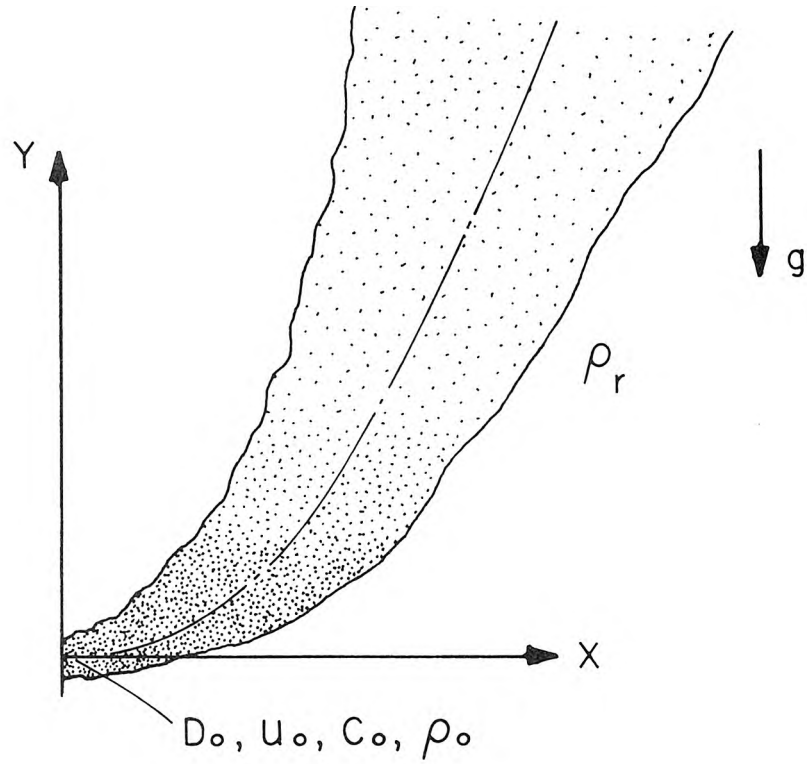

Figure 3. A horizontal, round buoyant jet into a stagnant, uniform fluid.

By combining Equations 9, and 14 through 22, inverting the left-hand side of the result and eliminating constants, we obtain:

$$\frac{S_m}{F_e} = f\left(\frac{y/D_e}{F_e}, \frac{1}{F_e}\right) \tag{23}$$

where S_m is the minimum dilution at a distance y above the jet exit.

Finally, by use of Equations 16 and 19 it can be shown that

$$\left.\begin{aligned} \frac{S_m}{F_e} &= C_c^{5/4}\,\frac{S_m}{F_o} \\ \text{and}\qquad \frac{y/D_e}{F_e} &= C_c^{3/4}\,\frac{y/D_o}{F_o}\ . \end{aligned}\right\} \tag{24}$$

Far above the jet exit, the flow behaves like a plume and the only governing parameters are B_o, y, and r, the radial distance from the centerline. The minimum dilution occurs on the centerline, so put $g' = g'_m$ at $r = 0$, to obtain:

$$g'_m = f(B_o, y)\ , \tag{25}$$

from which a dimensional analysis gives:

$$\frac{g'_m y^{5/3}}{B_o^{2/3}} = C_1\ , \tag{26}$$

where C_1 is a constant. By substituting Equations 9, 15, and 18 into 26, we obtain:

$$\frac{S_m}{F_e} = C_2\left(\frac{y/D_e}{F_e}\right)^{5/3}, \tag{27}$$

where

$$C_2 = \left(\frac{1}{C_1}\left(\frac{\pi}{4}\right)^2\right)^{1/3}. \tag{28}$$

Equation 27 is the asymptotic solution to Equation 23 as $y \to \infty$.

Experiments in which the centerline dilution has been measured have been performed by Cederwall (1967), Hansen and Schroder (1968), and Liseth (1970). Theoretical studies, which will not be discussed in detail here, have been made by Cederwall (1967), Abraham (1965), Fan and Brooks (1969), and Anwar (1972). All of these results are plotted in Figure 4. Hansen and Schroder, and Liseth used sharp-edged orifices, and the data in Figure 4 have been plotted assuming $C_c = 0.62$.

The value of the constant C_2 in Equation 27 can be estimated from the experiments of Rouse, Yih and Humphreys (1952). They measured temperature and velocity profiles in the radially symmetric plume above a point heat source (a cigarette), and expressed their results as:

$$g(\rho_r - \rho) = 11.0 \left(\frac{\rho_r (B_o \rho_r)^2}{y^5} \right)^{1/3} \exp\left(-71 \frac{r^2}{y^2}\right) . \tag{29}$$

To obtain the minimum dilution, put $r = 0$ and divide by ρ_r, obtaining:

$$\frac{g(\rho_r - \rho)}{\rho_r} = g'_m = 11.0 \frac{B_o^{2/3}}{y^{5/3}} . \tag{30}$$

The minimum dilution is then given by:

$$S_m = \frac{g'_o}{g'_m} = 0.091 \frac{g'_o y^{5/3}}{B_o^{2/3}} \tag{31}$$

On substituting the expression for B_o and F_e from Equations 15 and 18, Equation 31 becomes

$$\begin{aligned} \frac{S_m}{F_e} &= 0.091 \left(\frac{4}{\pi}\right)^{2/3} \left(\frac{y/D_e}{F_e}\right)^{5/3} \\ &= 0.107 \left(\frac{y/D_e}{F_e}\right)^{5/3} \end{aligned} \tag{32}$$

Equation 32, the asymptotic solution to Equation 23, is also plotted in Figure 4.

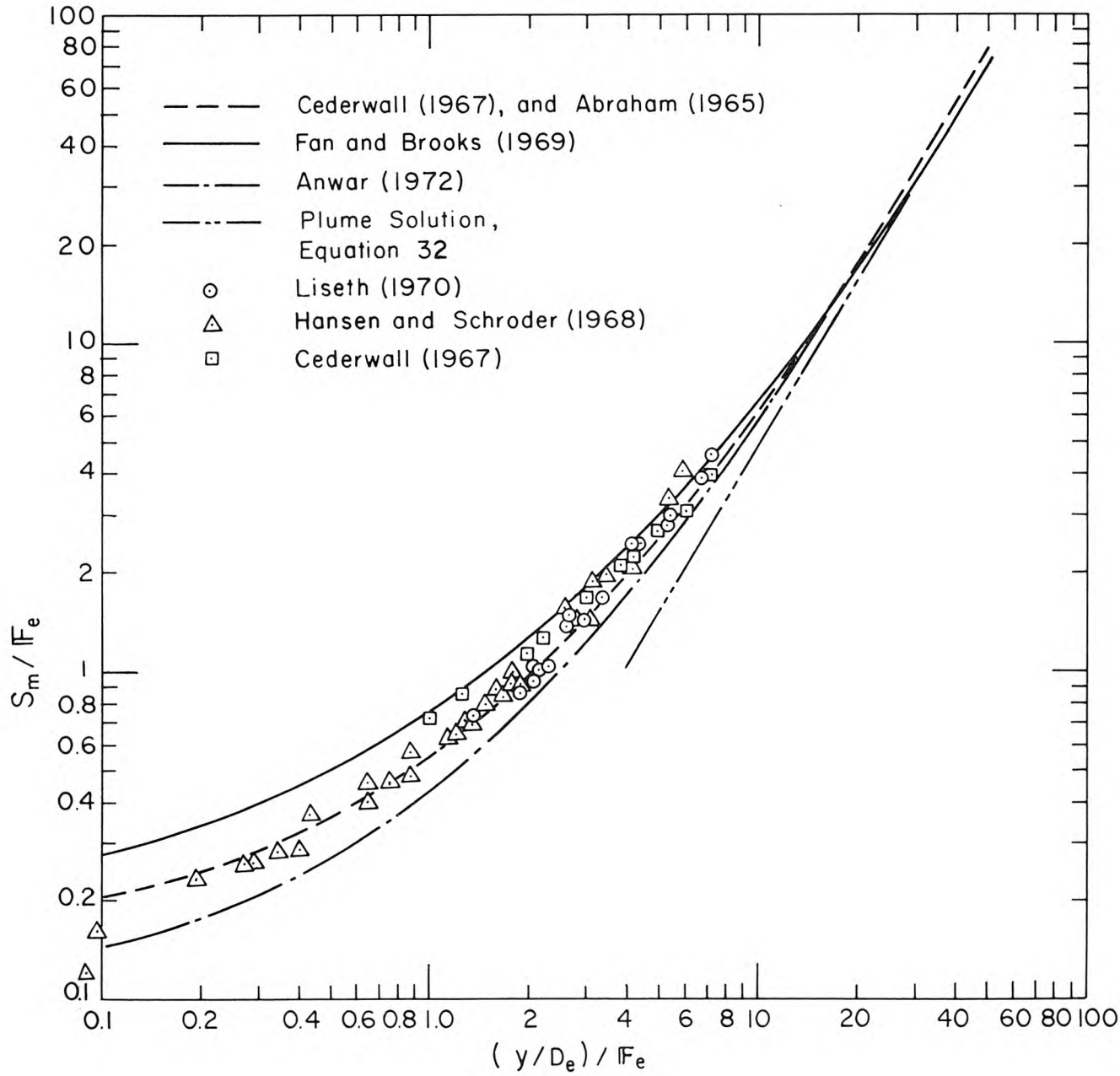

Figure 4. Centerline dilution of a horizontal, round buoyant jet in a stagnant, uniform fluid.

Figure 4 shows that there is good agreement between the results of the different experiments. For $(y/D_e)/F_e$ less than about 2 the theories of Abraham and Cederwall appear to describe the data best. For larger values of $(y/D_e)/F_e$, which are more typical of outfalls, there is little difference between the predictions, although the theory of Fan and Brooks appears to be best.

The predictions of Fan and Brooks (Brooks 1975), when replotted in the form of Equation 23, collapse to a single curve for $F_e > 8$. Therefore, as outfalls are generally designed such that $F_e > 10$, we can conclude that the initial volume flux is negligible for these cases, and that the minimum dilution can be expressed as:

$$\frac{S_m}{F_e} = f\left(\frac{y/D_e}{F_e}\right), \tag{33}$$

where the form of Equation 33 is shown in Figure 4.

We can now extend this argument to multiport diffusers, and write the minimum dilution immediately, by neglecting the port configurations and pipe diameter, as:

$$\frac{S_m}{F_e} = f\left(\frac{y/D_e}{F_e}, \frac{y}{\ell}\right) \tag{34}$$

Here, ℓ = the port spacing of the diffuser (2ℓ is the spacing on each side, see Figure 1).

Far above the source, as for the case of the individual round buoyant jet, the flow behaves like a plume, in this case from a line source. The only parameters which determine the minimum centerline dilution are now y, the height above the source, and b, the buoyancy flux per unit length. We can write, then:

$$g'_m = f(b,y) \ . \tag{35}$$

Dimensional analysis gives:

$$\frac{g_m' \, y}{b^{2/3}} = C_3 \ , \tag{36}$$

where C_3 is a constant. The minimum dilution is given by:

$$S_m = \frac{g_o'}{g_m'} = \frac{1}{C_3} \, g_o' \, y b^{-2/3} \ . \tag{37}$$

The buoyancy flux, b, per unit length from a diffuser with either staggered or opposed ports is given by:

$$b = g_o' q \ , \tag{38}$$

$$= \frac{u_o \pi D_o^2 g_o'}{4\ell} \tag{39}$$

On combining Equations 39, 37, 20, and 19, we obtain:

$$\frac{S_m}{F_e} = \frac{1}{C_3} \left(\frac{\pi}{4} \right)^{-2/3} \left(\frac{y}{\ell} \right)^{-2/3} \left(\frac{y/D_e}{F_e} \right)^{5/3} \ , \tag{40}$$

where the result is written in this way to agree with the form of Equation 34. Equation 40 is the asymptotic solution to Equation 34 as y/ℓ and $\frac{y/D_e}{F_e}$ both tend to infinity.

An alternative way of writing Equation 40 by using Equations 38 and 37 is:

$$S_m = \frac{1}{C_3} \, g_o'^{1/3} y q^{-2/3} \ . \tag{41}$$

The value of the constant C_3 can be estimated from the results of a number of experimental studies. Rouse, Yih and Humphreys (1952) studied the convection above a line burner, and measured velocity and temperature profiles. They expressed their results for temperature distribution as:

$$g(\rho_r - \rho) = 2.6 \left[\frac{\rho_r (b\rho_r)^2}{y^3} \right]^{1/3} \exp\left\{ -41 \, \frac{x^2}{y^2} \right\} , \tag{42}$$

where x is the horizontal distance from the plume centerline. For the centerline concentration, put x = 0 to obtain:

$$g_m' = 2.6\ b^{2/3}\ y^{-1} \quad . \tag{43}$$

Comparison of Equations 36 and 43 gives $C_3 = 2.6$.

Experiments have also been performed by Lee and Emmons (1961), who measured temperatures above a line fire; they also found the value of C_3 to be 2.6.

Recently, however, experiments have been performed by Kotsovinos (1975). He measured the velocity with a laser Doppler velocimeter and temperature by fast response thermistors above a two-dimensional heated water jet. Kotsovinos varied the source parameters of the jet to cover flow conditions ranging from a pure jet to a pure plume. He expressed his dilution measurements in terms of local conditions to account for the variability of the thermal expansion of water with temperature. Kotsovinos found the mean value of C_3 to be 2.37 for a pure plume, although his values ranged between 1.99 and 3.05 with a standard deviation of 0.20. As Kotsovinos' experiments appear to be the most accurate and reliable, we shall assume his value of $C_3 = 2.37$, with an estimated uncertainty of 10%. Equation 40 then becomes:

$$\frac{S_m}{F_e} = 0.50 \left(\frac{y}{\ell} \right)^{-2/3} \left(\frac{y/D_e}{F_e} \right)^{5/3} \quad , \tag{44}$$

and Equation 41 becomes

$$S_m = 0.42\ g_o'^{1/3} y q^{-2/3} \quad . \tag{45}$$

Experiments on merging buoyant jets from which the form of Equation 34 can be determined have been performed by Liseth (1970). He used a model manifold of 1.9 inches diameter with staggered ports of 3/16 inch diameter, whose spacing was varied from 7.5 cm to 0.83 cm. The model diffuser was fitted across the width of a flume 8 feet wide, 5 feet deep

and 180 feet long. The manifold was at the water surface and a heavy salt solution was discharged, which fell downwards. Dilutions in the plume were measured by means of a fluorescent dye tracer whose concentration in withdrawn samples was measured with a fluorometer. Liseth's data are shown plotted in the form of contours of constant values of $\frac{S_m}{F_e}$ in Figure 5. The data are plotted from the smooth curves drawn by Liseth through his data with the additional assumption that $C_c = 0.62$. The asymptotic plume solution, Equation 44, is also plotted in Figure 5.

Predictions of the dilution in merging round buoyant jets have been made by Koh (1971). Koh used the integral approach assuming a constant entrainment coefficient and Gaussian profiles. The jets are treated as individual round buoyant jets until a transition point is reached. At that point, the round jet solution is matched to the slot jet solution by matching mass, momentum and buoyancy fluxes. Two transition criteria were used, 1) where the jet width equals the jet spacing, and 2) where the entrainments for round and slot jets become equal. The two criteria gave practically identical results. For staggered ports, the jets are treated separately until their boundaries merge, then a single two-dimensional jet is assumed. For opposite ports, a region is allowed,if necessary, for pairs of two opposing jets to form single round jets which later merge to two-dimensional jets. This condition may occur for widely-spaced jets. Koh's solutions for staggered ports are shown in Figure 5. Similar results are presented by Shirazi and Davis (1972).

As can be seen from Figure 5, there is excellent agreement between Koh's theoretical and Liseth's experimental results. Koh's results give virtually identical results for staggered and opposing port configurations and, although there is no direct experimental verification of this, it is probable that the port arrangement is not important.

The reason for plotting the data as shown in Figure 5 is that the transition of the effluent flow from three-dimensional round buoyant jets to a two-dimensional plume can readily be seen by moving upwards on a 45° line (i.e., increasing y with other variables fixed). As can be

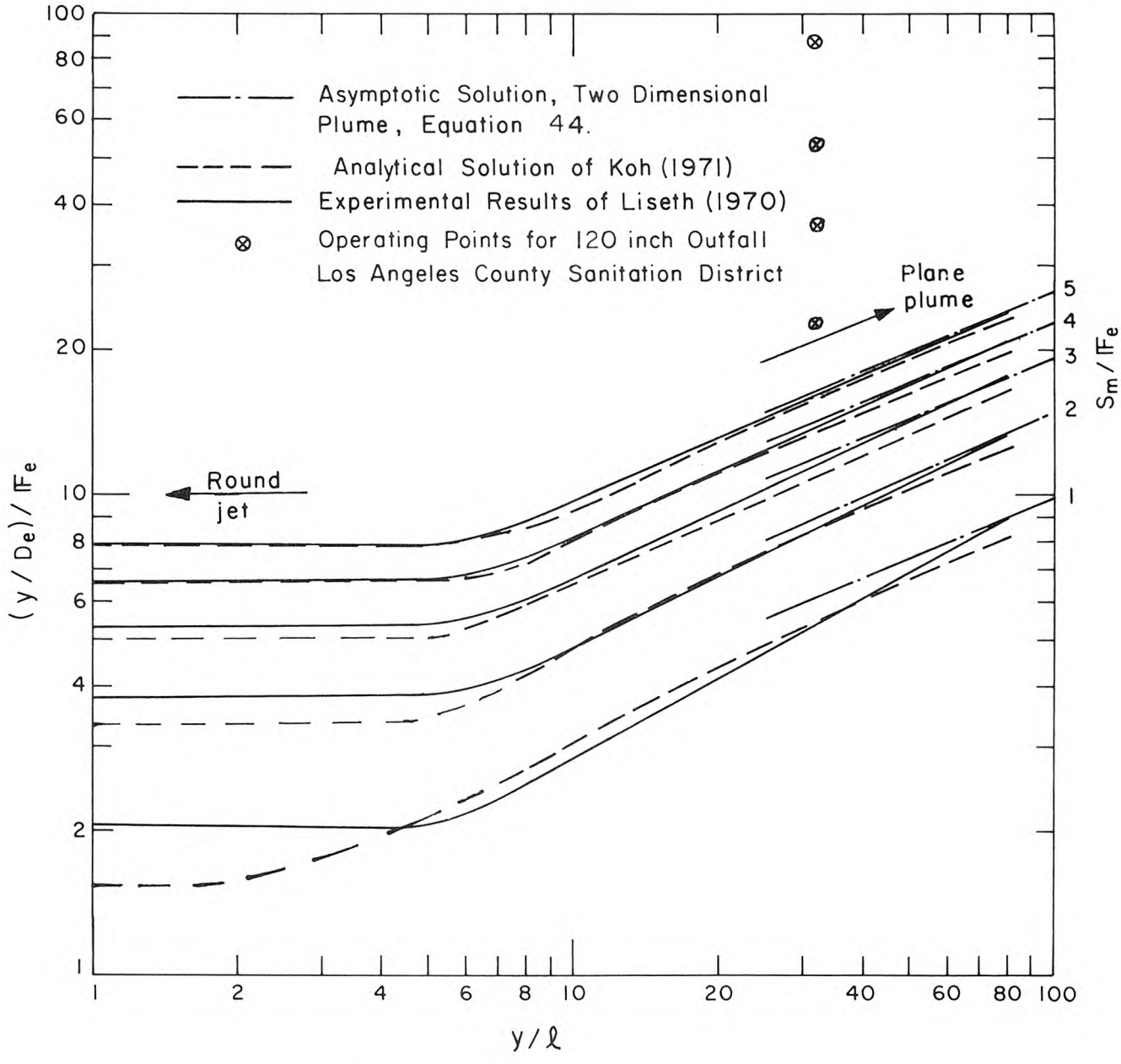

Figure 5. Contours of constant values of minimum dilution for merging, round buoyant jets above a multiport diffuser into uniform, stagnant water.

seen from the figure, there is little merging of the jets for $y/\ell < 5$, but as y increases further, merging causes a rapid decrease of dilution compared to the unrestricted round jet as the two-dimensional plume is approached.

Figure 5 can now be used to estimate the minimum dilution above a multiport diffuser in a stagnant, unstratified fluid. It can also be used to assess the degree to which the two-dimensional plume is approached at any height y. This is done by marking the operating point of the diffuser on the figure and observing how closely it lies to the plume solution curves in the upper right-hand corner.

APPENDIX C

DERIVATION OF DILUTION EXPRESSIONS

Consider an elemental volume, V, consisting of a mixture of volume V_o of effluent and V_r of receiving water. The dilution, S, is defined as:

$$S = \frac{V_o + V_r}{V_o} \quad . \tag{C1}$$

Conservation of mass states that:

$$\rho V = \rho_o V_o + \rho_r V_r \quad , \tag{C2}$$

where ρ, ρ_o, and ρ_r are the mass densities of the mixture, effluent, and receiving water, respectively. Suppose that these three components contain a species, for example salt, of concentrations c, c_o, and c_r and the density of each volume over the range of concentrations considered is linearly proportional to the species concentration, that is:

$$\left.\begin{aligned} \rho &= a_4 c + a_5 \\ \rho_o &= a_4 c_o + a_5 \\ \rho_r &= a_4 c + a_5 , \end{aligned}\right\} \tag{C3}$$

where a_4 and a_5 are constants. Conservation of species states that:

$$cV = c_o V_o + c_r V_r \quad . \tag{C4}$$

Substituting Eq. C3 into C2 and dividing through by a_5 yields:

$$\left(c+\frac{a_4}{a_5}\right) V = \left(c_o+\frac{a_4}{a_5}\right) V_o + \left(c_r+\frac{a_4}{a_5}\right) V_r \quad . \tag{C5}$$

Subtraction of Eq. C4 from C5 and division of the result by $\frac{a_4}{a_5}$ gives:

$$V = V_o + V_r \quad . \tag{C6}$$

Substitution of Eq. C6 into C2 yields:

$$\rho(V_o+V_r) = \rho_o V_o+\rho_r V_r \quad ,$$

hence

$$\rho = \frac{\rho_o V_o+\rho_r V_r}{V_o+V_r} \tag{C7}$$

Now, Eq. C1 can be written:

$$S = \frac{(\rho_r-\rho_o)(V_o+V_r)}{(\rho_r-\rho_o)\ V_o}$$

$$= \frac{(\rho_r-\rho_o)(V_o+V_r)}{\rho_r V_o+\rho_r V_r-\rho_o V_o-\rho_r V_r}$$

$$= \frac{(\rho_r-\rho_o)(V_o+V_r)}{\rho_r (V_o+V_r)-\rho_o V_o-\rho_r V_r}$$

$$= (\rho_r-\rho_o)/\left(\rho_r - \frac{\rho_o V_o+\rho_r V_r}{V_o+V_r}\right), \tag{C8}$$

and, on substitution of Eq. C7, Eq. C8 becomes:

$$S \equiv \frac{\rho_r - \rho_o}{\rho_r - \rho} \quad . \tag{C9}$$

A similar manipulation of Eqs. C1, C4, and C6 yields:

$$S = \frac{c_r - c_o}{c_r - c} \quad . \tag{C10}$$

If the density differences are due to variations in temperature and if, over a limited temperature range:

$$\rho \doteq \phi T + \sigma \quad , \tag{C11}$$

where T is the fluid temperature and ϕ and σ are constants, then application of the first law of thermodynamics to the mixture, assuming a constant specific heat, yields:

$$TV = T_o V_o + T_r V_r \quad , \tag{C12}$$

where T_r, T_o, and T are the temperatures of the receiving water, effluent, and mixture, respectively. Eq. C12, in combination with Eqs. C1 and C6, yields:

$$S = \frac{T_r - T_o}{T_r - T} \quad . \tag{C13}$$